

# Detecting myocardial ischaemia with optochemical sensing by using a fluorescent hydrogel

Combining optical and chemical sensing to save lives

Maurits Frans Vriesendorp



# Detecting myocardial ischaemia with optochemical sensing by using a fluorescent hydrogel

**Combining optical and chemical sensing to  
save lives**

by

Maurits Frans Vriesendorp

to obtain the degree of Master of Science  
at the Delft University of Technology,  
to be defended publicly on

Student number: 4391381  
Project duration: Augustus 20, 2020 – Augustus , 2021  
Thesis committee: Prof. dr. ir. P. J. French, TU Delft, supervisor  
Dr. G. de Graaf, TU Delft  
Dr. H. M. Amin Hassan, TU Delft  
Dr. M. Mastrangeli TU Delft

*This thesis is confidential and cannot be made public until December 31, 2021.*

An electronic version of this thesis is available at <http://repository.tudelft.nl/>.



# Abstract

Myocardial ischaemia induced by cardioplegia is the most prominent risk during open-heart surgery. To achieve adequate protection of the cardiomyocytes during surgery, the cardioplegia must arrive at all cardiomyocytes. Local obstruction can lead to regional ischaemia. For surgeons and perfusionist, the arrested heart is a black box. They know how much cardioplegia they are administering to the heart. However, they do not know if cardioplegia is reaching all cells. This work describes which parameters can be measured during cardioplegia induced cardiac arrest and compares the methods used in the literature to detect these parameters. Following this, it is the goal to create a proof-of-concept sensor for the detection of myocardial ischaemia. A literature review indicated that a fluorescent optochemical pH sensor has the most potential.

To be able to develop a proof-of-concept, optical, chemical, and medical knowledge needs to be combined. This is necessary to map what is required and what is possible for optochemical in vivo sensing. First, a framework is designed and used to select the best technique and material suited for this project. In this framework, the medical requirements and the resources available are combined. As a result, this thesis work will use a dual-wavelength pH-sensitive fluorescent dye encapsulated in a biocompatible hydrogel. In preparation for the proof-of-concept sensor, multiple samples are fabricated and extensively tested to achieve the optimal sensing layer. Using the optimised concentrations, a proof-of-concept sensor is created using a miniature reflection probe and an USB spectrometer.

This proof-of-concept sensor shows that it can measure the changes in pH and can be corrected for multiple interferences. It also shows the potential to be further miniaturised and to be used during cardiac surgery. Before this can happen, chemical optimisation of the sensing layer is needed and the consistency of the sensing layer needs to be improved. However, besides this, the work succeeded in selecting an optochemical sensing technique and material which shows the potential to be used in cardiac surgery.



# Preface

It all started a bit more than a year ago, when my brother notified me of the cardioplegia induced related death occurring after cardiac surgery. I was shocked to hear that the heart is like a black box for surgeons and they have no equipment to indicate if the cardiac tissue is becoming ischaemic. This motivated me to help develop a sensor which has the potential to save lives. During the past year, I had to combine the knowledge I gained during my Bachelor Clinical Technology and my Master Biomedical engineering.

I learned many new skills and challenged myself straight from the beginning. At times it was complex as I set up the research myself and could not build on previous work or knowledge within the bioelectronics research group. However, these challenges made sure I achieved the maximal results and that I grew personally and professionally. I would like to highlight the people around me which made this thesis possible.

First of all, I would like to thank my supervisors: dr. Ger de Graaf, Prof. dr. Paddy French and dr. Hitham Hassan. I already knew Ger and Paddy from my internship in Stellenbosch and they supported me in choosing my own project. They warned me of the challenges, but gave enough freedom to steer my own research. I want to thank them for their feedback and help during the process. The inexhaustible source of knowledge of both of them helped me a lot. The last weeks of my thesis were tight and without the help of Ger, I would not have the results I have now.

As my project was becoming increasingly chemistry-based, I came in contact with Hitham. It is incredible how he is able to explain complex chemistry processes in such a simplified way. This helped me to tackle challenges, which I could not have done without him. It was very inspiring and motivating to work together as he would break up my questions into small solvable pieces.

Futhermore, I would like to thank the EKL-team for the training and Stefaan Heirman of the PMVD group for the spectrometer equipment. Thanks to Stefaan, I had access to advanced equipment which helped to improve my results.

Last but not least, I want to thank Laura, my family and friends for support and help during my thesis. I am very lucky to have you all!

*Maurits Frans Vriesendorp  
Delft, August 2021*

# Contents

<b>Abbreviations</b>	<b>ix</b>
<b>Nomenclature</b>	<b>x</b>
<b>List of Definitions</b>	<b>xi</b>
<b>1 Introduction</b>	<b>1</b>
1.1 Background and Motivation	1
1.1.1 Cardiac Surgery	1
1.1.2 Motivation	2
1.2 Problem	3
1.2.1 Problem statement	3
1.2.2 Goal of thesis	3
1.3 Research Questions	3
1.3.1 Main Questions	3
1.3.2 Sub Questions	3
1.4 Organisation of thesis	4
1.4.1 Scope of thesis	4
1.4.2 Outline of thesis	4
<b>2 Theoretical Background</b>	<b>5</b>
2.1 Medical Background	5
2.1.1 Open heart surgery	5
2.1.2 Action Potential and Cardioplegia	7
2.1.3 Metabolism of the Cardiomyocyte	8
2.1.4 Parameters of ischaemia during Cardioplegia induced Cardiac Arrest	10
2.2 pH	12
2.2.1 Introduction pH	12
2.2.2 Factors related to pH	14
2.2.3 pH sensing in the human body	15
2.2.4 Differences in electrochemical and optochemical pH sensing	16
2.3 Biomedical sensor	17
2.3.1 Types of sensors used in biomedical sensors	17
2.3.2 Optical Sensing	18
2.3.3 Electrochemical sensing pH	19
2.3.4 Optochemical Sensing pH	20
2.4 (Photo)luminescence	22
2.4.1 Light-matter interaction	22
2.4.2 Single and Triplet Excited state	23
2.4.3 Internal Conversion	25
2.4.4 Fluorescence	25
2.4.5 Intersystem Crossing	27
2.4.6 Phosphoresence	27
2.4.7 <i>Fluorescent lifetime and Quantum Yield</i>	27
2.5 Fluorescence Measurement Techniques	28
2.5.1 Steady State Measurements	28
2.5.2 Time-resolved measurements	30
2.5.3 Luminescent Indicators	32
2.6 Hydrogels	33
2.6.1 Mechanism	33
2.6.2 Types	33

2.7	Challenges in optical pH sensing	34
<b>3</b>	<b>Narrowing the scope</b>	<b>35</b>
3.1	Literature review	35
3.1.1	Ischaemia parameters	35
3.1.2	Sensing Mechanism	36
3.1.3	Optical sensors	36
3.1.4	Consequences for thesis	38
3.2	Conditions for the sensor	39
3.2.1	Medical Requirements	39
3.2.2	Resources Available	39
3.2.3	State of the art sensors	41
3.2.4	Framework	42
3.3	Result	42
3.3.1	Selection of Optical Technique	42
3.3.2	Selection of pH Indicator	44
3.3.3	Selection of Support Matrix	44
3.3.4	Result	44
<b>4</b>	<b>Material and Methods</b>	<b>47</b>
4.1	General Materials and Instrumentation	47
4.1.1	Materials	47
4.1.2	Instrumentation	47
4.2	Methods	48
4.2.1	Fabrication of pH buffers	48
4.2.2	Fabrication of HPTS microbeads	48
4.2.3	Fabrication of sensing layer	49
4.2.4	Fabrication of different samples	50
4.3	Optical Experiments	50
4.3.1	Optical examination	50
4.3.2	Spectrometer Analysis Experiments	51
4.4	Analysing Data	53
4.4.1	Determining pKa of the HPTS microbeads	54
4.4.2	CMOS Imaging Processing	54
4.4.3	Reflection Measurements	54
4.4.4	Transmission Measurements	55
4.4.5	Absorption Measurements	55
4.4.6	Fluorescence Measurements	55
4.4.7	Reflection Probe	55
<b>5</b>	<b>Results</b>	<b>57</b>
5.1	First batch of samples	57
5.1.1	Goal of first batch	57
5.1.2	Experiment first batch	58
5.1.3	Results Experiments	58
5.1.4	Analysis of first batch	59
5.2	Second batch of samples	60
5.2.1	Goal of second batch	60
5.2.2	Experiment second batch	61
5.2.3	Results Experiments	61
5.2.4	Analysis of second batch	67
5.3	Reflection fibre USB spectrometer	70
5.3.1	Goal of USB spectrometer and Reflection probe	70
5.3.2	Experiment reflection fibre	70
5.3.3	Results Experiments	70
5.3.4	Analysis of reflection probe measurements	74

<b>6</b>	<b>Proof-of-concept sensor</b>	<b>75</b>
6.1	Goal of proof-of-concept sensor . . . . .	75
6.1.1	Concepts developed for sensor . . . . .	75
6.1.2	Fabrication of proof-of-concept sensor . . . . .	77
6.1.3	Experiments proof-of-concept sensor . . . . .	77
6.2	Results proof-of-concept sensor . . . . .	78
6.2.1	Optical investigation . . . . .	78
6.2.2	Reproducibility and Ionic Strength . . . . .	79
6.2.3	Transition Time . . . . .	81
6.3	Analysis of proof-of-concept sensor . . . . .	82
<b>7</b>	<b>Discussion</b>	<b>83</b>
<b>A</b>	<b>Appendixes</b>	<b>99</b>
A.1	Comparison table of different type of sensor . . . . .	99
A.2	Comparison table of different techniques sensor . . . . .	100
A.3	Protocol of producing phosphate buffers . . . . .	101
A.4	Protocol of producing HPTS loaded microbeads . . . . .	102
A.5	Overview different optical detection schemes by Steinegger et al. [139] . . . . .	103
A.6	Protocol of producing the hydrogel . . . . .	104
A.7	CMOS Data . . . . .	105
A.8	(Un)scaled Reflection Data for Perkin Elmer . . . . .	106
A.9	(Un)scaled Transmission Data for Perkin Elmer Lambda 1050 . . . . .	107
A.10	(Un)scaled Absorbance Data . . . . .	108
A.11	Fluorlog Data . . . . .	109
A.12	Fluorlog Sensitivity Samples A, B and D . . . . .	117
A.13	Extra Results Reflection Probe . . . . .	119
A.14	Results of the 1mm layer of the reflection probe measurements . . . . .	120
A.15	SOLIDWORK drawings . . . . .	121
A.16	Results of ionic strength measurement proof-of-concept sensor . . . . .	123
A.17	Results of reproducibility measurement proof-of-concept sensor . . . . .	124
A.18	Matlabcodes used in thesis . . . . .	125
	A.18.1 Scripts. . . . .	125
	A.18.2 Functions . . . . .	141
A.19	Literature Review . . . . .	146

# Abbreviations

- ATP** adenosine triphosphate. xiii, 8, 9
- AVR** Aortic Valve Replacement. 10
- BGA** Blood Gas Analysers. 16
- CABG** Coronary artery bypass graft. 2, 8, 10
- CCD** charge-coupled device. 31
- CMOS** Complementary metal–oxide–semiconductor. 31
- CPB** Cardiopulmonary bypass. 1, 5, 6, 11
- DLR** Dual Lifetime Referencing. 31, 41, 84, 87
- DWR** Dual Wavelength Referencing. 44, 84, 85
- ES** Excited State. 22, 23, 24
- fd-DLR** frequency-domain dual lifetime referencing. 31
- FLIM** Fluorescence Lifetime Imaging. 30
- FRET** Förster Resonance Energy Transfer/Fluorescence Resonance Energy Transfer. 43
- FRIM** Fluorescence Ratiometric Imaging. 29
- GS** Ground State. 23, 24
- HOMO** Highest Occupied Molecular Orbital. 23
- HPTS** 8-Hydroxypyrene-1,3,6-trisulfonic acid trisodium salt. 33, 41, 44, 45, 84
- IC** Internal Conversion. 25
- IS** Ionic Strength. 8, 14, 16, 33, 53, 72
- ISC** Intersystem Crossing. 27
- KCl** Potassium Chloride. 1, 6, 8, 85
- LED** Light Emitting Diode. 53
- LUMO** Lowest Unoccupied Molecular Orbital. 23
- MI** Myocardial Infarction. 2
- PDH** Pyruvate Dehydrogenase. 9
- PET** photoinduced electron transfer. 32, 44
- PIPT** photoinduced proton transfer. 32
- PMT** Photo Multiplier Tube. 53, 65
- td-DLR** time-domain dual lifetime referencing. 31

# Nomenclature

- $A_\lambda$  absorption coefficient. 19
- $E$  Electrical potential measured by electrode. 15
- $E^0$  the electrode potential. 15
- $F$  Farady constant. 15
- $I$  relative activity of ions in a solution. 14, 15
- $I$  measured light intensity. 19
- $I_0$  the intensity of the light at the source. 19, 27, 28, 29
- $K_w$  the ionisation constant of water. 13
- $R$  gasconstant. 14, 15, 29
- $T$  Temperature. 14
- $\Phi$  Quantum Yield. 26
- $\epsilon$  molar attenuation coefficient. 28, 29
- $\eta$  sensitivity of dissociation curve. 55
- $\lambda$  a sinusoidal waveform traveling at constant speed. 18
- $\mu_i$  the (molar) chemical potential of the species  $i$  under the conditions of interest. 14
- $\mu_i^\ominus$  the (molar) chemical potential of that species under some defined set of standard conditions. 14
- $\phi$  phase shift. 31
- $\rho_\lambda$  reflection coefficient. 19
- $\tau_0$  fluorescent lifetime of molecule. 27
- $\tau_s$  the lifetime of the singlet excited state. 26, 31
- $a_c$  activity of Ion C in a solution. 14
- $a_{H^+}$  activity of the hydrogen ion. 12
- $c$  molar concentration of each ion present in the solutions. 14, 28, 29
- $f$  frequency. 31
- $h$  Planck constant. 23
- $k_f$  fluorescence rate constant. 26
- $l$  thickness. 28, 29
- $\nu$  frequency of photon. 23
- $z$  Ionic valency charge of ion present in solution. 14

# List of Definitions

- acidosis** condition in which there is too much acid in the body fluids. 11
- aerobic** relating to, involving, or requiring free oxygen. 9, 10
- anaerobic** relating to or requiring an absence of free oxygen. 8, 9, 10, 11
- antegrade** In the direction of normal movement, as in blood flow or peristalsis. 1, 8
- cardiac arrest** a sudden, sometimes temporary, cessation of the heart's functioning. 1, 2
- cardiomyocyte** striated self-beating and cylindrical rod-shaped muscle cells that fundamentally govern the function of myocardium. xiii, 1, 2, 5, 7, 8, 9, 10, 11
- cardioplegia** chemical solution used to arrest (stop) the heart. 1, 2, 8
- chromophore** an atom or group whose presence is responsible for the colour of a compound. 22
- dye** a natural or synthetic substance used to add a colour to or change the colour of something. 22
- emission** the process of elements releasing different photons of color as their atoms return to their lower energy levels. xiii, xiv, 18, 22, 25, 28, 29, 30, 31, 32, 43, 54, 55, 61, 62, 65, 66, 72, 74
- excitation** the application of energy to something. xiii, 18, 22, 25, 28, 29, 30, 31, 43, 61, 62, 63, 65, 66, 68, 71, 75
- fluorescence** spontaneous emission of electromagnetic radiation after excitation by photon, which stops right after the excitation radiation is stopped (single state). xiii, 20, 23, 25, 26, 27, 29, 30, 31, 32, 43, 44, 58, 60, 61, 62, 65, 66, 67, 68, 70
- fluorescent lifetime** mean time elapsed between the activation of a fluorophore and emission of a photon from the fluorophore. 27, 30
- fluorophore** a fluorescent chemical compound that can re-emit light upon light excitation. 22
- glycolysis** the breakdown of glucose by enzymes, releasing energy and pyruvic acid.. 9, 10
- hydrogel** a crosslinked hydrophilic polymer that does not dissolve in water. 20, 33, 34, 39, 45, 50, 57, 59, 60, 69, 70, 84
- hypertrophy** increase and growth of muscle cells. 8
- hypothermia** the condition of having an abnormally (typically dangerously) low body temperature. 6
- indicator** a compound that changes colour at a specific pH value or in the presence of a particular substance, and can be used to monitor acidity, alkalinity, or the progress of a reaction.. 20, 21, 22, 28, 29, 31, 32
- ionisation constant** a constant that depends upon the equilibrium between ions and molecules that are not ionized in a solution or liquid. Additionally known as: dissociation constant, self-ionisation constant, ion product constant, or ionic product. 13
- ischaemia** inadequate blood supply to an organ or part of the body, especially the heart muscles. 1, 2, 3
- luminescence** spontaneous emission of light by a substance not resulting from heat. xiii, 19, 22, 24, 25, 27, 28, 29, 30, 31

- luminophore** an atom or functional group in a chemical compound that is responsible for its luminescent properties. 27, 28, 29, 31
- metabolism** the chemical processes that occur within a living organism in order to maintain life. xiii, 5, 6, 8, 9, 10, 11
- mitochondria** organelle found in large numbers in most cells, in which the biochemical processes of respiration and energy production occur. 8, 9
- morbidity** the condition of suffering from a disease or medical condition. 2
- mortality** state of being subject to death. 1, 2
- optrode** optical sensor device that optically measures a specific substance, usually with the aid of a chemical transducer. 21
- pH** decimal logarithm of the inverse of the hydrogen ion activity. xiii, 2, 3, 4, 5, 10, 11, 12, 13, 14, 15, 16, 17, 18, 19, 20, 21, 22, 28, 32, 33, 34, 35, 36, 37, 38, 39, 42, 43, 44, 47, 48, 49, 50, 52, 53, 58, 61, 62, 70, 75, 84
- phosphorescence** spontaneous emission of electromagnetic radiation after excitation by photon, which slowly decays with time and results in an afterglow (triplet state). xiii, 22, 23, 24, 27, 31
- phosphors** A phosphorescence chemical compound that can reemit light upon light excitation. 22
- photobleaching** loss of colour by a pigment (such as chlorophyll or rhodopsin) when illuminated. 21
- photodegradation** (of a substance or object) be decomposed by the action of light, especially sunlight. 32
- pKa** acid dissociation constant. 13, 14, 15, 20, 33, 34, 45, 54, 55, 73
- quantum yield** the ratio of the number of photons emitted to the number of photons absorbed. 25, 26, 27, 28, 29
- ratiometric** relating to the measurement of the ratio between two or more factors. 29, 30, 31
- sensor** a device which detects or measures a physical property and records, indicates, or otherwise responds to it. xiii, xiv, 16, 17, 18, 20, 21, 22, 29, 31, 34, 35, 36, 38, 39, 41, 42, 44, 57, 58, 61, 68, 70, 73, 74, 75, 76, 83, 84
- stenosis** the abnormal narrowing of a passage in the body. 1
- vibrational relaxation** relaxation of an excited-vibrational state molecule to less energetic vibrational modes through the transfer of vibrational energy. xiii, 23, 24, 25

# List of Figures

2.1	A cardiopulmonary bypass, the blood is extracted from the body at the veins and collected in a blood reservoir, from here roller pumps are used to pump the deoxygenated blood to the oxygenator after which the blood is pumped back into the body at the aorta. Reprinted from [40]	6
2.2	Anatomy of the heart. In red the layers of the heart which are of interest in this work. Reprinted from Bailey [14]	7
2.3	Normal action potential of cardiac muscle cell with different phases and ion gates flow illustrated. The membrane potential is -90mV and sodium influx causes a depolarisation which cause a contraction of the cardiomyocyte. Reprinted from [165]	7
2.4	A schematic of the effect of hyperkalemia and prolonged myocardial membrane depolarisation on Na <sup>+</sup> entry through the "window current" and the net influx of Ca <sup>2+</sup> into the cardiomyocyte via the reversal of the Na <sup>+</sup> /Ca <sup>2+</sup> exchanger. Reprinted from Dobson et al. [36]	8
2.5	Linkages between cardiac power, adenosine triphosphate (ATP) hydrolysis, oxidative phosphorylation, and NADH generation by dehydrogenase in metabolism. Reprinted from Stanley et al. [137]	9
2.6	The pathways and regulatory points of myocardial substrate metabolism. Reprinted from Stanley et al. [137]	9
2.7	Changes in the cardiomyocyte during ischaemia and reperfusion. Reprinted from Xia et al. [166]	10
2.8	Pearson correlation revealed a significant correlation between myocardial PtCO <sub>2</sub> and tissue lactate (B) and tissue pH (C). Single values displayed as baseline (squares), blood flow 75% (open triangles), 50% (filled triangles), and 25% (diamonds). Reprinted from Pischke et al. [112]	11
2.9	Effect of ionic strength on the pKa's of the membranes M1, M2 and M3. The charge of the support matrix has a large influence on the pKa value of the reaction. Reprinted from Weidgans [154]	15
2.10	Information flow from the body to the monitor provided by the biomedical sensor. As found in Tronstad [146]	17
2.11	Classification of Biomedical sensor developed for this literature review by combining classifications of Shavanova et al. [134], Sharma and Khurana [131], Hajian et al. [56] Singh et al. [135]	18
2.12	Interaction between light and matter. Different phenomena and their wavelengths. Only luminescence causes light of a different wavelength. Reprinted from A. et al. [1]	19
2.13	Absorption, transmission and reflection performance of the light: (a) in a transparent medium; (b) to face opaque medium. Reprinted from A. et al. [1]	19
2.14	Illustrations of the light matter interaction and the excited and ground state and excited states	23
2.15	Typical diagram of the electronic energy levels of a molecule with singlet and triplet systems. The most important radiative (fluorescence and phosphorescence) and non-radiative (internal conversion, vibrational relaxation, intersystem crossing) transitions are shown. Reprinted from Álvarez et al. [8]	24
2.16	Frank-Condon energy states and the absorption and luminescence spectra example	24
2.17	Stoke shift principle seen in fluorescence spectroscopy and the differences caused by the higher excitation states. Reprinted from Gupta and Mahapatro [55]	25
2.18	Intramolecular deactivation Processes	26
2.19	Dual excitation and single emission measurement methods. Reprinted from Weidgans [154]	30
2.20	Dual emission measurement methods. Reprinted from Kocincová [77]	30
2.21	Illustrations related to luminescence decay time measurements in time and frequency domain	31
2.22	Principle of the DLR The upper and the lower rows reflect the situations with "switched on" and "switched off" pH indicator, respectively. Reprinted from Steinegger et al. [139]	32
3.1	Classification of Biomedical sensor developed for this literature review by combining classifications of Shavanova et al. [134], Sharma and Khurana [131], Hajian et al. [56] Singh et al. [135]	36
3.2	Search terms used in literature search in Scopus	37
3.3	Flow diagram of records included in this literature review	37
4.1	Images of the different process steps described in section 4.2.1	49
4.2	Images of the HPTS-microbeads fabrication described in section 4.2.2	49
4.3	Picture of the 150 mm integrating sphere installed in a LAMBDA 1050+ with a top down view of the diagram of the sphere below. The red marked area is where transmission of the material is done, and the green area the reflectance of the material. Reprinted from [49]	51
4.4	Schematic representation of the fluorescence spectrophotometer Fluorolog 3 model FL3-22 from Horiba Scientific used for fluorescence spectrometry. Reprinted from horiba.com	52
4.5	Schematic representation of the set up with the 475nm LED and the Avantes Starline USB spectrometer	53
5.1	Optical Investigation of Sample A, C, E and G under Zeiss Microscope with 5-25x magnification	58
5.2	Images related to the first experiments with CMOS and first batch of Samples	59
5.3	The scaled output of the green channel of the thorlabs CMOS camera of Sample E	60
5.4	Samples in preparation of the fluorescent microscope	62
5.5	Sample of second batch under fluorescence microscope with GFP filter and 20x magnification	62
5.6	(a) Unscaled reflection output of Sample C in the lambda spectrophotometer, (b) Scaled output of Sample C in the lambda spectrophotometer and (c) the output of the samples at different pH	63
5.7	Images of Set up Transmission Measurements	63

5.8	(a) Unscaled transmission output of Sample C in the lambda spectrophotometer, (b) Scaled output of Sample C in the lambda spectrophotometer and (c) the output of the samples at different pH	64
5.9	(a) Unscaled absorbance output of Sample D, calculated using the transmission data from the lambda spectrophotometer, (b) Scaled output of Sample D and (c) the output of the samples at different pH	64
5.10	Results of determining pKa and sensitivity of the absorbance data of the samples C and D	65
5.11	Images of Set up Fluorlog	65
5.12	Fluorescence output of Sample C measured in Horiba Fluorlog 3	66
5.13	Fluorescent Output in Count per Seconds of Sample C and scaled Output of Sample C	67
5.14	Ratios, sensitivity and pKa determination for Sample C	67
5.15	Images of optical sensing layers on optical reflection fibre	71
5.16	Spectral output measured by Avantes Starline in counts per second, for the two layer thicknesses and at different pH and with different voltages. Measured in 150mM buffer solutions	71
5.17	Scaled output of the the layer at different light intensities (a and b) and at different pH at the same light intensity (c and d)	72
5.18	Spectral output measured by Avantes Starline in counts per second per different voltages, measured at the emission of 525nm. All values are scaled to the value of 475nm for the two layer thicknesses and at Ionic Strengths and with different pH	72
5.19	Outcome of the full range of the 0.5mm sample after submerging for 20 minutes in 150mM buffer solutions	73
5.20	Transition times when sensor is placed from a high/low sample to the other	73
5.21	Transition times vs. value at 525 emission wavelength, when sensor is placed from a high/low sample to the other	74
6.1	Concept design of a disposable planar sensor	76
6.2	Images related to the planar concept design	76
6.3	Design of the optical fibre proof of concept sensor. (1) 475 nm LED, (2) 405 nm LED, (3) SMA connector, (4) Avantes miniature reflection probe, (5) 3D printed connector, (6) rubber ring to hold sample in place, (7) Sample, (8) Avantes Starline USB Spectrometer, (9) Laptop to process data from Avantes Starline	77
6.4	Design of the optical fibre proof of concept sensor. (1) Avantes Reflection Fibre (2) pH Probe N64 of SI Analytics (3) Temperature Sensor, (4) Proof of concept needle, (5) Dark container	77
6.5	Set up of the final measurements	78
6.6	Set up of the proof-of-concept sensor needle	78
6.7	Zoomed Images of sensing layer on the tip of the needle. Left image with LED's turned of, middle image with 475nm LED on and right image with 405nm LED on	79
6.8	Non-Normalised Ratios of the measurement with 100mM buffer solutions and 5 minutes waiting time, green and blue line indicate the area where the sensor should be sensitive.	79
6.9	Results reproducibility measurements. Three measurement done with the same buffer solutions with and ionic strength of 100mM. Ratio of the emission peak divided by the excitation's peak (eq 4.7). pKa determined by Boltzmann sigmoid function (eq 4.5) Between each measurement 5 minutes waiting time	80
6.10	Results ionic strength measurements. Three measurement done with buffer solutions with IS of 50mM 100mM and 150mM. Ratio of the emission peak divided by the excitation's peak (eq 4.7). pKa determined by Boltzmann sigmoid function (eq 4.5) Between each measurement 5 minutes waiting time	80
6.11	Results of the measurements done with two different layers with the same concentration. The measurement done with buffer solutions with IS of 100mM. Ratio of the emission peak divided by the excitation's peak (eq 4.7). pKa determined by Boltzmann sigmoid function (eq 4.5). Between each measurement 5 minutes waiting time	81
6.12	Result of the transition time measurements with response time of each sensing layer. Measured in both directions	81
A.1	Advantages and Disadvantages of the Various Optical Detection Schemes and How Well They Can Compensate for Various Kinds of Undesired Interferences by Steinegger et al. [139]	103
A.2	The scaled output of the green channel of the thorlabs CMOS camera of Sample C	105
A.3	The scaled output of the green channel of the thorlabs CMOS camera of Sample G	105
A.4	Scaled Reflection of samples A-D	106
A.5	Reflection of samples A - D	106
A.6	Scaled Transmission of samples A-D	107
A.7	Transmission of samples A-D	107
A.8	Absorbance of samples A-D	108
A.9	Scaled Absorbance of samples A - D	108
A.10	Top view of fluorescence output measured by flourlog 3	109
A.11	Top view of fluorescence output measured by flourlog 3	110
A.12	Top view of fluorescence output measured by flourlog 3	111
A.13	Top view of fluorescence output measured by flourlog 3	112
A.14	Top view of fluorescence output measured by flourlog 3	113
A.15	Top view of fluorescence output measured by flourlog 3	114
A.16	Top view of fluorescence output measured by flourlog 3	115
A.17	Top view of fluorescence output measured by flourlog 3	116
A.18	Determining the pKa of Sample A at a emission wavelength of 525nm and excitation wavelengths 475/405nm	117
A.19	Determining the pKa of Sample B at a emission wavelength of 525nm and excitation wavelengths 475/405nm	117
A.20	Determining the pKa of Sample D at a emission wavelength of 525nm and excitation wavelengths 475/405nm	118
A.21	Spectral output measured by Avantes Starline in counts per second, scaled to the value of 475nm for the two layer thicknesses and at different voltages and with different pH. Measured in 100mM buffer solutions	119
A.22	Outcome of the full range of the 1mm sample after submerging for 20 minutes in 150mM buffer solutions	120
A.23	Full results of Ionic Strength measurements	123

A.24 Full results of reproducibility measurements . . . . .	124
---	-----

## List of Tables

2.1 Absorption and Emission Rate Comparison . . . . .	27
3.1 Comparison of different parameters with the (dis)advantages of measuring them to monitor myocardial ischaemia	35
3.2 Evaluation of all the sensors found in the literature on their capabilities to be in vivo ischaemia sensor. . . . .	38
3.3 Description of different requirements set by the cardiac thoracic surgeons of Leiden University Medical Centre. . .	40
3.4 Overview of the different optical techniques and their (dis)advantages. Compared on four different aspects . . . .	43
3.5 Indicators and Support Matrices found in literature . . . . .	46
4.1 Overview of different concentration used to fabricate different pH samples with different Ionic Strengths . . . . .	48
4.2 Concentrations of the sample mixtures used for the first optical experiments . . . . .	50
4.3 Concentrations of the solutions used for the second optical experiments and fluorescent microscopy images . . . .	50
5.1 Determining the optimal wavelength for dual wavelength referencing of Sample C . . . . .	66
5.2 pKa of samples and transition time from pH 10 to pH 4. Measured by visual output . . . . .	67
A.1 Comparison of different types of sensors for their potential to measure pH or Lactate with examples . . . . .	99
A.2 Overview of the different optical techniques and their (dis)advantages. Compared on four different aspects . . . .	100



# Introduction

Cardiovascular diseases are increasing all around the world. Due to the advancement in technology and understanding of the heart, it is possible to save many lives. Cardiac surgery is a growing field and more complex surgeries are being done. To facilitate the surgeon during an open heart surgery, the heart is temporarily arrested by administering cardioplegia. Cardioplegia is a pharmacological solution which "pauses" the heart muscle cells. Although cardioplegia exists since the 1960's, it is still causing postoperative mortality. This is because the condition of the heart is for the surgical team as a black box. They know the condition of the heart beforehand, they know how much cardioplegia they are administering, but they do not know if the cardioplegia reaches all cells. When heart muscle cell receives not any cardioplegia, this causes ischaemia, damage and eventually death of the cells. The goal of this thesis is to investigate the possibility to measure myocardial ischaemia and to design and produce a proof-of-concept sensor which can detect myocardial ischaemia during cardioplegia induced cardiac arrest.

## 1.1. Background and Motivation

### 1.1.1. Cardiac Surgery

Cardiac surgery is the field of medicine involved in the surgical treatment of the heart. With a variety of procedures, surgeons can treat acquired cardiovascular diseases and congenital malformations of the coronary arteries and/or heart valves. Although there are some exceptions (e.g.. off-pump bypass surgery), the heart is usually arrested (stopped) to enable surgeons to operate [128]. Before the heart can be arrested during such an operation, a heart-lung machine or Cardiopulmonary bypass (CPB) is first connected to the major blood vessels of the patient. This machine is design to replace the function of the heart and lungs during cardiac arrestKoning [78]; blood is drained from the vena cava/right atrium, oxygenated and then returned to the aorta. After connecting the heart-lung machine, the aorta is clamped, and cardioplegia is injected into the coronary artery to induce cardiac arrest [91].

Cardioplegia is the universal term used for pharmacological solutions that are administered during cardiac surgery to arrest the heart temporarily [23]. While there are many types of cardioplegia solutions, they are all primarily based on Potassium Chloride (KCl). KCl prevents repolarisation in the cardiomyocyte. The resulting diastolic cardiac arrest reduces the metabolism of the cardiomyocyte, preserving it without blood supply. Cardioplegia can reduce the oxygen demand by ten-fold; in combination with lowering the temperature, this can be even twenty-fold [2].

The standard method to administer cardioplegia is through antegrade perfusion in the aortic root or the ostia of the coronary arteries for around two minutes. Although the amount of administered cardioplegia solution can be measured at its entry point, the exact distribution of cardioplegia through the coronary system is unknown. To achieve adequate protection of cardiomyocytes during the procedure, cardioplegia must arrive at all cardiomyocytes. However, occlusion or stenosis of a distal coronary artery may obstruct the distribution of cardioplegia, resulting in regional ischaemia.

Ischaemia occurs as a consequence of an imbalance between oxygen supply and oxygen demand [138]. Local ischaemia will lead to myocardial damage. Drescher et al. [38] describe that myocardial damage is one of the most common causes of morbidity and mortality after heart surgery. These reasons are why the field of cardiac surgery is continuously looking for improvements of techniques to better preserve the cardiomyocytes during open-heart surgery. There is no blood flow during cardioplegia-induced cardiac arrest and therefore, normal parameters that are used to detect ischaemia are not applicable. These parameters include proteins like Troponin and Creatine Kinase MB (CK-MB), or mechanical parameters such as cardiac output [37]. The absence of tools or parameters to monitor the myocardium during cardiac arrest makes the administration of cardioplegia a black box. Only when the heart starts beating again, clinicians become aware whether cardioplegia was distributed well enough to preserve the myocardium. By then, the process of ischaemia is irreversible and myocardial function is lost.

Perioperative Myocardial Infarction (MI) is one of the most severe complications following cardiac surgery, especially Coronary artery bypass graft (CABG) surgery with a reported incidence of around 5% [34, 59]. In-hospital mortality rates are around 12%–40% after perioperative myocardial ischaemia [141]. After a CABG, the 30-day mortality is five times higher for patients with myocardial infarction than without [126]. In the Netherlands, around 13,000 patients received open-heart surgery in 2018 of which 6835 CABGs. Around 340 CABG patients are experiencing adverse effects from their heart surgery in the form of myocardial ischaemia. This number does not include patients who have aortic valve replacements, which are related to an even higher incidence of myocardial ischaemia after surgery. In some cases, this can be around 29% of patients [84]. In the USA, around 224,000 open-heart surgeries were performed in 2016 [32]. This shows the scale of patients who are at risk. Next to the short-term effects, myocardial ischaemia is associated with an increased risk of progressive heart failure in the years following the operation [104]. An additional downside of myocardial ischaemia is that it uses valuable healthcare resources and has a high economic impact [81]. The cost of a CABG in the USA can go up to \$ 151,886 (average \$75,345), while in the Netherlands this is around \$ 15,742 [159]. These numbers show the relevance of ischaemia monitoring during cardiac surgery. When clinicians would be able to detect the ischaemic response of the cardiomyocyte during cardiac arrest, this would improve outcomes, bypass time and costs through detection of (regional) ischaemia at a reversible stage and through tailor-made administration of cardioplegia.

### 1.1.2. Motivation

While healthcare is innovating very fast and many innovations that seem impossible have succeeded, still patients die from the problem of missing information. Both engineers and physicians learn as the basis of their education that to measure is to know. It was a shock to see how many processes in the hospital happen with educated guesses instead of obtained information. Cardiac surgery is one of the most demanding surgeries for the human body, and that crucial decisions are made on a black box model is a shock.

The black model box is as described above that the thoracic surgeons and perfusionist know how much cardioplegia they are giving to the patients. The dose and administering techniques are based on experience and animal models, but they do not get direct feedback if the cardioplegia is reaching the cardiomyocytes. Only when the heart is pumping again, the damage is visible. Therefore, instead of receiving direct feedback on the action, this can have a delay of more than 15 minutes. This delay can be deadly.

For many thoracic surgeons, the need for a system that can detect ischaemia is clear. In 1985 Khuri and Marston [73] showed the potential of measuring pH during cardiac surgery and Khabbaz et al. [72] developed a glass pH electrode for measuring the pH during surgery. In 1997 Tønnessen [144] started investigating the possibility to measure  $\text{PCO}_2$  to detect myocardial ischaemia, and this invention is still not finished [113]. It is incredible that with all knowledge available, no solution has reached the patient as the problem is so clear.

Most sensors which have been developed in the past are based on electrochemical sensing. Optical (chemical) sensing has many advantages over electrochemical sensing and has not yet been tested

to measure physical parameters. The motivation for this project is to fill the knowledge gaps needed to create an optical sensor which can detect myocardial ischaemia and with that solve the "black box problem" for surgeons and save patients lives.

## 1.2. Problem

### 1.2.1. Problem statement

This thesis aims to give an overview on the techniques which can be used to measure myocardial ischaemia to help thoracic surgeons during open heart surgery and to save patients lives. Following this, the thesis will implement the technique and investigate its characteristics and properties of the developed prototype sensor. The world of optical chemical sensing is not new, however, this work offers one of the first investigations into detecting myocardial ischaemia with an optochemical technique. This present work is expected to contribute to our understanding of the possibilities and pros/cons of using optical chemical sensing as a sensor during cardiac surgery. A number of knowledge gaps were identified. This thesis aims to fulfil the following knowledge gaps:

1. Parameters that can be measured during cardioplegia induced cardiac arrest to detect myocardial ischaemia
2. Combining optical, chemical and medical literature to investigate the possibility for a optical ischaemia sensor
3. An overview of what is needed and what is possible for in-vivo optical sensing

### 1.2.2. Goal of thesis

The aim of my thesis is to investigate the possibility to measure myocardial ischaemia with an optical-based sensor and create a proof of concept of this sensor. The goal is to investigate this while considering all different options by doing a narrowing-down approach. This approach allows for developing a sensor which satisfies the needs of the surgeon while keeping in mind the limited resources available. This approach works by investigating all different options and selecting the best option based on the information available. After this decision, all different options for the next step are investigated, after which the best option is chosen.

## 1.3. Research Questions

### 1.3.1. Main Questions

The scientific value of this work lies in the fulfilment of the knowledge gaps defined above and to reach the goal of the thesis by designing a proof of concept. While this thesis consists of a literature study and a design of a sensor, the process was driven by the need to answer a set of well-defined research questions. The main research question is defined as follows:

*Is it possible to measure myocardial ischaemia with an optical-based sensor?*

### 1.3.2. Sub Questions

To answer this research question, the question is split up in multiple subquestions:

1. **Literature: What are feasible methods to detect myocardial ischaemia during cardioplegia-induced arrest?**
  - Which physical parameters are related to myocardial ischaemia during a cardioplegia-induced arrest?
  - Which types of technologies are capable of measuring pH and Lactate during a cardioplegia-induced arrest?
  - What is the most feasible optical sensing technique for measuring pH or lactate during a cardioplegia-induced arrest?
2. **What are the conditions that the sensor must meet to be used in practice?**

- What are the medical requirements for the sensor?
- What are the resources available for designing a prototype?

### **3. What optochemical sensing technique can be used to measure pH difference induced by myocardial ischaemia?**

- Which optochemical sensing techniques are capable of measuring the pH difference induced by the myocardial ischaemia?
- Which techniques and materials meet the conditions of question 2 and can be developed into a proof-of-concept?

### **4. What are the characteristics and properties of the proof of concept developed?**

- What are the optimal concentrations and properties for the samples?
- What is the influence of temperature, light intensity, concentrations and ionic strength on the sensor
- What type of optical detectors can be used for this sensor?

## **1.4. Organisation of thesis**

### **1.4.1. Scope of thesis**

The aim of the thesis is to develop and test an optical sensor. Therefore, decisions will be made to ensure a prototype can be built. As a result, not the most advanced technologies can be used and can be delimited by the knowledge and resources available. The research is conducted at the section of Bio-electronics of the Department of Microelectronics at the faculty of Electrical Engineering, Mathematics and Computer Science at the TU Delft. Time frame of the thesis is an academic year and no test subjects will be used. The research will be conducted by a literature review and experimental design with testing.

### **1.4.2. Outline of thesis**

This thesis is structured as follows; the theoretical background necessary to this thesis is presented. This is followed by the outcome of the literature study and the selection of materials in Chapter 3. Chapter 4 will describe the materials and methods of fabricating the sensor and testing the sensors. In chapter 5, the results of the experiments are stated. These results are discussed in chapter 6 in combination with the interpretations and limitations. Finally, chapter 7 will state the concluding remarks and take a look back at the research questions and aim of the thesis.

# 2

## Theoretical Background

This chapter describes the background information which to understand the goal of the thesis and the working mechanisms of the different aspects of the prototype sensor and the challenges discovered surrounding myocardial ischaemia sensing. This chapter starts by describing the medical background, followed by describing the concepts related to pH. After these elaborations, biomedical sensing and different types of sensors are explained. To fully understand the mechanism behind fluorescent sensing, the (photo)luminescence principles are explained followed by different measurement techniques. As hydrogels will be used in the prototype sensor, the different types of hydrogels are explained. This chapter will finish by stating the challenges in using optochemical pH sensing.

### 2.1. Medical Background

In this section, the knowledge needed to understand the goal of this thesis is elaborated. With this background, the medical issue of myocardial ischaemia during cardioplegia induced cardiac arrest can be understood. First, the essential concepts to understand the need for the ischaemia sensor are introduced. This is followed by a comparison of the metabolism of the cardiomyocyte during normal and ischaemic conditions. This difference is the foundation which this research is built on.

#### 2.1.1. Open heart surgery

The golden standard for operating on a patient's heart is open heart surgery. This procedure is considered a high risk surgery with estimated postoperative in-hospital mortality rates of 1-2% for coronary artery bypass graft procedures, to 3-6% for all combined cardiac surgical procedures [59]. The risk for complications increases when patients are classified as high risk. Cardiac surgery is an extremely invasive surgery often done on deteriorated patients. During open heart surgery, the function of the heart and lungs is taken over by a heart-lung machine, called CPB. Standing outside of the patient's body, this machine oxygenates and pumps the blood (around in the body). To get access to the heart at the start of the operation, the sternum is split in two and an incision is made into the chest cavity, after which the cardiopulmonary bypass is connected. Following this, the heart is arrested with cardioplegia and the surgery is executed. At the end of the surgery, the CPB is disconnected and the heart is repolarised again. This is the moment when surgeons can look if there are any problems. When there are no visible complications, the sternum is closed. The steps taken are all highly dangerous and can lead to postoperative complications.

As Koning [78] describes in his dissertation: "Mortality after cardiac surgery can be predicted by patient characteristics and intraoperative factors. These characteristics include age, gender, cardiac function, preoperative comorbidities, and type of surgical procedure. The intraoperative factors are duration of bypass, hemodilution, blood transfusion, and postoperative renal failure." The most common reason for mortality is myocardial ischaemia caused by arresting the heart. Improving myocardial protection is a method to decrease mortality. Nowadays, myocardial protection is done by arresting the heart with cardioplegia, while in the early days of open cardiac procedures they were limited to 2 minutes of stopped blood flow.

In 1955 LAM et al. [83] reported that KCl injections induced a cardiac arrest which prolonged the intervention time. In the same year, Melrose et al. [96] described a method for chemical cardiac arrest using potassium citrate. However, due to inadequate testing, the results were disappointing and the use of chemical myocardial protection was delayed [46]. Some years earlier in 1950, Dr. Bigelow developed the idea that for cardiac surgery a motion and bloodless environment was needed and started using hypothermia to achieve this [91]. Between 1970-1975 new collaborations in Germany led to an increase of results with cardioplegia [36]. After the introduction of the CPB, cardiac surgeries surged and with that the development of new techniques. In 1990 there were cardiac surgeries performed which do not need a CPB. Since 2000 more operations are done minimally invasive, but it is not possible for all surgeries. The number of cardiac surgeries is growing due to ageing populations and the increase of cardiovascular diseases. This means many patients undergo a open heart surgery with cardiopulmonary bypass and cardioplegia. Full history of cardioplegia can be found in the article of Dobson et al. [36]

### *Cardiopulmonary bypass*

The cardiopulmonary bypass ensures that the body is perfused with oxygenated blood during the surgery. Figure 2.1 depicts the multiple parts of the CPB. The reservoir in the CPB uses gravity to collect deoxygenated blood. A roller pump is used to pump blood to the oxygenator, heat exchanger, and an arterial filter. Blood introduces an inflammatory response when it is in contact with foreign bodies. This is a large risk for patients and therefore blood thinners and heparin are used. Koning [78] states that: "The inflammatory response can lead to the development of postoperative organ dysfunction, including acute kidney injury, acute respiratory distress syndrome, neurological dysfunction, and bleeding disorders."

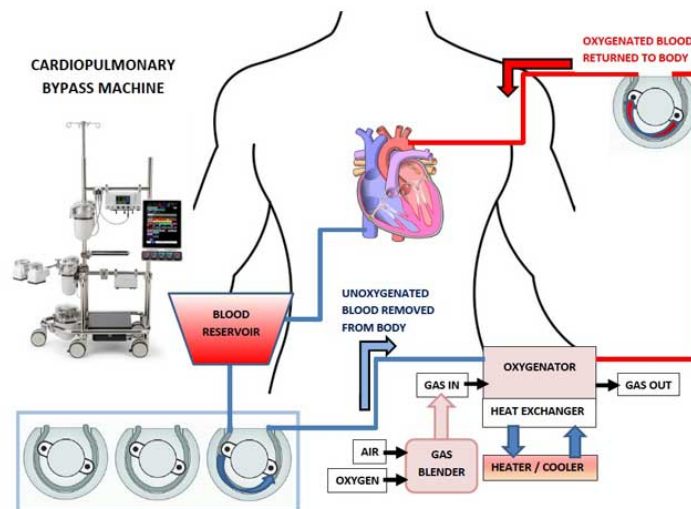


Figure 2.1: A cardiopulmonary bypass, the blood is extracted from the body at the veins and collected in a blood reservoir, from here roller pumps are used to pump the deoxygenated blood to the oxygenator after which the blood is pumped back into the body at the aorta. Reprinted from [40]

During a cardiopulmonary bypass, no oxygenated blood is going to the heart and this causes a change in the metabolism of the cardiomyocyte. The effects of the metabolism changes will be described in section 2.1.3. To save cardiomyocytes from ischaemia, cardioplegia has an essential role.

### *Anatomy of the heart*

Figure 2.2 shows the different parts of the heart on the inside. The red labels are the most important parts of the heart for this thesis work. These three layers form the heart muscle, which enables the heart to contract and pump the blood around the body. The endocardium is a thin layer at the inside of the heart wall. It lines the inner heart chambers and is also the inside of the large blood vessels. The myocardium is the middle layer of the heart wall and is composed of cardiomyocytes, heart muscle cells. This layer is thicker than the other layers and varies in different parts of the heart. The cardiac

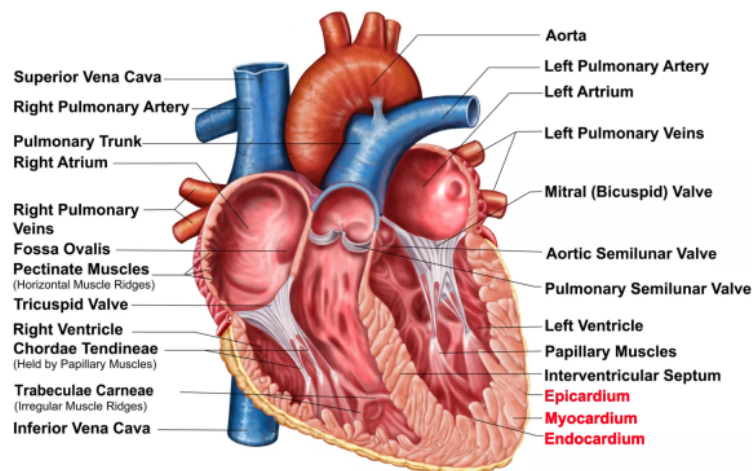


Figure 2.2: Anatomy of the heart. In red the layers of the heart which are of interest in this work. Reprinted from Bailey [14]

conduction electrical impulses which contract the heart, occurs in this layer. On the outside of the heart lays the epicardium, which in turn is the inside of the pericardium, the protective sack around the heart. In the epicardium, coronary vessels are found and this layer is also responsible for the production of pericardial fluid [14].

### 2.1.2. Action Potential and Cardioplegia

#### Action potential of cardiac muscles

Grigoriy Ikonnikov and Eric Wong

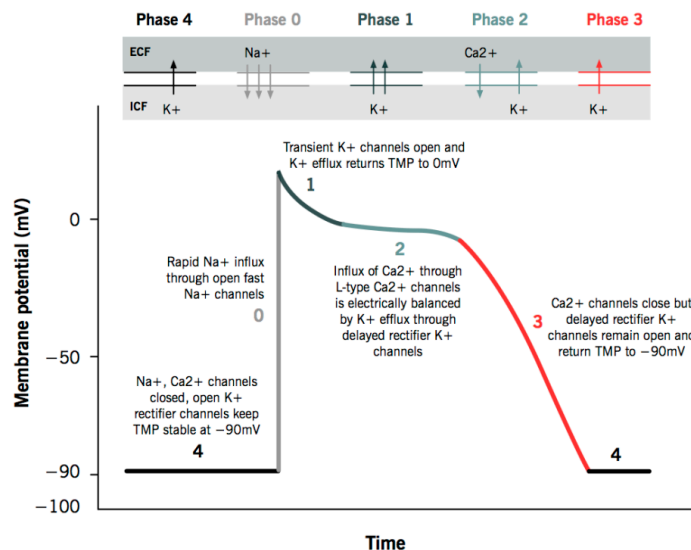


Figure 2.3: Normal action potential of cardiac muscle cell with different phases and ion gates flow illustrated. The membrane potential is -90mV and sodium influx causes a depolarisation which cause a contraction of the cardiomyocyte. Reprinted from [165]

Cardioplegia is a common term used for pharmacological solutions. With cardioplegia, the heart can be arrested temporally. Dr Melrose and dr. Lam discovered that a high level of potassium rich solution causes a temporal cardiac arrest [96]. A normal cardiomyocyte has a resting membrane potential of -90mV. The influx of sodium (Na<sup>+</sup>) leads to depolarisation of the membrane potential, causing the cardiomyocyte to contract. This process is illustrated in figure 2.3. The goal of cardioplegia is to target

voltage-gated channels. The presence of potassium reduces the membrane potential, making sure that the cardiomyocyte will not repolarise again. Resting potential is around  $-50\text{mV}$  when the voltage-gated channel will close, and the heart will go into a diastolic cardiac arrest [7].

Figure 2.4 gives an overview of the influence of potassium on the membrane potential and various channels. There are many types of cardioplegia; there is no clear consensus on what is the best practice. Many similarities are found between different solutions [7]. All solutions have high levels of KCl ( $15\text{-}35\text{mEq/L}$ ) and other electrolytes such as  $\text{Mg}^{2+}$ ,  $\text{Ca}^{2+}$ ,  $\text{Cl}^-$ ,  $\text{Na}^+$  and Bicarbonates are added just before administration [23]. Cardioplegia can be administered in a single dose or with multiple doses. Single is more used in minimally invasive cardiac surgery and basic CABG, because it reduces time and interruptions during the procedure. However, in more complex surgery, the multiple-dose cardioplegia achieves better myocardial protection [23].

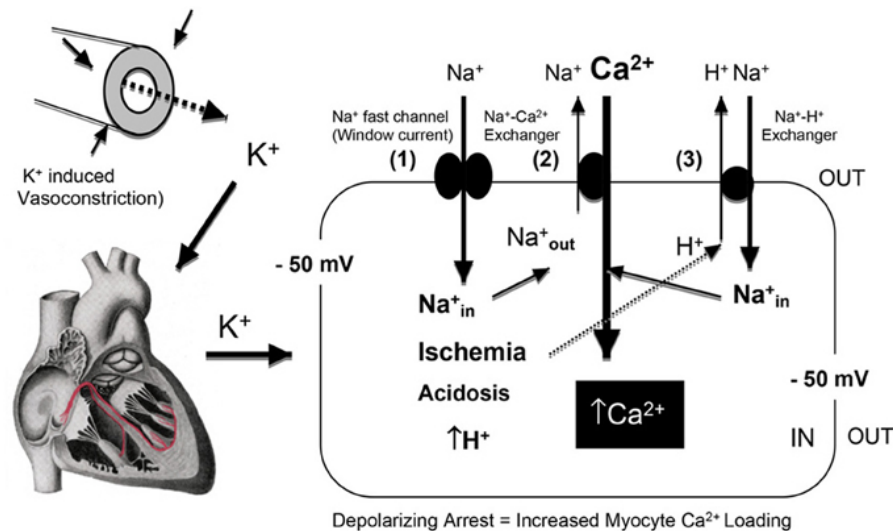


Figure 2.4: A schematic of the effect of hyperkalemia and prolonged myocardial membrane depolarisation on  $\text{Na}^+$  entry through the "window current" and the net influx of  $\text{Ca}^{2+}$  into the cardiomyocyte via the reversal of the  $\text{Na}^+/\text{Ca}^{2+}$  exchanger. Reprinted from Dobson et al. [36]

The use of electrolytes in cardioplegia can interfere with measurements if the sensor would be based on measuring the electrolyte concentration in and around a cell. That is why the focus of this research will be on the physical parameters and not on electrolyte concentrations. However, it is not clear how the electrolyte concentration will influence the sensitivity of the sensor because of the Ionic Strength (IS), section 2.1.4 describes this in more detail.

#### *Administering Cardioplegia*

The standard method to administer cardioplegia is through antegrade perfusion in the aortic root or the ostia of the coronary arteries for around two minutes. This process must be repeated multiple times throughout the procedure. This is when electrical activity begins to appear again due to diffusion of the cardioplegia and washout of its components along with products of anaerobic cellular metabolism. Although the amount of administered cardioplegia solution can be measured at its entry point, the exact distribution of cardioplegia through the coronary system is unknown. To achieve adequate protection of cardiomyocytes during the procedure, cardioplegia must arrive at all cardiomyocytes. However, occlusion or stenosis of a distal coronary artery may obstruct the distribution of cardioplegia, resulting in regional ischaemia. This narrowing can be the result of preexisting conditions such as coronary artery disease or left ventricular hypertrophy, but also iatrogenic complications (e.g., misplaced sutures, loose calcification's).

### **2.1.3. Metabolism of the Cardiomyocyte**

A cardiomyocyte is a heart muscle cell. It is different from a normal cell because it has multiple mitochondria. These mitochondria are important for the production of ATP. ATP is the organic compound that is used for intracellular energy transfer. ATP provides energy and is used in almost all forms of

life [76, 137]. The energy (ATP) demand of the cardiomyocytes is determined by the contractile state, the heart rate, the cardiac output, the sympathetic/parasympathetic balance, and the temperature. In normal conditions, 95% of all the ATP is produced by oxidative phosphorylation in the mitochondria [166, 138]. As illustrated in Figure 2.5 ATP is formed from ADP+P<sub>i</sub> by using oxygen to transfer an electron from NADH. This transfer produces water (H<sub>2</sub>O) as a by-product. The hydrogen is added to NAD<sup>+</sup> by the dehydrogenation of carbon fuels in the mitochondria. These carbon fuels are fatty acids, glucose and lactate. In Figure 2.6, the pathways of cardiomyocyte metabolism are illustrated.

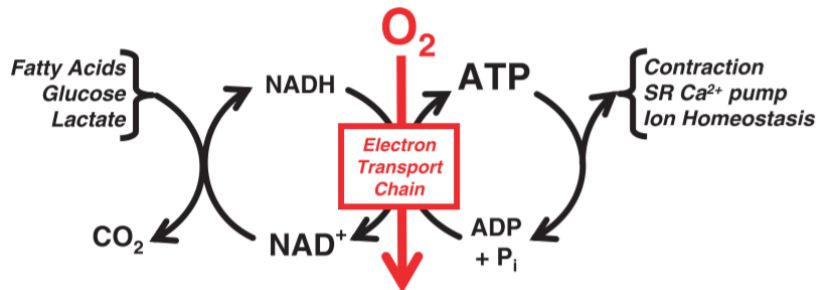


Figure 2.5: Linkages between cardiac power, ATP hydrolysis, oxidative phosphorylation, and NADH generation by dehydrogenase in metabolism. Reprinted from Stanley et al. [137]

This figure shows that acetyl-CoA is needed to produce NADH in the mitochondria. The distribution between acetyl-CoA formed by fatty acids and pyruvate is between 90:10% and 60:40%. The distribution of glucose and lactate contributing to pyruvate is approximately equal [137]. When the heart is functioning normally, it uses more lactate than it produces. So the cardiomyocyte absorbs lactate from the blood. The concentration of lactate in the cardiomyocyte will increase when the (anaerobic) glycolysis is producing more pyruvate than is being oxidated by the Pyruvate Dehydrogenase (PDH).

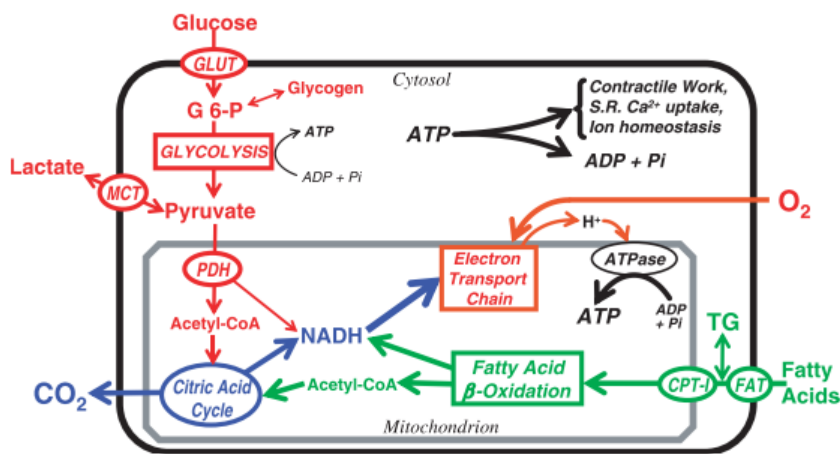


Figure 2.6: The pathways and regulatory points of myocardial substrate metabolism. Reprinted from Stanley et al. [137]

**Metabolism during ischaemia**

Ischaemia occurs as a consequence of an imbalance between oxygen supply and oxygen demand [138]. Ischaemia is besides an insufficient oxygen supply also associated with reduced availability of nutrients and the inadequate removal of metabolic waste products [138]. During ischaemia, the effects of oxygen deprivation cannot be separated from the effects of accumulating waste products. When the mitochondria of the cardiomyocyte cannot produce enough energy, because of a lack of oxygen, it switches to anaerobic glycolysis to produce energy. However, anaerobic glycolysis is less efficient than the aerobic process. The anaerobic produces only two ATP per glucose, while the optimised aerobic respiration produces thirty-two ATP per glucose.

The anaerobic glycolysis only produces 6% of what the aerobic process can produce [95]. This change of metabolism causes a negative energy balance in the cardiomyocyte, and thus anaerobic glycolysis uses high energy reserves. Besides the use of these reserves, it also causes an increase in lactic acid, which will immediately break down into lactate and hydrogen atoms because of the pH level in the cardiomyocyte [124]. The increase of the acid in the cardiomyocyte causes the pH to drop. Figure 2.7 illustrates how the cardiomyocyte tries to compensate for this drop of pH by exchanging  $H^+$  for  $Na^+$ . This increase of  $Na^+$  in the cardiomyocyte is compensated by the exchanging it for  $Ca^{2+}$ . This increase of  $Ca^{2+}$  damages the membrane of the mitochondrion and reduces the contractility of the cardiomyocyte [166]. After 1 minute of full ischaemia, there is almost no contractility of the cardiomyocyte left [138].

After reperfusion of the heart, this damage can be further worsened [138]. This is because when

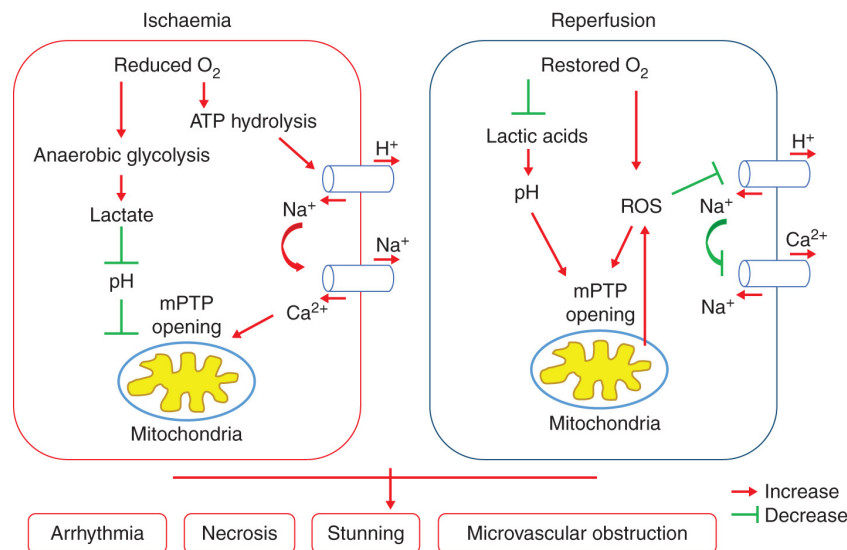


Figure 2.7: Changes in the cardiomyocyte during ischaemia and reperfusion. Reprinted from Xia et al. [166]

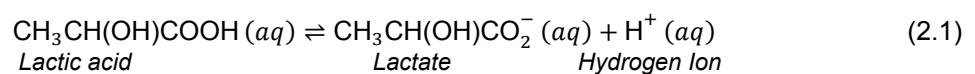
the heart is suddenly reperfused with oxygenated blood, the cardiomyocytes are exposed to extremes. This sudden change has a significant effect on the processes in the cell. Figure 2.7 shows that the  $Na^+/H^+$  pumps are inhibited, and the pH in the cardiomyocyte increases. Around 25%–45% of patients who die after CABG have histological evidence of the ischaemia/reperfusion injury [148]. When the condition of the heart is better monitored on ischaemia symptoms, the degree of the injury caused by the reperfusion can be decreased. Myocardial damage is one of the most common causes of morbidity and mortality after heart surgery as Drescher et al. [38] described in their work. The numbers of patients with myocardial damage after cardiac surgery can vary between 2–10% after CABG [148] and 29 % of Aortic Valve Replacement (AVR) [84].

#### 2.1.4. Parameters of ischaemia during Cardioplegia induced Cardiac Arrest

The simplified metabolism overview of figure 2.5 & 2.6 and the ischaemic processes illustrated in figure 2.7 give a few interesting parameters to look into.

##### Lactate

Starting with lactate, when the cardiomyocyte changes from an aerobic process to an anaerobic process, the metabolism of lactate changes. Lactate originates from the breakdown of lactic acid to lactate and hydrogen ions, see equation 2.1



As described in section 2.1.3, the cardiomyocyte uses lactate from outside of the cell to produce ATP during normal conditions. However, during the anaerobic process more lactate is being produced than

used [136]. This is called hyperlactatemia [79], and it causes an increase of lactate in the cell. This increase of lactate causes a drop of pH in the cell because of the acidity of lactate [79]. When the cell pH drops below 7.35, and the lactate levels are higher than 5mmol/L, it is called lactic acidosis [142]. Another marker of lactic acidosis is a bicarbonate level of lower than 20 mmol/L in blood. Bicarbonate ( $\text{HCO}_3^-$ ) levels can be measured in the blood because it is a buffer of  $\text{CO}_2$  and pH [153]. There are two different types of lactic acidosis. Type A is caused by impairment of tissue oxygenation, hypoperfusion, hypoxia, while type B is caused by toxin-induced impairment of cellular metabolism [99]. In this thesis, the focus will be on type A lactic acidosis. The disadvantage of the acidosis is that it stimulates cell apoptosis (cell death) when a cell is hypoxic. Lactate is not a physical parameter which is easy to measure [120]. Most lactate sensors that are being developed to measure lactate, measure lactate in sweat and tear fluid [50].

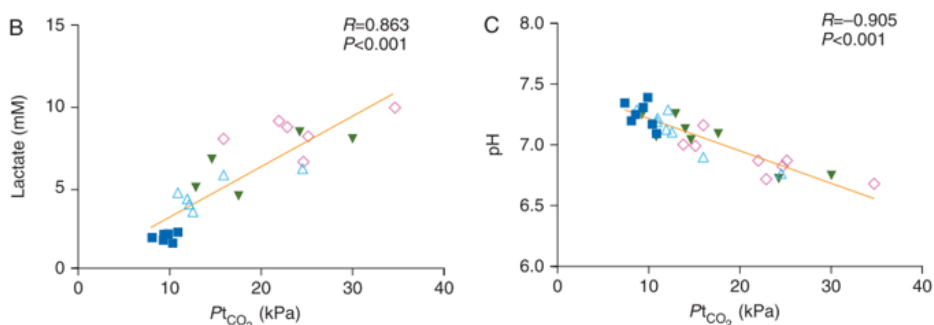
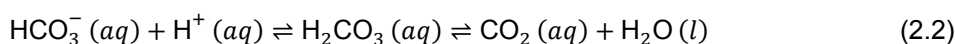


Figure 2.8: Pearson correlation revealed a significant correlation between myocardial PtCO<sub>2</sub> and tissue lactate (B) and tissue pH (C). Single values displayed as baseline (squares), blood flow 75% (open triangles), 50% (filled triangles), and 25% (diamonds). Reprinted from Pischke et al. [112]

### PCO<sub>2</sub>

PCO<sub>2</sub> stands for the partial pressure of carbon dioxide (CO<sub>2</sub>). Protons formed by the increase of lactate during anaerobic metabolism will react with  $\text{HCO}_3^-$  to form water and CO<sub>2</sub>:



Because there is no blood flow, CO<sub>2</sub> will not be transported away and will accumulate in the cell. Pischke et al. [112] showed in their research that there is a correlation between the tissue CO<sub>2</sub> (P<sub>t</sub>CO<sub>2</sub>) and the tissue lactate and tissue pH. This can be seen in Figure 2.8. Walters et al. [152] showed that it is possible to calculate PCO<sub>2</sub> from measured pH in a cardiomyocyte and vice versa. Tønnessen [144] started investigating in 1997 the possibilities of detecting PCO<sub>2</sub> as ischaemia detection, which led to the creation of the sensor tested by Pischke et al. [112]. This creation shows the potential of using CO<sub>2</sub> to measure myocardial ischaemia.

### O<sub>2</sub>

Oxygen is needed for the metabolism of the cardiomyocyte. StO<sub>2</sub> stands for the oxygen saturation of muscle tissue. During cardioplegia, the oxygen consumption of the cardiac cells can reduce up to 97% [52]. This means there is still a residual uptake of oxygen in the cell. This is slowly decreasing the oxygen level around the cardiomyocyte. Putnam et al. [116] showed that the StO<sub>2</sub> could detect regional changes before the change in lactate levels during CPB. On average, the lowest StO<sub>2</sub> was recorded 90 minutes before the highest lactate peak. Tissue oxygen saturation has the potential to be measured real-time, which makes it an interesting parameter. Most of the development of oxygen sensors are skin sensors. These type of sensors measure the oxygenation of a muscle or tissue by using Near Infra-Red and the absorption difference between oxygenated and deoxygenated blood cell. These type of sensors are getting more advanced such as the Humon Hex [63] or Moxy Monitor [102].

*pH*

The acidity of a cell is described by the measured pH. pH is the concentration of hydrogen ions in a solution inversely. It is the negative base 10 logarithm of the molar concentration of hydrogen ions [139]. pH is the parameter on which this thesis is focused and is further elaborated in section 2.2

**2.2. pH**

The background described in this section is based on Chapter 2 of the dissertation of Weidgans [154], if other literature is used, it is referenced. pH is a parameter used in chemistry and bioscience to specify the acidity or basicity of an aqueous solution. The definition of pH value was given by Sorensen in 1909, while the terms acidic and basic were described much earlier [139]. pH consists of two parts, p stands for the 'decimal cologarithm of a and not for power or potential [46]. The H stands for the hydrogen atom which determines the acidity.

A pH of 7 is neutral at 25 °C. Below 7 is acidic and a pH above 7 is considered as basic. The pH scale can have values outside of the range from 0-14, but this range is the most common in sciences. pH is important in life sciences, food and beverage processing, soil examination, and marine and pharmaceutical research and more, as it describes the local environment of the substance [139].

As the sensor described in this work is developed to measure pH it is important to understand what pH is and what factors influence pH. pH is not a constant value, it describes the activity of the hydrogen ion in a solution. The solution in which the hydrogen ion is located determines the activity of the ion and thus determines the pH. The following section will introduce pH and the factors related to pH and how these are of importance for this work.

**2.2.1. Introduction pH**

pH is defined as the decimal logarithm of the inverse of the hydrogen ion activity,  $a_{H^+}$ , in a solution [29]

$$\text{pH} = -\log_{10}(a_{H^+}) = \log_{10}\left(\frac{1}{a_{H^+}}\right) \quad (2.3)$$

While usually the formula is simplified to:

$$\text{pH} = -\log[H^+] = -\log[H_3O^+] \quad (2.4)$$

In water with a pH of 7 at 25 °C the formula states a hydrogen ion concentration ( $H^+$ ) of  $0.1\mu\text{M}$ . pH actually measures the activity of the hydronium ion  $H_3O^+$ , as hydrogen atoms are extremely reactive and are solvated by water. pH is a logarithmic scale which means that a change of 1 pH is a ten times increase/decrease of the number of hydronium ions. As the molar mass of the hydronium atom is 19.02 g/mol and in plain water the hydrogen concentration is  $0.1\mu\text{M}$  this results in only  $1.9\mu\text{g}$  of hydronium in a litre of water.



Equation 2.5 shows the dissociation of water molecules in neutral water. Only 2 out of the billion water molecules dissociate into a hydronium ion  $H_3O^+$  and a hydroxide ion  $OH^-$ :

*Equilibrium constant*

As chemical reactions in solutions are active processes, they reach an equilibrium state. The equilibrium state of a dynamical chemical system can be described by an equilibrium constant  $K_{eq}$ . This is the value for which two sides of the reaction are in equilibrium.

$$K_{eq} = \frac{a_{H_3O^+} \cdot a_{OH^-}}{a_{H_2O}^2} \approx \frac{[H_3O^+][HO^-]}{(1)^2} = [H_3O^+][HO^-] \quad (2.6)$$

In the ideal situation, the acid-base solutions are dilute and the activity of water is approximated as 1 and the activity of the solvents (ions) is equal to their concentration [6]. The right part of equation 2.6 is called  $K_w$  and is the equilibrium constant of water.

$$K_w = [H_3O^+][OH^-] = 1.01 \cdot 10^{-14} \quad (2.7)$$

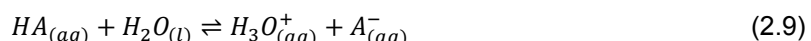
$K_w$  is equal to  $1.01 \cdot 10^{-14}$  at 25 °C and with an ionic strength of 0. The concentration of hydronium and hydroxide are both  $1.006 \cdot 10^{-7}$ , this means that in pure aqueous solutions pH and pOH combine to 14.

For this formula it is important to realise that it only stays constant if the activities of the ions are constant. The activity is related to the concentration, this will be elaborated in section 2.2.2. The concentration of water is constant (55.5M) and therefore, equation 2.7 can be derived from 2.6. Other names for the ionisation constant are: dissociation constant, self-ionisation constant, water ionproduct constant, or ionic product of water. The water ionisation constant can be notated with cologarithm just as with pH:

$$pK_w = -\log_{10} K_w = \text{pH} + \text{pOH} = 14 \quad (2.8)$$

#### Acid dissociation constants

The equilibrium constant  $K$  can also describe the equilibrium between an acid and a base in a solution. The reaction of a weak acid (HA) and its conjugated base ( $A^-$ ) in water is described by the following formula:



The magnitude of the equilibrium constant is used for determining the strength of acids and base. From equation 2.9 the acid dissociation constant  $K_a$  can be determined:

$$K_a = \frac{[H_3O^+][A^-]}{[HA]} \quad (2.10)$$

To avoid the exponential notation of constant  $K_a$ , it is defined as pKa:

$$pK_a = -\log_{10} K_a \quad (2.11)$$

The opposite of pKa is pKb, this is the basic dissociation constant. Together they are related to the water ionisation constant (pKw) in diluted solutions:

$$pK_a + pK_b = pK_w \quad (2.12)$$

In this thesis, an indicator dye is used which consists of an acidic and basic component. The activity of the acid component is measured. The activity of this component is described by the factors elaborated in section 2.2.2 and pH. pKa is related to pH as pKa specifies the equilibrium of a molecule at a certain pH.

pKa describes if a chemical will donate or accept a proton at a certain pH. pKa is the intrinsic property of an acid and it does not depend on how much acid there is in a solution. This means that a weak acid can have a lower pH than a diluted strong acid, while pKa is constant for each type of molecule. The relation between pKa and pH is described by the Henderson-Hasselbach equation:

$$\text{pH} = pK_a + \log_{10} \left( \frac{[\text{Base}]}{[\text{Acid}]} \right) \quad (2.13)$$

As the sensor developed in the thesis will use a fluorescent indicator, the concentration ratio between the base and acid is measured as the fluorescent output. pKa is the intrinsic property of an acid (here the indicator dye) and it does not depend on how much acid there is in a solution. This means that a weak acid can have a lower pH than a diluted strong acid, while pKa is constant for each type of molecule.

The lower the pKa is, the more acidic it is and the greater the ability of the molecule is to donate protons [61]. pKa is a constant for molecules and acidic solutions, however when different molecules are combined, the combined pKa has to be determined. This determination depends on the type of sensing used [122].

#### Nonideal situation

The formulas described above describe the relation in ideal situations. In these situations, there is one acid with conjugated base diluted in pure water. However, this is not how it is in real-life situations. There are multiple factors in a solution which influence the measurement of pH.

### 2.2.2. Factors related to pH

The goal of a pH measurement is to describe the pH of a solution. As equation 2.3 describes pH is the activity of the hydrogen ions. In section 2.2.1 the activity of water and acid is equalised to the concentration of the ions. This section will explain how pH measurements are actually measuring the activity of ions and how ionic strength (chemical potential), temperature, and solvent composition will influence the activity measurements. This is all combined in Nernst equation which is elaborated at the end of this section.

#### *Activity and acidity*

In comparison to the ideal situation, there are many different ions in the tissue and these ions interact with each other. Not all ions are occupied with interacting with other ions. The activity is an effective concentration of hydrogen ions, rather than the true concentration [94]. The difference is that the activity considers that the other ions around the hydrogen ions will shield them and affect how these ions react in chemical reactions.

$$a_i = f c \quad (2.14)$$

Where  $a_i$  is the relative activity,  $c$  the concentration and  $f$  the activity coefficient. In dilute mixtures, this factor is 1. Therefore, in the ideal situation, pH is described as the relation between the concentrations. However, in mixtures this is not the case. Relative activity  $a_i$  can also be defined as:

$$a_i = e^{\frac{\mu - \mu_i^\ominus}{RT}} \quad (2.15)$$

$\mu_i$  is the chemical potential of ion  $i$  (in molar) under the conditions of interest,  $\mu_i^\ominus$  is the chemical potential of ion  $i$  in standard conditions, the gas constant is  $R$ ,  $T$  is the thermodynamic temperature (in K) and  $e$  is the exponential constant [161]. The chemical potential of a reaction can be altered by all these factors and can make the exact measurement of the activity of hydrogen atoms challenging. Chemical potential is another name for Ionic Strength (IS). The activity coefficient depends on the ionic strength and temperature of the solution and approaches unity for infinitely dilute solutions. In very dilute solutions, pH can be related directly to the concentration of the hydrogen ions and this leads that equation 2.3 can be written as equation 2.4 in most cases.

#### *Ionic strength*

Ionic strength (IS) describes the chemical potential of ions in a solution [162]. It was first formulated by Randall and Lewis (equation 2.16) in 1921. Ions have an electric charge that can attract or repel each other. This effect results in behavioural changes for the ions. The  $I$  takes an important role in the Debye Huckel theory. This theory describes the deviations from the ideal situation that happens in ionic solutions [108].

$$\mu = \frac{1}{2} \sum_{i=1}^n c_i z_i^2 \quad (2.16)$$

So IS is the sum of the concentrations of the active ions present in a solution, divided by half because of the cations and anions.  $I$  is a quantitative measure the ionic strength a solution is.  $c$  is the molar concentration of each ion present in the solutions and  $z$  its charge.  $I$  is directly related to the activity  $a_c$  as described in equation 2.15

As ionic strength has a large influence on the activity and the activity is used to determine the pKa, the ionic strength influences the pKa. The greater the ionic strength, the higher the charge around the ion is and thus the less attraction to the ions by other influences. Weidgans [154] show that the charge of the membranes in combination with phosphate buffer results in different influences on the pKa as illustrated in figure 2.9

#### *Temperature*

The activity of ions is temperature depended, and thus the pH measurement is pH depended. At 100 °C, the pH of pure water is 6.14 and at 0°C this is 7.47. This does not mean that the solution gets more acidic, because not only the pH drops, but also the pOH drops [139]. So the total  $pK_w$  decreases and as pKa is related to pKw (equation 2.12) This is because of the Le Chaterliers principle. The Le Chaterlier principle can be simplified to: "Any change in status quo prompts an opposing reaction in the responding

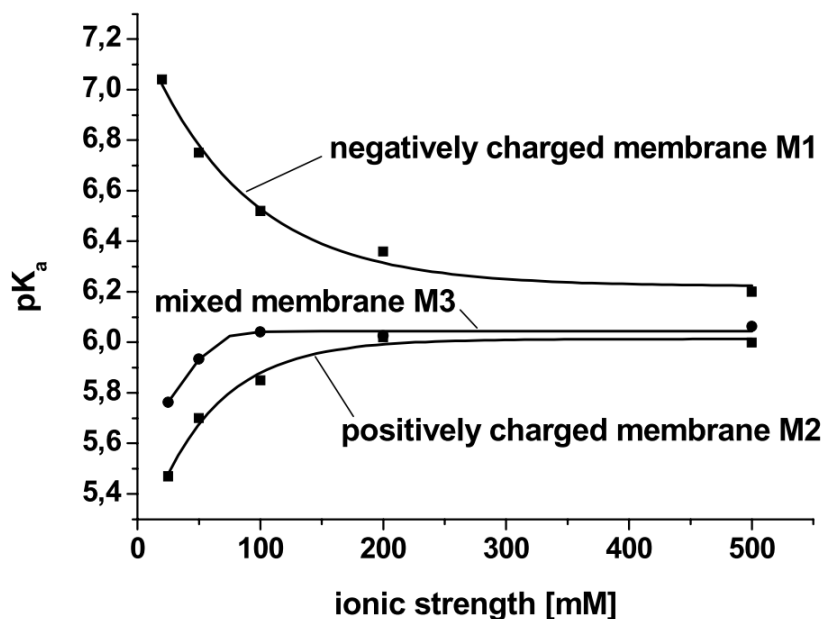


Figure 2.9: Effect of ionic strength on the pKa's of the membranes M1, M2 and M3. The charge of the support matrix has a large influence on the pKa value of the reaction. Reprinted from Weidgans [154]

system.". With increasing temperature,  $K_a$  increases and the  $pK_a$  decreases. All equilibrium constants vary with temperature according to the van t Hoff equation [11]. In general, the dissociation of acids and base is an endothermic process. This means that the  $pK_a$  decreases as temperature increases and as a results of that a pH measurement without temperature measurement is not accurate.

Temperature also influences the ionic strength [6] and the pH-indicators. Non-carboxylic acids are temperature sensitive. For example, phenol's decrease  $pK_a$  by 0.0012 per 1 °C increase. There are other effects related to the optical properties and temperature which can influence the measurements, these will be discussed in 3.3.1.

#### Solvent Composition

Reijenga et al. [122] describe that besides the influence of temperature and  $I$ , the solvent composition can influence the  $pK_a$  values. For example, if a solution contains organic solvents of more than 20% this solvent has effect on the activity of the proton and thus on the activity and thus on  $pK_a$  value. Other influences on  $pK_a$  are if the compositions contain large fractions of proteins or hydrophilic polymers [30]. So on both sides of the hydrogen atom transfer (solution and sensing material), there are factors which influence the pH measurement.

#### Nernst Equation

During electrochemical sensing, the activity of the hydrogen atom is measured, section 2.3.4 will go in more detail about this, but the electrode potential is described by the Nernst equation:

$$E = E^0 + \frac{RT}{F} \ln(a_{H^+}) = E^0 - \frac{2.303RT}{F} \text{pH} \quad (2.17)$$

$E$  is the potential measured by the electrode, it exists of  $E^0$  which is the electrode potential,  $R$  the gas constant,  $T$  temperature (in Kelvin),  $F$  the Faraday constant. When pH is defined in terms of activity 2.3 the electrode potential is proportional to pH [11]. This formula shows that the activity of the hydrogen ions is directly related to the pH measurement. However, with a factor that depends on the factors described above

### 2.2.3. pH sensing in the human body

Optochemical sensing of pH in the body is discussed extensively in the review by Steinegger et al. [139]. Only the optochemical sensing of tissue and blood pH is discussed in this work. Most research in

pH sensing is being done in the field of blood measurements. Researchers try to continuously monitor the blood gases in critically ill patients using optochemical sensors. This would make the blood gas analysers and blood tests redundant. These solutions achieved a good in vitro result, but the success was limited in vivo [139]. Different factors influenced the accuracy of the measurements and the cost-effectiveness is questioned because of the speed and quality of Blood Gas Analysers (BGAs).

pH sensing in tissues is being done on multiple targets, from monitoring brain pH during surgery to measuring the microenvironment changes of tumorous tissue. The scattering and absorption of light by the tissue make it difficult for accurate measurements.

#### *Challenges pH and blood*

Blood pH value ranges between 7.35 and 7.45 and values outside of 6.8-7.8 are seen as deadly. Intracellular pH is often around 7.0-7.4 and lower than the extracellular pH due to lower concentrations of  $\text{HCO}_3^-$ . In 2.2.1 the water concentration constant of 55.5mM was described, in blood, the apparent water concentration is around 40 M. The exact proton activity  $a$  of blood is unknown. The apparent concentration  $C$  is lower because of the influence of the large proteins. The concentration of different ions and buffer solutions in the blood have a significant influence on the  $pK_a$  value of blood. This effect on the IS by the ions can be compensated by using ion selective sensors for sodium and potassium because they make up 90% of the ionic strength IS of the blood [139].

Buffers are essential for the metabolism in the body. They make sure that the pH stays around 7.4 in the presence of both a weak acid and a conjugated base. The most important buffer of the blood is the bicarbonate buffer system.



The weak acid is  $\text{H}_2\text{CO}_3$  and the conjugated base is  $\text{HCO}_3^-$ . The  $pK_a$  of carbonic acid is 6.1 and the body regulates the bicarbonate to carbonic acid ratio (20:1) to keep the pH stable. The breathing frequency can be increased to decrease the  $p\text{CO}_2$  and increase the pH [60].

#### *Expected challenges cardioplegic arrest and pH measurements*

There are three main challenges expected in measuring the right pH during Cardioplegia Induced Cardiac Arrest:

1. First of all, measuring the pH is done in aqueous solutions, measuring the pH off the heart tissue on the epicardium/pericard 2.2. The main muscle tissue of the heart, the myocard, is laying below these layers. An essential part in sensing the ischaemia is if the pH changes of the Myocard can be measured on the epicard and if the environment is aqueous enough to assist the transfer of the hydrogen ions.
2. Secondly, as described in section 2.1.2 Cardioplegia consists of many ions to depolarise the cells. These ions change the ionic strength inside of the heart. Instead of blood the coronary arteries are filled with a solutions containing different ions. The concentration of these ions depends on the technique and the type of cardioplegia used. As described, ionic strength and solvent composition have significant effects on the measurements op pH.
3. At last, the temperature is known to vary during the operation and the difference in administering cardioplegia (cold or body temperature) will certainly influence the measurements. Therefore the pH sensing should be combined with a temperature measurement or calibrations.

#### **2.2.4. Differences in electrochemical and optochemical pH sensing**

In 1987 Janata [64] described the differences between optochemical en electrochemical pH sensing. Here he describes that the thermodynamic components are stronger in optochemical sensor in comparison to the electrochemical sensors. Optochemical sensors measure the solute-solvent interaction of the immobilised indicator and the relationship between the surface and the bulk value of pH and of all other involved species. Electrochemical measurements measure the activity of pH, while the optochemical sensor measure the concentration of the cell. There is a difference between the concentration and activity. Optochemical sensors measure the concentration of the acidic and the basic form of the pH

indicator [33]. Another problem with optochemical sensing is that local pH in the optochemical sensor is different than that of pure water, because the sensor is not only pure water. Optochemical pH sensors are cross sensitive towards ionic strength which should be kept in mind when using this type of sensing [156]. In 2007 Hanson et al. [57] showed only a difference of 0.04 pH between an electrochemical and optochemical sensor, but since then no one-to-one comparisons have been done.

## 2.3. Biomedical sensor

A sensor is described as; *a device that responds to a physical stimulus (such as heat, light, sound, pressure, magnetism, or a particular motion) and transmits a resulting impulse (as for measurement or operating a control)* by Merriam and Webster Dictionary [98]. Yeow [167] states that "biomedical sensors are a subset of specialised sensors responsible for sensing physiological or biological measurands." Most biomedical sensors measure a physical property which they translate in a property which can be used in diagnostics or therapeutics. Figure 2.10 illustrates that to extract the information from the body a transducer is needed. This part converts the output of the body to a signal which can be handled and quantified. When a transducer is not working correctly, the information will be useless [146]. The second part of a sensor is the instrumentation. This is where the measurement is controlled. The output of the instrumentation will be processed into a signal which can be used and read. The definitions of sensors and transducers are often used interchangeably. Although the definitions are not the same, this thesis will use the term sensor. This is done because there is no agreement on the use of these terms in literature and to avoid confusion the term sensor is used.

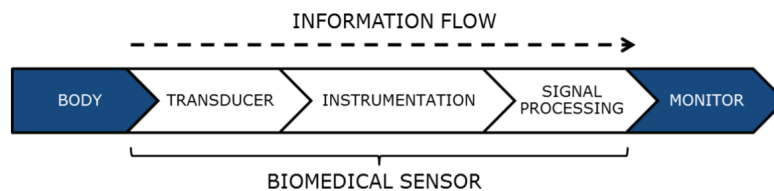


Figure 2.10: Information flow from the body to the monitor provided by the biomedical sensor. As found in Tronstad [146]

Two other definitions that are often used interchangeably are "biosensor" and "biomedical sensor". This is wrong because a bio sensor is a type of biomedical sensor. It is a type of sensor which senses biological signals like enzyme, antigen, antibody, hormone, DNA, RNA and microbes. While a biomedical sensor is the umbrella term for all the sensors used in the biomedical field [173].

### 2.3.1. Types of sensors used in biomedical sensors

There are different methods of classifying biomedical sensors. It is possible to categorise all the biomedical sensors in physical or chemical sensors [173]. Physical sensors can be split up into electrodes, measuring electrical changes or optrodes, where light is used as measurand. The chemical sensors include electrochemical, biosensors and chemiluminescence. This classification is not optimal for this research, because physical sensing can be more than only electrical or optical. Therefore, as part of the literature review described in chapter 3 a classification was made which is more optimal. This classification will exist out of the following types. A short description of the type of sensors:

1. *Electrochemical*: Electrochemical sensors are biosensors that make use of the electrical charge which is made by chemical reaction with the biological element. This reaction comes from a chemically selective layer which is called the recognition element [18]. Most electrochemical sensors are based on the potentiometric and amperometric principle. Potentiometric sensors measure the electrical potential with a high impedance meter and do not need an external source. Potentiometric sensors always need a reference electrode to measure the potential current [111]. Amperometric also need a reference electrode, but it measures the current generated by enzymatic or bio-affinity reaction at the surface of the electrode. A constant working potential is given on the working electrode. A redox reaction is always occurring at amperometric sensors [65]. Voltammetric sensors have a similar working principle but measures the current as the potential is varied and is less used in the biosensing. Impedimetric sensors are less used, and conductometric sensors are a subset of impedimetric sensors [132]. Amperometric sensors are most

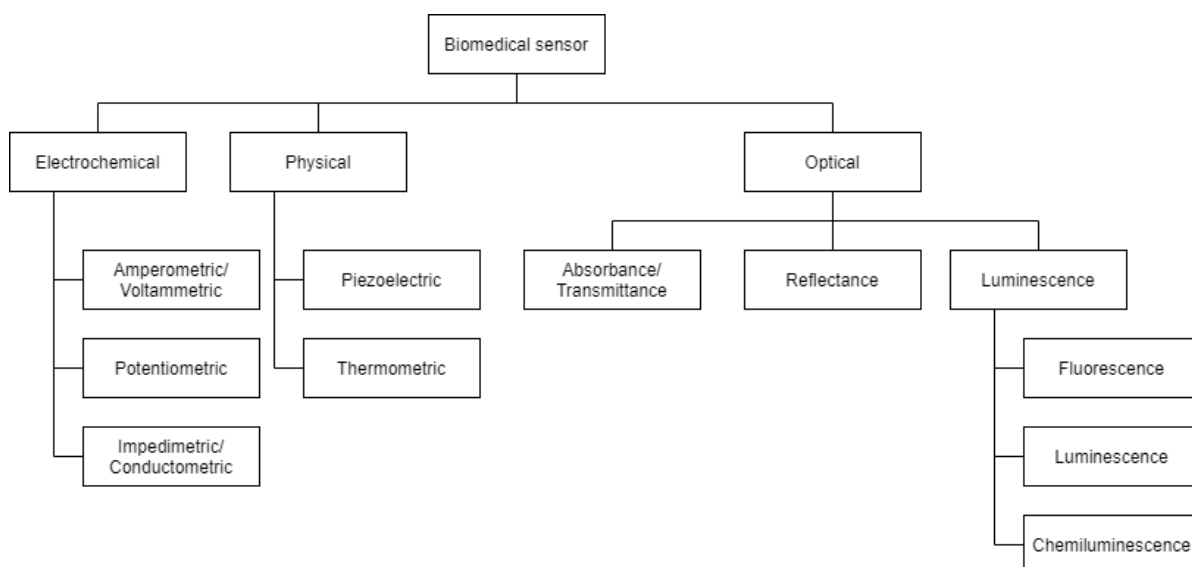


Figure 2.11: Classification of Biomedical sensor developed for this literature review by combining classifications of Shavanova et al. [134], Sharma and Khurana [131], Hajian et al. [56] Singh et al. [135]

successfully commercialised devices [134].

2. *Physical Sensors*: Physical sensors are based on their type of signal. This signal can be from a mechanical sensor which is measured by a piezoelectric principle. Piezoelectric sensors can be used to measure pressure, acceleration, strain or force [121]. A thermal sensor measures, for example, temperature by the thermometric principle. In thermometric sensing, the heat that occurs when a recognition element interacts with an enzyme is measured [134].
3. *Optical*: Optical sensors are sensors that measure a change of light. This change can come from absorption, reflection or scattering of light. Absorption is related to transmission and therefore combined. The last light principle is (photo)luminescence; this is the emission of light of matter after excitation[1]. The differences will be explained in section 2.3.2. Absorption based sensors measure the change in light by absorption of the tissue or solution [90]. Reflection based sensors measure the change of reflected light of the tissue or solution. Figure 2.12 shows the differences between the light principles. In the sensing of pH optical sensors are actually optochemical sensors, as a chemical process is measured using light.

As result of the literature review, this work will focus on optochemical sensing. In the next section, the basis of optical sensing is explained, followed by stating the (dis)advantages of electrochemical and optochemical sensing.

### 2.3.2. Optical Sensing

There are several phenomena caused when light and matter interact. Light is defined by  $\lambda$  and the unit nm is used for the size of the wavelength. When light gets reflected, scattered or transmitted, it keeps the same wavelength as the excitation light has ( $\lambda_1$ ). However, as illustrated in figure 2.12 a different wavelength ( $\lambda_2$ ) can be emitted after absorbed light interacts with electron or molecules. When light hits matter, it can be absorbed, reflected or transmitted. For example, if light passes through a colour filter, some wavelengths will be absorbed while others will be transmitted. During absorption, the frequency of the light is almost equal to the energy level of the electrons in the matter [21]. This causes the electrons to absorb the energy of the wavelength. This absorption causes a change in energy state. When the excitation light exists of multiple wavelengths, the wavelength corresponding to the energy level of the matter will be absorbed. Absorbance, reflection and transmittance are closely related in transparent matter because in a transparent material, there is always transmitted light and almost no reflection. In opaque material, there is no transmitted light and the incident light is absorbed or reflected [1]. In figure 2.13, this difference between absorbance and reflection is illustrated with the different denominations. When analysing light after absorption, a dip is seen in the transmission spectra, and a peak is seen in the absorption spectra. Absorbance has a logarithmic relationship with transmittance, as shown in

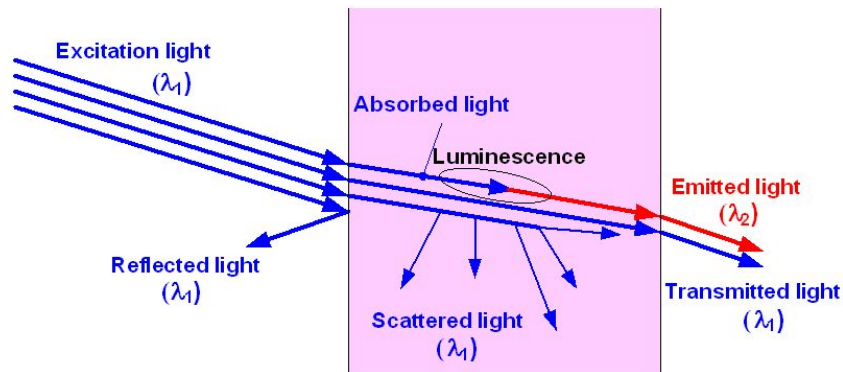


Figure 2.12: Interaction between light and matter. Different phenomena and their wavelengths. Only luminescence causes light of a different wavelength. Reprinted from A. et al. [1]

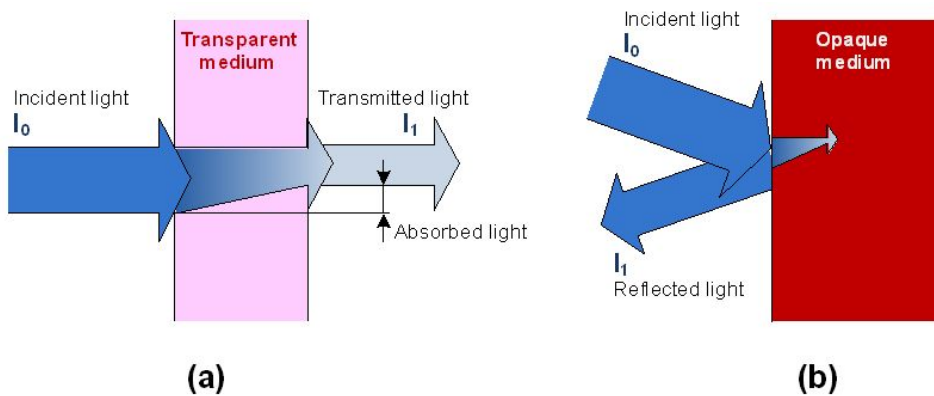


Figure 2.13: Absorption, transmission and reflection performance of the light: (a) in a transparent medium; (b) to face opaque medium. Reprinted from A. et al. [1]

equation 2.18; with an absorbance of 0 corresponding to a transmittance of 100% and an absorbance of 1 corresponding to 10% transmittance [41].

$$A_\lambda = -\log T = -\log\left(\frac{I}{I_0}\right) = 2 - \log(\%T) \tag{2.18}$$

$A_\lambda$  is the absorption coefficient, and it is possible to measure the change of intensity to relate this to the matter.  $I$  is the measured light intensity and  $I_0$  the light intensity at the source. Analysing the spectral distribution of light gives information about the matter the light has passed through. In an optical fibre, reflection is the main factor of the functioning of an optical fibre. The internal reflection is almost 100% in optical fibres, and this makes it an excellent media to transfer information. If the cladding is removed of a fibre, this can change the internal reflection. Equation 2.19 shows the formula to calculate the coefficient of reflectance ( $\rho_\lambda$ ). This equation shows a one-to-one relationship between the incident light and the reflected light.

$$\rho_\lambda = \frac{I_0}{I_1} \tag{2.19}$$

Figure 2.12 shows two other light phenomena when matter is excited by light. Scattered light cannot be used to measure properties of matter because it is random and hard to detect. Scattered light is mostly seen as noise or loss of information. The last phenomenon is luminescence and will be described in section 2.4.

### 2.3.3. Electrochemical sensing pH

Electrochemical sensors are the largest and oldest group of chemical sensors [64]. pH electrodes give information about the activity of the hydronium ions. In 1906 Cremer discovered electrical potential with the use of a glass electrode [16]. This principle is still used as golden standard, it is a combination

electrode of a reference electrode and a working electrode. This sensor exists out of two Ag/AgCl electrodes, one electrode is in contact with a known solution and the other electrode is in contact with an unknown sample solutions. The electrical potential over the membrane is measured ( $E_m$ ) as described in equation 2.17. A electric potential exist because the differences in electron between the solution. Glass membranes, which are used in a Glass electrode are selective for  $H_3O^+$ , but also  $Na^+$ ,  $Li^+$ ,  $K^+$ ,  $Ag^+$ , and  $NH_4^+$ . Most used type of electrical sensing is potentiometric, but also voltametric sensors have been used for measuring pH. Potentiometric sensors work with a working and a reference electrode as described above. A voltametric sensor adds a counter electrode to supply a current to the electrodes. The changes of electrical field caused by the hydrogen atoms are used to determine the pH [149]

#### *Advantages and Disadvantages of electrical pH sensing*

Wencel et al. [156] and Weidgans [154] describes the following advantages of pH electrodes:

1. A pH electrode is reliable and easy to operate
2. A pH electrode has relatively low cost
3. A pH electrode facilitates rapid measurement
4. A pH electrode has high sensitivity and wide dynamic range
5. A pH electrode has small power requirements
6. A pH electrode measures activities rather than concentrations
7. A pH electrode has good performance in electrolyte sensing
8. A pH electrode allows for a two point calibration strategy

The disadvantages:

1. A pH electrode has poor performance at extreme pHs
2. A pH electrode has difficulties in remote sensing
3. A pH electrode has the need for a reference electrode
4. A pH electrode is sensitive for electrical fields
5. A pH electrode hard to miniaturise
6. A pH electrode lacks in specificity
7. A pH electrode is not suitable for long term measurements due to electrode signal drift
8. A pH electrode only facilitates single point measurements
9. A pH electrode is mechanically fragile

### **2.3.4. Optochemical Sensing pH**

This section is based on the work done by Wencel et al. [156] and Steinegger et al. [139]. There are multiple light phenomena which can be used for sensing pH. The optical pH sensors are optochemical sensors as the light is used to translate a chemical proces into information. Absorption, Reflection, Luminescence are the most used phenomena used to sense pH. These techniques will be elaborated. Other principles which can be used to measure pH with use of light are: Refractive Index, Surface Plasmon Resonance, Photonic Crystal, IR and Raman Spectroscopy, Interferometric Based sensing. These techniques will not be discussed in this work. Optochemical sensors are named Optrodes. Optrodes use indicator dyes which are typically organic acids or bases with optical properties associated with their protonated (acid) and deprotonated form (basic).

The absorption or the fluorescence properties will change depending on the hydronium concentration. As described in 2.2.2 Ionic strength, temperature and solvent concentration all can influence the measurements of pH. These changes result in shifts of the calibration plots and pKa is only valid for given IS, temperature and concentration per buffer solution. To support the interaction of the test sample with the indicator often a uncharged hydrogel matrix is used. This matrix acts as a support for the indicator dye. The interaction of the hydrogel and the indicator determine the selectivity and sensitivity

of the sensor. Optochemical sensors usually have a dynamic range of 1.5-3.0 pH. A narrow dynamic range results in high resolution, because the smallest changes of pH will result in a difference of the emitted light.

#### *Advantages and disadvantages of Optical pH sensing*

Wencel et al. [156] and Weidgans [154] describes the following advantages of pH optrodes:

1. A pH optrode has no additional reference element needed
2. A pH optrode does not suffer from electrical or electromagnetic interferences
3. A pH optrode is easily to miniaturise
4. A pH optrode has smaller dynamic range but higher resolution
5. A pH optrode can transmit more information than electrical signals
6. A pH optrode can be used for simultaneous multianalyte analysis
7. A pH optrode is non invasive
8. A pH optrode can be used as disposable sensor
9. A pH optrode has production cost and is suitable for mass production
10. A pH optrode allows for continuous measurements

The disadvantages:

1. A pH optrode can be interfered by ambient light
2. A pH optrode have a narrow dynamic range
3. A pH optrode photobleaching and leaching of indicator can limit the long term stability
4. A pH optrode measures concentrations instead of activities
5. A pH optrode is IS and temperature depended. Varying IS will cause surface potentials which affect the sensor

#### *Types of optical pH sensors*

There are three types of platforms used in optical sensing:

1. Planar sensors: Planar sensors are more robust than optical fibres and can be used for measuring pH in samples while the measurement is done from the outside without direct contact, this make planar sensor suited for disposable sensors and can be easily be mass produced for low costs. There are three types of planar sensors:
  - (a) Planar nonwaveguiding sensors: In this type of sensing the indicator particles are embedded in a matrix and the light is sent directly onto the matrix and the emitted/reflected light is detected
  - (b) Planar nonwaveguiding sensor particles: In this type of sensing the indicator particles can move freely in a fluid
  - (c) Planar waveguiding sensors: In this type of sensing mirrors are used to sent the light through the hydrogel, this type of sensing is more advanced but allows better direction of light. Mostly used in reflection and absorption based sensing.
2. Fibre optic sensors: Fibre optic sensors exist out of small glass or plastic fibres. These fibres have the size of less than 1 mm. The fibres are flexible and allow for remote sensing. They are more difficult to produce than planar sensors and reproducibility is a significant issue. Optical fibres divided into two categories:
  - (a) Fibre optic tip sensor: In this type of sensing the tip of the optical fibre (single or multi-fibre) is coated with the indicator dye (and matrix) and light is emitted and detected through the optical fibre.

- (b) Fibre optic evanescent field sensor: In this type of sensing the cladding is replaced by a coating with the indicator dye or gratings are added on the fibre. This change of cladding changes the optical properties of the light sent through the fibre. This change can be related to the pH changes.
3. Nanosensors: Nanosensors can be used to measure pH difference inside of cell or other small media. The advantage of nanosensors is that they are less affected by proteins or other molecules. This can improve the reliability of pH sensors. The disadvantage of nano sensor is that it has issues with intracellular delivery, distribution of cells, selectivity, toxicity and in-vivo calibration [139]

## 2.4. (Photo)luminescence

For this section the books by Bernard Valeur and Mário Nuno Berberan-Santos [17] and Lakowicz [82] are used as main reference. Luminescence is the umbrella term for all that is associated with the emission of light. Okabe [106] defined luminescence as: "spontaneous emission of radiation from an electronically excited species or from a vibrationally excited species not in thermal equilibrium with its environment." There are three different types of luminescent compounds: Organic Compounds, Inorganic Compounds and Organometallic compounds [17]. This research will focus on photoluminescence, this is luminescence excited by the absorption of photons. There are three types of photoluminescence:

1. Fluorescence: spontaneous emission of electromagnetic radiation after excitation by photon, which stops right after the excitation radiation is stopped (single state)
2. Phosphorescence: spontaneous emission of electromagnetic radiation after excitation by photon, which slowly decays with time and results in an afterglow (triplet state)
3. Delayed fluorescence: extremely weak emission of electromagnetic radiation after excitation with delayed response

There are multiple terms used around (photo)luminescence which are closely related to each other but are different. Distinction between the terms is needed for the following sections:

- *Chromophore*: "The part (atom or group of atoms) of a molecular entity in which the electronic transition responsible for a given spectral band is approximately localised. The term arose in the dyestuff industry, referring originally to the groupings in the molecule that are responsible for the dye's colour." [103]
- *Luminophore*: "A part of a molecular entity (or atom or group of atoms) in which electronic excitation associated with a given emission band is approximately localised. (Analogous to chromophore for absorption spectra)." [80]
- *Fluorophore*: "Molecular entity (often organic) that emits fluorescence. Fluorophores typically contain several combined aromatic groups, or planar or cyclic molecules with several  $\pi$  bonds" [140]
- *Phosphors*: "A phosphorescence chemical compound that can re-emit light upon light excitation. Phosphors are often transition-metal compounds or rare-earth compounds of various types." [19]
- *Dye*: "As a colored substance that chemically bonds to the substrate to which it is being applied. The color of a dye is dependent upon the ability of the substance to absorb light within the visible region of the electromagnetic spectrum (400-700 nm)." [13]
- *Indicator/Probes*: "Are synthetic dyes that undergo colour changes on interaction with chemical species. The purpose of using a so-called indicator chemistry (i.e., a dye in or on a polymeric support) in optical sensing is to convert the concentration of a chemical analyte into a measurable optical signal." [163]

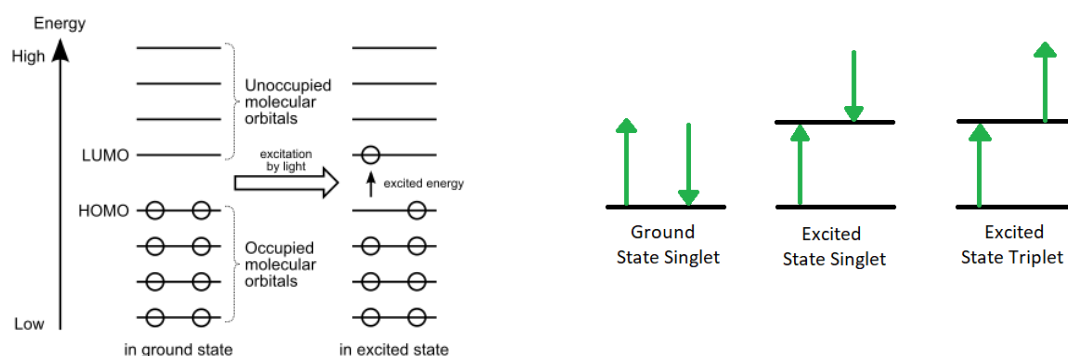
### 2.4.1. Light-matter interaction

There are different types of light-matter interactions. Some examples are absorption, reflection, transmission, diffraction and scattering described in section 2.3.2. Photoluminescence depends on the absorption of light. The other interactions can influence the luminescence. When photons are absorbed by a material that is capable of luminescence, this material will create an Excited State (ES). In this

ES the material has more energy present than the material had in the Ground State (GS). The energy difference also energy gap is the energy of the photon absorbed:

$$E_{ES} - E_{GS} = h\nu \quad (2.20)$$

Where  $h$  is the Planck constant and  $\nu$  the frequency of the absorbed photon. When a molecule absorbs a photon it results in moving up an electron from the Highest Occupied Molecular Orbital (HOMO) to the Lowest Unoccupied Molecular Orbital (LUMO) [162]. The reverse move can result in the luminescence. However, not all molecular transitions are visible in the form of emitted photons (light). Both HOMO and LUMO refer to the ground state of the molecule (see figure 2.14a). There are intramolecular deactivation processes which are related to the photoluminescence of single molecules and intermolecular deactivation processes. Intermolecular deactivation processes are the processes which can influence the photoluminescence of molecules. The following sections describe the intramolecular processes and section 2.4.6 will describe the intermolecular processes.



(a) Diagram of the HOMO and LUMO of a molecule. Each circle represents an electron in an orbital; when light of a high enough frequency is absorbed by an electron in the HOMO, it jumps to the LUMO. Reprinted from Wikipedia [160] (b) Transition from Ground State to Excited Singlet and Triplet States. Ground state and Singlet state are spin paired. In the triplet state the spin is in the same direction and thus not spin paired. Reprinted from Libretexts Chemistry [86]

Figure 2.14: Illustrations of the light-matter interaction and the excited and ground state and excited states

### 2.4.2. Single and Triplet Excited state

The difference between fluorescence and phosphorescence is caused by the difference in the state of electrons. Electrons can be in a singlet or triplet state. Two electrons in an orbital of a molecule must have opposite spin states, this is called spin pairing. When electrons are spin paired the molecule does not exhibit a magnetic field. Singlet state is formed when one electron is excited to a higher energy level and the electron has the same orientation as it was in the ground state [82]. Triplet state is formed when the electron is excited to a higher energy level state and the electron has a parallel orientation with the electron in the ground state. Figure 2.14b illustrates the difference between the triplet and singlet states. The change in electronic state the transition from singlet to singlet occurs more often than singlet to triplet (or reverse).

An electron in the triplet state has a longer lifetime than that of singlet state electrons, because of the change in spin orientation. The triplet excited state has a lower energy than the singlet excited state as it costs energy to change the orientation [17]. The different states and the transitions are visualised in the Jablonski diagram illustrated in figure 2.15. This diagram shows the energy levels of the singlet ( $S_{0,1,2,\dots}$ ) and triplet ( $T_{0,1,2,\dots}$ ) excited states and the intramolecular deactivation processes (radiative and non-radiative transitions). At room temperature most electrons are in the ground state, when these electrons absorb the energy of a photon, this electron is excited to an excited state.

#### Vibrational Relaxation

In almost every case the first effect is the vibrational relaxation, a non-radiant relaxation bringing the electron to its vibrational ground state ( $S_{1,2,\dots}$ ). During vibrational relaxation the lost energy of the electron is converted to heat. When an electron is in a vibrational ground state it can change to another vibrational level, this can be *Internal Conversion (IC)*, *Fluorescence*, *InterSystem Crossing (ISC)* or

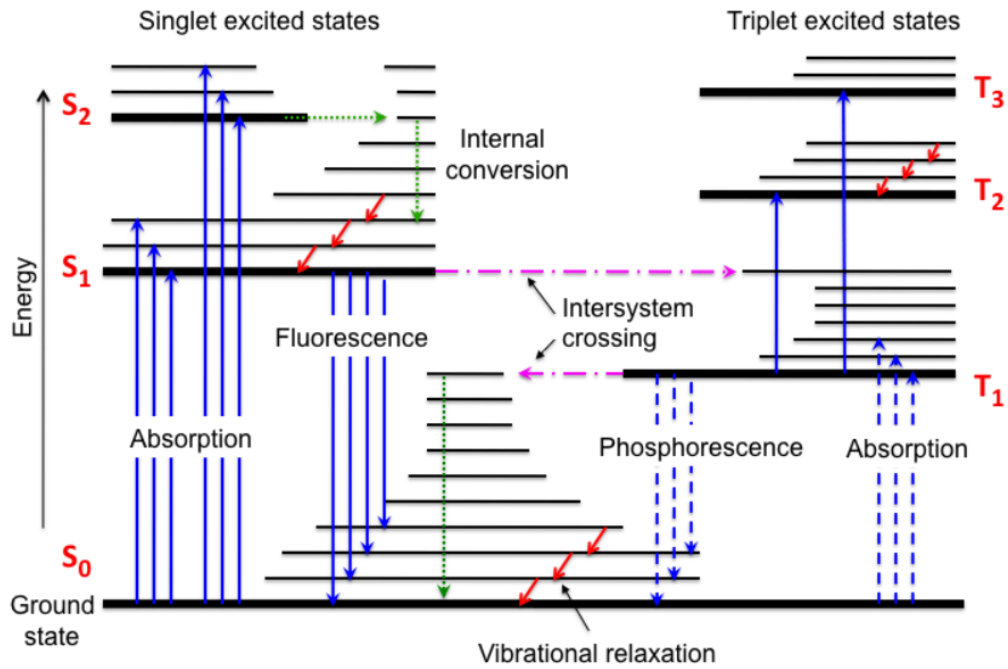


Figure 2.15: Typical diagram of the electronic energy levels of a molecule with singlet and triplet systems. The most important radiative (fluorescence and phosphorescence) and non-radiative (internal conversion, vibrational relaxation, intersystem crossing) transitions are shown. Reprinted from Álvarez et al. [8]

**Phosphorescence.** The photon always chooses the path of the least resistance when it falls back to the ground state. Before discussing these other transition, Stokes shifts and the Frank-Condon principle are explained. These two principles are essential for the luminescence processes.

### Frank-Condon Principle

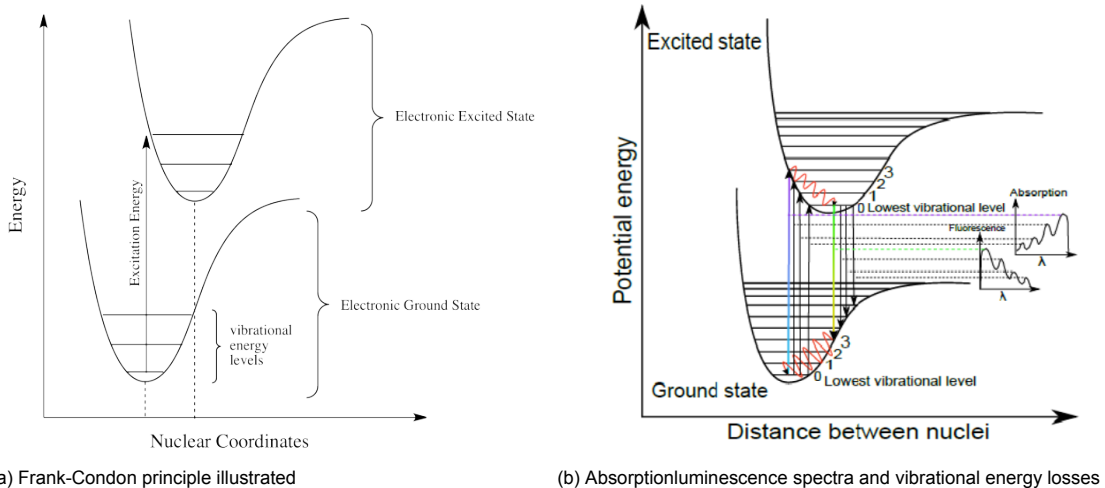


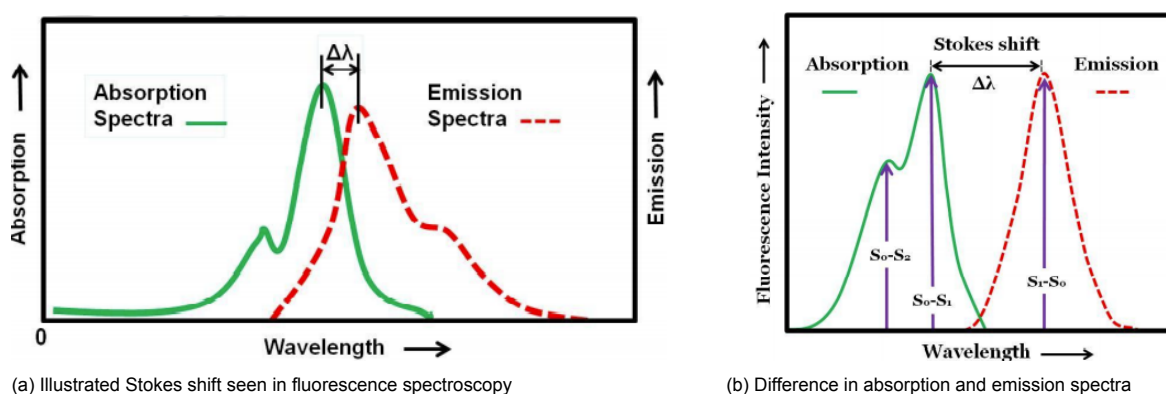
Figure 2.16: Frank-Condon energy states and the absorption and luminescence spectra example

The Franck-Condon principle describes that during an electronic transition (GS to an ES) a change from one vibrational energy level to another will be more likely to happen if the two vibrational wave function overlap significantly [11]. Simplified, when electrons get to an excited state, it will change to the vibrational level of this excited state overlaps with the wave function (figure 2.16a). This causes the energy in the excited state to directly transfer to vibrational energy, which is lost as heat or molecular

collision. So instead of dropping straight down, the electrons first loses heat to go down to its excited ground state [86]. From here on it will drop to the ground state matching its wave function, which is usually a higher vibrational level of the ground state. This results in a lower wavelength of the photon when the electrons fall to the ground state, shown in figure 2.16b. When chromophores are dissolved in liquid the Franck Condon principle can be applied to the electronic transitions [86].

### Stokes shift

As the electron loses energy due to vibrational relaxation before it falls back to the ground state. This lower energy causes the emission of light to have a lower energy than the absorbed light. As a result the emission spectra moves toward the longer wavelengths (figure 2.17a). This occurring shift towards longer wavelengths is called the Stokes shift, in which the wavelength changes with ( $\Delta\lambda$ ). As the value of the Stokes shift increases, it becomes easier to separate the excitation from the emission light using fluorescence filters [55]. The loss of energy of electron in the excited state  $S_1$ , is the total energy loss observed during the emission process. Differences between the absorption and the emission peak can be seen when an electron transitions from the ground state to the higher electronic levels  $S_2$  or  $S_3$  and loses energy to relax to the first excited state  $S_1$  (figure 2.17b). From here the energy emission peak is shifted from the  $S_1$  absorption peak with the Stokes shift ( $\Delta\lambda$ ).



(a) Illustrated Stokes shift seen in fluorescence spectroscopy

(b) Difference in absorption and emission spectra

Figure 2.17: Stokes shift principle seen in fluorescence spectroscopy and the differences caused by the higher excitation states. Reprinted from Gupta and Mahapatro [55]

Stokes shift only occurs in radiative deactivation transitions. Non-radiative transitions do not emit photons. Radiative transitions are Fluorescence and Phosphorescence and non-radiative transitions are Internal Conversion and Intersystem Crossing [17]. All these intramolecular deactivations are illustrated in figure 2.18.

### 2.4.3. Internal Conversion

Internal Conversions (ICs) is the non-radiative transition between electronic states of the same spin multiplicity. During this de-excitation no photons are emitted [87]. The energy is converted into vibrations and rotations of the excited molecule itself or it can be transferred to other molecules upon collision [3]. Internal Conversion is less effective when the energy gaps between the states is increased. This causes that between  $S_0$  and  $S_1$  mostly other modes of deactivation are occurring, while between higher excited states  $S_{2,3,\dots}$  and  $S_1$ , IC is causing the higher states to lower to  $S_1$ . The energy gap between  $S_0$  and  $S_1$  is determined by the excitation wavelength. IC is more efficient than luminescence in the red-light absorbing dyes.

### 2.4.4. Fluorescence

Fluorescence is a radiative deactivation of an electronic excited state to the ground state that has the same spin multiplicity [22]. Most of the time fluorescence happens from  $S_1$  to a vibrational excited  $S_0$ . This causes direct vibrational relaxation. The energy of the emitted photons during fluorescence is less than the energy of the photons absorbed during excitation [3]. The fluorescent quantum yield

describes the efficiency of the fluorescence process. It is the ratio of the number of photons emitted to the number of photons absorbed [158] (equation 2.21). The maximum ratio is 1, which results in that each photon absorbed will be emitted in a photon. Materials with a quantum yield of 0.10 are still considered fluorescent [86].

$$\Phi = \frac{\text{Number of photons emitted}}{\text{Number of photons absorbed}} \quad (2.21)$$

Quantum yield  $\Phi$  can also be defined by the excited state decay rates (equation 2.22) where  $k_f$  is the fluorescence rate constant ( $s^{-1}$ ) and  $\tau_s$  is the lifetime of the singlet excited state ( $s^{-1}$ ). The excited state decay times of material are around 0.5-20 nanoseconds.

$$\Phi = \frac{k_f}{\sum_i k_i} = \tau_s k_f \quad (2.22)$$

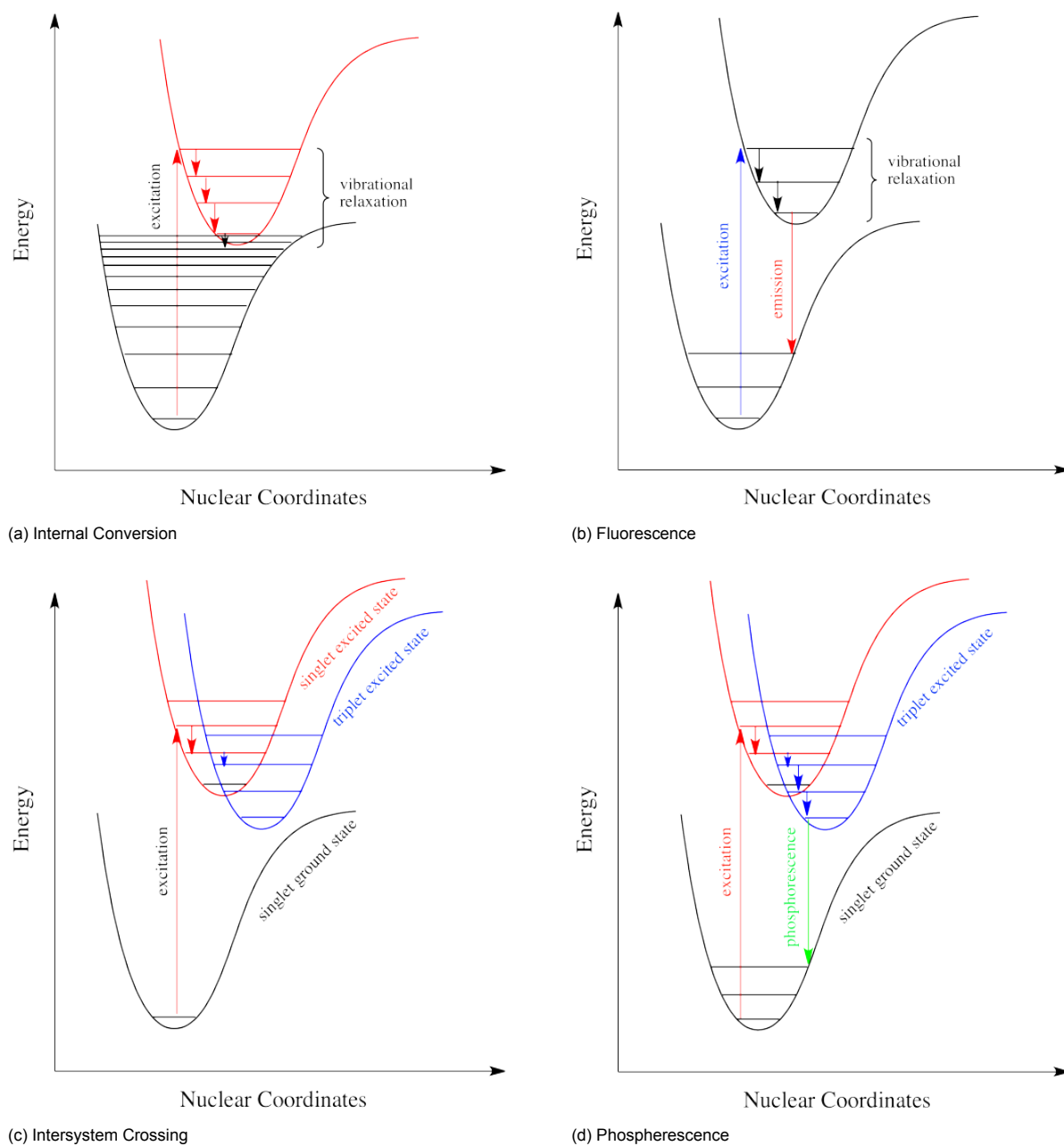


Figure 2.18: Intramolecular deactivation Processes

### 2.4.5. Intersystem Crossing

Intersystem Crossing (ISC) is a non-radiative transition between excited states but differs from Internal Conversion by the change in spin [17]. So the molecule changes from a singlet state to a triplet state. It is not possible to go from the singlet ground state directly to the triplet state, but sliding down vibrationally onto the triplet state from the singlet state is possible because there is no absorption of a photon. The probability of reversing the spin occurs when the vibrational levels over the singlet and triplet overlap, as shown in figure 2.18c. The process is spin forbidden but through quantum mechanics it still occurs. Because the energy level of T1 is lower than S1 the reverse is improbable. The Intersystem Crossing Quantum yield is:

$$\Phi_{isc} = \frac{k_{isc}}{\sum_i k_i} = \tau_s k_{isc} \quad (2.23)$$

Where  $k_{isc}$  is the Intersystem Crossing rate constant.

### 2.4.6. Phosphorescence

When an electron changes from an excited state to the ground state with an opposite spin it is called phosphorescence [86]. In phosphorescence, the excited state lifetime is inversely proportional to the probability that the molecule will transition back to the ground state [87]. The lifetime of a molecule in the triplet state is long, this causes the transition to continue after the irradiation has stopped. This makes it easy to differentiate between fluorescence and phosphorescence. Organometallic heavy-metal complexes or low temperatures allow for Intersystem Crossing and therefore phosphorescence.

Table 2.1 gives an overview of the deactivation process described above and the timescale for the deactivation processes.

Process	Transition	Timescale (sec)
Light Absorption (Excitation)	$S_0 \rightarrow S_n$	ca. $10^{-15}$ (instantaneous)
Internal Conversion	$S_n \rightarrow S_1$	$10^{-14}$ to $10^{-11}$
Vibrational Relaxation	$S_n^* \rightarrow S_n$	$10^{-12}$ to $10^{-10}$
Intersystem Crossing	$S_1 \rightarrow T_1$	$10^{-11}$ to $10^{-6}$
Fluorescence	$S_1 \rightarrow S_0$	$10^{-9}$ to $10^{-6}$
Phosphorescence	$T_1 \rightarrow S_0$	$10^{-3}$ to 100
Non-Radiative Decay	$S_1 \rightarrow S_0$	$10^{-7}$ to $10^{-5}$
	$T_1 \rightarrow S_0$	$10^{-3}$ to 100

Table 2.1: Absorption and Emission Rate Comparison

#### *Intermolecular deactivation processes*

Besides the intramolecular deactivation processes there are many different types of intermolecular deactivation processes. These processes can decrease the luminescence intensity of a luminophore in presence of another molecule. Quenching, Energy and Electrons Transfers are such processes, but will not be discussed as deactivation process in this thesis. More information is given in the book Molecular Fluorescence by Bernard Valeur and Mário Nuno Berberan-Santos [17].

### 2.4.7. Fluorescent lifetime and Quantum Yield

Lifetime and quantum yield are the fundamental parameters of luminescence emission. Together they determine the intensity and the temporal behaviour. Intermolecular non-radiative decay has a strong influence on these two parameters and provide the basis for sensing. Fluorescent lifetime is the average time a molecule stays in the excited state before returning to the fundamental state [154]. Nonradiative and radiative mechanisms determine the fluorescent lifetime  $\tau_0$

$$\tau_0 = \frac{1}{k_r^s + k_{nr}^s} \quad (2.24)$$

The radiative transition from  $S_1 \rightarrow S_0$  is described by  $k_r^s$  and the sum of the nonradiative rates (internal conversion and intersystem crossing) is described by  $k_{nr}^s$ . When the molecules are excited by a pulse of light, the intensity of the excited molecules will decrease with a rate of  $1/\tau_0$ . The initial intensity ( $I_0$ ) is

determined by the concentration of excited molecules by the light. The fluorescent intensity at a certain time is given by the following formula:

$$I(t) = I_0 e^{-\frac{t}{\tau_0}} \quad (2.25)$$

$I(t)$  is the impulse response of the system, when the molecule is excited by complex patterns, the convolution of this function can be used to determine the output response.

Quantum yield is the measure of luminescent efficiency described in 2.4.4. Quantum yield is determined by the relative magnitudes of the (non)radiative constant. Higher quantum yield results that it is easier to detect the luminescent signal of a sample. These two parameters can change when the luminescent molecules interact with other molecular species. This interaction can promote or demote the impact of these parameters. Measuring this impact is the basis for fluorescent sensing techniques

## 2.5. Fluorescence Measurement Techniques

For this section Chapter 6 of Handbook of Optical Sensors by Jorge [68] is mainly used as reference. Jorge [68] describes two types of measurements. Steady state and time resolved measurements. Steady state is based on recording luminescence intensity while the molecules are continuously illuminated with an excitation source. Time resolved measurements are based on the intrinsic characteristics of the luminophores. Lifetime is an intrinsic characteristic of the luminophore. This causes that it is not vulnerable for how the light is aligned to the luminophore and it doesn't depend on concentration or photodegradation.

### 2.5.1. Steady State Measurements

Steady state measurements can be divided into three techniques and two methods. The techniques are absorption, reflection and luminescence intensity. The measurements can be done with a single or dual wavelength excitation.

#### *Absorptiometry*

Absorption based sensing is a very common optical sensing technique, but not often used in the continuous sensing of pH [139]. This is because it is based on the transmission of light, therefore a transparent support, sensing layer and sample are needed. This is to overcome scattering, leaking and absorption of other materials. In spectroscopy, absorption is used a lot. The absorption efficiency can be determined by taking the logarithm of the excitation Intensity ( $I_0$ ) and the measured transmission intensity ( $I_T$ ):

$$A_\lambda = -\log T = -\log\left(\frac{I}{I_0}\right) = 2 - \log(\%T) \quad (\text{revisited 2.18})$$

The luminescent emission should not be measured, because that is a different technique. The Beer-Lambert law describes the absorption in equation 2.26:

$$A(\lambda) = \epsilon(\lambda)lc \quad (2.26)$$

It describes the absorbance to be proportional to the concentration of the dye ( $c$ ), the thickness ( $l$ ) and the molar absorptivity  $\epsilon$ .  $\epsilon$  is always related to the wavelength corresponding to the maximum of the absorption band of lower energy [51]. This formula implies that the sample absorbance is linear to the concentration. However, this is not valid for higher concentrations. This as a result of the saturation effects, possibly leading to dye aggregates which change the scattering of light or modify the absorption. Equation 2.36 in section 2.5.3 shows how the absorption can be used to determine the pKa of an indicator.

#### *Reflectometry*

Reflection based sensing is more suitable for optical pH sensing. Simple pH indicator stripes are based on this principle, as the impermeable material is scattering a wavelength dependable on the pH. Often the scattering is increased by adding white scattering particles [139]. The Kubelka and Munk formula describes the relation between the concentration and the reflected light:

$$c = \frac{S(1 - R_d)^2}{2\epsilon_R R_d} \quad (2.27)$$

$R_d$  is the intensity of the reflected light,  $S$  is the constant for the support,  $\epsilon$  the molar absorbance of the material.  $c$  is the concentration of the basic or acidic form of the concentration. More advanced sensors use dual wavelength sensing, this makes the sensor more accurate and less vulnerable to concentration differences. An advantage of reflection based sensing in advanced sensors is that the emitter and the detector can be on the same side compared to absorption-based sensing. This allows for surface sensing.

#### *Luminescence intensity*

The last type of steady state sensing is the luminescence intensity based sensing. This is based on the parameters described in section 2.4.6. As the luminophore is continuously excited it attains a steady state. The relation between the quantum yield and the luminescence output is described by the following formula:

$$I_L = I_0(1 - 10^{-\epsilon c l})\phi \quad (2.28)$$

This formula shows that luminophores with high quantum yield are more advantageous, because smaller quantum yield have to be compensated by increasing excitation intensity. This higher excitation will increase photodegradation. When photons are emitted, they have a certain energy distribution which is the emission spectrum. The relation between the concentration and the luminescence intensity is described by Parker's law:

$$I_L(\lambda_{Ex}, \lambda_L) = 2.3kF(\lambda_L)I_0(\lambda_{Ex})\epsilon(\lambda_{Ex})lc \quad (2.29)$$

Where luminophore intensity  $I_L$  is related to the excitation intensity  $I_0$ , the molar absorbance of the indicator  $\epsilon$ , the concentration  $c$ , the penetration length  $l$  and the parameter  $k$  which accounts for a diversity of experimental factors affecting the detected signal [68]. This law is an approximation at low luminophore concentration and when the absorbance of the luminophore increases, it stops to have this linear relations. This formula shows that the luminescence intensity is not only affected by the concentration of the luminophore, but also by the penetration depths, the intensity, change in sensitivity and a drop of concentration by leaching or photobleaching. Some of these factors can be compensated by ratiometric or time-resolved sensing. Another big disadvantage of fluorescence intensity sensing is the background fluorescence of the samples and the intrinsic fluorescence of optical and other components. Equation 2.29 allows for obtaining the emission spectrum when the excitation wavelength is fixed, and for obtaining the excitation spectrum when the luminescent intensity is measured when changing the excitation wavelength.

#### *Dual-Wavelength Referencing (two wavelength ratiometric luminescence intensity)*

Dual-wavelength referencing is a sensing method that can overcome problems such as concentration differences, changes in light path and drifts of optical source or detectors. Dual-wavelength referencing uses two different wavelengths and is also called ratiometric referencing. Dual-wavelength referencing increases the robustness of the system by measuring the emission with two different excitation wavelengths. Reflection dual-wavelength referencing and luminescence dual-wavelength referencing are the most common. In reflection dual-wavelength referencing two LEDs are used, one is emitting a wavelength that is absorbed by the indicator and another that is indifferent to the indicator. Subtracting the second emission from the first can get rid of interferences. In fluorescent dual wavelength referencing or Fluorescence Ratiometric Imaging (FRIM) the dual wavelengths can be applied in multiple methods.

Weidgans [154] and Kocincová [77] describes three different types of FRIM:

1. Two excitation and one emission wavelength: Most fluorescent indicators allow for this ratio  $R$ . Figure 2.19 shows this principle.

$$R = \frac{I(\lambda_1^{ex}, \lambda^{em})}{I(\lambda_2^{ex}, \lambda^{em})} \quad (2.30)$$

2. One excitation and two emission wavelengths: Possible when indicator exhibit dual emissions or if a reference dye is added to the indicator. Figure 2.20 shows these possibilities.

$$R = \frac{I(\lambda_1^{em}, \lambda^{ex})}{I(\lambda_2^{em}, \lambda^{ex})} \quad (2.31)$$

3. Two excitation and two emission wavelengths: When indicators exhibit dual emissions, this type can be used. Not a popular option

$$R = \frac{I(\lambda_1^{ex}, \lambda_1^{em})}{I(\lambda_2^{ex}, \lambda_2^{em})} \quad (2.32)$$

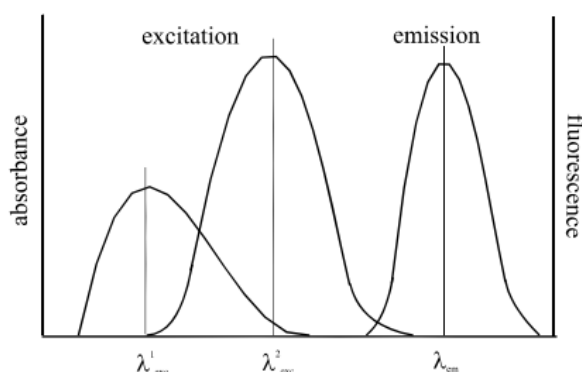
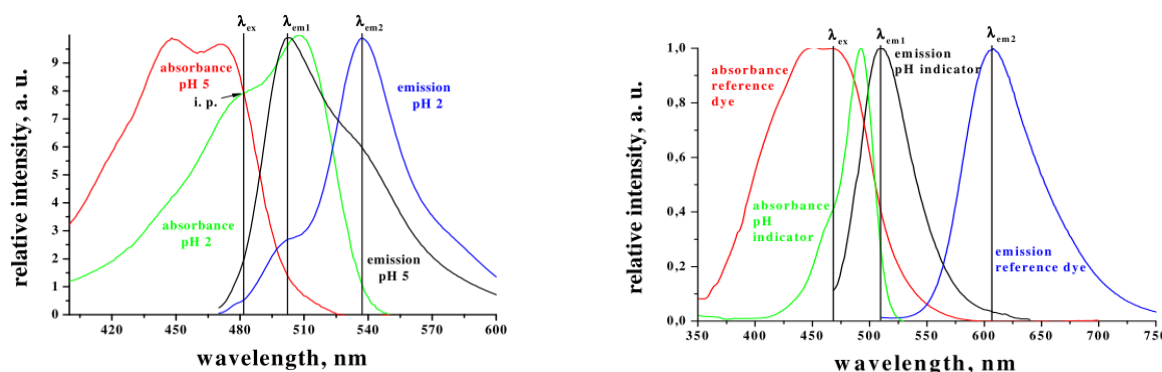


Figure 2.19: Dual excitation and single emission measurement methods. Reprinted from Weidgans [154]



(a) A typical example of ratiometric approach where excitation is performed at isosbestic point (i. p.) and dual emission is monitored at two different wavelengths.

(b) A typical example of ratiometric approach in which excitation of indicator/reference dye system is performed at a single wavelength and emission of both is monitored at two different wavelengths.

Figure 2.20: Dual emission measurement methods. Reprinted from Kocincová [77]

### 2.5.2. Time-resolved measurements

Time-resolved measurements are focused on the intrinsic characteristics of the luminophore. This causes the measurements to be invulnerable to system changes, such as optical alignment, dye concentration, and photobleaching. Time-resolved measurements are focused on the luminescence decay time and are influenced by less parameters than intensity measurements [3]. This makes it a robust alternative for steady state measurements. The disadvantage of this measurement is that more advanced instrumentation is needed, because the decay time of fluorescence is very short. Phosphorescence lifetimes are more easy to measure and are used in applications [3]. Time-resolved measurements can be divided into two methods and can be in the time or frequency domain: luminescence decay time, dual-lifetime referencing.

#### Luminescence Decay Time

Luminescence Decay Time is based on fluorescent lifetime ( $\tau$ ), which is the average time for a molecule to stay in the excited state and is also called pulse fluorimetry, time-resolved luminescence intensity or Fluorescence Lifetime Imaging (FLIM) [77]. Because  $\tau$  is a statistical consideration, it can be described as the time after  $1/e$  of the initial excited molecules are not deactivated yet [154]. Equation 2.25 shows this relation and is illustrated in figure 2.21a. The advantage of luminescence decay measurements

is that two types of sensing are possible, in the time domain/pulse or in the frequency domain/phase modulation [88]. In the time domain, the sample is excited with a short pulse of light and the decay of the sample is measured, as shown in figure 2.21b. The intensities of the luminophore are measured with a photodetector, charge-coupled device (CCD) or Complementary metal–oxide–semiconductor (CMOS). In the frequency domain, the sample is excited by a sinusoidal modulated light [17]. The decay time of the luminophore phase shifts  $\phi$  the same waveform with a frequency  $f$ .

$$\tau = \frac{\tan \phi}{2\pi f_{mod}} \quad (2.33)$$

Here,  $f_{mod}$  is the modulation frequency of the excitation light. The modulation  $M$  is the relative peak-to-peak amplitude of the modulated emission in relation to the modulated excitation light [82]. This type of sensing is mostly used for the determination of relatively long decay times (mili- and microseconds), for shorter decay time the equipment becomes too complicated. This is because for these indicators high-frequency modulation is needed.

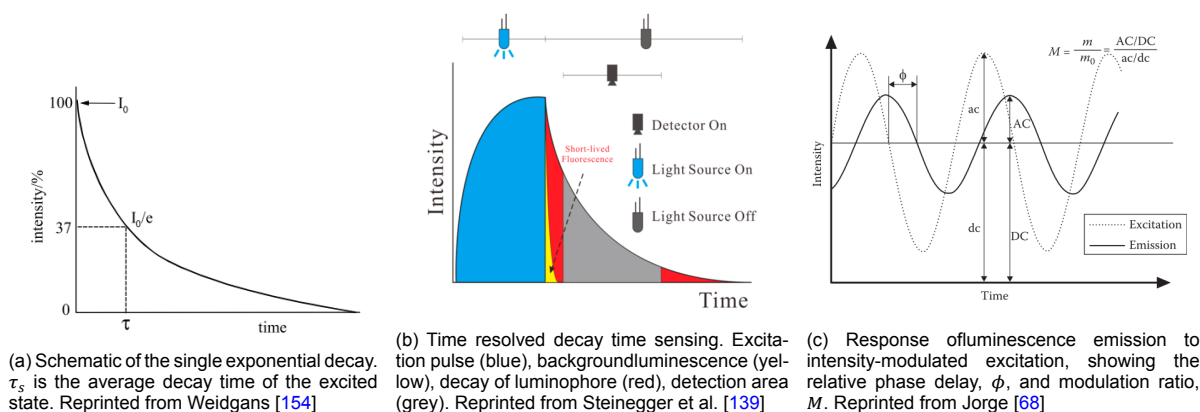


Figure 2.21: Illustrations related to luminescence decay time measurements in time and frequency domain

### Dual Lifetime Referencing

Dual Lifetime Referencing (DLR) uses two luminophores with different decay times. This is a chemical sensitive indicator with a short-lived decay time and a nonsensitive reference indicator with longer decay time [154]. Both luminophores have overlapping excitation and emission spectra and are excited at the same wavelength. Just as with the phase modulation luminescence decay time, the indicator is excited sinusoidal and therefore its fluorescence emission is also modulated sinusoidal, showing a shift of the phase. DLR is a method to turn fluorescence intensities into ratiometric signals. During Time-domain dual lifetime referencing (td-DLR), the detector is turned on during the excitation and during the emission (figure 2.22a). The reference dye has a much longer decay time, the ratio between the two measurements determines the concentration of the analyte. In the second window only the phosphorescence is measured of the reference. Therefore, it is important to only start the sensing after the fluorescence is completely decayed. The ratio  $R$  of the td-DLR is determined by the following equation:

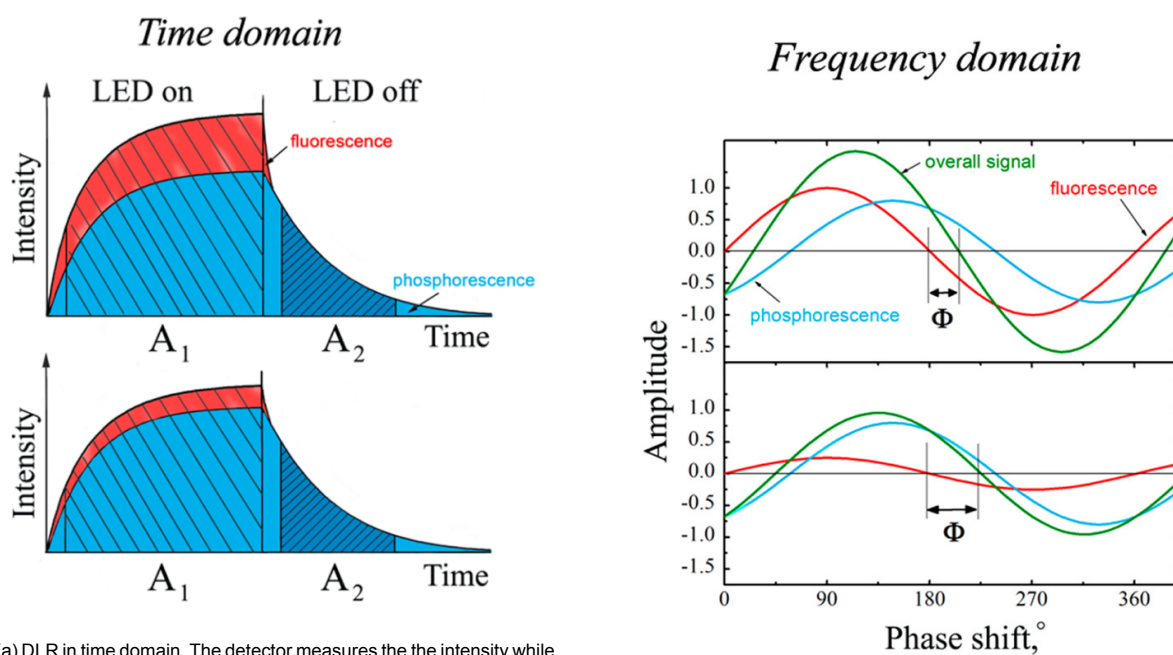
$$R = \frac{A_{ex}}{A_{em}} = \frac{A_{ex}(ind) + A_{ex}(ref)}{A_{em}(ref)} \quad (2.34)$$

In the frequency-domain dual lifetime referencing (fd-DLR), the phase shift of the overall luminescence is depended on the ratio of the intensities of the reference and the indicator [77]. The reference gives a constant background signal while the analyte concentration changes the fluorescence signal of the indicator. The overall phase shift of the overall luminescence  $\phi_m$  is determined by  $\phi_{ref}$  and  $\phi_{ind}$ :

$$\cot \phi_m = \cot \phi_{ref} + \frac{1}{\sin \phi_{ref}} \cdot \frac{A_{ind}}{A_{ref}} \quad (2.35)$$

Where  $A$  is the amplitude and  $\phi$  the phase shift. This type of sensing allows to have a dual sensor capable of simultaneous detection of the two analytes. For such applications, a long-lived phosphorescence indicator acts as an reference for a short-lived fluorescent indicator [75]. This causes that the

observed phase shift is dependable on the concentration of both analytes and is called modified-DLR. More information on m-DLR and fd-DLR can be found in [21] and [75]. Steinegger et al. [139] made a table of the various optical detection schemes and rated capabilities for interference compensation. This table can be found in Appendix A.5.



(a) DLR in time domain. The detector measures the intensity while the LED is on and when the LED is off, after the fluorescence is decayed.

(b) DLR in frequency domain with phaseshift  $\phi$

Figure 2.22: Principle of the DLR. The upper and the lower rows reflect the situations with "switched on" and "switched off" pH indicator, respectively. Reprinted from Steinegger et al. [139]

### 2.5.3. Luminescent Indicators

Luminescent indicators/probes are essential for luminescent based sensing and determine the quality of the sensor. The sensing technique and equipment depend on the characteristics of the indicator. Luminescent indicators are not all interchangeable within one set-up, so selecting the right indicator is an important step in building an optical sensor. Indicators depend on the analyte you want to measure, but can also be interchangeable. Since early on, the characteristics have been studied and many natural or synthesised compounds are available for luminescent sensing. There are intrinsic and extrinsic luminophores.

Intrinsic luminophores are organic materials and called organic probes. Most naturally occurring probes have absorption and emission in the UV or blue region spectrum. This makes them more harming and expensive to use and they also have short lifetimes (3-5ns) [68]. More interesting dyes are the synthesised organic luminophores. There are more than thousands of synthesised luminophores available for sensing application [68]. These luminophores mostly bound to the molecule of interest or have a type of chemical affinity. For analytes, the sensitivity is achieved through photoinduced electron transfer (PET) or photoinduced proton transfer (PIPT). Most organic dyes present a high degree of photodegradation hindering their use in long-term sensing applications. Steinegger et al. [139] describe the following types of luminophores which can be used for pH sensing; Phenolic luminophores (HPTS and Fluoresceins), luminophores with aromatic rings of protonable nitrogen atoms (Pyridines, quinines, oxazines) and luminophores with dissociated groups attached to a chromophore. For this research, the focus will be on the phenolic luminophores. These types of probes can have a phenol group which is part of the chromophoric system. This group can be phenol and phenolates depending on the local pH value. The phenolate is photoexcited and causes fluorescence. If the pH value drops, there is less absorption of the phenolate form and the fluorescence will fade out.

Extrinsic luminophores are Metal-ligand complexes, also called long-lived Transition Metal Complexes.

These luminophores have longer decay times existing of a transition metal containing one or more organic ligands. The most used metal complex is platinum metal ruthenium. Metal-ligand complexes have the advantage that they have longer decay times and larger Stokes shift compared to organic luminophores because of a lower energy of the triplet state. The disadvantage is that the brightness is lower and the quantum yields are low. Another big limitation is that the metal-ligand complexes are sensitive to oxygen, which influences the decay time. The last category of luminescent indicators are luminescent quantum dots, but because of their bad biological response, this is not further explained in this research.

#### *pKa of luminescent indicators*

To determine the pKa, usually the Eistert equation is used in combination with photo/fluormetry.

$$pK_a = pH + \log \frac{(A_x - A_b)}{(A_a - A_x)} \quad (2.36)$$

Equation 2.36 describes, that  $A_x$  is the absorbance at a pH value.  $A_b$  and  $A_a$  are the absorbance of the dye in basic and acidic form (with very high or low pH). With unknown ionic strengths which affect the equilibrium constant and more thorough calibration is needed. However, in dual wavelength/lifetime referencing usually a sigmoid function is fitted to the measured ratios between the two measurements.

#### *Sigmoid function for pKa*

Reijenga et al. [122] describe fourteen methods of determining the acid dissociation constant and evaluate the different methods. Most of these methods use curve fitting of a sigmoid curve to obtain the inflection point which is the pKa. In the literature, different sigmoid functions are used to fit the dissociation curve. However, the most used function is the Boltzmann fitting curve and is also used by the OriginLab Chemistry Software [107, 154, 150]

In 1988 Edmonds et al. [42] described that an increase of ionic strength can shift the pKa up to 1.2 units. Different dyes have different effects on the pKa. Fluorescein dyes have been described to lower the ionic strength while 8-Hydroxypyrene-1,3,6-trisulfonic acid trisodium salt (HPTS) has been described to increase the IS. This is because HPTS has multiple negative charges that are sensitive to IS. Therefore it is important when an indicator is used, it needs to be calibrated.

## 2.6. Hydrogels

Hydrogels exist out of a polymer network. This polymeric network has a double function in the optical sensors. It is the solvent for the indicator and a permeation-selective membrane which prevents cross talk. For a pH sensor, this network has to be permeable for protons. Therefore, mostly hydrophilic polymer networks are used. Polymeric networks made out of inorganic materials are called sol-gels. In this thesis, the focus is on the organic hydrophilic polymer networks called hydrogels.

### 2.6.1. Mechanism

Hydrogels hydrophilic characteristic causes that the network can absorb between 0.1 and 2000 times their dry weight. This results in a swelling of the network. This swelling is needed for proton transfer. Proton transfer means that protons of  $H_3O^+$  transfer to a neighbouring  $H_2O$  molecule. This means that when a hydrogel wants to react with the pH changes, it is not permeable for one proton, but allows proton transfer. Charged polymers and hydrophobic polymers make this harder and are therefore not used very often and will not be discussed. Proton diffusion is determined by the polymer volume fraction and influences the response time of the hydrogel. This fraction is the amount of water retained by the hydrogel in the swollen state. Besides the proton diffusion, this fraction also influences the mechanical stability. Because the swelling of the hydrogel can negatively effect the mechanical properties of the hydrogel. The elastic nature of the hydrogels allows them to fully recover from small deformations (up to 20%). Larger deformation can influence the mechanical properties and detach the hydrogel from the mechanical support.

### 2.6.2. Types

There are different structures the hydrogel can exist of. It can exist out of hydrophilic linear polymers, hydrophobic and hydrophilic polymers and cross-linked hydrophilic polymers. The differences will be

discussed in section 3.3.3. Dyes can be attached to the hydrogel in different methods. The immobilisation methods are: Physical entrapment, covalent immobilisation, non covalent entrapment, electrostatic binding, copolymerisation and ion pairing. These methods are extensively elaborated by Steinegger et al. [139].

## 2.7. Challenges in optical pH sensing

A lot of research has been done in the field of optical sensing and for this application the following challenges are synthesised from the work of Steinegger et al. [139] and Weidgans [154],

1. **Ionic Strength:** need for IS effect compensation, blood electrolyte concentration vary a lot.
2. **Temperature:** a pH sensor is a temperature sensor. Therefore the changes in temperature should be taken seriously in obtaining the right data.
3. **Small Volume:** indicator error in small sample volume. Indicator is a (weak) buffer itself, as well as for any (de)protonable (and thus swellable) polymer or conductive polymer. If small volumes of unbuffered samples are used the error can be significant.
4. **Degradation:** leaching and bleaching of the indicator material influence the stability of the sensor.
5. **Support Matrix:** hydrogels or sol-gels. For hydrogels the use of swellable polymers influence the sensitivity, these polymers contain numerous protonable sites which make them sensitive to ionic strength. The pKa changes and the swelling depends on the IS.
6. **Time:** diffusion of the protons cost time and this has direct influence on the response time of the sensor.
7. **Sterilisation:** sterilisation of the sensor.
8. **Noise:** storing the sensors, background light/fluorescence.
9. **Body fluid interaction:** blood clotting, coating with protein and fouling.
10. **Concentration vs Activity:** as described in 2.2.2, fluorescent dyes measure the concentration of the protons not directly the activity.
11. **Fluid:** for transmission of protons to the fluorescent indicator liquid is needed and dry surfaces can influence the result.

Not all challenges can be tackled by this thesis work. Certain decisions are made due to limited resources (time, money, and available knowledge). The following chapter will go deeper into these decisions and how they influence the challenges listed above.

# 3

## Narrowing the scope

This chapter will focus on the work done to narrow down the scope of this project. The first step was done in an extensive literature review which can be found in Appendix A.18.2. This literature review showed that there are many possibilities to measure pH and all have their (dis)advantages. The decisions made in the literature review greatly impact this thesis work. To focus on the outcome of a proof-of-concept sensor, many decisions are made in a structured manner. This chapter will first summarise the outcome of the literature review and what the influence of the goal of this thesis work is. After this elaboration, conditions are introduced which impact the possibilities for this work and a framework will be introduced for decisions. After this, a second literature search is used to decide on the method chosen for this proof of concept.

### 3.1. Literature review

The literature review was done to find feasible methods to monitor myocardial ischaemia. This was done in three parts, the first focusing on what parameters to measure, the second part was deciding between electrochemical and optical sensing, and the main part was comparing different optical sensing techniques. The goal of the literature review was to lay the groundwork for the development of ischaemia sensor and to make an overview of what has been done. The goal of the literature review was to answer the following question:

*What are feasible methods to detect myocardial ischaemia during a cardioplegia-induced arrest?*

#### 3.1.1. Ischaemia parameters

The first question which is answered in the literature review is:

*Which physical parameters are related to myocardial ischaemia during a cardioplegia-induced arrest?*

To answer this question, the parameters related to ischaemia were elaborated and the following 4 parameters were compared:  $\text{PCO}_2$ ,  $\text{O}_2$ , Lactate, and pH. These parameters are all directly related to the ischaemia of the heart cell as described in 2.1.4. Table 3.1 describes the (dis)advantages of sensing

Parameter	Advantages	Disadvantages	Depended on	Used to measure ischaemia
Lactate	Direct product of anaerobic glycolysis	Enzyme needed to measure lactate	pH	only in sport Payne et al. [110]
pH	Direct information about acidity in the cell	Buffer system in cell try to keep pH steady	Lactate Various buffers ( $\text{CO}_2$ , phosphate)	Khuri and Marston [73] Khabbaz et al. [72]
$\text{PCO}_2$	Measures the pH and the accumulation of $\text{CO}_2$	Influenced by the buffer system of pH	pH	Pischke et al. [112]
$\text{O}_2$	Oxygen is used by the cell and a decrease Indicates a cell using too much oxygen	Only partial pressure or oxygen in Haemoglobin can be measured easily	Oxygen uptake cell	Nichols et al. [105]

Table 3.1: Comparison of different parameters with the (dis)advantages of measuring them to monitor myocardial ischaemia

these parameters. In the review, the decision was made to focus on both lactate and pH. Although lactate is challenging to measure, lactate was selected because it is the direct product of ischaemia. pH was selected as the second parameter because multiple studies show the direct correlation between pH and lactate [112, 92, 151] and Khabbaz et al. [72] already showed the capability to monitor ischaemia in the heart with pH. At the end of the literature study the decision was to focus solely on pH because it is more accurate and better suitable for fluorescent sensing as the fluorescent indicators react with pH.

### 3.1.2. Sensing Mechanism

The second question which is answered in the literature review is:

*Which types of technologies are capable of measuring pH and Lactate during a cardioplegia-induced arrest?*

To answer this question, an overview of the different biomedical sensors was synthesised from the literature. The classification developed in this literature review is shown in figure 3.1.

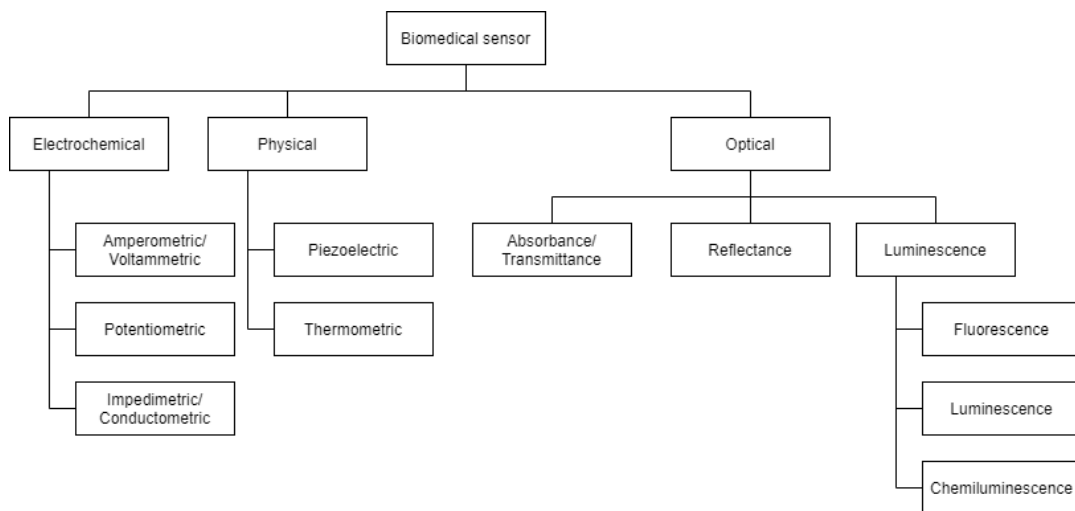


Figure 3.1: Classification of Biomedical sensor developed for this literature review by combining classifications of Shavanova et al. [134], Sharma and Khurana [131], Hajian et al. [56] Singh et al. [135]

Table A.1 shows an overview of the sensors discussed in figure 3.1 with the (dis)advantages per sensor type. Of course, there are many types of sensor per measuring principle, but it gives a good indication of which type of sensors are capable of measuring the pH of tissue or solutions. The physical sensors are not capable of measuring pH, and for the other type of sensors, there are already sensors made in the research field. Because the electrochemical sensors are more related to chemistry, can interfere with the oxidation and have lower specificity. The decision to focus on optical sensors are elaborated in section 2.3.4.

### 3.1.3. Optical sensors

The third and main part of the literature review is focused to answer the question:

*What is the most feasible optical sensing technique for measuring pH or lactate during a cardioplegia-induced arrest?*

This question was answered by reviewing the literature. To find the best possible sensor, a search strategy was constructed. This search strategy exists in multiple parts which are shown in figure 3.2 and was performed in Scopus. It was done to include all possible sensors which show the potential to be able to measure within the physiological range. The following selection criteria were used to only assess the sensors with the most potential:

1. Not a review article

AND					
Parameter	Transducer	Type of sensing	Tissue	NOT	
OR	"pH"	*sensor*	*optic*	"in vivo"	nerve
	lactate*	*transducer*	*fibre*	myocyte*	kinematics
	*lactic*		*luminescent*	cardiomyocyte*	
			*fiber*	myocard*	
			*fluorescent*	tissue	
			blood*		
			*muscle*		

Figure 3.2: Search terms used in literature search in Scopus

2. Set up described with an optical sensor
3. Sensing lactate or pH
4. Can measure in or around the physiological range of lactate (0-5mM) and pH (6.0-8.0)
5. Has the possibility to measure in-vivo

A total of thirty-seven studies were identified for inclusion in the review. The search of the SCOPUS database provided a total of 1,004 articles, while 298 other records were found through other sources such as PubMed and Google Scholar. After duplicate removal 1,050 records remained eligible for screening. Succeeding the title abstract screening, 154 full-text articles were assessed for eligibility. Of these, 129 were articles were excluded for various reasons, which can be found in figure 3.3. In total, it resulted in thirty-seven articles which are included in the literature review. Seven articles found were designed to measure lactate levels. Thirteen articles are absorption-based optical sensors, fourteen are fluorescent-based sensors, and five are sensors based on the reflection. Elaboration on all thirty-seven sensors are described in the review. The extensive results of the literature review can be found

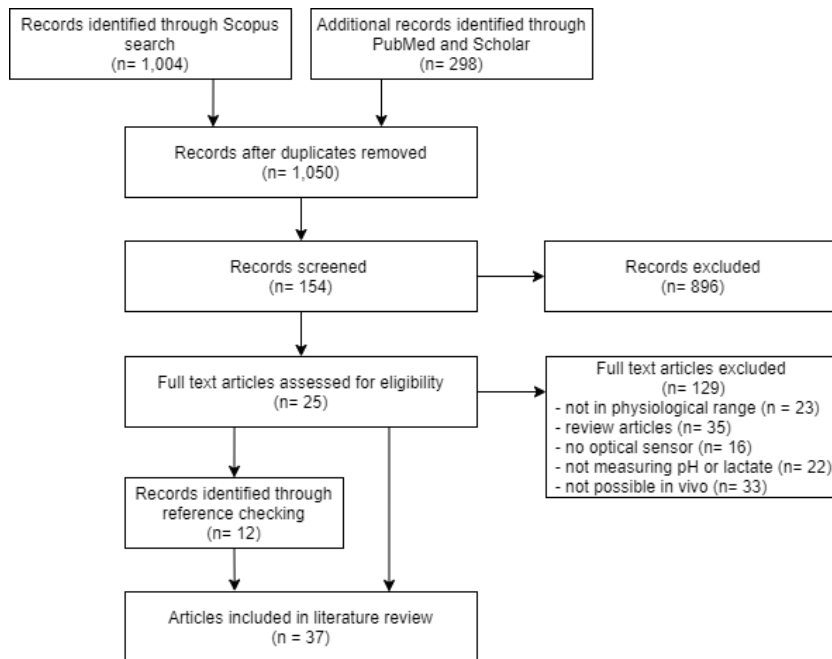


Figure 3.3: Flow diagram of records included in this literature review

in Appendix A.18.2, but Table 3.2 summarises the results. Looking at the literature found, the following deductions are made. First of all, the lactate-based sensors found in this review are not very applicable for in vivo measurements. It has various reasons, but the need for oxygen for enzymatic reactions to occur limits the possibilities for these types of sensors. The second problem with lactate sensors is that

the manufacturability of these sensors is difficult. This is the reason that this thesis will not focus on lactate.

Another conclusion which can be made from this review is that fluorescent fibre based techniques are most advanced. These types of sensors are already being used in-vivo and show great potential. Only one sensor by Aigner et al. [5] can certainly not be used as an ischaemia sensor, because of the short shelf-life of the planar sensor. The applicability is the most significant uncertainty of the reflection sensors as to whether they are suitable as a potential sensor. Just as with the lactate sensor, the manufacturability is a reason why the focus of the rest of the research will not be on reflection based sensors.

Absorption based sensors are considered relatively easy to manufacture. This is mainly because only a dye and a hydro/sol-gel matrix are needed. No fluorophores, lasers, or nanoparticles have to be used to test these sensors. The main disadvantage of these sensors is that they are only tested in test solutions or biosamples. This makes it hard to determine if they would succeed in measuring the pH of the tissue of the heart. The last hurdle which should be investigated with the absorption-based sensor is the size of the fibres used. Most of them are above 300  $\mu\text{m}$  and this is still invasive for the tissue. Fluorescent based optical fibres are smaller but have problems with dry bleaching and response time.

Ref	Parameter	Principle	Type of Sensing	Physiological Range	Applicable for in vivo	Resolution/Accuracy	Response Time	Easy to Manufacture	Potential Sensor
Jernelv et al. [67]	Lactate	AB	Fibre	✓	X	?	✓	X	X
Baishya et al. [15]	Lactate	AB	Fibre	✓	X	?	✓	X	X
Zheng et al. [172]	Lactate	FL	Fibre	X	X	?	?	X	X
Biswas et al. [20]	Lactate	FL	Fibre	X	X	?	?	X	X
Sharma et al. [133]	Lactate	RE	Fibre	✓	X	✓	✓	X	X
Driller et al. [39]	Lactate	AB	Planar	✓	X	?	?	X	X
Andrus et al. [9]	Lactate	FL	Planar	X	X	?	X	X	X
Florea et al. [48]	pH	AB	Fibre	✓	X	?	?	✓	X
Raoufi et al. [119]	pH	AB	Fibre	✓	✓	X	?	✓	✓
Jeon et al. [66]	pH	AB	Fibre	✓	?	?	✓	✓	?
Tou et al. [145]	pH	AB	Fibre	✓	?	✓	✓	?	?
Zajic [169]	pH	AB	Fibre	✓	X	✓	?	✓	X
Tamayol et al. [143]	pH	AB	Fibre	✓	X	X	X	✓	X
Kim et al. [74]	pH	AB	Fibre	✓	?	✓	✓	✓	✓
Mishra et al. [100]	pH	AB	Fibre	✓	X	✓	✓	X	X
Hartings et al. [58]	pH	AB	Fibre	✓	X	?	X	✓	X
Hiruta et al. [62]	pH	AB	Planar	✓	✓	?	✓	X	✓
Ellerby et al. [44]	pH	AB	Planar	✓	X	✓	✓	✓	X
Chen and Gu [27]	pH	AB	Planar	✓	?	✓	✓	?	?
Kattippambil Rajan et al. [70]	pH	AB	Planar	✓	X	✓	?	✓	X
Kasik et al. [69]	pH	FL	Fibre	✓	?	X	✓	✓	?
Weizhong Jin et al. [155]	pH	FL	Fibre	✓	?	✓	✓	?	?
Aigner et al. [4]	pH	FL	Fibre	✓	✓	✓	✓	?	✓
Qi et al. [117]	pH	FL	Fibre	✓	✓	?	✓	?	✓
Cui et al. [31]	pH	FL	Fibre	✓	?	✓	✓	✓	✓
Chen et al. [26]	pH	FL	Fibre	✓	✓	✓	?	X	?
Ehrlich et al. [43]	pH	FL	Fibre	✓	✓	✓	✓	X	?
Wencel et al. [157]	pH	FL	Fibre	✓	✓	✓	?	?	✓
Choudhary et al. [28]	pH	FL	Fibre	✓	✓	✓	✓	X	?
Gong et al. [53]	pH	FL	Fibre	✓	✓	✓	✓	X	?
Aigner et al. [5]	pH	FL	Planar	✓	X	?	?	?	X
Liu et al. [89]	pH	FL	Planar	✓	?	✓	✓	X	?
Cattini et al. [24]	pH	FL	Planar	✓	?	✓	✓	✓	?
Li et al. [85]	pH	RE	Fibre	✓	?	✓	✓	X	?
You et al. [168]	pH	RE	Fibre	✓	?	✓	✓	X	?
Zhao et al. [170]	pH	RE	Fibre	✓	?	✓	✓	?	?
Elsherif et al. [45]	pH	RE	Fibre	?	X	✓	✓	?	X
Ran et al. [118]	pH	RE	Fibre	✓	✓	✓	✓	X	?

Table 3.2: Evaluation of all the sensors found in the literature on their capabilities to be in vivo ischaemia sensor.

### 3.1.4. Consequences for thesis

Extracting the information from the literature review narrowed down the scope of a potential ischaemia sensor. The consequence of these results is that the focus of the thesis work is focused on fluorescent

optochemical sensing. As described in section 2.4 and 2.5 many different techniques, hydrogels, and pH indicators can be used. To choose the right materials for the thesis, some recommendations were made in the literature review: First of all, the manufacturability has to be further investigated to see what is possible with limited resources. Secondly, it is essential to elaborate on which risks are accompanied by using fluorophores and dyes. In the third place, further investigation into the hydrogel/sol-gel material is required. It needs to be done to make sure it does not damage the tissue of the heart. At last, the possibility to combine planar and optical fibre techniques in a sensor needs to be examined. It can be an advantage to place a hydrogel with a planar LED on the tissue and only use optical fibres to receive the information of the tissue. These recommendations were taken into consideration for setting the conditions for the sensor.

## 3.2. Conditions for the sensor

As result of the literature study, this thesis is focused on developing a pH-sensitive optical sensor based on fluorescence. This section describes the medical requirements, available resources, and selection criteria of the material which are taken into consideration for the development of the proof-of-concept sensor. Following this description, some state-of-the-art sensors are described and the first concepts are elaborated. To finish, a framework is described which is used to select the materials and techniques for the development of the sensor. The aforementioned requirements influence each other and that is why the framework was devised to choose the best combination for this research.

### 3.2.1. Medical Requirements

In consultation with cardio-thoracic surgeons of the Leiden University Medical Centre (LUMC), a list of requirements was synthesised which is shown in Table 3.3. These requirements were developed without any technological constraints and should give an understanding of what is wanted by the surgeons to help them during the surgery and what will improve the possibility of adaption by the surgeons. These requirements are set for the final design of the sensor, so it is accepted if the prototype does not meet these requirements. However, it should show enough potential to overcome the problems.

### 3.2.2. Resources Available

Now that the requirements and wishes for medical success are elaborated, it is necessary to evaluate the resources (costs, time, tools, devices, materials) available to set up the selection criteria and approach for the proof of concept. Different resources are discussed and their influence on the final criteria are given. As the goal of this thesis is to develop a proof of concept, the limitations lay in the complexity, time and devices needed. While time, cost, and materials are limitations because this research is only a thesis work.

- *Cost*: The availability of financial resources is limiting the development of the sensor. Many sensors found in the literature describe expensive processes or the use of expensive devices to fabricate the sensor. These options are not very attractive for proof-of-concept research. The ultimate sensor can definitely be expensive as this is a life saving application, but this sensor should fall in the budget of the department.
- *Time*: The second scarce resource is the time available for the research and development of the sensor. As this research is focused on selecting the right method for detecting myocardial ischaemia and making a proof-of-concept, limited time can be spent on selecting the method and material and on developing the proof of concept.
- *Knowledge*: As found in the literature, many sensors are based on difficult chemistry and need extensive processing steps. Chemistry is not the main background of the author, supervisors, or department and not the goal for this sensor. Many different combinations of hydro/sol-gels and indicators are described in the literature and can be interchanged in some cases [154, 156, 157, 28, 47, 71, 164]. This allows that the chemical knowledge needed to create a proof-of-concept sensor can be minimised as with further development this can be made more complex. However, the method and materials chosen should be able to be interchanged.

Requirement	Minimally	Optimally	Remarks
<i>Location</i>	3 sensors (in proximity of each coronary artery)	Complete 3D map under coronary sinus	As described in section 2.1.2 the cardioplegia is administered antegrade in the aortic root or in the ostia of the coronary artery. Minimally it is necessary that the ischaemia is measured distal of each of the coronary arteries. The ultimate goal would be to measure ischaemia all around the heart.
<i>Response time</i>	± 30 seconds	± 1 seconds	The faster the surgeon can react to the ischaemia, the better the tissue is preserved. The surgeon needs time to react to changes and therefore a response time of 30 seconds should be the aim of the sensor. Longer times will increase the risks for damaging the tissue.
<i>Installation time (placement on heart)</i>	Max. 5 minutes	<1 minute	The placement of the sensor will cost time, surgeons will counterwork the implementation if the installation of the sensors takes too long. The time is depended on the effectiveness, but installation times above 5 minutes can have negative consequences
<i>Time of use</i>	6 hours	48 hours	Open heart surgery usually takes between three to six hours. There are cases that a CPB is connected for more than 10 hours. However, six hours should be enough for most operations. The ultimate goal would be to keep the sensor in the heart for 48 hours to detect postoperative ischaemia.
<i>Size patch</i>	3x3 cm	<1x1 cm	When the sensor exists out of a sensitive patch, this patch should not be bigger than 9 cm <sup>2</sup> . Bigger patches will interfere with the accuracy and the ease of use. Smaller patches are better because of this
<i>Invasiveness</i>	Myocardia/Epicardia	Myocardia/Epicardia	Myocardia is the muscle tissue of the heart and the epicardia is the upper layer of this muscle tissue. It still needs to be determined on which layer the sensor would work the best.
<i>Transmission</i>	Cabled	Wireless	The surgical area is already narrow and many cables, tubes and catheters are limiting the surgical area. If it would be possible for the signal to be transmitted wirelessly it would be optimal, but it is not an essential requirement.
<i>Toxicity/ degradation</i>	Biocompatible 2x time of use	∞ Biocompatible	The sensor should not be toxic for the tissue because it is already very weak. The degradation of the sensor should be at least to 2x the planned use and would be optimal to be zero
<i>Sensing parameters</i>	Ischaemia in general	All different parameters related to ischaemia	The surgeons are interested in measuring the ischemia of the tissue. It is no requirement that the sensor measures pH, Lactate, O <sub>2</sub> or pCO <sub>2</sub> , but if it would be possible to measure all these parameters independently this would improve the outcomes and the possibilities for researching the effects.
<i>Reference sensors</i>	-	Intercostale muscle	To measure the changes in the heart it is relevant to have a reference sensor connected to other muscle tissue for example the intercostal muscle.
<b>pH specific requirements</b>			The surgeons do not require a pH sensor. They are just interested in the ischaemia of the tissue, however pH is chosen as the sensing parameter. Therefore the following requirements were made
<i>Measurement range pH</i>	6 - 7.5 (error 0,01)	5-8 (error 0,001)	pH in the body is in a range between 7.35-7.45. Values lower than 7 should be measured as this is when the tissue is at risk. For safety margin the minimal pH which should be measured is 6. The maximal pH value is less important for the surgeon
<i>Drift</i>	± 0,01 pH per hour	± 0,0001 pH per hour	Accuracy is very important in this type of sensing, because you do not want that the sensors start to drift and the surgery is halted. Therefore, only a small drift is wanted by the surgeons.
<i>Temperature drift</i>	± 0,01 pH per C	± 0,0001 pH per C	Temperatures can vary during the surgery. pH is depended on temperature as described in 2.2.2. These temperature changes need to be measured, but it is also necessary that these temperature changes can be corrected by the same factor during the surgery

Table 3.3: Description of different requirements set by the cardiac thoracic surgeons of Leiden University Medical Centre.

- *Devices:* Surface Plasmon Resonance and Raman Scattering are devices which enhance the complexity of the measurement. These devices have high purchase costs and are not available for this research. Gratings and Quantum Dots need specialised devices to be fabricated and are also not available for this research. However, the devices of the Else Kooi Lab are available for this research. These devices have the advantage that they are scalable for mass production and will not interfere with the end goal of the project. Additionally, all different kinds of spectrometers are available to test the sensors.
- *Materials:* All materials should be available for purchase or fabrication. The fewer materials needed will simplify the proof of concept but should not be at the expense of accuracy. Secondly, the materials used should be biocompatible as the devices will be implanted for hours inside of the body. The tissue should not be influenced by the sensor and the sensor should comply with the ISO 10993-1:2018.

### 3.2.3. State of the art sensors

Before a new design is developed, it is important to investigate what the current state of the art is in the scientific community and with what you need to compare the new sensor. It can also be of added value to see for the possibility to combine work and build on the knowledge already acquired. This section will describe the sensor developed by Wencel et al. [157], Gong et al. [53], Cattini et al. [24] and Presens. All sensors are published in the last three years and are the results of multiple research groups trying different methods.

Wencel et al. [157] designed a sensor using HPTS and a sol-gel consisting of ETEOS and GPTMS. The sensor used a 400  $\mu\text{m}$  multimode fibre with 37 cores. at the end of this fibre the sol-gel with encapsulated HPTS was coated. The achieved intensity ratio of maximal 4.0 at pH of 8.5 and a reaction time of 2 minutes. They even tested the sensor in vivo and showed an resolution of 0.0013 pH. However, this sensor is expensive and needs custom opto-electronics and advanced processing.

Gong et al. [53] describes an hydrogel-based sensor using two fluorophores (5(6)-FAM and Porphyrin) were Porphyrin was the insensitive indicator and 5(6)-FAM the sensitive pH indicator. The hydrogel was selected by combining different kinds of hydrogels at varying concentrations. Followed by selecting the one with the most potential. The achieved an response time of only 30 seconds and proved to detect the acidity of lung tumors in ex vivo measurements. The disadvantage of the sensor is that it is expensive and needs advanced processing, which would be hard to adapt for this work.

Finally Cattini et al. [24] developed a much simpler sensor for in-line blood pH measurements using HPTS encapsulated in microbeads in an hydrogel. They demonstrated that the sensor had an error of only a few thousands of pH over a 6h measurement. The advantage of the sensor was that the sensing part could be disposable and the electronics reusable. They clearly described the fabrication method which can be an advantage to other sensors.

pH sensors developed by Presens use the patented technology of Dual Lifetime Referencing. These sensor are used in determining pH in tumour micro environment and tissue engineering solutions. They have a micro sensor which can be used to measure pH in solutions and semisolids. They have a range between 5.5 and 8.5 and a resolution of 0.02 pH and an accuracy of 0.1 pH (with calibration). However, their sensors are very fragile and need special pH equipment.

For this research, it will try to develop a sensor which has the potential to compete with these sensors and be an added value to the scientific community. Secondly, these sensors are all designed with different applications in mind and this work will focus on myocardial ischaemia related pH changes.

### 3.2.4. Framework

To select the right method for producing and measuring pH, both the medical requirements and the available resources have to be taken into consideration. However, their weight for each of these considerations is different. Some criteria can be easily set, such as costs, devices, measurement range, and time of use. While others like material are depended on the process possibilities and the knowledge available. The following core criteria are used at the onset of the research to determine to which techniques and material proof-of-concept sensor is built. These criteria are then used to select different measuring techniques and materials (pH indicator and Support Matrix) which can be used for this application. These different techniques and materials are then evaluated and compared. As the materials used can not be used with different techniques, combining the results will lead to a method to fabricate a proof-of-concept sensor. The core criteria for a proof of concept sensor are that:

1. The prototype material needs to be bio-compatible
2. The prototype needs to be sensitive for pH between 6.5 and 8
3. The prototype needs an accuracy of at least 0.1 pH
4. The prototype cost should not exceed 1000 euro
5. The prototype needs to easily allow for remotely sensing
6. The prototype needs no complex chemistry for fabrication
7. The prototype needs no complex optical measurement technique
8. The prototype needs to handle interferences

#### *Approach*

The literature review described in Section 3.1 reviewed the possible optical options for sensing pH, following this outcome, the framework is set up to find and compare different fluorescent-based pH sensors. The first step is to evaluate the different measuring techniques as not all pH indicators and support matrices can be used for certain measuring techniques. All possible techniques should be evaluated on cost, difficulty, material/devices needed, and type of sensing. For the most promising outcome, the literature has to be evaluated to ensure the latest advancements are included in the comparison. Following this, an overview should be made of these methods and materials. Here the different methods found in the literature are compared on indicators, polymers, their potential, materials used, fabrication method, and pH sensing properties. Subsequently, the support matrices and pH indicators are elaborated. The final step is to compare the methods, which have the most potential, with the core criteria. Finally, this will result in an optical sensing technique and materials which will be used for the continuation of the project.

## 3.3. Result

This section will describe the outcome of the framework described in section 3.2.4. As every study has different goals, it was difficult to compare all different results with each other. By comparing the pros and cons of different studies, overviews were created. These overviews allow for combining a technique and materials which meet most of the requirements and allows for the development of a sensor despite the limited resources.

### 3.3.1. Selection of Optical Technique

The different fluorescent measurement techniques described in section 2.3.2 were compared on the ability to handle interferences, the expected costs, the difficulty of fabrication, and the material and devices needed. Of course, the techniques described can be applied in various applications and set-up, but this overview gives an overall description of the (dis)advantages of these technologies. Table 3.4 shows these criteria and ratings. Each criterium is rated from (--) to (++). The ability of handling interferences is rated an (--) when the technique has no option to prevent the results from interferences outside of the wanted signal. A (++) is rated when the technique can almost completely compensate for the interferences. The costs are rated on the same scale where (--) is rated when high costs are

expected and (++) is rated when the technique is expected to be inexpensive. The difficulty of using the techniques ranged from problematic (--) to straightforward (++) . Materials and devices needed are not only based on cost, but also the process steps needed and the availability of all necessary materials and devices. At last, the table shows if it is possible to use the techniques for planar or fibre-based sensors. The possibility to use the technique for both types has the preference as the future design is not yet fully excogitated.

Technique	Advantages	Disadvantages	Interferences	Costs	Difficulty	Material/ Devices	Planar/ Fibre
<i>Steady State Measurements</i>							
Absorptiometry	Relatively simple	Need for clear sensor material	--	++	++	+	Both, fibre only ATR
	Commonly used technique	Clear sample to prevent scattering					
	Can be used for optical fibre cladding	Not used for fluorescence Sensitive for interferences					
Reflectometry	Simple	Optical isolation layer advisable	-	++	++	+	Both
	Ratiometric sensing	Weak signal					
Luminescence intensity	Commonly used sensing	Scattering particles advisable	-	+	++	+	Both
	Used a lot in research.	Influenced by a lot of factors not only the concentration (see Section ??)					
	Known principle. Commercially available	Indicators with high quantum yield needed					
Dual-wavelength referencing	Less scattering	Still interferences of optical components	+	+	+	+	Both
	Less instrumental drift	Background fluorescence and dye bleaching					
	Less optical alignment interferences	More difficult than luminescence intensity					
<i>Time-Resolved Measurements</i>							
Luminescence decay time (TD-FD)	Independent of intensity fluctuations.	Expensive.	++	-	-	--	Both
	Very good in handling interferences.	Need for long life indicators.					
	Self referencing and sensitive	Complex					
Dual Lifetime Referencing (TD-FD)	Almost no interferences	Dyes needed with different lifetimes	++	+	-	+	Both
	Time or domain frequency.	More complex					
	Simple calibration. Precise	Metal Ligand Complex needed					
<i>Energy Transfers</i>							
FRET	Low cost instrumentation	Two dyes needed in close proximity of each other.	+	+	-	-	Both
Inner Filter Effect	No need for close proximity.	Not much information available.	n.a.	-	-	-	n.a.
	No influence on decay time	Mostly seen as unwanted effect of fluorescence spectroscopy.					
Fluorescence Quenching	Used in extreme sensing	Inadequate detection levels	n.a.	+	-	-	n.a.
PET	Speed and simplicity	More chemistry based	n.a.	+	-	-	n.a.
	Fast and reversible.	Inefficient for long wavelengths.					
	Thermodynamically favourable	More chemistry based					

Table 3.4: Overview of the different optical techniques and their (dis)advantages. Compared on four different aspects

### Energy Transfers

Besides steady-state measurements and time-resolved measurements described in section 2.5 the table also describes the techniques involving Energy Transfer. The Energy Transfer techniques were added in the comparison as multiple sensors described in the literature use these techniques.

First of all, Fröster Resonance Energy Transfer/Fluorescence Resonance Energy Transfer (FRET). FRET exists in two different types of dyes. One dye is pH responsive while the other normally not (can be possible). Photonic energy can be transferred from the first to the second dye. The emission band of the first dye overlaps with the excitation band of the second and as reaction the second dye will have an emission occurring. The ratio between these peaks can indicate the level of pH. FRET can also be used in combination with nanoparticles. The disadvantage is that it has to be clearly differentiated from the Inner Filter Effect [139].

Inner Filter Effect works by adding an extra dye which is pH independent which during photo-excitation emits fluorescence which interacts with the fluorophore. This working is often found with upconversion nanoparticles and quantum dots. In comparison to FRET, the indicator does not have to be in close proximity to the inert fluorophore. Inner Filter has no effect on the decay time.

In classical fluorescence quenching, a quencher, such as iodide, a metal ion, a nitro compound, or even the hydronium ion ( $H_3O^+$ ), quenches the fluorescence of a fluorophore or a particle. In other words, the photonic energy is no longer emitted by the quencher. Quenching may be static or dynamic. In the former case, the decay time remains unaffected, while in the latter case, it is reduced.

PET is an excited state electron transfer process where a photoexcited electron is transferred from the donor (receptor group) to the fluorophore. With respect to sensing, the PET caused by the unpaired electrons of amino or phenolate groups has received the most attention. Therefore, PET efficiency is high if the PET group is easily oxidised (readily loses an electron in the excited state) and the fluorophore is easily reduced.

### 3.3.2. Selection of pH Indicator

There are over 900 different fluorophores, which can be found [147]. Fluorophores.org shows that 37 of these fluorophores can be used as a pH indicator. This gives researchers in optical pH sensing many possibilities to select a pH indicator for their application. To narrow down these options, a selection is made between the pH indicators described in the literature. Table 3.5 shows the different indicators. HPTS, DHPDS, fluoresceins, 5(6)-FAM, and SNARF-DE are all phenolic luminophores based on photoinduced proton transfer (PIPT). While porphyrin, PET-rhodamines, and 4-ANI are aliphatic amines luminophores based on PET. As this research is mainly focused on optical pH sensing and not comparing chemistry-based principles, the selection of the pH indicator depends mostly on the ease of manufacturing a sensing layer with a pH indicator and which can be sensed easily. As well, the decision was made to select a combination of the support matrix and the indicator described in the literature to make sure this would not slow down the fabrication of the sensor. Therefore are the indicators evaluated in combination with the support matrix. The full sensor was rated on their potential, materials used, fabrication steps, and sensitivity to pH. Table 3.5 shows these ratings and (dis)advantages of the fourteen sensors found in the literature.

As all sensors were preselected, they are all capable of measuring the pH in the desired range and selectivity. Therefore, they are rated from (-) to (+++). A (+++) is given when the sensor satisfies the optimal criteria. The (++) is given when it is sufficient and (+) is okay. A rating of (-) is only given once because the processing steps were very complex.

### 3.3.3. Selection of Support Matrix

In the literature, two types of support matrices are mainly used. These are hydrogels and sol-gels. Hydrogels are described in section 2.6 and sol-gels is: "a wet chemical process that involves the formation of an inorganic colloidal suspension (sol) and gelation of the sol in a continuous liquid phase (gel) to form a three-dimensional network structure" [10].

Meng [97] describe the following advantages of sol-gels in comparison with hydrogels; Sol-gel material is chemically, photochemically, thermally, and mechanically stable, Sol-gel material is optically transparent (down to 250 nm), Sol-gel material is formed at low temperature and under mild chemical conditions, Sol-gel can be cast as various forms including monoliths, thin films, fibers, and powders.

However, this process is much more chemically complex and can make the process steps more difficult. As table 3.5 shows, indicators can be used with sol gels and with hydrogels. As using hydrogels will allow for a more iterative developing process and can be handled fairly easily, it can be a big advantage. Especially when it is possible to switch to a sol-gel later in the process.

### 3.3.4. Result

As sections, 3.3.2, 3.3.1 and 3.3.3 shows, selecting an optical technique depends on many factors and interconnects with the decision of the material. Keeping in mind that there are limited resources available, first an optical technique was chosen:

The decision was made to choose the Dual-Wavelength Referencing (Dual Wavelength Referencing (DWR)) as optical technique. This technique has as main advantages that it can cope with interferences and is a steady state measurement. This allows for much simpler instrumentation and makes testing

less difficult than Time Resolved or Energy Transfers. Another advantage is that it can be easily optimised to more complex materials if the fundamental of the technique works for the desired application.

Selecting the support matrix was dependable on the indicator, so secondly the indicator was chosen. As many indicators in table 3.5 need advanced chemical processing, the decision was made to use HPTS. This is a very known dye with well-known specifications and characteristics. This will make the processing easier and to validate the results with the literature. A disadvantage of HPTS is that it is prone to bleaching and displays strong sensitivity to ionic strength. The pKa of HPTS is 7.4, which is suitable for the wanted range. Mobilising HPTS can increase the pKa, depending on the charge of the support membrane [154]. When testing the HPTS, the influence of the ionic strength should be kept in mind.

For the support matrix, a decision was made not to use sol-gel because of the chemical processing and materials needed to fabricate the sol-gels. One of the most used and proven biocompatible hydrogels, which does not need activation is HydroMed D4. This hydrogel can be developed by dissolving the HydroMed D4 polymer in ethanol and mixing it with the indicator. A disadvantage is that the HPTS can not be mixed directly with the hydrogel, therefore an dye immobiliser has to be used. For this, an anion exchange resin is used. AmberChrom 1x8 is chosen as this is used in the literature by Kermis et al. [71] and Cattini et al. [24]. This does influence the sensitivity to ionic strength, but is a relatively simple method to immobilise the HPTS in the hydrogel.

Reference	Indicator	Support Matrix	Potential	Materials	Fabrication	pH	Assessment of potential	Fabrication method
Cattini et al	HPTS <sup>a</sup>	Hydromed D4	+++	+++	+++	++	Advantages: Relative simple hydrogel, clear instruction Optical lay-out described. Planar sensor Disadvantages: designed for use in In-Line monitoring of blood, Compensates influences of temperature	Described clearly
Wencel et al	HPTS <sup>a</sup>	ETEOS:GPTMS <sup>1</sup>	+++	+	++	+++	Advantages: Very good results, tested in vivo in tissue, optical fibre with no bending influences,minimal invasive, good long term stability. PEG coating tested Disadvantages: Use of Sol-Gel, multimode fiber, custom build optoelectronics, relative slow response time (2 min)	Described, but missing information
Gong et al	5(6)-FAM <sup>b</sup> Porphyrin	HBMA/DMAEA <sup>2</sup>	+++	++	++	++	Advantages: high speed, multiple combination of polymers tested, highest potential selected, tested in vivo in the lung, optical fiber Disadvantages: Expensive set up needed, dual referencing	Described, but missing information
Aigner et al	PET rhodamines	pHEMA <sup>3</sup> and silica gel	+++	++	+++	+	Advantages: use of PET rhodamines, tested with silica gels and polyHEMA, use of click chemistry, good fluorescence Disadvantages: not very high accuracy (0.2pH), not tested in vivo/vitro	Described
Choudary et al.	5(6)-FAM <sup>b</sup>	Silica microspheres with TAMRA <sup>4</sup>	+++	+	-	++	Advantages: tested in vivo, combined pH/O <sub>2</sub> measurements,accuracy (0.02 pH), instantaneous results, small sensor Disadvantages: Difficult fabrication, Expensive material	Described clearly
Kocincova et al	HPTS <sup>a</sup>	pHEMA microbeads	+++	++	+++	++	Advantages: multiple parameter sensor, use of pHEMA with HPTS Disadvantages: glass fibre optic, brittle, expensive set-up needed, slow response time	Described clearly
Tian et al	Fluorescein	pHEMA-co-PAM <sup>5</sup>	+++	+++	++	+	Advantages: different ratio of polymers compared, Polymeric based, cheap Disadvantages: read-out not described	Described clearly
Qi et al	4-ANI <sup>c</sup>	Hydromed D4	++	+++	+	++	Advantages: more controllable pKa through use of ionophores, large range, fast response time Disadvantages: More chemical approach, read-out set up not described,	Described, but missing information
Cui et al	CTAB-HPTS <sup>d</sup>	ETES:GLYMO <sup>6</sup>	++	+	++	++	Advantages: tapered optical fiber, small size, use of HPTS, fast response time, good accuracy (0.07) Disadvantages: fragile, difficult to reproduce, use of sol-gel	Described
Hakonen et al.	DHPDS <sup>e</sup>	Cellulose acetate	++	++	+	++	Advantages: accurate, ratiometric measurement, not clear if planar or fiber Disadvantages: slow, use of HPTS derivative, read-out not described	Described, but missing information
Hiruta et al	QD fluorescein rhodamine B	TEOS <sup>7</sup> Ph-TriEOS <sup>8</sup>	++	+	+	++	Advantages: combination of absorption and fluorescence. High durability with continuous light exposure, planar sensor Disadvantages: Difficult fabrication (Quantum Dots, sol-gel)	Described, but missing information
Borisov et al.	Cr-YAB <sup>f</sup> SNARF-DE <sup>9</sup>	Hydromed D4	++	++	++	+	Advantages: multiparameter sensor, set up described Disadvantages: pH not focus of sensor, expensive set up needed, high complexity	Described
Nivens et al	HPTS <sup>a</sup>	TEOS <sup>7</sup>	++	+	+	++	Advantages: multiparameter, good storability Disadvantages: sol-gel, poor accuracy, read out not described, older research	Described
Kermis et al	HPTS (MA-HPDS)	PEG-DA <sup>9</sup>	++	+++	++	+	Advantages: Relative simple material, tested in cuvette, HPTS analog which is easier polymerisable, sterilisable Disadvantages: low accuracy, older technique	Described

<sup>a</sup> 8-Hydroxypyrene-1,3,6-Trisulfonic Acid

<sup>b</sup> 5-(and-6)-Carboxyfluorescein

<sup>c</sup> 4-amino-1,8-naphthalimide

<sup>d</sup> Cetrimonium bromide

<sup>e</sup> 6,8-Dihydroxy-1,3-pyrenedisulfonic acid

<sup>f</sup> Chromium Yttrium Aluminum Borate

<sup>9</sup> Seminaphthorhodafloer decyl ester

<sup>1</sup> ethyltriethoxysilane:(3-glycidoxypropyl)trimethoxysilane

<sup>2</sup> hydroxybutyl methacrylate:Dimethylaminoethyl acrylate

<sup>3</sup> Polyhydroxyethylmethacrylate

<sup>4</sup> Carboxytetramethylrhodamine

<sup>5</sup> Polyacrylamide

<sup>6</sup> Ethyltriethoxysilane:glycidoxypropyltriethoxysilane

<sup>7</sup> tetraethylorthosilicate

<sup>8</sup> phenyltriethoxysilane

<sup>9</sup> Poly(ethylene glycol) diacrylate

Table 3.5: Indicators and Support Matrices found in literature

# 4

## Material and Methods

This chapter gives an overview of the materials and instrumentation used to develop all what is used in this work. Following this, the methods of developing the pH buffer, HPTS-microbeads, sensing layer, and different samples are elaborated. Subsequently, the different experiments are described and how the data is obtained and processed. All information needed to imitate the research can be found in this section

### 4.1. General Materials and Instrumentation

All materials and instrumentation used in this work are described in this section.

#### 4.1.1. Materials

The following chemicals were used for this work: 8-Hydroxypyrene-1,3,6-trisulfonic acid trisodium salt (HPTS, product no. H1529), AmberChrom® 1X8 chloride form, strongly basic, 200-400 mesh (Dowex 1X8, product no. 44340), Ethanol (product no. 443611), Sodium phosphate dibasic dihydrate (Na<sub>2</sub>HPO<sub>4</sub> · 2H<sub>2</sub>O, product no. 71643), Sodium Chloride 99.9% (NaCl, product no. S9888), Sodium Hydroxide 98% (NaOH, product no. S8045), Hydrochloric acid 37% (HCl, product no. 320331) were all obtained from Sigma Aldrich ([www.sigmaaldrich.com](http://www.sigmaaldrich.com)). pH buffer solutions with pH of 4, 7, 10 fabricated by Mercks ([www.mercks.com](http://www.mercks.com)) (product no. 1.09884.0001, 1.09887.0001, 1.09890.0001) were obtained via VWR ([www.vwr.com](http://www.vwr.com)). Hydromed D4 (product no. 100028) was purchased from AdvanSource Biomaterials Corp., USA ([www.advbiomaterials.com](http://www.advbiomaterials.com)). All materials are of analytical grade and used without any purification. 50 mL and 15 mL Centrifuge tubes (product no.) were obtained via VWR ([www.vwr.com](http://www.vwr.com))

#### 4.1.2. Instrumentation

##### *pH meter*

For measuring the pH of the samples, the Lab 850 was used in combination with the pH sensor N64. Both the sensor and the meter are fabricated by Schott Instruments Analytics ([www.sianalytics.com](http://www.sianalytics.com)). The pH meter Lab 850 was already owned by the department and the pH meter N64 was purchased via VWR ([www.vwr.com](http://www.vwr.com)). For measuring the temperature, a temperature probe was used. For creating the buffers, a microscale was used and a magnetic stirrer by Schott Instruments. A 200-1000 µL and a 10-100 µL pipette of VWR were used for precise pipetting.

##### *Optical examination*

For the optical examination of the samples, a Zeiss Microscope in combination with an optical camera is used. For the fluorescent examination, the Zeiss Axiovert 200M was used and the Thorlabs DC1656 CMOS. The Triax 1080 Monochromator is used for creating excitation light of certain wavelengths.

##### *Spectrometric measurements*

For measuring the transmittance and reflection, the Perkin Elmer Lambda 1050 is used. For the transmittance measurements, a lens was added in front of the sample to focus the light on the sample. For fluorescence measurements the Horiba Fluorlog 3 is used. The 3-22 configuration is used in this

research. For the reflection fibre measurements, the Avantes Starline is used in combination with the reflection probe FCR-7UVIR200-2-2.5×100. A UV5TZ-400-15 Bivar, UV LED and the luxeon LXHL-PB01 475nm LED are used for the excitation light.

## 4.2. Methods

This section elaborates the methods used to fabricate the different solutions and sensing layers.

### 4.2.1. Fabrication of pH buffers

For testing the influences of pH and Ionic Strength in total 40 different pH buffers were fabricated. Buffers were prepared by mixing a stock solution with different concentrations of sodium chloride and adjusting to the right pH with hydrochloric acid and sodium hydroxide. An acidic stock solution was prepared by mixing 2.3405 g  $\text{NaH}_2\text{PO}_4 \cdot 2\text{H}_2\text{O}$  in 1.5L of water. This results in a concentration of 1.2 g  $\text{NaH}_2\text{PO}_4$  per litre (0.06 g per 50 mL). The buffer calculator developed by Liverpool University was used to calculate the concentration of NaCl, Phosphate Buffer for the right pH and IS (<https://www.liverpool.ac.uk/pfg/Research/Tools/BufferCalc/Buffer.html>). Table 4.1 shows an overview of the concentration used.

Ionic Strenght	pH	6.2	6.6	7	7.4	7.8	8.2
100 mM	$\text{NaH}_2\text{PO}_4$ (g)	0.06	0.06	0.06	0.06	0.06	0.06
	NaCl (g)	0.2529	0.2427	0.2295	0.218	0.2109	0.2074
	$\text{H}_2\text{O}$ (mL) <sup>a</sup>	45	45	45	45	45	45
150 mM	$\text{NaH}_2\text{PO}_4$ (g)	0.06	0.06	0.06	0.06	0.06	0.06
	NaCl (g)	0.3984	0.3877	0.3744	0.3634	0.3568	0.3536
	$\text{H}_2\text{O}$ (mL) <sup>a</sup>	45	45	45	45	45	45
200 mM	$\text{NaH}_2\text{PO}_4$ (g)	0.06	0.06	0.06	0.06	0.06	0.06
	NaCl (g)	0.5441	0.5331	0.5198	0.5091	0.5028	0.4998
	$\text{H}_2\text{O}$ (mL) <sup>a</sup>	45	45	45	45	45	45

<sup>a</sup> after achieving the right pH the buffers were filled to 50mL with  $\text{H}_2\text{O}$  to achieve the right concentrations.

Table 4.1: Overview of different concentration used to fabricate different pH samples with different Ionic Strenghts

To achieve the buffers with the right pH and ionic strength, 45mL of  $\text{NaH}_2\text{PO}_4$  stock solution was poured into a 50 mL glass beaker. Using a magnetic stirrer, the concentration of NaCl was mixed into the stock solution. NaCl was weighted on the microscale for precise concentrations (figure 4.1a). The pH electrode and temperature sensor were inserted in the concentration (figure 4.1c). While the magnetic stirrer mixed at 100 rpm ((figure 4.1b), 0.01M HCl and 0.01M NaOH buffers were used to bring the buffer to the right concentration. Pipettes were used for controlled addition of the acid and base. Mostly NaOH was used as the stock solution was acidic. pH buffers were stored at room temperature in the dark. Every time a test was done, the pH of the buffer was checked (figure 4.1d). The full protocol of fabricating the pH buffers can be found in Appendix A.2

### 4.2.2. Fabrication of HPTS microbeads

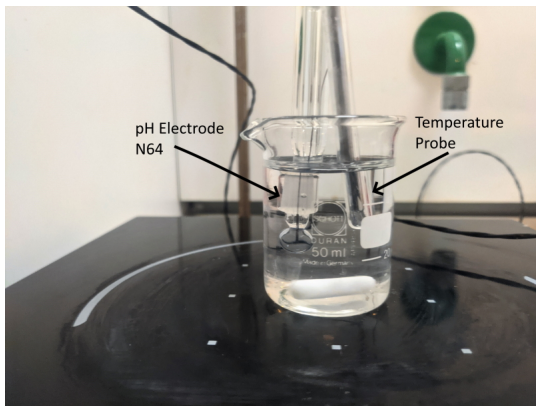
To test the properties of the HPTS loaded into the Amberchrom microbeads, these had to be fabricated. For this fabrication, three different samples were made, the first existing of 35 mg HPTS dissolved in 100 mL and the others of 70 mg and 105 mg in 100 mL demineralized water. This solvent was labelled compound 1 and was mixed with compound 2 existing of 10 g of microbeads in 10 mL of demineralised water. The two different concentrated mixtures were then mixed for 6h at 400 rpm (figure 4.2a). Following this, the mixtures were rested and 80 mL of clear water was extracted from the samples. After this, the samples were stored in a dark location. Before storage, the samples were centrifuged at 2000 rpm and the microbeads were extracted. To check the process, a small sample of microbeads were mixed with a solution of pH 6 and pH 8. If a visual difference was visible, the process went well and the loaded microbeads were ready to be stored (figure 4.2). The protocol for producing the HPTS



(a) Image of measuring the NaCl for the pH buffer



(b) Image of the magnetic stirrer used for mixing the buffer



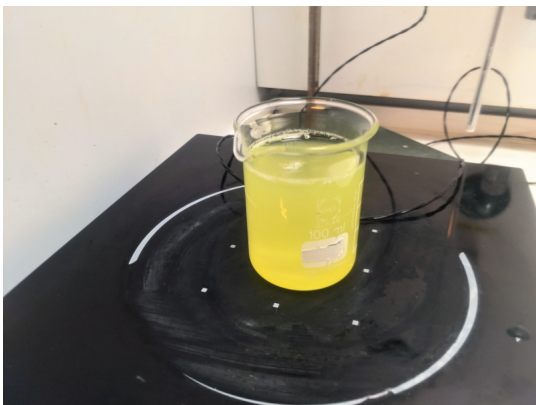
(c) Image of the pH electrode and the temperature probe in the buffer solution



(d) Image of the output of the Lab 850 pH meter

Figure 4.1: Images of the different process steps described in section 4.2.1

microbeads can be found in appendix A.2



(a) Image of the HPTS and Microbeads Mixture during the mixing stage



(b) Image of the microbeads in acidic (left) and basic (right) environment

Figure 4.2: Images of the HPTS-microbeads fabrication described in section 4.2.2

### 4.2.3. Fabrication of sensing layer

The final step of the fabrication of the sensor exists out of combining the HPTS microbeads with the hydromed D4 hydrogel. First, 1 gram of crushed hydromed D4, 1 mL of demineralised water, and 9

mL of ethanol (96%) were poured together and mixed for 6 hours until the hydromed D4 was fully dissolved into ethanol. Meanwhile, the water should be extracted from the HPTS microbeads. The HPTS microbeads were mixed with the hydrogel solution with the ratio of 1 ml of hydrogel to 350 mg of microbeads and stirred for one hour to ensure a good mixture. To create a sensing layer, a pipette was used to drop 0.1 mL of this mixture on microscopic glass slides of 10x15x1mm.

#### 4.2.4. Fabrication of different samples

##### *First batch of samples*

To examine the optical properties of the hydrogel and HPTS-microbeads, 8 different samples were fabricated, existing out of 2 samples per concentration level of HPTS. Three different concentrations of HPTS microbeads were produced and are depicted in table 4.2. One hydrogel solution was divided over

Sample	Hydromed D4	Microbeads	HPTS
A	1gr/10mL	-	
B	1gr/10mL	-	
C	1gr/10mL	1gr/1mL	105mg/ml
D	1gr/10mL	1gr/1mL	105mg/ml
E	1gr/10mL	1gr/1mL	70mg/ml
F	1gr/10mL	1gr/1mL	70mg/ml
G	1gr/10mL	1gr/1mL	35mg/ml
H	1gr/10mL	1gr/1mL	35mg/ml

Table 4.2: Concentrations of the sample mixtures used for the first optical experiments

four different beakers of which 3 with different HPTS-microbeads concentrations. The final solutions were mixed for one hour. Of all four solutions, two small doses were deposited on microscopic glasses (10x15mm). In total, 8 different samples were fabricated and dried in ambient temperature for 2 hours.

##### *Second batch of samples*

Second batch of samples were created with less HPTS and thinner layers for measurement with a fluorescent microscope. The same steps were followed as for the first batch except lower concentrations of HPTS were used and one sample without HPTS was fabricated as a reference, see table 4.3 To

Solution	Hydromed D4	Microbeads	HPTS
A	1gr/10mL	1gr/1mL	
B	1gr/10mL	1gr/1mL	3.5mg/ml
C	1gr/10mL	1gr/1mL	17.5 mg/ml
D	1gr/10mL	1gr/1mL	35 mg/ml

Table 4.3: Concentrations of the solutions used for the second optical experiments and fluorescent microscopy images

achieve thinner samples, the hydrogel solutions were diluted with 1mL of ethanol before pouring them in containers of 1mm height and a surgical knife was used to scrape off the excessive solution. Per solution (4.3) 6 different samples were made, so these could be used for the pH determinations.

### 4.3. Optical Experiments

During this research, multiple different experiments are done on different samples. Each subsection describes the equipment used and how it is used to obtain data on the samples.

#### 4.3.1. Optical examination

##### *Microscopic examination*

The first batch of samples described in section 4.2.4 were investigated under the Zeiss Microscope. In figure 5.1 the different samples are shown with different magnifications. The standard light source of the microscope was used for the optical images. A smartphone (Google Pixel 4a) was used to capture images of the samples. The images were taken with 10x, 25x, 50x, and 60x magnification.

#### CMOS camera examination of emission

The first batch of samples were examined for their fluorescent response at the wavelengths 405nm and 475nm and measured with the Thorlabs DC 1656 CMOS camera. The camera was positioned 2cm above a reflective mirror on which the samples are placed, see figure 5.2b. The TRIAX monochromator is used to excite the sample with specific wavelengths. The light of the monochromator is transferred to the sample through a slit optical fibre and aimed at the sample at an angle of 65 ° at a distance of 1 cm. The lightsource of the monochromator is powered by 21.3V and 10.6A and the entrance slit is set to 2 mm while the exit slit is set at 1 mm. The settings of the camera were set as followed: all gains = 1, fps = 1, pixel clock = 40 MHz, exposure time = 999.2 ms. The images were analysed in Image J by splitting the channels and determining the histogram values of the green channel on the sample.

#### Fluorescent Microscope examination

The second batch of samples are examined under the Zeiss Axiovert 200M. This is an inverted microscope with fluorescence filters. The different types available were (**DAPI-1160A** Excitation: 387/11; Emission: 447/60, **GFP-3035B** Excitation: 472/30; Emission: 520/35, **TX-RED4040B** Excitation: 562/40; Emission: 624/40, **CY5-4040A** Excitation: 628/40; Emission: 692/40 ), but only the GFP-3035B is of interest for the samples. The outcome is processed by the software included with the microscope. The disadvantage of this is that it was not possible to set the camera settings. The camera automatically corrected for white balance and contrast. Therefore, it is not possible to compare the values/histograms of the samples.

### 4.3.2. Spectrometer Analysis Experiments

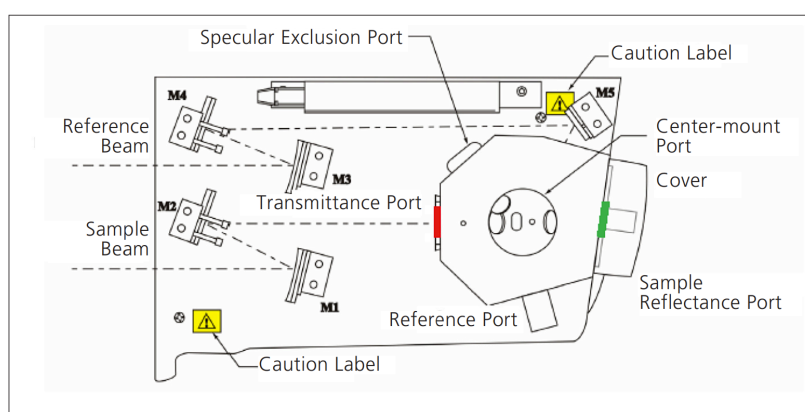


Figure 4.3: Picture of the 150 mm integrating sphere installed in a LAMBDA 1050+ with a top down view of the diagram of the sphere below. The red marked area is where transmission of the material is done, and the green area the reflectance of the material. Reprinted from [49]

#### Transmission measurements

The transmissions of the samples were measured with the LAMBDA 1050 spectrophotometer by Perkin Elmer. The range was set from 350 nm to 700 nm in steps of 5 nm and the wavelength was set at 1 nm. Normally, the set-up is used for reflection measurement, so a converging lens was put in front of the sample holder to focus the light straight at the sample. This lens created a focal area of around 25 mm<sup>2</sup>. Using the align function, a white light beam was projected on the focal area. The sample was placed in front of the entrance of the integrating sphere (red part figure 4.3). Therefore, all light going through the sample is detected by the sensor and allows for the measurement of the total transmittance. The light beam comes from a Tungsten Halogen light source and the specific wavelength is determined by a double monochromator set-up and a common beam depolarizer is used to correct for inherent instrument polarization. Before measuring the samples, a 0 and 100 % measurement were done to calibrate the system.

The samples were prepared by taping them to a microscopic glass, as they do not stick to the glass

when the sample is wet. The samples were submerged for 5 minutes in the prepared pH buffers discussed in section 4.2.1. After 5 minutes, the samples are taken out of the buffer solution. They are dried with cleanroom wipes to get rid of water on the samples. Following this, the samples were placed in the sample holder of the spectrophotometer and aligned correctly using the white light beam. When the samples were correctly placed, the lid was closed and the measurement would run. For each type of sample described in section 4.2.4 these steps are repeated for the six different pH buffers with the ionic strength of 150 mM described in section 4.2.1. An ionic strength of 150mM were selected as this matches with the physical ionic strength of the body and the resources were not available to test all different ionic strengths.

#### *Reflection measurements*

The reflections of the samples were measured with the LAMBDA 1050 spectrophotometer. The range was set from 350 nm to 700 nm in steps of 5 nm and the wavelength was set at 1 nm. The samples are placed at the exit of the integrated sphere to detect the total reflection of the sample (green part figure 4.3). The focal area of the light is set around 25 mm<sup>2</sup> with the use of slits. The same samples as in the transmission measurements are used and as in the transmission experiments, they are submerged in the 150 mM pH buffer for 5 minutes before they are dried and placed into the sample holder. The align function of the spectrophotometer is used to check if the sample is placed correctly at the focal area of the light.

#### *Fluorescence Spectrometer*

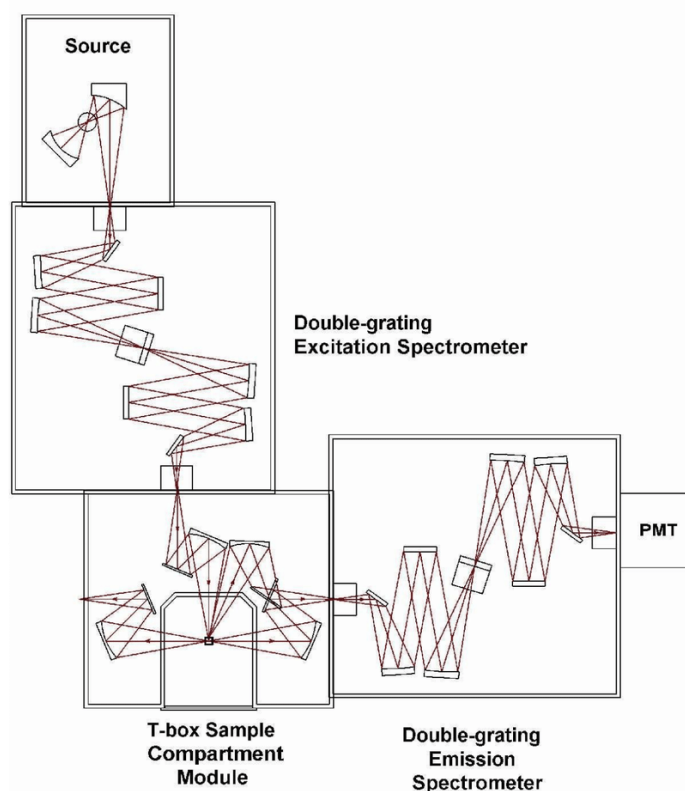


Figure 4.4: Schematic representation of the fluorescence spectrophotometer Fluorolog 3 model FL3-22 from Horiba Scientific used for fluorescence spectrometry. Reprinted from horiba.com

The fluorescence spectra of the samples were measured using the Horiba Fluorolog 3. Fluorolog®-3 modular spectrofluorometer, developed by Jobin Yvon. Fluorolog®-3 delivers the ultimate in sensitivity, speed, and automation for all types of steady-state fluorescence research. Fluorolog®-3 is completely computer-controlled and delivers high-quality fluorescence data throughout the ultraviolet, visible, and near-IR regions of the electromagnetic spectrum. For these measurements the FL3-22 configuration is used. In this configuration, the light from a 450 W Xenon arc lamp passed through two monochromators

to achieve an excitation light of a specific wavelength. This light comes in contact with the sample in the sample chamber at an angle of 45 degrees. The fluorescent response is measured at 90 °angle of the excitation light. The fluorescent response first goes through two monochromators for measuring the light at a single wavelength. This measuring was done with a Photo Multiplier Tube (PMT).

For the measurements the samples were excited with light from 350-500nm, and the emissions were measured from 350-600 nm. A entrance and exit slit of 1nm were chosen and the PMT was powered to 1350V to achieve the wanted accuracy. The corrected and scaled outcomes from the system were exported to .CSV files to be analysed with MATLAB. As with the reflection and absorption measurements, the samples were submerged for 5 minutes in the 150mM pH solution before measurement. Before the samples are placed in the Fluorlog, they were dried to get rid of the influence of water. The full spectrum light is used to align the sample in the chamber.

#### *USB Spectrometer with reflection probe*

Following the recipe of Sample C, new samples are fabricated. The samples are placed inside the 100 um pipettips. The pipettips are fitted with the reflection fibre (type) of Avantes. Three different thicknesses are fabricated to investigate the transition times. These layers have a thickness of 0.5mm and 1 mm. The output is measured by the Avantes Starline. The excitation light comes from an Luxeon LH-LB01 blue emitter. The light from the Light Emitting Diode (LED) is focused inside of a 0.5 inch tube with a converging lens and SMA adapter. This light is focused on the tip of the 6 fibres of the reflection probe. The measuring fibre is connected to the Avantes Spectrometer, as illustrated in figure 4.5. Using the Avasoft 8 software, the spectra are measured with different specifications.

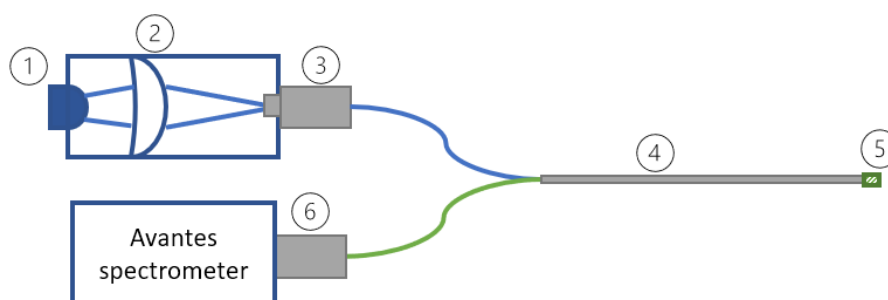


Figure 4.5: Schematic representation of the set up with the 475nm LED and the Avantes Starline USB spectrometer

The first test was to determine the differences between voltage, pH and thickness. For this measurement, the probe is fitted with a layer and doped into the buffer solutions. After 3 minutes, a measurement is done at 5 different amperes through the LED (100, 150, 200, 300, 350mA). These measurements are done in buffer solution with varying ionic strengths IS (100mM, 150mM, and 200mM). The second experiment was imaging the spectrum over the full pH range. To ensure that the samples reach an equilibrium, the reflection fibre is placed inside of the buffer sample for 20 minutes before measuring the output. As a third experiment, the transition time is measured for the layers, during this experiment, the probe was first doped into an extreme pH buffer (low or high) and then transferred to the other extreme. Just before this transfer, the LED and spectrometer are turned on to measure the output. The output is saved every 10 seconds and to preserve the LED 300mA is used and the temperature is checked using a thermometer.

## 4.4. Analysing Data

To analyse the data obtained from the optical experiments, the data needs to be processed. This section describes how the data is processed and which steps are done to describe the optical characteristics of the samples.

#### 4.4.1. Determining pKa of the HPTS microbeads

The overall absorbance  $A$  measured by the spectrometer exists out of the absorbance of the cuvette, the HPTS-microbeads, and the buffer solution:

$$A_{\text{overall}} = A_{\text{cuvette}} + A_{\text{HPTS-microbeads}} + A_{\text{buffer}} \quad (4.1)$$

$A_{\text{HPTS-microbeads}}$  exists out of the indicator HPTS and the anion exchange microbeads. The  $A_{\text{HPTS}}$  at a wavelength  $\lambda_1$  exist out of the indicator in acidic form (HIn) and basic form (In<sup>-</sup>):

$$A(\lambda_1) = A(\lambda_1)_{\text{HIn}} + A(\lambda_1)_{\text{In}} \quad (4.2)$$

pKa is described in section 2.2.1 and the determining the pKa is based and the following formula:

$$\text{p}K_a = \text{pH} + \log \frac{(A_x - A_b)}{(A_a - A_x)} \quad (4.3)$$

This is derived from the following formula:

$$\text{p}K_a = \text{pH} - \log \left( \frac{[\text{In}^-]}{[\text{HIn}]} \right) \quad (4.4)$$

For these measurements, extreme values are needed to give accurate pKa values

##### *Numerical pKa determination*

Weidgans [154] describes using the Boltzmann function to estimate the pKa by curve fitting a sigmoid function to the output of the measurements. This Boltzmann function is as follows:

$$\text{pH}(R_{475/405}) = \frac{a - b}{1 + e^{(R_{475/405} - c)/d}} + b \quad (4.5)$$

where  $a$ ,  $b$ ,  $c$ , and  $d$  are empirical parameters describing the initial value ( $a$ ), final value ( $b$ ), center ( $c$ ) and the width of the fitting curve ( $d$ ).  $R_{475/405}$  is the scaled value of the emission wavelength, divided by the ratio between the dual reference wavelengths (see equation 4.7). Using sigmoid functions to determine pKa is common in chemical engineering as described in section 2.5.3 [122, 25].

HPTS has a pKa of 7.30 in 0.066 M phosphate buffers at 22 C [139]. As described in section 2.2.2 there are many factors which influence pH. These same factors have influence on the pKa of a sensor. Factors such as ionic strength and the dielectric constant of the surrounding medium have a large impact on the sensor. In this research, it is necessary to determine the pKa of each sample as different concentrations and thicknesses are used.

#### 4.4.2. CMOS Imaging Processing

The images obtained by the Thorlabs camera are processed in ImageJ. First, the channels of the images are split. Because the interest lays in the green channel, only the green channel is used for the examination. From the green channel, a histogram is made and the mean values, minimum, maximum, and intensity densities are extracted from the full image and a small section. These values are compared per sample and different pH. The ratio of the intensity per area at the wavelength of 475nm is divided by the ratio of the intensity per area at the wavelength of 405nm:

$$R = \frac{\text{Intensity green channel 475nm per area}}{\text{Intensity green channel 405nm per area}} \quad (4.6)$$

These ratios are then plotted against pH to investigate if there is a relation between the ratios and pH.

#### 4.4.3. Reflection Measurements

The data obtained from the Perkin Elmer Lambda 1050 is imported into MATLAB. Here, the sample data is corrected by extracting the background and glass sample from the data. After this, the images are compared and the ratios between the first and last values are compared as well as the values between 405nm and 465nm. 465nm is chosen because a preliminary test showed that the reflection of the samples is the highest at 465nm. Finally, the samples are scaled to the value at 405 nm and compared.

#### 4.4.4. Transmission Measurements

The data obtained from the Perkin Elmer Lambda 1050 is imported into MATLAB. Here, the sample data is corrected by extracting the background and glass sample from the data. Following this, the images are compared and the ratios between 405 and 475nm are compared. At the wavelength of 475nm, the differences between the pH are most distinct. After this comparison, the data is divided by the value measured at 405 nm to scale the data for the ratiometric measurements

#### 4.4.5. Absorption Measurements

For the absorption measurement, the same data of the transmission measurements is used. This data is converted to absorption following the Beer's Law:

$$A_{\lambda} = -\log T = -\log\left(\frac{I}{I_0}\right) = 2 - \log(\%T) \quad (2.18 \text{ revisited})$$

After this conversion, the same steps as with the transmission measurements are done to analyse the data.

#### 4.4.6. Fluorescence Measurements

The numerical data obtained from the Horiba Fluorlog 3 is imported into MATLAB. Here, 3D surface graphs are constructed. Following this, the right wavelength is chosen by examining the fluorescence response at the emission wavelengths between 500-600nm and the excitation wavelength 350-500nm. The most dominant differences between the 405 and 475nm wavelengths are then further analysed and scaled to the value at 405nm. The ratios between emissions measured at excitation by 405nm and 475nm are plotted against the pH values.

$$R_{475/405}(i, \text{pH}) = \frac{P(i, \lambda_{em}, \lambda_{ex_2}, \text{pH})}{P(i, \lambda_{em}, \lambda_{ex_1}, \text{pH})} \quad (4.7)$$

For  $\lambda_{em}$  525nm is used and for  $\lambda_{ex_1}$  and  $\lambda_{ex_2}$  405nm and 475nm are used. Following this, a sigmoid Boltzmann function is fitted to these data points as described in section 4.4.1

$$\text{pH}(R_{475/405}) = \frac{a - b}{1 + e^{(R_{475/405} - c)/d}} + b \quad (4.8)$$

Using the line fitting tool supplied by MATLAB, the coefficients are estimated. These coefficients are used to plot the estimated function of pH for each ratio. From this line, a derivative is plotted to show the sensitivity  $\eta$  by function `estimatepKa.m` Appendix A.18 A.17.

$$\eta = \frac{\partial R}{\partial \text{pH}} \quad (4.9)$$

To determine the pKa of the sensor, a derivative is taken from the sensitivity. The pKa is when the second derivative is equal to zero:

$$\text{pK}_a = \text{pH} : \frac{\partial^2 R}{\partial^2 \text{pH}} = 0 \quad (4.10)$$

#### 4.4.7. Reflection Probe

The data, which was obtained from the Avantes Starline Spectrometer, was outputted to Excel files. These files are loaded into MATLAB. For all measurements, the spectral output is scaled to the value at 475nm. For plotting the Ionic Strength and pH sensitivity, the scaled value at 525nm is divided by the value at 475nm. This relation is used to correlate with the pH value of the solutions with the MATLAB function `estimatepKa.m` Appendix A.18 A.17



# 5

## Results

The goal of this thesis is to give an overview of the possibilities to measure myocardial ischaemia with optical-based sensors and to create a proof of concept. The possibilities are described in Chapter 3 and this chapter gives the results of the experiments done to test the HPTS-HydroMed D4 sensing layer. As no previous work on this type of sensing was done at the faculty, many experiments were done to characterise the materials and to test different concentrations and thicknesses. Multiple sensing layer samples are created so each time the findings of the measurements could be used for the next measurements. Using this method, an optimal combination of dye concentration, hydrogel concentration, microbeads, and thickness is derived, which is used in the final proof-of-concept sensor. This chapter exists out of 4 sections, each describing a step towards a proof-of-concept sensor.

The first section describes the measurements done to fabricate the first sensor, get used to the processing steps and to test the first assumptions. The second section describes the measurements done to fully investigate the optical properties of the sensing layers created. In this section, different concentrations and different thicknesses are fully analysed. On the basis of these results, measurements with a reflection probe were developed and are described in Section 5.3. The last section describes the proof-of-concept sensor results. This sensor is the final product of the thesis, and is combining all findings of this thesis into a final product.

### 5.1. First batch of samples

This section describes all information related to the results of the first batch of samples. A brief explanation is given on what the goal of this batch is and how they are fabricated. Following this, an explanation per experiment is given and then the results of the experiments are described. Finally, this section describes the analysis of these results and what the consequences are for the next batch.

#### 5.1.1. Goal of first batch

The first batch were created with the goal to get familiar with the fabrication method, to test different concentrations of dye in the microbeads, to have a first optical investigation on the samples under a microscope, to see how the samples can be stored the best and investigate the potential to use a CMOS camera as a detector for the fluorescence. Different concentrations of the fluorescent dye HPTS were mixed in the microbeads to investigate if these differences could be detected. Besides 3 different concentrations a sample was created existing only out of the hydrogel. This sample was created to have a reference sample and to see what characteristics of the sole hydrogel are.

##### *Fabrication of first batch*

The fabrication steps of the HPTS-microbeads are described in section 4.2.2 and the full batch of first sensing layers in 4.2.4. The difference between the samples is the concentration. Samples A and B are only Hydromed D4 dried at room temperature, while samples C to H had microbeads which were mixed with different concentrations of HPTS in water. Two samples of each mixture were developed to investigate if the two samples give comparable results.

### 5.1.2. Experiment first batch

To investigate the characteristics of the first batch, an optical investigation is used to evaluate the difference between the concentration and the reference samples. Other experiments done in preparation for the next samples are storage and transition time (between basic and acid solutions). At last, the samples are tested on their ratiometric capabilities, using a set-up existing out of a monochromator and a CMOS camera. This method is tested to see if this method can be used in for future experiments.

#### *Optical investigation*

Besides the optical investigation with the eye, a simple microscope was used to evaluate the difference of the samples. The results found by the microscope will tell if the second batch will need more or less microbeads/HPTS/hydrogels.

#### *Storage*

A side experiment was done on the first batch on how to store the samples. Literature describes that the samples are dried and after this stored wet. For each of the different concentration samples, one was stored dry and one was stored wet.

#### *Transition Time*

To investigate if the sensor layers show potential to be used inside of the body, a preliminary test was done to check how long the samples took to transition from no fluorescence to maximal fluorescence and back. This experiment indicates if the next samples should be thicker or thinner.

#### *Dual wavelength referencing*

To test the dual wavelength referencing possibilities of the HPTS-microbeads, a set-up was developed consisting of a CMOS and a monochromator. The set-up is illustrated in figure 5.2b. To first see the difference between the pH and fluorescence, a drop of pH 6.2 solution and a drop of pH 8.2 were dropped on the samples. This difference should show the ability to use this sensing layer for the proof of concept sensor and to compensate for the different interferences. Following this first test, all samples are doped into a solution of the highest and lowest pH and the output is measured by a CMOS camera. The idea is that using the green channel of the CMOS, the differences in fluorescent output can be measured.

### 5.1.3. Results Experiments

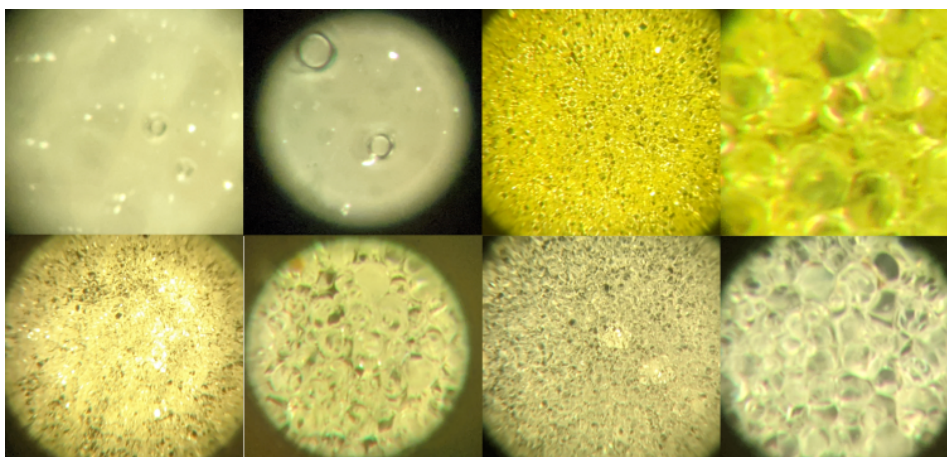


Figure 5.1: Optical Investigation of Sample A, C, E and G under Zeiss Microscope with 5-25x magnification

The first batch of samples is fabricated following the steps in section 4.2.4. All samples are relatively thick (+ 2mm) and have high concentration microbeads. The samples were stored dry and had a frail appearance. However, all samples were relatively elastic. The elasticity is increase when they were doped with water. All samples showed a yellow glow, samples C and D showed the most present yellow colour, while G and H the least. When the samples were dried after they had been soaked in water, they became much more fragile and broke more easier. As the samples were quite thick, the transition time from low to high pH was long (+20 minutes).

### Optical investigation

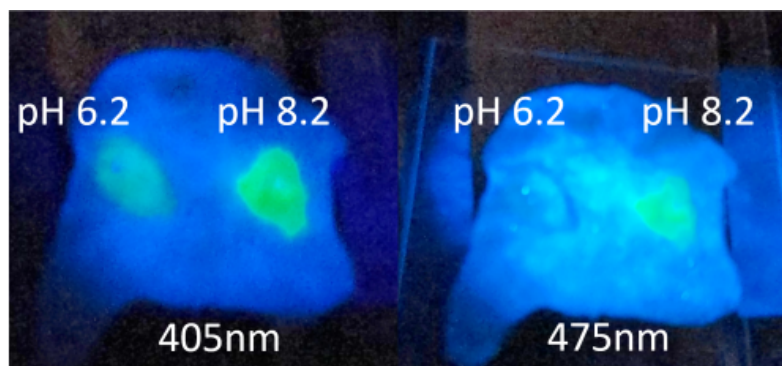
The samples under the microscope show that sample C has a much more yellow colour in comparison to the other samples. The sample A has no microbeads and this is clearly visible in the images. The thickness of the samples is clearly visible as there are multiple layers visible. The microbeads are quite consistent in size, but it is hard to distinguish between the different microbeads as there are so many of them. These images are taken from the dry samples. This is visible in the crystallic structure of the microbeads.

### Storage and transition time

Storage of the samples gave better results when stored wet instead of dried. The dried stored sample became brittle after each use and showed more cristalic microbeads in comparison to the wet samples. Another disadvantage of the dried samples is that each time the sample got wet, the sample increased in size. This was expected as hydromed D4 is a hydrogel that can take up to 40% of water. However, the disadvantage of this is that the sample curls up every time it gets wet. This causes that it is more difficult to excite the sample with proportionate light. The transition time of the samples was long (25+ minutes, one way). This can be caused by the thickness of the samples and the high amount of microbeads.

### CMOS and monochromator

Analysing the data obtained by the Thorlabs camera was done following the steps described in section 4.3.1. This resulted in the following figure 5.3, the other figures can be found in Appendix A.7. In the graph, it is clear that there is no relation visible between the pixel intensity of the green channel and the pH value of the sample. Sample E shows an increasing line with a dip at the end, while other samples gave similar incoherent results (see Appendix A.7). While the differences were visible to the naked eye, it was not possible to extract this with a CMOS camera in combination with the monochromator. All samples had higher concentrations than found in the literature, which could lead to oversaturation of the microbeads (section 2.5.1) or a large influence on Nernst Equation (equation 2.17 in section 2.2.2) by the fluorescent dye. No differences were found using different ionic strength buffer solutions (50 mM, 100mM, 150m, and 200mM). It was important to set all the settings the same for all measurements as the auto gain and white balance of the camera could lead to different outputs.



(a) Sample E of first batch with drop of solution with pH6.2 and pH8.2 at excited at wavelength 405nm and 475nm with TRIAX monochromator



(b) Set up with Thorlabs camera, a sample and the silicon Mirror

Figure 5.2: Images related to the first experiments with CMOS and first batch of Samples

Another observation during the measurements was that small shifts in the set-up led to different outputs of light (intensity and colour), as the connector of the fibre and monochromator had a small amount of slack. It was also not clear which wavelengths were passed through the slit of the monochromator.

### 5.1.4. Analysis of first batch

Combining the results of the experiments of the first batch, the following analysis can be made. First, that a lower concentration of HPTS should be used in the samples. The samples showed that they could be over saturated and as described in the theoretical background, this can influence the measurements. Secondly, samples with different thicknesses should be made to test the influence of the thickness and density of the microbeads on the results. The reference hydrogel without any microbeads was

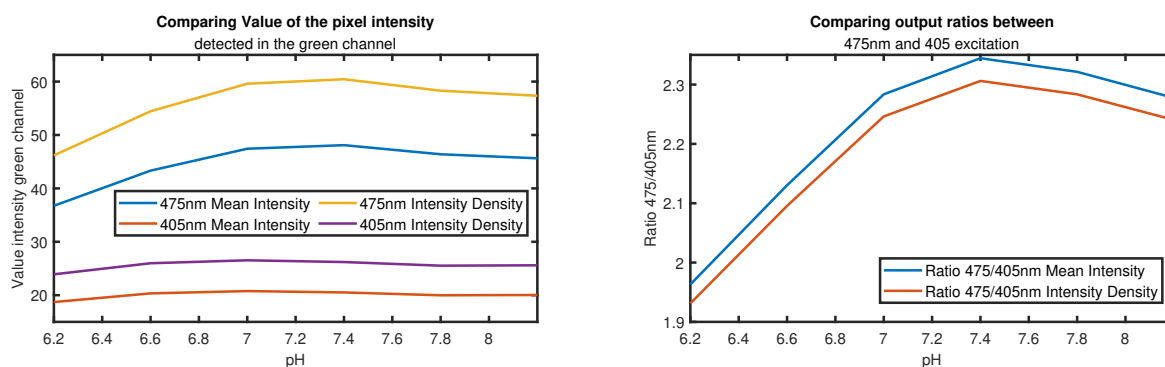


Figure 5.3: The scaled output of the green channel of the thorlabs CMOS camera of Sample E

not a good reference sample, as the microbeads take up almost the full sample and the hydrogel is solely the connecting material. Therefore, the next sample should have a reference sample with unloaded microbeads. The optical investigation does not say anything on the fluorescent and therefore the next samples should be fully characterised optically. Absorption, reflection, and fluorescence should be investigated off different samples. In addition, a fluorescent microscope will tell much more about the loaded microbeads instead of the normal microscope.

#### Interim Conclusions:

- Concentration of the dye in the sample shows a strong influence on the measurements and properties
- Samples can be stored dry, but after contact with water they need to stay moist
- Thick samples have a slow transition time and absorb a lot of light.
- Using a CMOS camera in combination with a monochromator does not show a lot of potential for the proof-of-concept sensor.

## 5.2. Second batch of samples

This section describes all information related to the results of the second batch of samples. These samples are created with the outcome of the first batch in mind and try to further characterise the optical hydrogel. A brief explanation is given on what the goal of this batch is and how they are fabricated. Following this, an explanation per experiment is given and then the results of the experiments are described. Finally, this section describes the analysis of these results and what the consequences are for the next batch

### 5.2.1. Goal of second batch

The second batch of samples were created with the goal to process the findings of the first batch and to optimize the concentration, thickness, and density of the samples. First, the samples are investigated by the eye and with a fluorescent microscope. This will make the differences between the samples clear. Following this, different spectrophotometric measurements are done to characterise the 4 samples. The outcome of these measurements can be used to measure the pKa and the sensitivity of the sensors. As with the first batch, the transition time of the samples is measured. The first sample is a reference sample without any HPTS and the others have increasing concentrations of HPTS. However, the concentration of HPTS is much lower than in the first batch to overcome the saturation.

#### *Fabrication of second batch*

The fabrication steps of the HPTS-microbeads are described in section 4.2.4. The difference between the samples is the concentration of HPTS. Sample A has no HPTS in the microbeads, but followed the same steps. Sample B had the concentration of HPTS described in the literature as well as sample D.

Sample C was chosen as it is the middle between the two described concentrations in the literature. Per concentration, multiple samples were created by using plastic molds of different sizes.

### 5.2.2. Experiment second batch

As with the first batch, an optical investigation of the samples is done. This to investigate the topology of the samples. This time the samples are investigated under a fluorescence microscope. This will make the differences between the samples more clear. Following this, the optical properties are investigated with the use of two types of spectrophotometers (Transmission/reflection and fluorescence). Finally, the pKa and sensitivity of the different samples are calculated based on the results of the fluorescence spectrophotometry. This will describe which concentration is the best for the proof of concept sensor.

#### *Optical investigation*

Next to the investigation by the eye, a fluorescent microscope was used to evaluate the differences between the samples. The results will show if the differences in thickness and concentration are visible. While under the fluorescent microscope, a droplet with a pH of 6.2 and 8.2 are placed on the sensor to measure the differences.

#### *Spectrophotometry*

First, all samples are tested on their reflection using a spectrophotometer. Following this is the transmission measurements. The transmission can be converted to absorption of the samples. Different concentrations and thicknesses will influence the absorption of the results. For both measurements the same spectrophotometer is used, but the sample is placed at different locations. This spectrometer can only change the excitation wavelength and measures all photons emitted. Thus, these measurements do not give information on the emission wavelengths. To investigate this, a fluorescent spectrophotometer is used. In the machine, both the excitation and emission wavelengths can be independently measured. This measurement can be used to find the best emission wavelength were the differences between the dual wavelengths of the HPTS are the best for the proof-of-concept sensor.

#### *Sensitivity & Response times*

Using the measurements of the two spectrophotometers, the pKa value and the sensitivity of the sensing layers can be determined. This will help to figure what the optimal thickness and concentration is for the proof-of-concept sensor. Finally, the response time of the different samples is measured as this is an important factor for the final design.

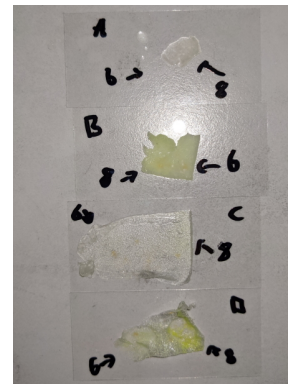
### 5.2.3. Results Experiments

Inspecting the samples, it was clear that there are big differences between the samples. The differences are visible to the naked eye as figure 5.4 shows. *Sample A* can be described as thick, rigid, and opaque. The sample has a thickness of around 0.5mm and many microbeads are visible. Due to the mold used for the sample, the size is quite small and compact. There is not colour visible in normal conditions and inspected with the eye. *Sample B* has a comparable structure as sample A. However, the size is larger because of the mold used and the a yellow/green colour is visible to the eye. The sample is relatively thick and therefore it is not possible to watch through the sample. This thickness causes a rigidity which is comparable to Sample A. *Sample C* is much thinner than samples A and B, therefore also more elastic. In this sample, single microbeads are visible and in some parts just the hydrogel. As a result, the sample is much more transparent, and the colour difference is more local (where the microbeads are). The overall size of the sample is also larger. *Sample D* is much more comparable to sample C than A and B. This sample has a larger size, is more elastic, more transparent, and single microbeads are visible. The difference with sample C is that the colour differences are better visible to the eye.

Unfortunately, this batch did not result in consistent samples, while the process steps were kept constant. The only difference was the mold used to create the sample as there were only two larger moulds and two smaller. This led that the larger moulds are more spread out and thinner, while the smaller moulds led to thicker samples.



(a) Sample D in sample holder of Fluorescent microscope with pH 6 drop on the left and pH 8 drop on the right

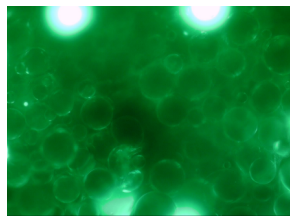


(b) Comparison of the samples with pH drops on both sides

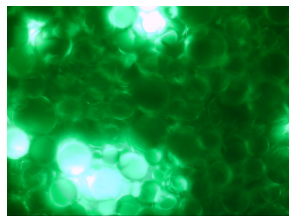
Figure 5.4: Samples in preparation of the fluorescent microscope

### Optical investigation

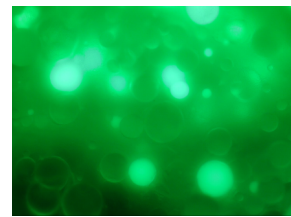
In figure 5.5 the different samples are shown under the Zeiss fluorescent microscope. As the camera of the microscope was automatically controlled, so the intensity differences can not be explained by the pH values. The filter used in this image is the GFP-3035B, with an excitation filter of 472/30 and an emission filter of 520/35. Therefore, in theory, the values with an higher pH should show more fluorescence. As described above, Sample A was fabricated without any HPTS in the microbeads. However, on the images from the fluorescent microscope, there are some microbeads visible with fluorescence. This shows that there has been contamination in the process. Furthermore, it is visible that there is a thick



(a) Sample A at pH 6.2 under fluorescence microscope 20x magnification



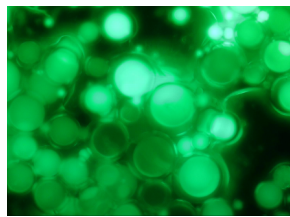
(b) Sample A at pH 8.2 under fluorescence microscope 20x magnification



(c) Sample B at pH 6.2 under fluorescence microscope 20x magnification



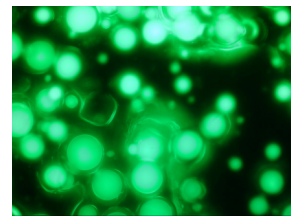
(d) Sample B at pH 8.2 under fluorescence microscope 20x magnification



(e) Sample C at pH 6.2 under fluorescence microscope 20x magnification



(f) Sample C at pH 8.2 under fluorescence microscope 20x magnification



(g) Sample D at pH 6.2 under fluorescence microscope 20x magnification



(h) Sample D at pH 8.2 under fluorescence microscope 20x magnification

Figure 5.5: Sample of second batch under fluorescence microscope with GFP filter and 20x magnification

layer of microbeads as there is no black background visible and the microscope is not fully focused on all microbeads. This corresponds to the images of the sample. The manufacture of the microbeads describes that they have a size of 200-400 mesh, which is 37 to 75 microns. In all samples these size differences are visible. Sample B shows more microbeads with fluorescence than Sample A but less than C and D. The thicker layer is clearly present in the microscopic images, visible in figure 5.5e. Sample C shows that almost all microbeads are filled with fluorescence. As this sample has a much thinner layer, the background is visible and all different sizes of the microbeads. Sample D shows that all microbeads are filled with fluorescence and the background is visible thanks to the thin thickness of the sample.

### Reflection

Figure 5.6 gives an example of the (un)scaled measured reflection by the lambda spectrophotometer and the results of all different samples per pH. The full reflection results of all samples can be found in Appendix A.8, figure A.5 shows the unscaled reflection measurements, and figure A.4 the scaled reflection. The glass slide on which the samples were pinned had a background reflection of around 8-10%, therefore the values of the glass slide are subtracted from the data obtained per sample. In Sample A, there is only a small bump visible at 405 nm. In Samples B, and D there is a significant increase visible at excitation wavelengths lower than 420nm. However, there are differences between Samples B and C/D. In samples C and D, there is an increasing reflection when the values of excitation wavelengths is lower. While in sample B there is a small decrease between 420-500 with a peak at 475nm.

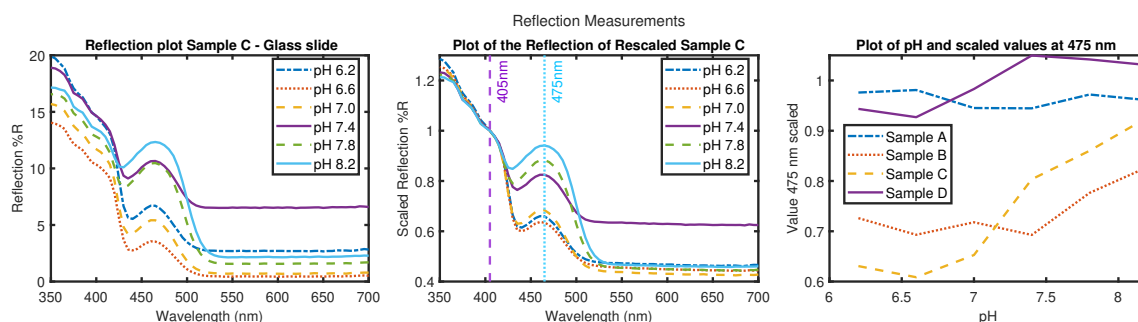


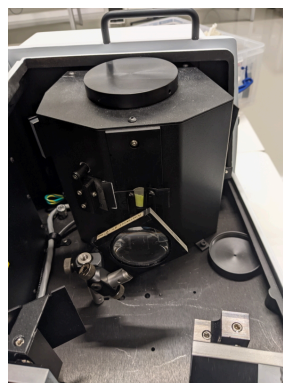
Figure 5.6: (a) Unscaled reflection output of Sample C in the lambda spectrophotometer, (b) Scaled output of Sample C in the lambda spectrophotometer and (c) the output of the samples at different pH

### Transmission/Absorption

The samples of the second batch were placed inside of the spectroscope as shown in figures 5.7. For the transmission measurements, the samples were placed in front of the integrating sphere. From the transmittance, the absorption can be calculated 2.18 as described in section 4.4. Figure 5.8 gives an



(a) Set up Transmission Measurements Sideview



(b) Set up Transmission Measurements Topview

Figure 5.7: Images of Set up Transmission Measurements

example of the (un)scaled measured transmission measured by the lambda spectrophotometer and the results of all different samples per pH. The full transmission results of all samples can be found in Appendix A.9, figure A.7 shows the unscaled reflection measurements, and figure A.6 the scaled reflection. First, the results of all samples are described and then the absorbance of all samples are shown.

The thickness of Sample A allows for a maximal transmission of 88% with the a pH of 8.2 and only a transmission of 84% at pH of 6.2. Total decrease of the sample at different pH is only around 10%. between 510nm and 700nm only there are small changes visible. ALL lines show a small dip at 475nm and another one at 405nm. Looking at the unscaled graph in figure A.7 no relation is visible between pH

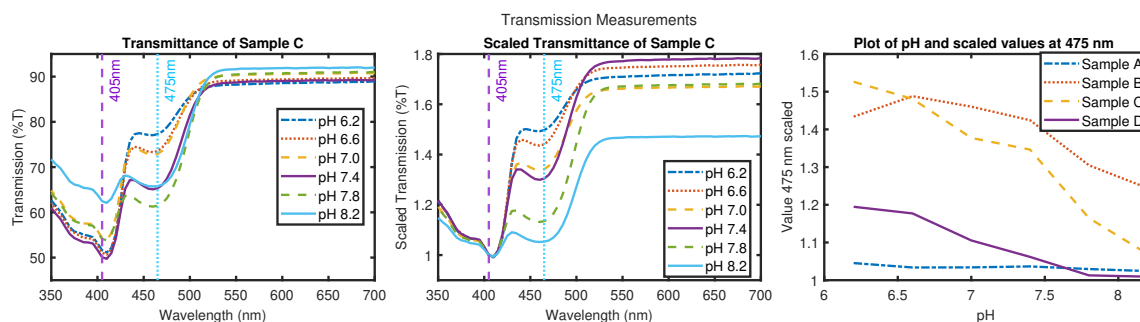


Figure 5.8: (a) Unscaled transmission output of Sample C in the lambda spectrophotometer, (b) Scaled output of Sample C in the lambda spectrophotometer and (c) the output of the samples at different pH

and the transmission. However, in the scaled transmission graph, there is less transmission with higher pH than with the lower pH. The values between 6.6 and 7.4 are unrecognisable from each other. As Sample B is the thickest sample, the maximal transmission is only 60%. The total decrease in transmission is around 35% which is more than in Sample A. The scaled transmissions in figure A.6 show that there is a relation between the transmittance of the samples and the pH. Except for the sample with a pH of 6.2, this is an outlier in the trend of the percentual decrease between 475nm and 405nm. Sample C is thinner than samples A and B and this results in a transmission of around 90% between 520 and 700 nm. As with Sample B, this sample shows a decrease of around 50% of the maximal transmission. While the transmission of pH 8.2 appears to be an outlier, it is not when the samples are scaled to the value at 405nm. In figure 5.8 it is clearly visible that there is a negative relation to the transmission with increasing pH values. Sample D has an even higher transmission value than sample D. However, in comparison with the other two samples, the difference between the maximal value and minimal value is lower. This is between 30-40%, the difference between pH 6.2 and pH 8.3 is large. However, the higher values pH 7.8 and 8.2 show almost identical lines in the scaled graph, see Appendix A.9.

Figure 5.9 show the absorbance plots related to Sample D. Sample D is illustrated as Sample C is just the inverse plot of figure 5.8. As the logarithm scales the output of the samples, the plot in 5.9 (c) shows a steeper line for sample D than 5.8. The scaled absorbance graphs in Appendix A.10 figure A.9 show this inverse in all plots. Using equation 2.18 as described in section 4.4 the absorbance data can be obtained. The absorbance graphs correspond to results found in the literature. Samples C and D are illustrated as these show the most potential after the first spectrometric analysis. Based on the

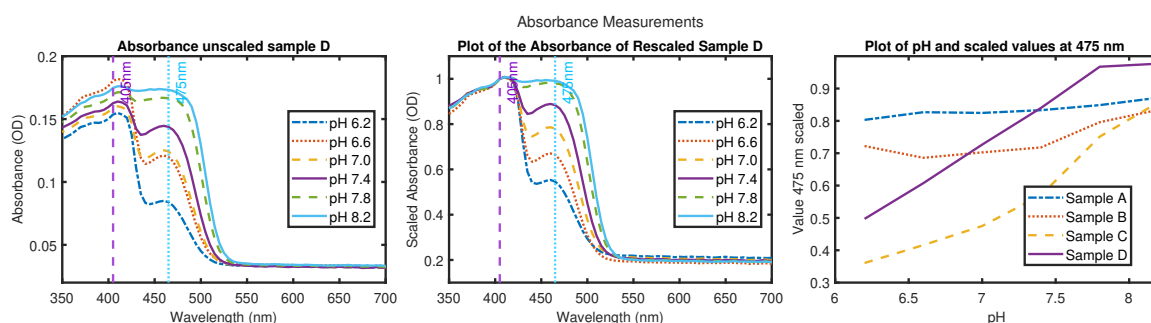


Figure 5.9: (a) Unscaled absorbance output of Sample D, calculated using the transmission data from the lambda spectrophotometer, (b) Scaled output of Sample D and (c) the output of the samples at different pH

relation between the dual wavelength properties and the absorbance difference of the 405 nm and 475 nm wavelengths, the pKa and sensitivity of the samples can be calculated. 5.9 (c) show the relation between the samples and the scaled absorbance and pH. Figure 5.10 show the pKa curves fitted to the data for samples C and D. Samples A and B did not have data on which a sigmoidal curve can be plotted. Using the Boltzmann function described in section 4.4.1, the following pKa,  $\eta$  and curves can be extracted. A big difference is visible in this data. This can be explained by that only a part of the curve is measured with the pH between 6.2 and 8.2. To overcome this, in the future analysis, a measurement with the pH of 4 and with the pH of 12 will be added to better fit the data.

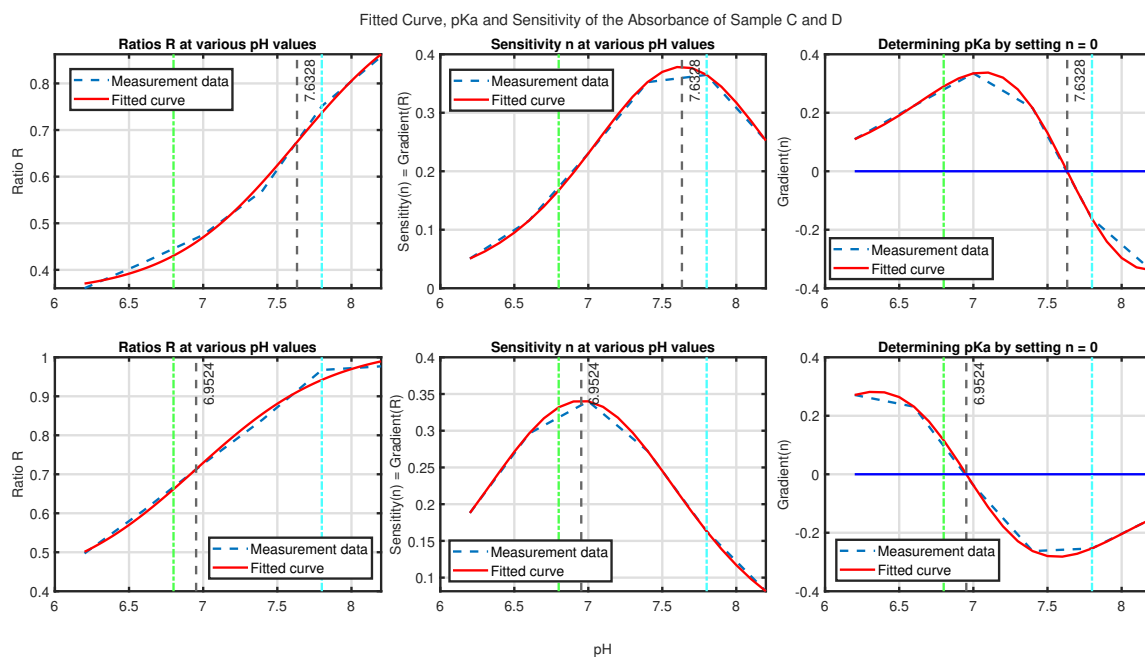
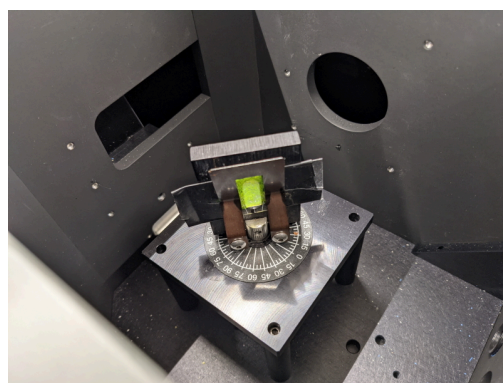


Figure 5.10: Results of determining pKa and sensitivity of the absorbance data of the samples C and D

### Fluorescence



(a) Set up with Sample in Fluorlog 3



(b) Topview of Sample in Fluorlog 3

Figure 5.11: Images of Set up Fluorlog

The samples of the second batch were placed inside of the spectroscope as shown in figures 5.11. The fluoropsectrophotometer gave the output in count per second detected by the PMT. As the light-beam excites the sample at an angle of  $45^\circ$ , the output measured by the PMT is only the fluorescence output and not the reflection from the sample. Figure 5.12 shows a summary of the 3D plot of the output measured by Fluorlog 3. This figure shows the fluorescence output at pH 4, 7, and 10. The full results can be found in Appendix A.11. In this section, all samples will be briefly discussed, but the focus is on the results of Sample C. As this sample showed the most potential for future work.

Sample A is a sample which should not contain any fluorescent material. However, images from the fluorescent microscope show that there is little contamination of HPTS loaded microbeads in the sample. Therefore, instead of saying that the sample is a background test, this will now be a layer with a low dose of loaded HPTS microbeads. The plots show that there is a transition going on from a fluorescent peak from 415nm excitation and 445nm emission to higher values at the emission of 520nm figure A.11 and A.10. A peak in the lower left corner is also visible, which is decreasing per increasing pH.

Sample B shows the same characteristics as Sample A with decreasing values at the lower left corner and increasing values at the 525-emission line. Figure A.13 show the spectral images of sample B. The only difference with the sample A is that the values are more than 10 times as big. While being measured with the same settings. This increase shows that there is more fluorescent material excited in this sample.

Sample C shows the same characteristics as samples A and B with decreasing values at the lower left corner and increasing values at the 525-emission line. The values are lower than for Sample B and show that there is less fluorescent material excited. The values are much higher than sample A.

Figure A.17 illustrates that sample D shows the same characteristics as samples A, B and C with decreasing values at the lower left corner and increasing values at the 525-emission line. However, this decrease goes much faster and at pH 7.0 already nearly visible. This shows that after a pH of 7.0, no more extra fluorescence is excited in the sample. An outlier is visible in the maximal value of the sample as there is an lower value of output visible. Zooming in on the 525nm emission wavelength, it is visible that there is a plateau reached. This shift is visible in figure A.16 where the peak of the spectral plot is around 535nm emission wavelength and not measured on the 525 nm line.

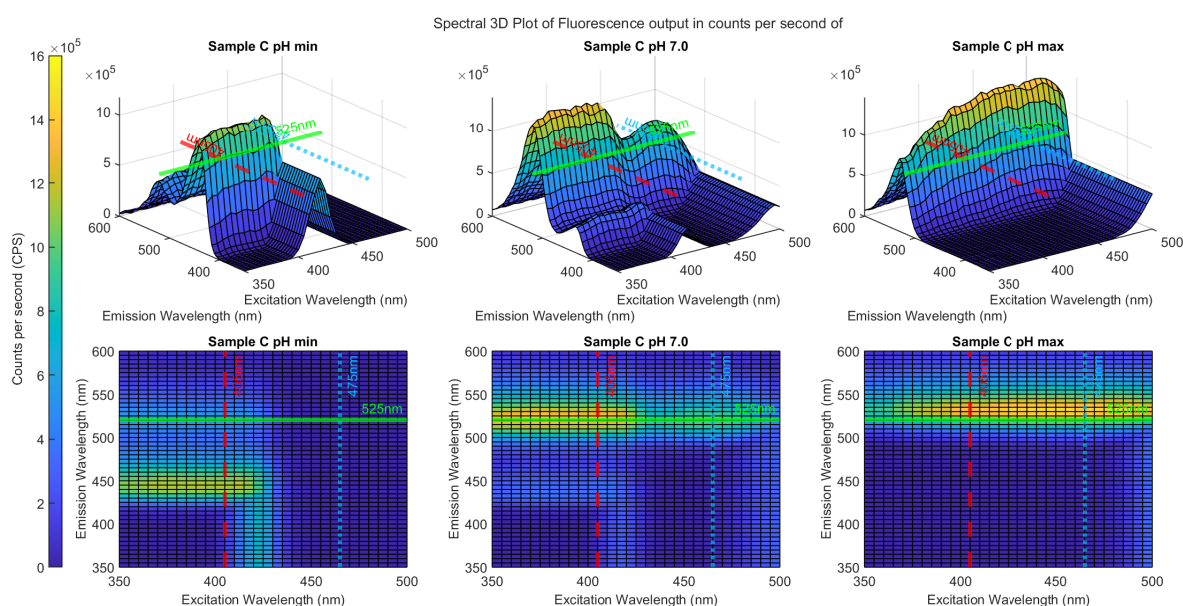


Figure 5.12: Fluorescence output of Sample C measured in Horiba Fluorlog 3

### Sensitivity & Response times

To determine the sensitivity and pKa of the samples, the Boltzmann function is used to fit the curve, as described in section 4.4.1. Before this could be done, the dual wavelengths for the ratiometric sensing had to be determined. For this, all emission wavelengths between 500nm and 600nm were compared with the ratio between 475nm and 405nm. Table 5.1 show the outcome for Sample C. Clearly, the max relative difference is found at the emission wavelength of 520-525 nm. Other samples showed comparable results.

Sample C	pH min	pH 6.2	pH 6.6	pH 7.0	pH 7.4	pH 7.8	pH 8.2	pH max
Maximal difference (cps)	531220	937244.4	739949.6	450801.3	270000	260000	220000	8789.75
Wavelength with max diff.	525	525	525	525	520	520	525	590

Table 5.1: Determining the optimal wavelength for dual wavelength referencing of Sample C

Figure 5.13 shows the fluorescent output measured at an emission wavelength of 525nm for all excita-

tion wavelengths of sample C. Unscaled output does not show any relation, however the scaled output shows a clear relation between the measured output and the increasing pH. Using this data, a curve could be fitted following the procedure described in section 4.4.6.

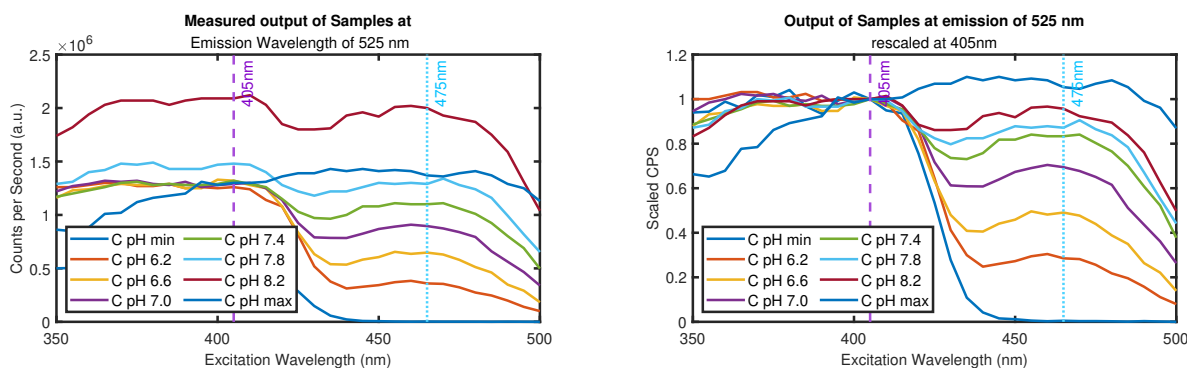


Figure 5.13: Fluorescent Output in Count per Seconds of Sample C and scaled Output of Sample C

Figure 5.14 shows the fitted curve of the data from the fluorlog. By plotting the gradient function of R, the sensitivity is calculated. The function obtained by reversing the sigmoid shown in figure 5.14 is:

$$F = \frac{a - b}{1 + e^{(x-c)/d}} + b \quad (5.1)$$

where  $a = 0$ ,  $b = 1.0357$ ,  $c = 6.7679$ ,  $d = 0.7592$ .  $a$ ,  $b$ ,  $c$ , and  $d$  are empirical parameters describing the initial value ( $a$ ), final value ( $b$ ), center ( $c$ ) and the width of the fitting curve ( $d$ ). Appendix A.12 shows the plots of the other samples. Compared to other samples, it shows that sample C has a more narrow sensitivity than sample B and comparable sensitivity as sample A 5.14 and a higher pKa than A and D, but lower than B.

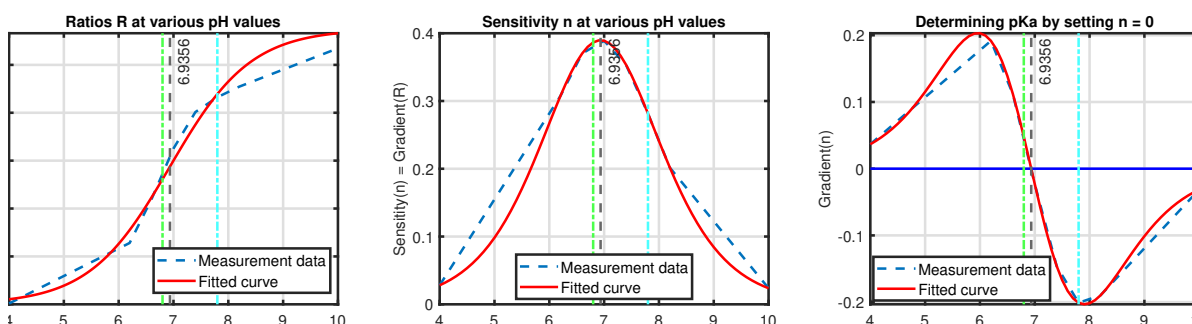


Figure 5.14: Ratios, sensitivity and pKa determination for Sample C

Table 5.2 shows the response times of the different samples and their pKa determined from the fluorescence output. It clearly shows the influence of the thickness of the sample and the concentration. Sample B takes much longer to transfer from maximal fluorescence to no fluorescence.

Sample	A	B	C	D
pKa	6.9879	7.729	6.9356	6.201
Transition time (pH 10 - pH 4 (min))	5	25	10	12

Table 5.2: pKa of samples and transition time from pH 10 to pH 4. Measured by visual output

### 5.2.4. Analysis of second batch

The results of the second batch definitely show the potential to use this hydrogel-HPTS combination as a sensing layer for the ischaemia sensor. The different sensors all showed that they had a relation be-

tween the fluorescent output and pH. Still there are some inaccuracies, but these experiments showed that results from the literature can be matched. Some analysis that can be made are the following: First of all, differences in thickness and concentration are clearly visible in all measurements. The fluorescent microscope showed the partly filled microbeads in samples A and B and the black background of samples C and D. The absorption and reflection outputs measured using the Perkin Elmer Lambda 1050 were also higher for samples A and B than for samples C and D. While in fluorlog 3, the higher total concentration of HPTS caused that sample B had the most fluorescent output measured. The next experiment should take a look at samples with the same concentration but with different thicknesses and at different power of the excitation wavelengths.

Secondly, the calculated pKa and sensitivity of the samples differ between the absorption and fluorescence values. For sample C this was a difference between 7.6 and 6.9 and for sample D, it was between 7.0 and 6.2. Both a large difference and this should be taken into account. The final sensor will be based on fluorescent, but these differences indicate that the sensing layer should be calibrated to the full pH range. As a small deviation can have now a large influence on the sigmoid curve. Therefore, the next experiments should measure the full range. Another experiment should be focused on the response time over time. Now the measurement was done from max to zero, but it should be interesting to see if this transition is linear or exponential.

Thirdly, for these experiments advanced equipment and controlled environments are used. The goal of the thesis is to develop a proof-of-concept sensor to show the potential for ischaemia sensing. Therefore, the next experiments should be done with less advanced equipment to see if it is possible to measure the results with less.

At last, the size of the samples is quite large and the following experiment should try to minimize this to see if the scale has influence on the outcomes. As well as the influence of the ionic strength is not yet tested. This is an essential relation described in the literature and should be investigated.

**Summary Experiments & Interim Conclusions:**

- Summary experiments:
  - Fluorescent microscopy:
    - ◊ Sample A had pollution which was visible in the results
    - ◊ Due to software of the camera, it was not possible to compare the light intensity of the samples
    - ◊ Sample C and D much thinner and less microbeads than A and B
  - Transmission/Absorbance:
    - ◊ When scaling the absorbance to the value of 405nm, there is a relation visible between the absorbance and the pH value
    - ◊ Higher dose of dye showing an earlier peak in absorbance
    - ◊ Clear relation visible in samples C and D
  - Reflection:
    - ◊ No clear relation between the reflection and pH
    - ◊ Fluorescence is difficult to detect with a spectrophotometer as the spectrophotometer uses a photo multiplier tube to measure the reflection at a certain wavelength but does not look at the wavelength of this reflection
  - Fluorescence Spectrophotometry
    - ◊ Higher fluorescent dye concentrations lead to lower pKa values.
    - ◊ Thicker samples/microbeads lead to higher transition times
    - ◊ pKa and sensitivity depends on the layer thickness and dye concentration
- Interim Conclusion:
  - The potential to use fluorescent hydrogel is shown in the experiments
  - Thickness and concentration should be optimised
  - Advanced equipment show clear difference between the samples
  - Spectroscopic analysis shows a lot of potential

### 5.3. Reflection fibre USB spectrometer

This section describes all information related to the experiments done with Starline Spectrometer and the Avantes reflection probe as the final experiments for designing the proof-of-concept sensor. These experiments are done to show the potential of the hydrogel and to show the potential for fluorescence reflection sensing. A brief explanation is given on what the goal of this batch is and how they are fabricated. Following this, an explanation per experiment is given and then the results of the experiments are described. Finally, this section describes the analysis of these results and what the consequences are for the proof-of-concept sensor are.

#### 5.3.1. Goal of USB spectrometer and Reflection probe

The experiments of this section are done to show the potential of using a USB spectrometer and a reflection probe for the proof-of-concept sensor, while optimising for light intensity, thickness and to work out the influence of the ionic strength. A reflection probe is chosen to see if needle-based sensor shows more potential than a planar sensor. The advantage of using a reflection probe with the usb spectrometer is that the full spectrum can be used for analysis, if the results show that this is possible. As with the other experiments, this section will start with an optical investigation. However, in this section no microscope is used. After this, two different thickness are compared to the influence of light intensity of a 475nm LED and are measured in different ionic strengths. Following this, a full range measurement of both sensors is done from a pH of 3.2 to 12.1 and the response is measured over time.

##### *Fabrication of layers*

For the experiments, identical samples of varying thickness are created. The samples were made following the concentration of Sample C of section 5.2. Thus, 1mg/mL of microbeads to 17.5 mg/mL of HPTS. The layers were created in small tubes with a 1.5mm size, which is equal to the diameter of the reflection probe. One had the thickness of 1mm and the other of 0.5mm. The samples were surrounded by plastic except from the two sides. At one side the reflection probe could be mounted and the other side was in direct contact with the liquid.

#### 5.3.2. Experiment reflection fibre

First, the sensing layers were investigated by the eye to see if the colour differences are clear to the eye and to see how much light from the light source is absorbed by the layer at the end of the reflection probe. One set-up will then be used for the other experiments. Here, the final necessary measurement will be done before the final proof-of-concept sensor can be created.

##### *Thickness, light intensity, and Ionic Strength*

During these experiments, the reflection probe with a sensing layer of 1 or 0.5mm is first doped in the liquid with an ionic strength of 150 mM with varying pH. During these measurements, the current through the LED is adjusted. The currents used are 100 mA, 150 mA, 300mA, 350mA, and 450 mA. This is done to see if a higher light intensity affects the output of the spectrometer. Following this, the current is set and the probe is put in all pH samples of the 3 ionic strength buffer solutions. This to see if the expected issues with ionic strength described in section 2.2.2 are visible in the measurements.

##### *Full range measurements and Response time*

As described in the analysis of the previous experiments, a measurement of the full range of pH is needed to better determine the pKa of a sample. For this experiment, pH buffer solutions from 3.2 to 12.2 are used. With the setup described, it is also possible to do timed measurements. Therefore, to see how fast the change of pH is detected by the sensor, first the sensor is doped in a low/high concentration and then transferred to the opposite concentration. After this, every second a measurement of the spectrometer is saved to see the changes over time. This experiment will be used to see if the differences between 0.5 and 1 mm are significant.

#### 5.3.3. Results Experiments

##### *Optical investigation*

The differences between the 1mm and 0.5mm layers are the most clear when the light of the LED was turned on. With the lights turned off, only a difference in length is visible, see figure 5.15a. However,

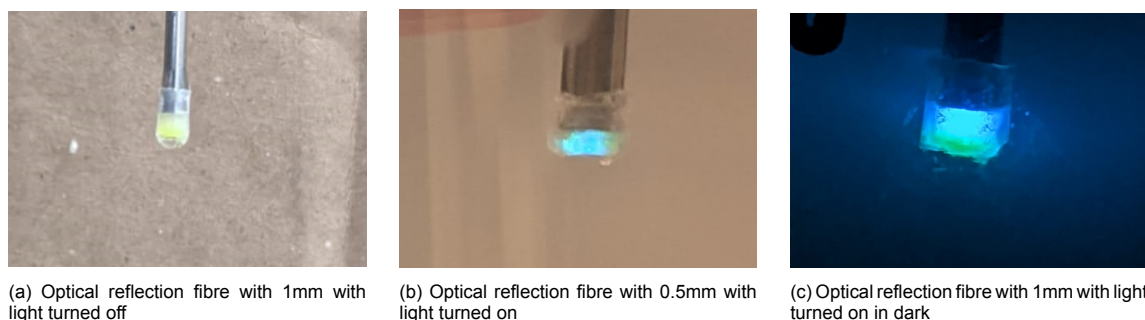


Figure 5.15: Images of optical sensing layers on optical reflection fibre

when the light is turned on and the sensing layer is in a buffer solution, a colour difference is visible see figure 5.15b. When the sensing layer is just submerged, a clear line can be seen on where the buffer solution has diffused. This difference is even bigger in the thicker sensing layer, see figure 5.15c. In the 0.5mm sensing layer, the colour is more equally divided and the transitions go faster.

#### Thickness, light intensity, and ionic strength

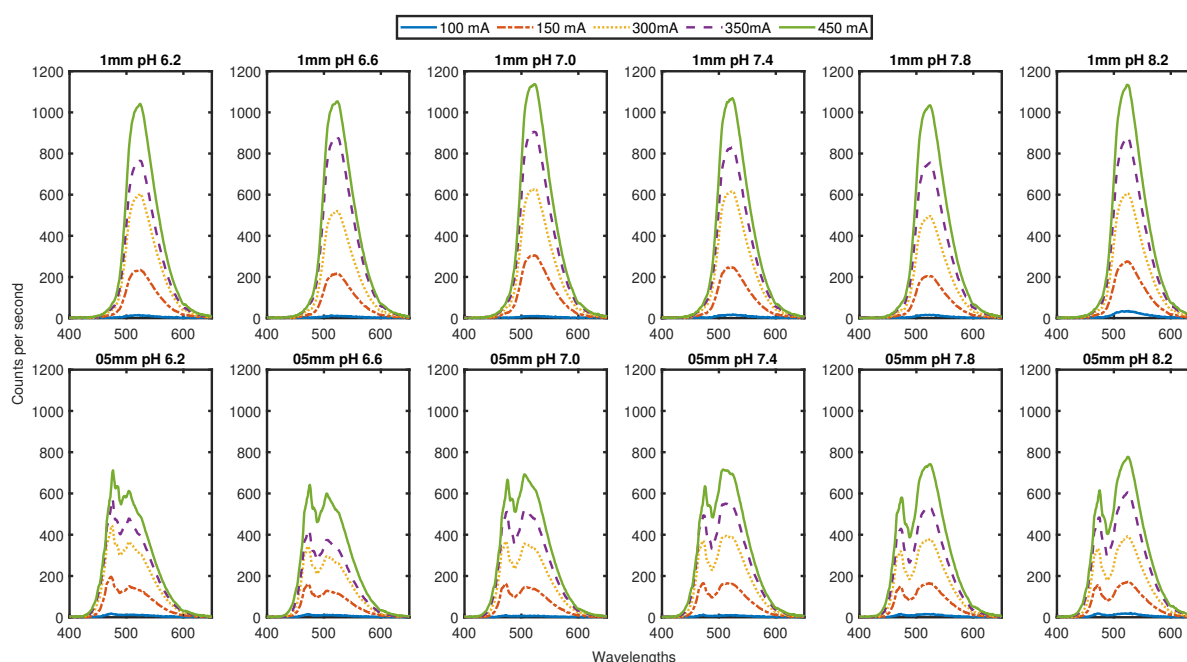


Figure 5.16: Spectral output measured by Avantes Starline in counts per second, for the two layer thicknesses and at different pH and with different voltages. Measured in 150mM buffer solutions

In figure 5.16 the results are shown for the measurements with the reflection probe and hydrogels of two different thicknesses. As described in the section 4.3.2 the probe was inserted in the pH buffer solution for 3 minutes before the measurement was taken. The peaks are higher in the thicker sample. Higher voltages and thus more excitation light has a positive correlation with the output measured. In the 0.5mm sample, more difference in peaks is visible, while for the 1mm layer only the peak around 525nm is visible. This match with the figure 5.15b and 5.15c. In this figure it is visible that in the 0.5mm layer there is a consistent colour of the layer, while in the 1mm layer there is a difference between the bottom and top of the layer. As the solution diffuses through the layer, a thicker layer can influence the time. This is increased by the restriction of the plastic holder. Therefore, the diffusion can only occur in one direction.

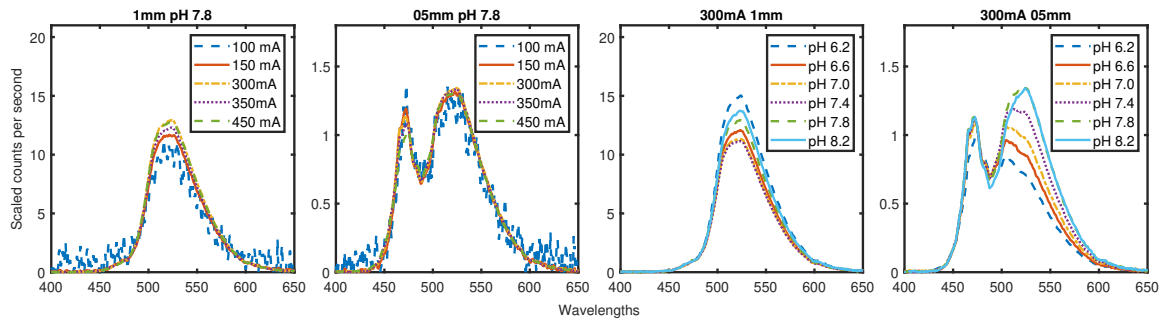


Figure 5.17: Scaled output of the the layer at different light intensities (a and b) and at different pH at the same light intensity (c and d)

Scaling the output by dividing it by the value at 475nm gives a ratio which shows that a thinner layer shows more similarity with each other than with the thicker sample. This is shown in Appendix A.13. Analysing the scaled ratio per ampere shows that each ampere of the 0.5mm layer has a relation to the pH. The relation between ampere and pH is illustrated in figure 5.17.

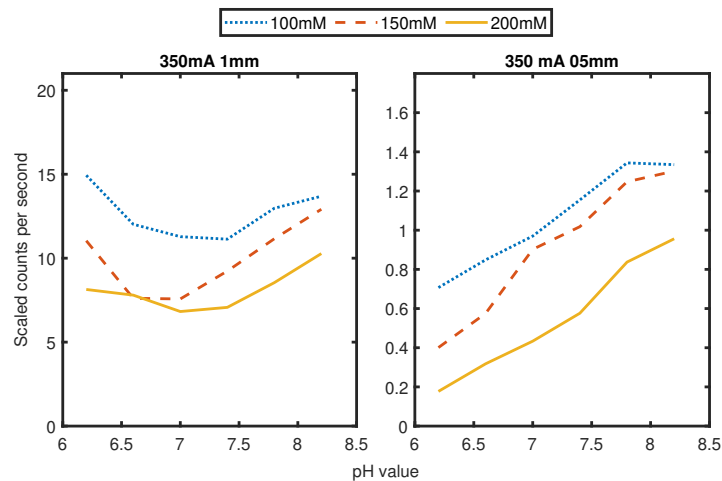


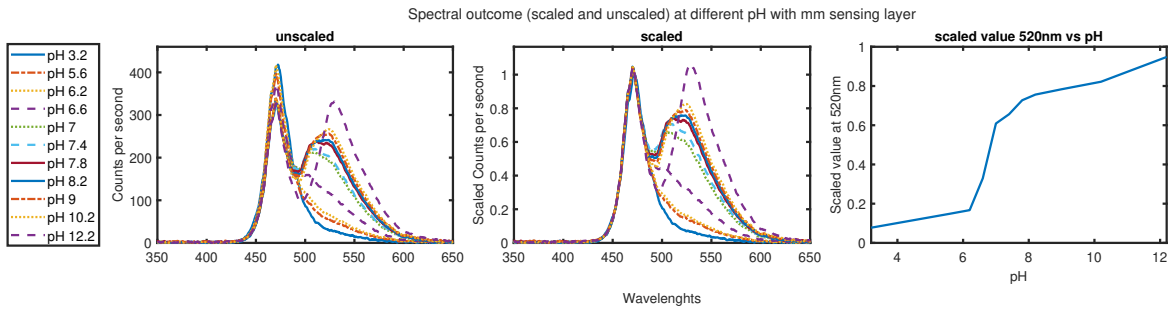
Figure 5.18: Spectral output measured by Avantes Starline in counts per second per different voltages, measured at the emission of 525nm. All values are scaled to the value of 475nm for the two layer thicknesses and at Ionic Strengths and with different pH

Comparing the scaled ratios per different Ionic Strength buffers (100mM, 150mM, and 200mM) gives clear relations with the 0.5mm sample, figure 5.18. This verifies the influence of IS on the ability to measure the pH correctly with fluorescent dyes, which is described in Section 2.2.2 of the Theoretical Background. The ionic strength has influence on the diffusion and the transition between the conjugated base and acid. This effect is visible at all different voltages. The higher the pH, the less clear this difference becomes. This figure also indicates that the angles of the relation between the scaled output and pH are comparable. For the sample of 1mm this is not visible and are no relations visible between the samples.

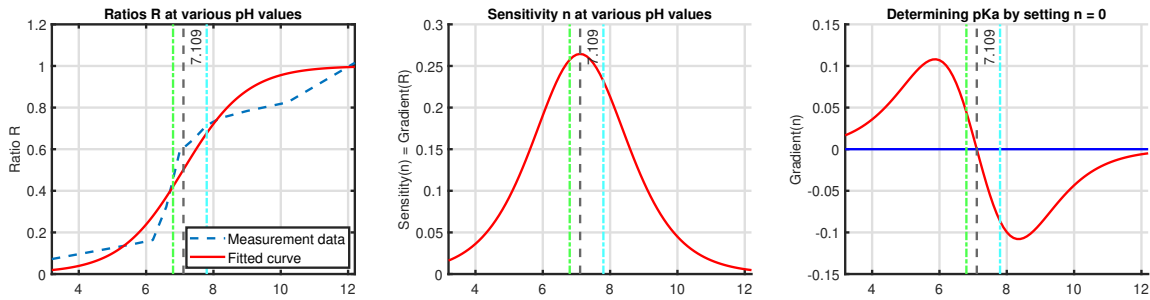
#### Full range pH

After the differences between the voltages, ionic strength and layer thickness, the full range of the two thicknesses were investigated. The probe with the sensing layer was submerged for 20 minutes before measuring the spectral output. It was done with the Ionic Strength of 150mM as this is comparable to the Ionic Strength in the human body. Figure 5.19 show the results of the 0.5mm sample. The results of the 1mm sample can be found in Appendix A.14.

The scaled ratios of the sample with 1mm thickness are more in a linear line in comparison with the 0.5mm sample. Figure 5.19b shows that the scaled ration of 0.5mm sample shows more of a sigmoid



(a) Full range of 0.5mm sensing layer and relation between output and pH



(b) Sensitivity, pKa of 0.5mm layer

Figure 5.19: Outcome of the full range of the 0.5mm sample after submerging for 20 minutes in 150mM buffer solutions

line. The scaled values are comparable to the values of the previous experiment, however they are below 1. In the previous experiment, the maximal value was 1.2. pKa is higher than in the previous experiments and shows that a full range can estimate the sigmoid curve more accurately.

Transition times

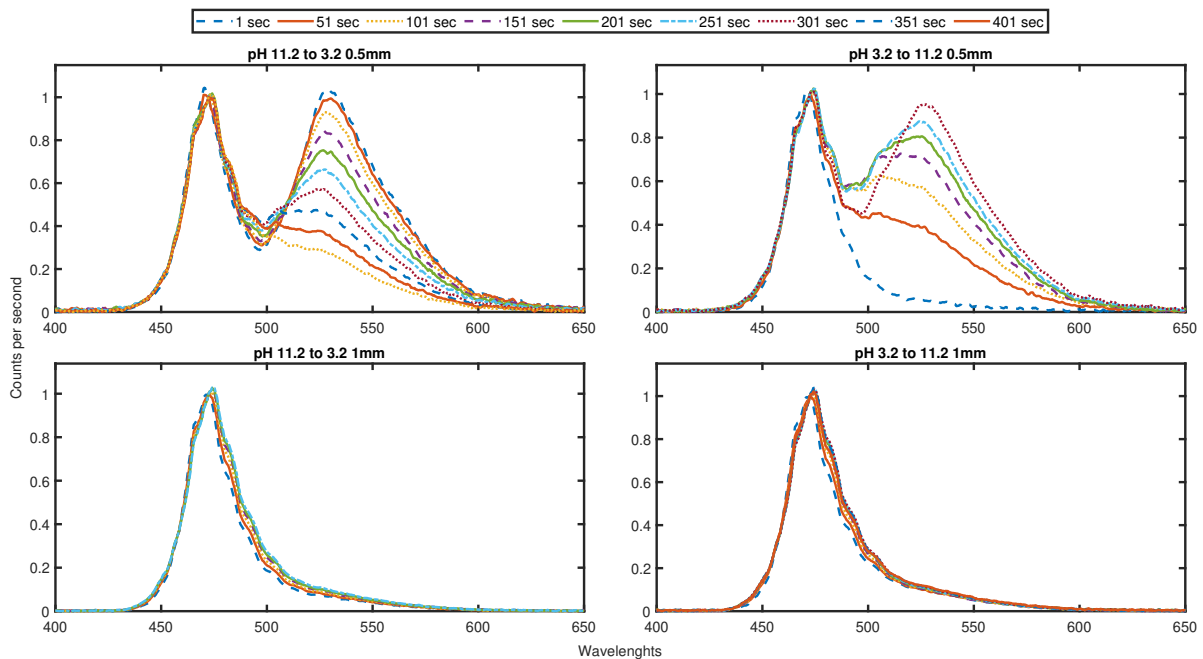


Figure 5.20: Transition times when sensor is placed from a high/low sample to the other

Figure 5.20 and 5.21 show that the sensing layer of 1mm is not changing a lot within 7 minutes, while

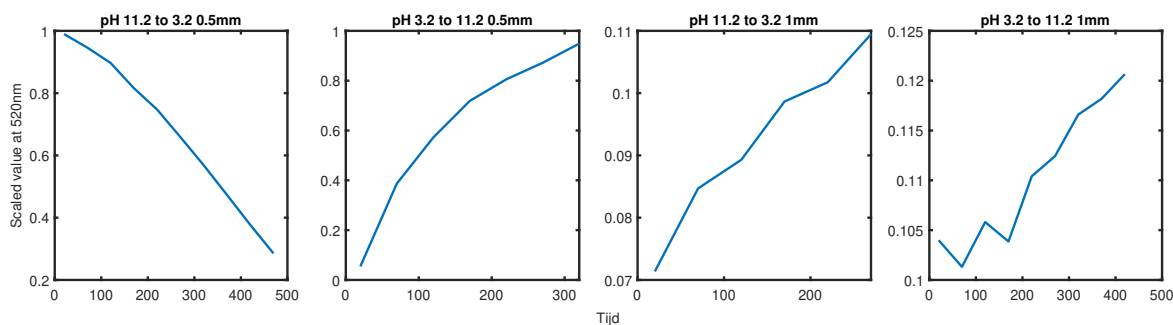


Figure 5.21: Transition times vs. value at 525 emission wavelength, when sensor is placed from a high/low sample to the other

the 0.5mm layer shows a fast transition time when changed to another buffer solution. During the tests, the reflection probe with sensing layer was submerged for 20 minutes in a very high or low pH buffer solution. After this, the light was turned on and the probe was transferred to the other extreme. Both measurements done on the 0.5mm layer show a fast change between the scaled values at 525nm. This is not visible in the 1mm sensing layer.

With this sensing layer decreasing pH led to even higher outcomes, see figure 5.21. The scale of the 1mm layer is ten-fold lower than with the 0.5mm layer. Another difference is that even when the samples are submerged for a longer period in the high pH value, the peak at 525nm is not visible. This suggest that the waiting time was not sufficient for the pH solution to fully diffuse into the sensing layer.

### 5.3.4. Analysis of reflection probe measurements

The results of the measurements done with the reflection probe show the potential for a ischaemia sensor by using a reflection probe with a sensing layer in combination with a USB spectrometer. The differences in layer thickness have a significant influence on the results and multiple measurements did not go as expected because of the slow transition time of the 1mm sample.

Secondly, the influence of the ionic strength is mapped and is larger than expected. This will be a challenge for future development of the sensor but can be done with different chemical processes. For calibration of the sensor, the use of a full range will better estimate the pKa of the sensor. As well as smaller steps can improve the estimation done by MATLAB.

Thirdly, light intensity does not have a large effect on the results, it should be tested with two LEDs as these measurements were done only with a 475nm LED.

#### Interim Conclusions:

- Thinner layers lead to faster and more accurate results
- Not much difference between the output measured at different light intensities
- Clear influence of ionic strength visible in the results, hard to compensate for
- 1mm sample can need a very long time before the buffer solution is fully diffused into the sample, this effect may have influenced the measurements
- Scaling the emission wavelength 525 by dividing it by the value at 475 shows potential, but should be combined with 405nm LED

# 6

## Proof-of-concept sensor

The final part of this thesis is the proof-of-concept sensor. This specific sensor's goal is to prove the viability of using such sensor for the detection of ischaemia. In section 3.2.4 a list of requirements for the proof-of-concept is described and the final product is tested against these criteria. First, the goal of the sensor is elaborated, followed by different concepts developed during the design period of this thesis. Subsequently, the fabrication, design of the sensor and the experiments to test the sensor are described. Finally, the outcomes of the experiments are stated and a final analysis is made.

### 6.1. Goal of proof-of-concept sensor

The initial goal of the proof-of-concept sensor is to see if fluorescent sensing would be a viable method to detect the pH changes which occur during myocardial ischaemia. However, as described in chapter 3, there are many optical techniques and the results depend on the material used. Therefore, the final goal of the proof-of-concept sensor is to investigate if optochemical sensing of pH with a sensing layer existing out of HydroMed D4, AmberChrom microbeads and HPTS shows the potential to measure pH changes which occur during myocardial ischaemia. While meeting the criteria described in section 3.2.4:

1. The prototype material needs to be bio-compatible
2. The prototype needs to be sensitive for pH between 6.5 and 8
3. The prototype needs an accuracy of at least 0.1 pH
4. The prototype cost should not exceed 1000 euro
5. The prototype needs to easily allow for remotely sensing
6. The prototype needs no complex chemistry for fabrication
7. The prototype needs no complex optical measurement technique
8. The prototype needs to handle interferences

By selecting HPTS, HydroMed D4 and Dual Wavelength Referencing, criteria 1, 6, 7, and 8 are met. The next step is to create concepts which would satisfy criteria 4 and 5. While testing the optimal proportions of the materials to see if criteria 2 and 3 are met with the material and techniques used.

#### 6.1.1. Concepts developed for sensor

At the start of the development, two types of concepts are established. The first concept is a planar design which could be used as a patch and would process the information in the patch. This design is similar to the Philips Healthdot, however, has the addition of being capable of measuring in vivo. This patch would use photosensitive electronics (CMOS/CCD/PD) for processing the image and LEDs placed on a PCB for excitation of the sensing layer. Even a concept is made to design the sensor as

disposable. Figure 6.1 shows the a concept design of a patch sensor with a fluorescent hydrogel.

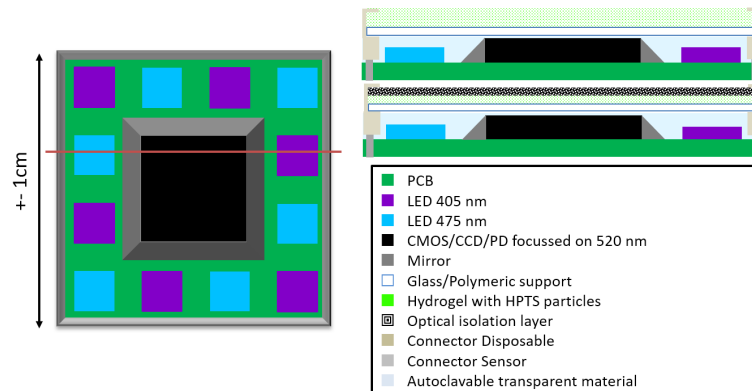
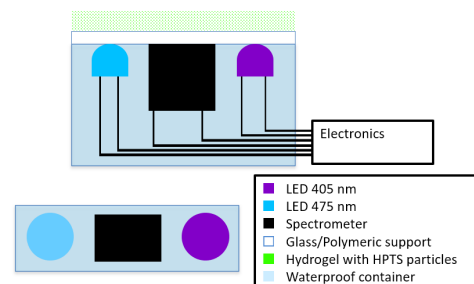


Figure 6.1: Concept design of a disposable planar sensor

Figure 6.2 shows the healthdot (6.2a), which is an inspiration of this first concept and a trimmed design (6.2b) of the first concept, which is able to test the potential of a planar sensor. However, this concept is abandoned after the results of the CMOS and monochromator showed that the CMOS is not able to detect the differences and that the advanced electronics necessary is a thesis project in itself. Instead of a CMOS, a photodetector can be used to detect the fluorescent reaction. However, such a design is tested and described by Cattini et al. [24] and would increase the cost of the proof-of-concept sensor as new materials need to be ordered.



(a) Philips healthdot, used as inspiration for a patch like design of the sensor



(b) Schematic design of trimmed down design to test the viability of full planar sensor, figure 6.1

Figure 6.2: Images related to the planar concept design

Eventually, the other concept showed more potential to be validated using the materials available. The second concept developed is an optical fibre-based sensor. The advantage of using optical fibres is that the processing of the information can be done outside of the body and more advanced equipment can be used. The disadvantage is that optical fibres are vulnerable and prone to small changes. First, the goal is to develop a needle with custom fibres to imitate the miniature probe of Avantes. This set-up proved to give useful results as described in section 5.3.

However, due to the hydrophilic characteristic of the sensing layer, it cannot be coated on the optical fibres or metal of the needle. Eventually, the decision is made to design a connector piece for the reflection probe. The advantage of a connector piece is that it would be able to test different samples, uses available equipment, and it gives reliable results. It is designed with a pointed shape, which can be miniaturised into small needles. Eventually, the final design can exist of multiple needles with coatings which are placed on the heart and optical fibres to transfer the information outside of the body.

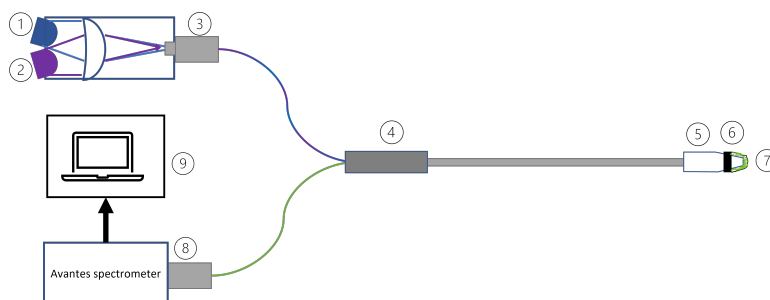


Figure 6.3: Design of the optical fibre proof of concept sensor. (1) 475 nm LED, (2) 405 nm LED, (3) SMA connector, (4) Avantes miniature reflection probe, (5) 3D printed connector, (6) rubber ring to hold sample in place, (7) Sample, (8) Avantes Starline USB Spectrometer, (9) Laptop to process data from Avantes Starline

### 6.1.2. Fabrication of proof-of-concept sensor

For the fabrication of the proof-of-concept sensor, different types of connector pieces are designed and 3D printed using an Ultimaker S5. The design can be found in Appendix A.14. In the design, a slit is extruded so a rubber ring could be used to fix the sensing layer sample. Besides the connector pieces, four different moulds are printed. These moulds have a notch in the middle of different depths. These holes are made to test the difference in layer thickness. The samples are held in place by a rubber ring, which also seals the connector.

#### *Set-up final measurements*

To make sure the measurements are done in a controlled environment, a dark container is developed with different sensors attached to it. This ensured that all measurements are done in the same way. Figure 6.4 shows this container with the sensors. For each measurement with a buffer solution, the developed buffer solution is transferred to the dark container.

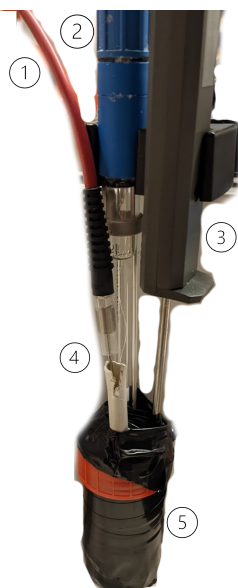


Figure 6.4: Design of the optical fibre proof of concept sensor. (1) Avantes Reflection Fibre (2) pH Probe N64 of SI Analytics (3) Temperature Sensor, (4) Proof of concept needle, (5) Dark container

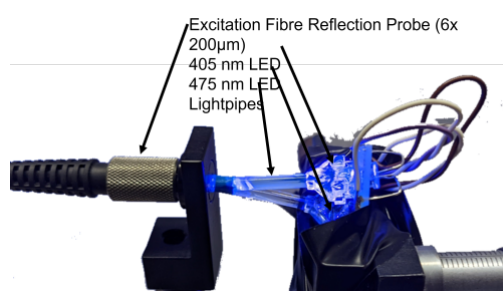
### 6.1.3. Experiments proof-of-concept sensor

As with the other samples, the sensing layer placed on the connector piece is optical investigated. This is done to see how the microbeads are positioned relative to the reflection probe fibres. Following this, comparable measurements are done as described in section 5.3. The influence of ionic strength,

reproducibility, thickness, and response time are measured and calculated. All experiments are done with the same buffer solutions and the time between measurements.

## 6.2. Results proof-of-concept sensor

Figure 6.5 shows how the LED's are connected to the reflection probe and the equipment used for the final experiment. All solutions are kept at 40 °C. Then pH and temperature are measured, while the probe is submerged. After 5 minutes, the pH and temperature are checked again. If the temperature is at 37 °C, a measurement is done. First, the optical response of the 405nm LED is measured and after of the 475nm LED. The integration time is set to 5 ms and averaged 1000 times. This is done to increase the measured light intensity and to smooth out the spectral image. In total, two different sample thicknesses are tested. For all experiments, a 0.5mm layer thick sample is used. While to compare the pKa related to thickness and response time to thickness, a 1mm sample is used. During the response time measurements, the buffers are at an ambient room temperature of 22 °C as it is not possible to keep the buffer solutions for a longer time at 37 °C. All results of the ratios are normalised in a range from 0 to 1 to allow a better comparison between the different measurements.



(a) Set up of the LED's, two LED's (405nm and 475nm) are connected through solid light pipes to the excitation fibres of the Avantes reflection fibre. LED's are controlled by tabletop power supply



(b) All devices used for the final measurements. pH meter with SI Analytics pH probe, temperature sensor and the Avantes probe with spectrometer.

Figure 6.5: Set up of the final measurements

### 6.2.1. Optical investigation

The sensing layers, created using a mold, are fitted on to the 3D printed needle tip. Using a rubber band, the sensing layer is fixed in position. The needle tip is glued onto a pipe to ensure no solution will leak into the needle tip and interfere with the measurement. This pipe is fixated to the cap of the dark container so the measurement could be the same with each measurement. Figure 6.6b shows that only a tiny part of the sensing layer is used for the measurement.



(a) Image of the final needle with sensing layer and rubber ring



(b) Image of the final needle with sensing layer and rubber ring

Figure 6.6: Set up of the proof-of-concept sensor needle

#### Microscope

Figure 6.7 shows the images taken with the Zeiss Microscope. Here it is better visible how little HPTS-microbeads are located at the tip of the needle. In the middle and right image, it is visible that the

position of the LED light pipes is translated to the optical fibres of the tip. As the camera used to take the pictures is less sensitive towards UV, the 405nm LED light is less visible on the image. On the image, it is visible that the size of the needle can be minimised a lot more as only a small part is taken up by the optical fibres.

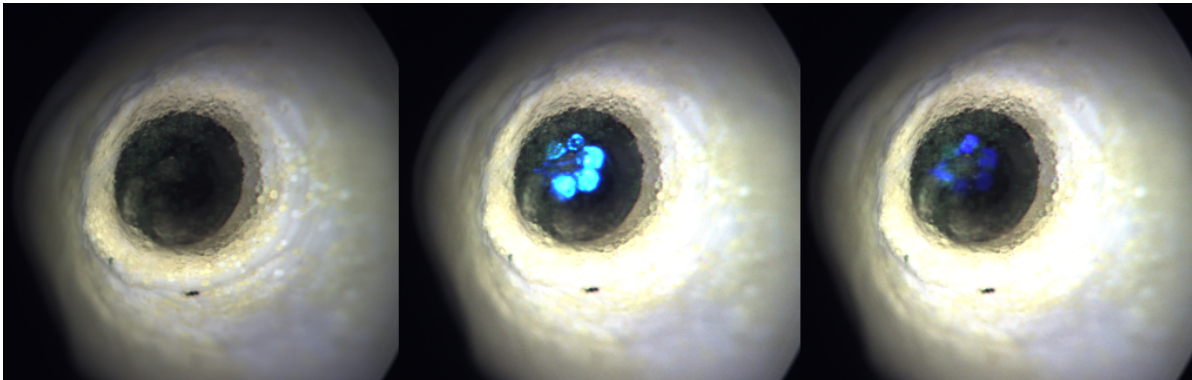


Figure 6.7: Zoomed Images of sensing layer on the tip of the needle. Left image with LED's turned of, middle image with 475nm LED on and right image with 405nm LED on

### 6.2.2. Reproducibility and Ionic Strength

Figure 6.8 shows the results of the measurements done with the 100mM buffer solutions. The ratios calculated as described in section 4.4.6 with formula 4.7 are fitted with a Boltzmann sigmoid function. Figure 6.8 shows this curve with the corresponding sensitivity and pKa values.

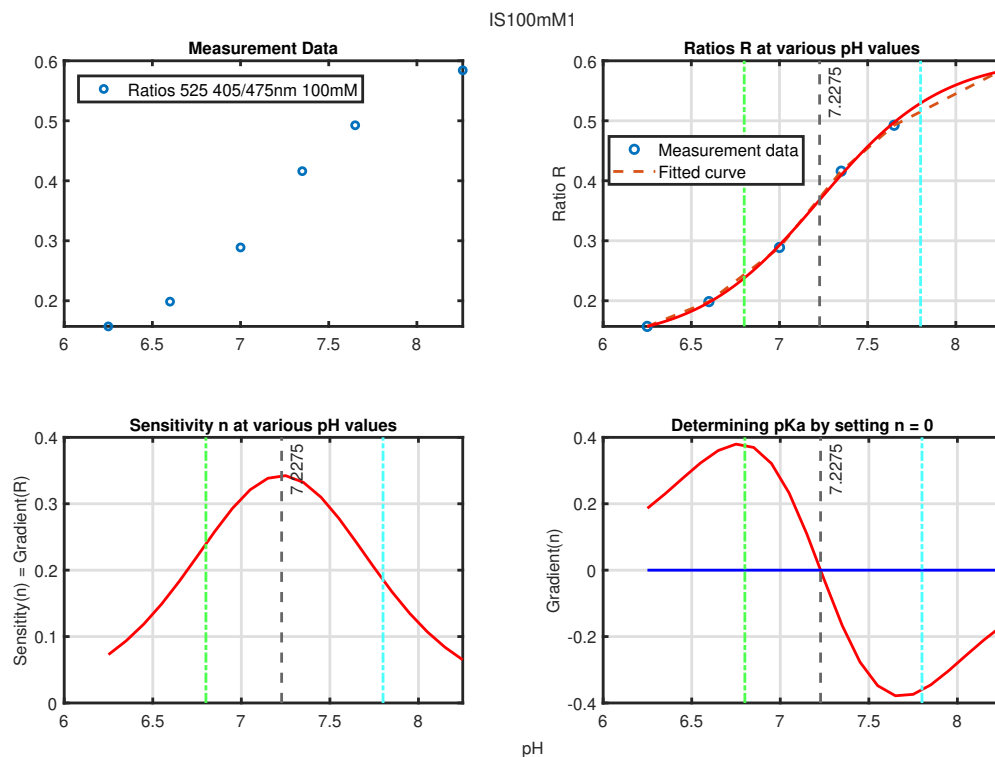


Figure 6.8: Non-Normalised Ratios of the measurement with 100mM buffer solutions and 5 minutes waiting time, green and blue line indicate the area where the sensor should be sensitive.

### Reproducibility

To investigate the reproducibility of the sensing layer, the experiment is repeated three times. Figure 6.9 show the results and figure A.24 in Appendix A.17 shows the extensive results. In the results it is visible that with no changes in the sensing layer, temperature or time between measurements, the measurements do vary. Between measurements 1 and 3, there is an estimated pKa difference of 0.6 points, which is very big. The pKa is estimated by fitting a curve to the measured ratios and a tiny difference can make a large difference here. Measurements 2 and 3 are in the same range of ratios, between 0.14 and 0.45. While in the first measurement the ratios are 10% higher (0.15 - 0.58). However, figure 6.9 shows the normalised ratios and here the differences are compensated.

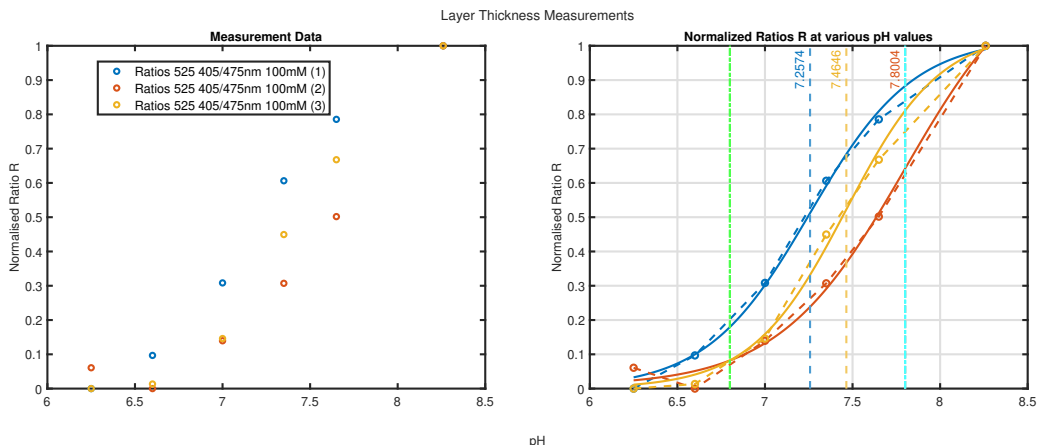


Figure 6.9: Results reproducibility measurements. Three measurement done with the same buffer solutions with and ionic strength of 100mM. Ratio of the emission peak divided by the excitation's peak (eq 4.7). pKa determined by Boltzmann sigmoid function (eq 4.5) Between each measurement 5 minutes waiting time

### Ionic Strength

To measure the influence of the ionic strength, measurements are done in buffer solutions with three different ionic strengths. Figure 6.10 shows these results. As described in the literature, it is visible that a higher ionic strength lowers the pKa of the indicator [154]. The sensitivity of the samples is comparable between the ionic strengths. This is visible in figure A.23 in Appendix A.16. The pKa of the measurements in a buffer solution of 150mM is less than the third reproducibility measurement and therefore this result could also be explained by the inconsistency of the measurements.

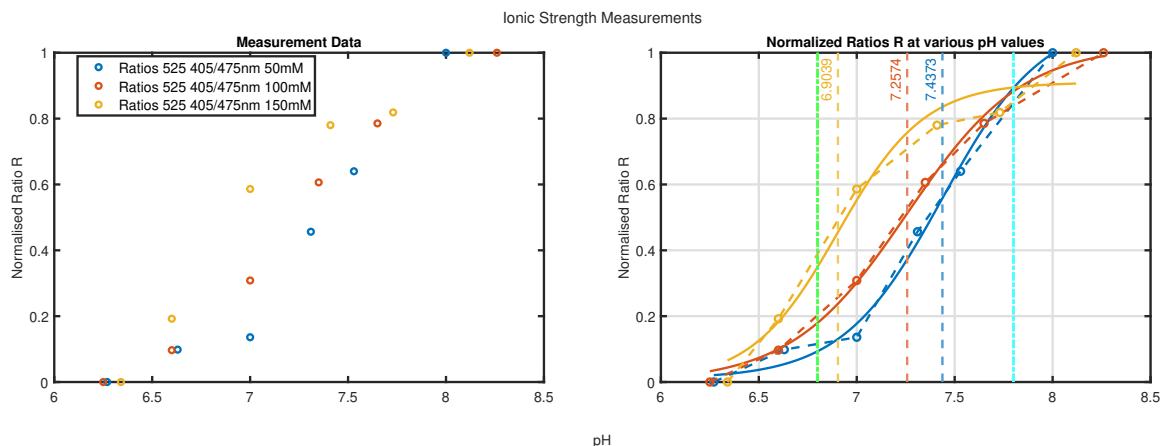


Figure 6.10: Results ionic strength measurements. Three measurement done with buffer solutions with IS of 50mM 100mM and 150mM. Ratio of the emission peak divided by the excitation's peak (eq 4.7). pKa determined by Boltzmann sigmoid function (eq 4.5) Between each measurement 5 minutes waiting time

Layer Thickness

To investigate the difference of thickness and speed, a measurement is done with a layer of 1mm thick next to the sample of 0.5mm thick, depicted in figure 6.11. The ratios for the thicker sample are higher. This can be a result of more HPTS-microbeads in front of the optical fibre. However, in figure 6.11 normalised ratios are used and the thicker sample is a bit more sensitive than the thinner sample. The thicker sample has a higher pKa than that of the thinner sample. However, if you compare it to the second measurement of figure 6.9 it is much closer. The sensitivity of the thicker sample is higher. This can be explained by the larger range between ratios of the sample. This makes the sensor more capable of detecting small changes.

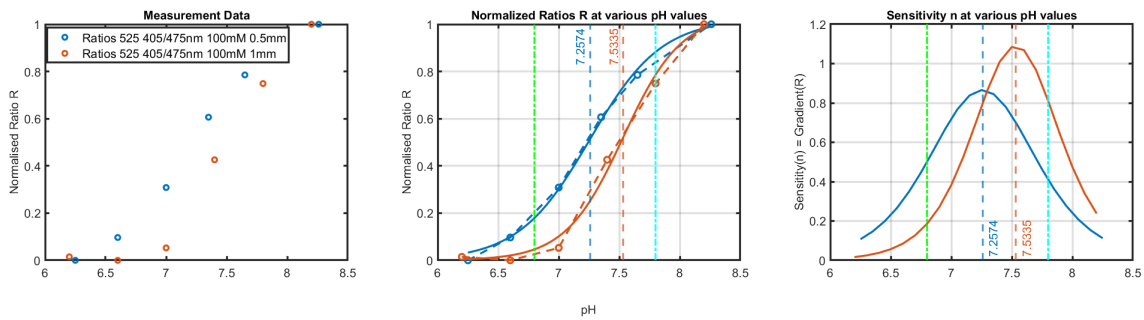


Figure 6.11: Results of the measurements done with two different layers with the same concentration. The measurement done with buffer solutions with IS of 100mM. Ratio of the emission peak divided by the excitation's peak (eq 4.7). pKa determined by Boltzmann sigmoid function (eq 4.5). Between each measurement 5 minutes waiting time

6.2.3. Transition Time

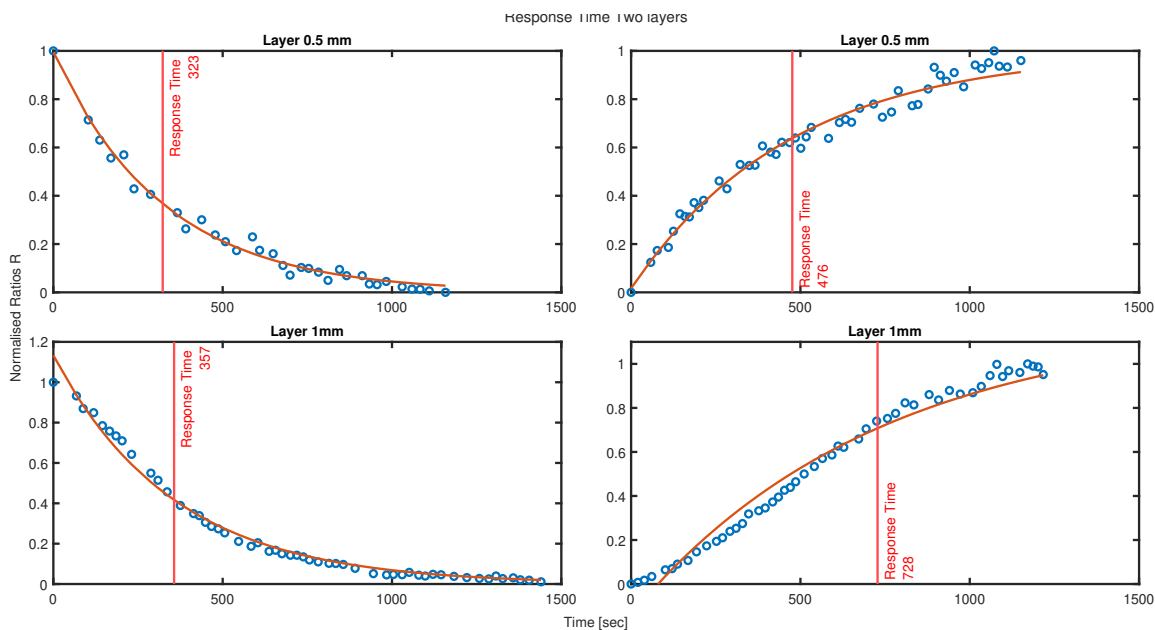


Figure 6.12: Result of the transition time measurements with response time of each sensing layer. Measured in both directions

To measure the speed of the sensor and the time constant, the sensor is submerged into a solution of pH of 8.2 and transferred to a solution with a pH of 6.2 and the other way around. During 20 minutes, multiple measurements are done to calculate the change of ratio over time. With these ratios, an exponential line can be fitted:

$$R = C + ae^{b*t} \tag{6.1}$$

From the fitted exponential function, the response time  $T$  can be calculated by:

$$T = 1 / -b \quad (6.2)$$

Figure 6.12 show the results of the measurement done to determine the response time of the sensor. As expected, the response time of the thicker sample is slower as more diffusion has to occur and this is limited by the physical processes of diffusion of hydrogen ions. However, the transition time from a pH of 8.2 to 6.2 is much closer than that of the other way around. Secondly, the response times from a buffer solution with high pH to low pH (left) are faster than the other way around. Almost twice as fast from low to high.

To achieve reliable measurements, a time of 3 times  $T$  has to be taken. This to have a measurement within 5% of the final value. For all layers, this exceeds the 1 minute time asked by the surgeons at the onset of the project. At most, the minimal response time (0.5mm and high-low) is 323 seconds, which implies a reliable measurement time of 969 seconds which is 16.16 minutes. However, the response time can be shorted by extrapolating the data during the measurement.

### 6.3. Analysis of proof-of-concept sensor

The results of the proof-of-concept sensor show the potential of using this type of sensing for measuring myocardial ischaemia. Almost all measurements had a pKa in between the range of 6.8 and 7.8, which is described as the range in which cells can survive. This is a positive result.

The sensing layer is sensitive to ionic strength as expected, and unfortunately the reproducibility is low. This is essential for a sensor and should be a focus for the future. Another focus would be to decrease the transition times. As these are still way to long. However, a clear relation could be extracted from the time measurements which correspond to the literature.

Thickness improves the fluorescent intensities measured. This enlarges the ratio differences and causes a higher sensitivity. However, the transition time is slower for the thicker sample. Future research is needed to investigate how the sensitivity can be increased without increasing the response time of the sensor.

In the onset of the project, a list of criteria is set up for the proof-of-concept sensor. The created sensor is: bio-compatible, sensitive to pH between 6.5 and 8, costs less than 1000 euro to fabricate, allows for remote sensing, and no complex chemistry is needed to create the sensor. However, the sensor is not able to handle interference, as its own reproducibility is low. It had not an accuracy of 0.1 pH. It did use complex equipment for the optical measurements, but the technique is not that complex. The role of the spectrometer in the measurements can be easily taken over by photo diodes and filters.

#### Interim Conclusions:

- The developed proof-of-concept sensor is sensitive in the predetermined range.
- Response time is slow, the thicker sample is even slower.
- Thicker sample leads to higher values, and thus a higher sensitivity.
- Reproducibility of the sensor needs to be improved as the differences are still large.
- Ionic strength results correspond to the literature

# 7

## Discussion

The aim of the thesis was to investigate the possibility to measure myocardial ischaemia with an optical-based sensor and to develop a proof-of-concept of the sensor. The goal is to investigate this, while considering all different options by using a structured approach. The main research question of the thesis was: Is it possible to measure myocardial ischaemia with an optical-based sensor? This main question was split up into subquestions related to the feasible methods, the conditions the sensor must meet, which technique can be used to achieve this, and what the characteristics and properties of the developed sensor are. Overall, this thesis succeeded in answering the main question. However, some limitations and disadvantages are discovered and are discussed in this chapter. These limitations and disadvantages are manageable and therefore this thesis shows a lot of potential for the future. As this research is new within the department, a lot of new information is gathered and many options are considered. Combining the information and findings of this thesis, it seems viable to measure myocardial ischaemia with an optical-based sensor.

First, the research questions will be restated and answered with the information gathered in this thesis. Secondly, the results of this thesis are compared with the literature and state how this research filled in the knowledge gaps. Finally, the limitations and clinical relevance are evaluated and recommendations for future research are done.

To answer the research question and to develop a proof-of-concept sensor, it was split up into four subquestions. These questions concerned the feasible methods (**SQ:1**), the condition which the sensor must meet (**SQ:2**), the optical sensing technique (**SQ:3**), and the characteristics and properties of the proof of concept developed (**SQ:4**). As subquestion 1 was the research question of the literature review (Appendix A.18.2) it is extensively discussed in the review and will only be shortly discussed here.

### **(SQ:1) What are feasible methods to detect myocardial ischaemia during cardioplegia-induced arrest?**

The goal of the literature review was to lay the groundwork to develop a proof of concept sensor. To lay this ground work, the literature review first examined which physiological parameters can be measured in an arrested heart. Lactate and pH were chosen to be further investigated in the literature review. Following this, an overview of all types of technologies capable of sensing pH and lactate were compared. The decision was made to further investigate the optical sensing technologies. In total, thirty-seven different pH and lactate were compared in three optical methods. These methods were reflection, absorption, and fluorescence. The results from the literature review show that fluorescence pH sensing has the most potential and that is why the remainder of the thesis focused on this.

### **(SQ:2) What are the conditions that the sensor must meet to be used in practice?**

To develop a proof-of-concept sensor and to select an optochemical sensing technique, it is important to design it with the end goal in mind. Therefore, cardio-thoracic surgeons of the Leiden University

Medical Center were consulted to see what the medical requirements are for the sensor. For the surgeons, it is important that it needs to measure the ischaemia reliable and safe, be easy to handle, and does not get in the way during the operation. It did not matter which parameter the sensor would measure and the costs. They need at least 3 sensors as the flow areas of all coronary arteries should be investigated and Khabbaz et al. [72] showed that three sensors are reliable. The largest limitation in this work compared to the literature lays in the resources available for this project. As this research is a proof-of-concept and exploration in the field of ischaemia detection, there were limited resources available. As a result, expensive and chemically advanced processes could not be used. Therefore, the use of sol-gels and Time-Resolved optical measurements were not available for this project, while these show a lot of potential [157, 28, 53]. However, Cattini et al. [25] showed that with relative simple methods and materials impressive results could be obtained. However, the research of Cattini et al. [24] did not state any information about optimising the sensing layer and concentrations. It was also focused on measuring the pH of blood in extracorporeal circulation, and as described in section 2.2.3 and in the review article of Steinegger et al. [139] this can be challenging. Combining the literature, medical requirements and the resources available, a list of criteria was developed to make sure that a proof-of-concept sensor could be created and tested in this research. This work is the first to describe the requirements of the surgeon on ischaemia detection, which can support many other researchers for developing ischaemia detecting sensors.

### **(SQ:3) What optochemical sensing technique can be used to measure pH differences induced by myocardial ischaemia?**

In the literature review, the articles found were divided into three optical techniques. However, other types of these techniques are described in the literature. Table 3.4 shows that there are 12 different optochemical techniques which can be measured by using fluorescence. The more advanced the sensing principle is, the better it can compensate for the interferences. Time-Resolved measurements show the most potential as they are already used in optochemical pH sensors [139]. Presens sensors use Dual Lifetime Referencing sensing which they patented [115]. However, dual wavelength referencing shows also a lot of potential for low cost sensors and has the ability to overcome interferences. As the resources available for this work are the main restriction, the dual wavelength referencing method is chosen in this work. This decision influences the indicator used for the prototype. As not all indicator dyes have dual wavelength (ratiometric) properties. By selecting the technique and dye, it is not yet possible to fabricate a sensor. For this, a support matrix is needed, and as described sol-gels could not be used in this work. Therefore, a selection is made between the different hydrogels. For this, HydroMed D4 was chosen, as it is a proven bio-compatible hydrogel and does not need any processing (UV/temperature/etc.) which can interfere with the indicator dye. As the hydrogel is transparent, it did not interfere with the optical measurements of the indicator dye. To encapsulate the indicator dye, anion exchange microbeads are used. This is done before in the literature and showed some limitations [24, 71, 139], which were accepted to develop a proof-of-concept sensor. This work is not the first to use this combination of dye, support matrix and microbeads. However, it is the first to compare the different techniques and materials by rating them on their ability to be developed into an in vivo sensor.

### **(SQ:4) What are the characteristics and properties of the proof of concept developed?**

Research published which fabricated HPTS-HydroMed D4 sensing layers did not describe an optimisation of the sensing layer. Therefore, this work used optical investigations and spectrometric analysis to optimise the concentration of HPTS, the density, and thickness of the sensing layer. This work clearly showed that changes in the layer have a result on the optical measurements. As the sensing layer contains microbeads of varying sizes, it is not possible to use methods like spin-coating. As a result, it is depended on where you measure on the sample. The goal of Dual Wavelength Referencing (DWR) is to overcome the problem of varying sample structures. However, this work shows that varying thicknesses and concentration have influence on the result. It also showed that the factors described in section 2.2.2 have a significant effect on the measurements and should be tackled before the sensor can be used in vivo. A lot of research described in the literature does not describe the influence of ionic strength in their pH measurements [139], because of the lack of knowledge on the chemistry taking place at the molecular scale. This research tried to map this and how the support matrix and

microbeads also have a relation to the accuracy of the sensor.

As final result a needle proof-of-concept sensor is developed, on which different types of sensing layers could be tested. This needle used an miniature reflection fibre, a sensing layer, two LED's (405nm and 475nm), and a USB spectrometer. At the onset of the project, a list of 8 criteria were set up for the proof-of-concept sensor. Eventually, the sensor did meet 6 of the criteria and shows the potential to solve the other two. The influence of ionic strength and the lack of reproducibility are the greatest concern for the continuation of the project. However, it did meet all other criteria. The measurements done with an thicker sample show that more microbeads improve the sensitivity, but slows down the response time

## Limitations

As consequence of the decisions made in this work, some limitations have influenced the outcomes of this work. The most relevant limitations will be discussed

### *Resources*

As described in section 3.2.2 the resources available were a limiting factor. The decision to design a sensor based on Dual Wavelength Referencing with an hydrogel and HPTS was made to reduce the complexity and cost and time. Due to the delivery problems of materials, time was a scarce resource and did not allow for much further testing. If more time, financial, and devices were available, other decisions would have been made. However, the selection of the materials and techniques made allowed for the development of a proof-of-concept sensor, which was the main goal of the thesis.

### *Ionic Strength*

As the results show, the ionic strength of the solutions has a large influence on the fluorescent output measured. This influence is essential as the sensor needs to be accurate during a cardiac surgery. Secondly, the influence of electrolytes in cardioplegia should be investigated. As cardioplegia exist out of KCl,  $Mg^{2+}$ ,  $Ca^{2+}$ ,  $Cl^-$  and  $Na^+$ . All these ions have a valency which changes the ionic strength in the environment. However, cardioplegia is administered in coronary arteries and it is not clear if on the epicard the influence of the ionic strength of the electrolytes is present. The proof of concept results show that the ionic strength has a substantial influence on the ratios calculated from the spectrometer measurements.

### *Chemical Knowledge*

As at the beginning of the project it was not yet clear which type of sensing would be the best for detecting myocardial ischaemia, all different types were compared. Eventually, the most potential sensors were optochemical sensors. The limitation which comes with this is that the background of the main author is not a chemical background. While the processes influencing the sensor are mostly chemical processes. As a result, the influence of ionic strength and immobilisation of the indicator where not fully understood when the selection was made to use microbeads and a negatively charged hydrogel. If more chemical knowledge were available, other techniques (more advanced) such as Wencel et al. [157] and Gong et al. [53] could be attempted. As results in the literature show that sol-gels have their advantages in stability and immobilisation of the dye

### *In vivo sensing*

The goal of this thesis was to develop a proof-of-concept sensor and test this sensor in vivo. However, due to delivery problems and limited time, it was not possible to test the sensor in vivo. As the in vivo results can be different than those of the buffer solutions, the viability of the sensor is not yet fully clear. In the final design, it is also not yet suitable to test on the heart as the design still has to be miniaturised. This miniaturisation has to be optimised as the chemical processes change at a small scale.

### *Consistency and interference*

As the results show, it was hard to achieve a consistent sensing layer and results. As the process steps in this work were tried to be kept the same for the fabrication of the sensing layer, this was difficult. This resulted in different types of sensing layers, which were difficult to compare. The Dual Wavelength Referencing is used to overcome the interference between the layers, but was not efficient

enough. Other interferences were that water was accumulating on the backside of the sensing layer. This caused that the light from the reflection fibre was first going from the probe to the sensing layer to water, and after a while from probe to water to the sensing layer to water. Different media have different effects on light and these effects should be investigated in future research. Another interference which should be kept in mind is that the sensor will need to be calibrated. However, for calibration, the precise environment is needed which accords with the measurement environment. As this environment changes, the calibration needs to be changed.

### **Clinical relevance**

This project started with a clinical problem: Cardiac patients die after surgery because the cardioplegia did not protect all cardiomyocytes and that this is a black box for surgeons and perfusionists. As there is no golden standard or even a device which is possible, there were many different options to create a sensor. Unfortunately, it was not possible to test the sensor in vivo or in tissue, and the sensor will need to be further developed before these tests can be done. However, this work definitely helped in solving the clinical problem of cardioplegia induced myocardial ischaemia.

First of all, this is the first research which compared the potential of electrochemical and optochemical sensing for detecting changes in tissue pH. This work explicated the challenges for optochemical sensing during cardiac surgery and showed the potential of fluorescent sensing.

Secondly, this work tested if a sensing layer consisting of HPTS-microbeads and HydroMed D4 could be used for detecting the pH changes of the tissue. The sensing layers created show a lot of potential, but as stated before, the consistency of the layers should be increased to validate the potential.

In third place, this work identified challenges on which subsequent research should focus and tackle before in vivo measurements can be done. For example, the relation between ionic strength and electrolyte concentration should be investigated. As well as the possibility to use sol gels instead of hydrogels to have a neutral charged sensing layer, which could improve the accuracy.

Finally, this work describes the relation between the thickness/concentration and sensitivity of the sensing layer. In this work, the relation between thickness of the sample and the transition time is substantial. Therefore, it is important to focus future work on creating thin sensing layers.

### **Recommendation**

The following recommendation for improvement of the current sensor and future research can be made. These recommendations are not only for the continuation of research at TU Delft, but all future research on detecting cardioplegia induced cardiac arrest. First, sensor-related recommendations are made and these are followed by the recommendation on which physiological effects need to be further investigated.

#### *Optimisation sensor*

It has been already described multiple times in this research, but improving the consistency of the samples can make the sensor more viable. The sensor should be more reproducible than it is now. The differences between samples had too much influence on the outcome of the measurements. If this can be reduced, it is possible to calibrate the sensor. Besides the reproducibility, the response times have to be reduced a lot, before this sensor can be used in practice. Secondly, scattering particles and optical isolation layer can be used to improve the light detected by the spectrometer. Thirdly, minimisation and biocompatibility testing are needed before the sensor can be used for in vivo measurements. At last, the optical system can be simplified by using filters and photodetectors instead of a spectrometer.

#### *Collaboration Chemical Engineering*

As stated in the limitation, the chemical know-how limited the processes to develop more advanced sensing layers. Sensing layers such as Gong et al. [53] and Wencel et al. [157] are more complex in fabrication, but also have better results. Combining the optical and medical knowledge of the department of Bio-electronics with that of chemical engineering, it can improve the success of the project.

As the latest sensors in the literature all use sol-gels as this has less influence on the sensitivity related to ionic strength, this would be the first recommendation. Sol-gels also allow for better immobilisation of the indicator dye and do not need microbeads as intermediaries. As the charge of the microbeads can also influence the pH measurement. Other indicators than HPTS are being used as the negative charge of HPTS makes it vulnerable for ionic strength changes.

#### *Compare with existing sensors in vivo*

Since the research of Khabbaz et al. [72] in 2001 no pH meter is used to detect myocardial ischaemia. While many different sensors have been developed since then. The advantage of using commercial pH sensors is that they have been approved by the authorities, this can speed up the process of in vivo sensing. The sensors of Presens have the most potential and they have a monopoly on Dual Lifetime Referencing (DLR) sensors. The sensors use a fluorescent hydrogel which can be vulnerable and needs liquids to work. It is already used in food and biological measurements, however not yet in vivo. They did a test with fluorescent sensor foils on tissue [125].

Another commercial available pH sensor is the ISFET pH sensor of Wellingq. This sensor is using the ISFET technology, which is sensitive to drift but showed good results in in vivo measurements done by Goodman et al. [54]. The sensor is FDA approved and thus can be tested in vivo without much problems. It would be interesting to test both sensors at the same time, as they use different technologies. Where the ISFET sensor measures the direct activity of the hydrogen ions the DLR sensor measures the concentration. Both sensors describe an accuracy of 0.1 in the diluted solution, so it should be interesting to see how this holds up in vivo.

#### *Cardioplegia electrolytes and other tissue*

The final recommendation is to focus a research on the influence of cardioplegia electrolytes on the pH measurements. As described multiple times, the influence of the electrolytes is unknown and could potentially have a great influence on the measured values. It would be interesting to evaluate this. Another aspect of this research would be to see if a reference measurement, for example on the muscles of your ribs, would be enough to indicate ischaemia. As the surgeons only want to know if the cardiomyocytes are becoming ischaemic and not the exact pH value is of importance.

Most pH sensors developed right now are focused on the differentiation of tumorous tissue [53, 5, 101, 35] or wound healing [130, 93]. It would be interesting to see the potential of this sensor in these applications.

## **Conclusion**

It is possible to measure myocardial ischaemia with an optical-based sensor. This worked showed the potential of optical-based sensors and indicates that myocardial ischaemia can be detected by using a fluorescence hydrogel. To develop a proof-of-concept sensor, a list of requirements is synthesised and a structured analysis of all options and techniques possible is conducted. This led to a proof-of-concept sensor, which is a needle-based sensor with an fluorescent hydrogel and two LED's to allow for dual wavelength referencing. This sensor is capable of measuring pH changes in the range requested by thoracic surgeons and can help them protect the patients during surgery.

Improvements can be made on the consistency of the sensing layers, the reproducibility, and the miniaturisation. However, this project succeeded in developing a sensor for a problem given by surgeons in 10 months time. Besides developing a sensor, this work brought together different sections of the scientific world to give an overview of all possibilities to measure ischaemia and the challenges ischaemia sensors are facing. Future investigation will optimise the current sensor and see if the sensor gives similar results in vivo.

Optochemical pH sensors will be the future in biomedical pH sensing as it shows a lot of potential and the accuracy is improving. Not only cardiac surgery patients can be helped by these types of sensors, but it is also capable of recognising tumorous tissue and other applications.



# Bibliography

- [1] A., M., Gonzalez, O., and R., J. (2013). Optical Fiber Sensors for Chemical and Biological Measurements. In *Current Developments in Optical Fiber Technology*. InTech.
- [2] Abdominal Key (2020). Myocardial Protection | Abdominal Key.
- [3] Aigner, D. (2010). *Synthese und Charakterisierung von polymerisierbaren optischen Indikatoren und deren kovalente Anbindung an magnetische optische Sensorpartikel*. PhD thesis, TU Graz, Graz.
- [4] Aigner, D., Borisov, S. M., Orriach Fernández, F. J., Fernández Sánchez, J. F., Saf, R., and Klimant, I. (2012). New fluorescent pH sensors based on covalently linkable PET rhodamines. *Talanta*, 99:194–201.
- [5] Aigner, D., Ungerböck, B., Mayr, T., Saf, R., Klimant, I., and Borisov, S. M. (2013). Fluorescent materials for pH sensing and imaging based on novel 1,4-diketopyrrolo-[3,4-c]pyrrole dyes. *Journal of Materials Chemistry C*, 1(36):5685–5693.
- [6] Albert, A. and Serjeant, E. P. (1984). *The Determination of Ionization Constants*. Springer Netherlands.
- [7] Ali, J. M., Miles, L. F., Abu-Omar, Y., Galhardo, C., and Falter, F. (2018). Global cardioplegia practices: Results from the global cardiopulmonary bypass survey. In *Journal of Extra-Corporeal Technology*, volume 50, pages 83–93. American Society of Extra-Corporeal Technology.
- [8] Álvarez, V., Agramunt, J., Ball, M., Batallé, M., Bayarri, J., Borges, F. I., Bolink, H., Brine, H., Cárcel, S., Carmona, J. M., Castel, J., Catalá, J. M., Cebrián, S., Cervera, A., Chan, D., Conde, C. A., Dafni, T., Dias, T. H., Díaz, J., Esteve, R., Evtoukhovitch, P., Ferrando, J., Fernandes, L. M., Ferrario, P., Ferreira, A. L., Ferrer-Ribas, E., Freitas, E. D., García, S. A., Gil, A., Giomataris, I., Goldschmidt, A., Gómez, E., Gómez, H., Gómez-Cadenas, J. J., González, K., Gutiérrez, R. M., Hauptman, J., Hernando-Morata, J. A., Herrera, D. C., Herrero, V., Iguaz, F. J., Irastorza, I. G., Kalinnikov, V., Labarga, L., Liubarsky, I., Lopes, J. A., Lorca, D., Losada, M., Luzón, G., Marí, A., Martín-Albo, J., Méndez, M., Miller, T., Moisenko, A., Monrabal, F., Monteiro, B., Monzó, J. M., Mora, F. J., Muñoz Vidal, J., Natal Da Luz, H., Navarro, G., Nebot, M., Nygren, D., Oliveira, C. A., Palma, R., Pérez Aparicio, J. L., Pérez, J., Radicioni, E., Quinto, M., Renner, J., Ripoll, L., Rodríguez, A., Rodríguez, J., Santos, F. P., Dos Santos, J. M., Seguí, L., Serra, L., Shuman, D., Sofka, C., Sorel, M., Soriano, A., Spieler, H., Toledo, J. F., Torrent Collell, J., Tomás, A., Tsamalaidze, Z., Vázquez, D., Velicheva, E., Veloso, J. F., Villar, J. A., Webb, R., Weber, T., White, J. T., and Yahlali, N. (2012). SiPMs coated with TPB: Coating protocol and characterization for NEXT. *Journal of Instrumentation*, 7(2).
- [9] Andrus, L. P., Unruh, R., Wisniewski, N. A., McShane, M. J., and Bukkapatnam, S. (2015). Characterization of lactate sensors based on lactate oxidase and palladium benzoporphyrin immobilized in hydrogels. *Biosensors*, 5(3):398–416.
- [10] Asmatulu, R. (2012). Nanocoatings for corrosion protection of aerospace alloys. In *Corrosion Protection and Control Using Nanomaterials*, pages 357–374. Elsevier.
- [11] Atkins, P. and Paula, J. d. (2006). *Atkins' Physical chemistry*. Oxford University Press.
- [12] Awasthi, P., Mukherjee, R., O Kare, S. P., and Das, S. (2016). Impedimetric blood pH sensor based on MoS<sub>2</sub>-Nafion coated microelectrode. *RSC Advances*, 6(104):102088–102095.
- [13] Bafana, A., Devi, S. S., and Chakrabarti, T. (2011). Azo dyes: Past, present and the future.
- [14] Bailey, R. (2019). The 3 Layers of the Heart Wall.

- [15] Baishya, N., Momouei, M., Budidha, K., Qassem, M., Vadgama, P., and Kyriacou, P. A. (2020). Near infrared spectrometric investigation of lactate in a varying pH buffer. *Journal of Near Infrared Spectroscopy*, 28(5-6):328–333.
- [16] Baucke, F. G. K. (1985). The Origin of the Glass Electrode Response. In *Glass ... Current Issues*, pages 481–505. Springer Netherlands.
- [17] Bernard Valeur and Mário Nuno Berberan-Santos (2011). *Molecular Fluorescence*. Wiley-VCH.
- [18] Bhalla, N., Jolly, P., Formisano, N., and Estrela, P. (2016). Introduction to biosensors. *Essays in Biochemistry*, pages 60–61.
- [19] Birkel, A., Denault, K. A., George, N. C., Doll, C. E., Héry, B., Mikhailovsky, A. A., Birkel, C. S., Hong, B. C., and Seshadri, R. (2012). Rapid microwave preparation of highly efficient Ce 3+-substituted garnet phosphors for solid state white lighting. *Chemistry of Materials*, 24(6):1198–1204.
- [20] Biswas, A., Bornhoeft, L. R., Banerjee, S., You, Y. H., and McShane, M. J. (2017). Composite Hydrogels Containing Bioactive Microreactors for Optical Enzymatic Lactate Sensing. *ACS Sensors*, 2(11):1584–1588.
- [21] Borisov, S. M., Neurauter, G., Schroeder, C., Klimant, I., and Wolfbeis, O. S. (2006). Modified dual lifetime referencing method for simultaneous optical determination and sensing of two analytes. *Applied Spectroscopy*, 60(10):1167–1173.
- [22] Carrara, S. (2017). Towards new efficient nanostructured hybrid materials for ECL applications. (January):1–226.
- [23] Carvajal, C., Goyal, A., and Tadi, P. (2020). *Cardioplegia*. StatPearls Publishing.
- [24] Cattini, S., Accorsi, L., Truzzi, S., and Rovati, L. (2020a). On the Development of an Instrument for In-Line and Real-Time Monitoring of Blood-pH in Extracorporeal Circulation. *IEEE Transactions on Instrumentation and Measurement*, 69(8):5640–5648.
- [25] Cattini, S., Truzzi, S., Accorsi, L., and Rovati, L. (2020b). Performances and Robustness of a Fluorescent Sensor for Nearly Neutral pH Measurements in Healthcare. *IEEE Transactions on Instrumentation and Measurement*, 69(10):7658–7665.
- [26] Chen, S., Yang, Q., Xiao, H., Shi, H., and Ma, Y. (2017). Local pH monitoring of small cluster of cells using a fiber-optic dual-core micro-probe. *Sensors and Actuators, B: Chemical*, 241:398–405.
- [27] Chen, X. and Gu, Z. (2013). Absorption-type optical pH sensitive film based on immobilized purple cabbage pigment. *Sensors and Actuators, B: Chemical*, 178:207–211.
- [28] Choudhary, T. T. R., Tanner, M. M. G., Megia-Fernandez, A., Harrington, K., Wood, H. H. A., Marshall, A., Zhu, P., Chankeshwara, S. S. V., Choudhury, D., Monro, G., Dhaliwal, K., Bradley, M., Ucuncu, M., Yu, F., Duncan, R. R., Thomson, R. R., Dhaliwal, K., and Bradley, M. (2019). High fidelity fibre-based physiological sensing deep in tissue. *Scientific Reports*, 9(1):1–10.
- [29] Covington, A. K. (1985). International union of pure and applied chemistry: Analytical chemistry division commission on electro analytical chemistry and physical chemistry division commission on electrochemistry definition of pH scales, standard reference values, measurement of pH and related terminology. *Pure and Applied Chemistry*, 57(3):531–542.
- [30] Cox, B. G. (2013). *Acids and Bases*. Oxford University Press.
- [31] Cui, Q., Podrazky, O., Mrazek, J., Probostova, J., and Kasik, I. (2015). Tapered-Fiber Optical Sensor for Physiological pH Range. *IEEE Sensors Journal*, 15(9):4967–4973.
- [32] D’agostino, R. S., Jacobs, J. P., Badhwar, V., Fernandez, F. G., Paone, G., Wormuth, D. W., and Shahian, D. M. (2018). The Society of Thoracic Surgeons Adult Cardiac Surgery Database: 2018 Update on Outcomes and Quality. *The Annals of Thoracic Surgery*, 105:15–23.

- [33] Daniel, A. (2014). *Design and Development of New Sensitive Materials in Fluorescence pH Sensors*. PhD thesis.
- [34] Davierwala, P. M., Verevkin, A., Leontyev, S., Misfeld, M., Borger, M. A., and Mohr, F. W. (2013). Impact of expeditious management of perioperative myocardial ischemia in patients undergoing isolated coronary artery bypass surgery. *Circulation*, 128(SUPPL.1).
- [35] Delehanty, J. B. J., Susumu, K., Manthe, R. R. L., Algar, W. R., and Medintz, I. I. L. (2012). Active cellular sensing with quantum dots: Transitioning from research tool to reality; a review. *Analytica Chimica Acta*, 750:63–81.
- [36] Dobson, G. P., Faggian, G., Onorati, F., and Vinten-Johansen, J. (2013). Hyperkalemic cardioplegia for adult and pediatric surgery: end of an era? *Frontiers in Physiology*, 4:228.
- [37] Donald, S. and Barry E, B. (2018). Cardiac Markers: Definition and Efficacy, Cardiac Troponins, Creatine Kinase–MB.
- [38] Drescher, C., Diestel, A., Wollersheim, S., Berger, F., and Schmitt, K. R. (2011). How does hypothermia protect cardiomyocytes during cardioplegic ischemia? *European Journal of Cardiothoracic Surgery*, 40(2):352–359.
- [39] Driller, M., Plews, D., and Borges, N. (2016). Wearable near Infrared Sensor for Determining an Athlete's Lactate Threshold during Exercise. *NIR news*, 27(4):8–10.
- [40] ebme (2021). Cardiopulmonary bypass machine - CPB.
- [41] Edinburgh Instruments (2021). Beer Lambert Law | Transmittance & Absorbance |.
- [42] Edmonds, T. E., Flatters, N. J., Jones, C. F., and Miller, J. N. (1988). Determination of pH with acid-base indicators: Implications for optical fibre probes. *Talanta*, 35(2):103–107.
- [43] Ehrlich, K., Kufcsák, A., McAughtrie, S., Fleming, H., Krstajic, N., Campbell, C. J., Henderson, R. K., Dhaliwal, K., Thomson, R. R., and Tanner, M. G. (2017). pH sensing through a single optical fibre using SERS and CMOS SPAD line arrays. *Optics Express*, 25(25):30976.
- [44] Ellerby, G. E., Smith, C. P., Zou, F., Scott, P., and Soller, B. R. (2013). Validation of a spectroscopic sensor for the continuous, noninvasive measurement of muscle oxygen saturation and pH. *Physiological Measurement*, 34(8):859–871.
- [45] Elsherif, M., Hassan, M., Yetisen, A., and Butt, H. (2019). Hydrogel optical fibers for continuous glucose monitoring. *Biosensors and Bioelectronics*, 137:25–32.
- [46] Ericsson, A. B. (2000). From the Cardioplegia and Cardiac Function Evaluated by Left Ventricular Pressure-Volume Relations Stockholm 2000. Technical report.
- [47] Ferrari, L., Rovati, L., Fabbri, P., and Pilati, F. (2013). Continuous haematic pH monitoring in extracorporeal circulation using a disposable fluorescence sensing element. *Journal of Biomedical Optics*, 18(2).
- [48] Florea, L., Fay, C., Lahiff, E., Phelan, T., O'Connor, N. E., Corcoran, B., Diamond, D., and Benito-Lopez, F. (2013). Dynamic pH mapping in microfluidic devices by integrating adaptive coatings based on polyaniline with colorimetric imaging techniques. *Lab on a Chip*, 13(6):1079–1085.
- [49] Frank, P. (2019). Perkin Elmer Application Note UV/Vis Spectroscopy.
- [50] French, P. (2020). In-vivo microsystems: A review.
- [51] Galler, N. (2013). *Investigation of optical pH sensors below 10 mM ionic strength*. PhD thesis, University of Technology, Graz.
- [52] Glenn P. Gravlee (2008). *Cardiopulmonary Bypass: Principles and Practice*. Wolters Kluwer Health/Lippincott Williams & Wilkins.

- [53] Gong, J., Tanner, M. G., Venkateswaran, S., Stone, J. M., Zhang, Y., and Bradley, M. (2020). A hydrogel-based optical fibre fluorescent pH sensor for observing lung tumor tissue acidity. *Analytica Chimica Acta*, 1134:136–143.
- [54] Goodman, A., Bacon, W., Murphy, K., Austin Client, M., Doro Advisor, C., and Jeremy Rogers, P. (2020). Improving acute compartment syndrome diagnostic technology by measuring intramuscular pH with an Ion-Sensitive Field Effect Transistor Critical Emergency Room Question Acute Compartment Syndrome Acknowledgements. *Sensors*.
- [55] Gupta, V. and Mahapatro, A. K. (2008). Material science Characterization Techniques for Materials II Characterization of Fluorescence Emission Paper No. : Characterization Techniques for Materials II Module : Characterization of Fluorescence Emission Development Team Principal Investigator Pap. Technical report.
- [56] Hajian, R., Mehrayin, Z., Mohagheghian, M., Zafari, M., Hosseini, P., and Shams, N. (2015). Fabrication of an electrochemical sensor based on carbon nanotubes modified with gold nanoparticles for determination of valrubicin as a chemotherapy drug: Valrubicin-DNA interaction. *Materials Science and Engineering C*, 49:769–775.
- [57] Hanson, M. A., Ge, X., Kostov, Y., Brorson, K. A., Moreira, A. R., and Rao, G. (2007). Comparisons of optical pH and dissolved oxygen sensors with traditional electrochemical probes during mammalian cell culture. *Biotechnology and Bioengineering*, 97(4):833–841.
- [58] Hartings, M. R., Castro, N. J., Gill, K., and Ahmed, Z. (2019). A photonic pH sensor based on photothermal spectroscopy. *Sensors and Actuators, B: Chemical*, 301(July):127076.
- [59] Head, S. J., Milojevic, M., Taggart, D. P., and Puskas, J. D. (2017). Current practice of state-of-the-art surgical coronary revascularization. *Circulation*, 136(14):1331–1345.
- [60] Heinemann, H. O. and Goldring, R. M. (1974). Bicarbonate and the regulation of ventilation. *The American Journal of Medicine*, 57(3):361–370.
- [61] Helmenstine, A. M. (2020). pH, pKa, and the Henderson-Hasselbalch Equation.
- [62] Hiruta, Y., Yoshizawa, N., Citterio, D., and Suzuki, K. (2012). Highly durable double sol-gel layer ratiometric fluorescent pH optode based on the combination of two types of quantum dots and absorbing pH indicators. *Analytical Chemistry*, 84(24):10650–10656.
- [63] Humon (2020). Humon - The World's First Muscle Oxygen Sensor for Endurance Sports.
- [64] Janata, J. (1987). Do Optical Sensors Really Measure pH? *Analytical Chemistry*, 59(9):1351–1356.
- [65] Janata, J. and Janata, J. (2009). Amperometric Sensors. In *Principles of Chemical Sensors*, pages 201–239. Springer US.
- [66] Jeon, D., Yoo, W. J., Seo, J. K., Shin, S. H., Han, K. T., Kim, S. G., Park, J. Y., and Lee, B. (2013). Fiber-optic pH sensor based on sol-gel film immobilized with neutral red. *Optical Review*, 20(2):209–213.
- [67] Jernelv, I. L., Strøm, K., Hjelme, D. R., and Aksnes, A. (2019). Infrared spectroscopy with a fiber-coupled quantum cascade laser for attenuated total reflection measurements towards biomedical applications. *Sensors (Switzerland)*, 19(23):5130.
- [68] Jorge, P. A. d. S. (2014). Interferometric Measurement: Principles and Techniques. In *Handbook of Optical Sensors*, pages 130–163. CRC Press.
- [69] Kasik, I., Mrazek, J., Martan, T., Pospisilova, M., Podrazky, O., Matejec, V., Hoyerova, K., and Kaminek, M. (2010). Fiber-optic pH detection in small volumes of biosamples. *Analytical and Bioanalytical Chemistry*, 398(5):1883–1889.

- [70] Kattipparambil Rajan, D., Patrikoski, M., Verho, J., Sivula, J., Ihalainen, H., Miettinen, S., and Leikkala, J. (2016). Optical non-contact pH measurement in cell culture with sterilizable, modular parts. *Talanta*, 161:755–761.
- [71] Kermis, H., Kostov, Y., Harms, P., and Rao, G. (2002). Dual Excitation Ratiometric Fluorescent pH Sensor for Noninvasive Bioprocess Monitoring: Development and Application. *Biotechnology Progress*, 18(5):1047–1053.
- [72] Khabbaz, K. R., Zankoul, F., and Warner, K. G. (2001). Intraoperative metabolic monitoring of the heart: II. Online measurement of myocardial tissue pH. *Annals of Thoracic Surgery*, 72(6):S2227–S2233.
- [73] Khuri, S. F. and Marston, W. A. (1985). On-line metabolic monitoring of the heart during cardiac surgery. *Surgical Clinics of North America*, 65(3):439–453.
- [74] Kim, S., Lee, S. H. S. Y., Min, S. Y., Byun, K. M., and Lee, S. H. S. Y. (2017). Dual-modal cancer detection based on optical pH sensing and Raman spectroscopy. *Journal of Biomedical Optics*, 22(10):1.
- [75] Klimant, I., Huber, C., Liebsch, G., Neurauder, G., Stangelmayer, A., and Wolfbeis, O. S. (2001). Dual Lifetime Referencing (DLR) — a New Scheme for Converting Fluorescence Intensity into a Frequency-Domain or Time-Domain Information. pages 257–274. Springer, Berlin, Heidelberg.
- [76] Knowles, J. R. (1980). Enzyme-catalyzed phosphoryl transfer reactions. *Annual review of biochemistry*, 49(1):877–919.
- [77] Kocincová, A. S. (2007). New pH Sensitive Sensor Materials. Luminescent Fiber-Optic Dual Sensors for Non-Invasive and Simultaneous Measurement of pH and pO<sub>2</sub> (Dissolved Oxygen) in Biological. Technical report.
- [78] Koning, N. J. (2017). *Protection of the microcirculation during cardiac surgery with cardiopulmonary bypass*.
- [79] Kraut, J. A. and Madias, N. E. (2014). Lactic Acidosis. *New England Journal of Medicine*, 371(24):2309–2319.
- [80] Kricka, L. (2003). *No Titl Optical Methods: A Guide to the "Escences"*. American Association for Clinical Chemistry.
- [81] Laimoud, M. and Qureshi, R. (2020). Outcome of Postcardiac Surgery Acute Myocardial Infarction and Role of Emergency Percutaneous Coronary Interventions. *Cardiology Research and Practice*, 2020.
- [82] Lakowicz, J. R. (2006). *Principles of Fluorescence Spectroscopy*. Springer US, Boston, MA.
- [83] LAM, C. R., GEOGHEGAN, T., and LEPORE, A. (1955). Induced cardiac arrest for intracardiac surgical procedures; an experimental study. *The Journal of thoracic surgery*, 30(5):620–5.
- [84] Lee, C. H., Ju, M. H., Kim, J. B., Chung, C. H., Jung, S. H., Choo, S. J., and Lee, J. W. (2014). Myocardial injury following aortic valve replacement for severe aortic stenosis: Risk factor of post-operative myocardial injury and its impact on long-term outcomes. *Korean Journal of Thoracic and Cardiovascular Surgery*, 47(3):233–239.
- [85] Li, W., Cheng, H., Xia, M., and Yang, K. (2013). An experimental study of pH optical sensor using a section of no-core fiber. *Sensors and Actuators, A: Physical*, 199:260–264.
- [86] Libretexts Chemistry (2020a). Molecular Fluorescence.
- [87] Libretexts Chemistry (2020b). The Franck-Condon Principle.
- [88] Liebsch, G., Klimant, I., Krause, C., and Wolfbeis, O. S. (2001). Fluorescent imaging of pH with optical sensors using time domain dual lifetime referencing. *Analytical Chemistry*, 73(17):4354–4363.

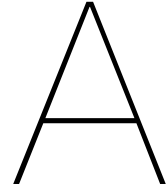
- [89] Liu, M., He, D., Yang, T., Liu, W., Mao, L., Zhu, Y., Wu, J., Luo, G., and Deng, J. (2018). An efficient antimicrobial depot for infectious site-targeted chemo-photothermal therapy. *Journal of Nanobiotechnology*, 16(1).
- [90] Lobnik, A. (2006). ABSORPTION-BASED SENSORS. pages 77–98. Springer, Dordrecht.
- [91] Lowenstein, E. (1997). Cardiac Surgery in the Adult. *Anesthesia & Analgesia*, 85(6):1418.
- [92] Marzouk, S. A., Buck, R. P., Dunlap, L. A., Johnson, T. A., and Cascio, W. E. (2002). Measurement of extracellular pH, K<sup>+</sup>, and lactate in ischemic heart. *Analytical Biochemistry*, 308(1):52–60.
- [93] Meier, R., Schreml, S., Wang, X.-D., Landthaler, M., Babilas, P., and Wolfbeis, O. (2011). Simultaneous photographing of oxygen and pH in vivo using sensor films. *Angewandte Chemie - International Edition*, 50(46):10893–10896.
- [94] Meirose (2014). The World Leader in Serving Science. *Spectrochimica Acta - Part A: Molecular and Biomolecular Spectroscopy*, pages 1–19.
- [95] Melkonian, E. A. and Schury, M. P. (2019). *Biochemistry, Anaerobic Glycolysis*. StatPearls Publishing.
- [96] Melrose, D. G., Dreyer, B., Bentall, H. H., and Baker, J. B. (1955). ELECTIVE CARDIAC ARREST. *The Lancet*, 266(6879):21–23.
- [97] Meng, Z. H. (2012). Molecularly Imprinted Sol-Gel Sensors. In *Molecularly Imprinted Sensors*, pages 303–337. Elsevier.
- [98] Merriam-Webster (2021). Sensor | Definition of Sensor by Merriam-Webster.
- [99] Miesse, P. (2020). *Flexible Electrochemical Lactate Sensor*. PhD thesis, Old Dominion University.
- [100] Mishra, S. K., Zou, B., and Chiang, K. S. (2017). Wide-Range pH Sensor Based on a Smart-Hydrogel-Coated Long-Period Fiber Grating. *IEEE Journal of Selected Topics in Quantum Electronics*, 23(2):284–288.
- [101] Moon, C. M., Kim, Y. H., Ahn, Y. K., Jeong, M. H., and Jeong, G. W. (2019). Metabolic alterations in acute myocardial ischemia-reperfusion injury and necrosis using in vivo hyperpolarized [1-13C] pyruvate MR spectroscopy. *Scientific Reports*, 9(1):1–11.
- [102] Moxy Monitor (2021). Moxy Monitor - Muscle Oxygen Monitor.
- [103] Muller, P. (1994). Glossary of terms used in physical organic chemistry: (IUPAC Recommendations 1994). *Pure and Applied Chemistry*, 66(5):1077–1184.
- [104] Namay, D. L., Hammermeister, K. E., Zia, M. S., DeRouen, T. A., Dodge, H. T., and Namay, K. (1982). Effect of perioperative myocardial infarction on late survival in patients undergoing coronary artery bypass surgery. *Circulation*, 65(6):1066–1071.
- [105] Nichols, S. P., Balaconis, M. K., Gant, R. M., Au-Yeung, K. Y., and Wisniewski, N. A. (2018). Long-term in vivo oxygen sensors for peripheral artery disease monitoring. In *Advances in Experimental Medicine and Biology*, volume 1072, pages 351–356. Springer New York LLC.
- [106] Okabe, Yuka, U. o. C. I. (2007). Advantages of quantum dots over conventional fluorophores. pages 7–8.
- [107] OriginLab (2021). Origin Help - Boltzmann.
- [108] Outhwaite, C. W. (2003). Extension of the Debye–Hückel Theory of Electrolyte Solutions. *The Journal of Chemical Physics*, 50(6):2277.
- [109] Park, H. J., Yoon, J. H., Lee, K. G., and Choi, B. G. (2019). Potentiometric performance of flexible pH sensor based on polyaniline nanofiber arrays. *Nano Convergence*, 6(1):9.

- [110] Payne, M. E., Zamarayeva, A., Pister, V. I., Yamamoto, N. A., and Arias, A. C. (2019). Printed, Flexible Lactate Sensors: Design Considerations Before Performing On-Body Measurements. *Scientific Reports*, 9(1):1–10.
- [111] Picó, Y. (2012). *Chemical Analysis of Food: Techniques and Applications*. Elsevier Inc.
- [112] Pischke, S., Hyler, S., Tronstad, C., Bergsland, J., Fosse, E., Halvorsen, P., Skulstad, H., and Tønnessen, T. (2015). Myocardial tissue CO<sub>2</sub> tension detects coronary blood flow reduction after coronary artery bypass in real-time †. *British Journal of Anaesthesia*, 114(3):414–422.
- [113] Pischke, S. E., Tronstad, C., Holhjem, L., Halvorsen, P. S., and Tønnessen, T. I. (2012). Perioperative detection of myocardial ischaemia/reperfusion with a novel tissue CO<sub>2</sub> monitoring technology. *European Journal of Cardio-thoracic Surgery*, 42(1):157–163.
- [114] Pohanka, M. (2017). The Piezoelectric Biosensors: Principles and Applications, a Review. *Int. J. Electrochem. Sci*, 12:496–506.
- [115] PreSens (2021). Sensor Basics: Measurement Principle of Optical Sensors.
- [116] Putnam, B., Bricker, S., Fedorka, P., Zelada, J., Shebrain, S., Omari, B., and Bongard, F. (2007). The correlation of near-infrared spectroscopy with changes in oxygen delivery in a controlled model of altered perfusion. *American Surgeon*, 73(10):1017–1022.
- [117] Qi, J., Liu, D., Liu, X., Guan, S., Shi, F., Chang, H., He, H., and Yang, G. (2015). Fluorescent pH Sensors for Broad-Range pH Measurement Based on a Single Fluorophore. *Analytical Chemistry*, 87(12):5897–5904.
- [118] Ran, Y., Xiao, P., Zhang, Y., Hu, D., Xu, Z., Liang, L., and Guan, B.-O. (2020). A Miniature pH Probe Using Functional Microfiber Bragg Grating. *Optics*, 1(2):202–212.
- [119] Raoufi, N., Surre, F., Sun, T., Rajarajan, M., and Grattan, K. T. (2012). Wavelength dependent pH optical sensor using the layer-by-layer technique. *Sensors and Actuators B: Chemical*, 169:374–381.
- [120] Rassaei, L., Olthuis, W., Tsujimura, S., Sudhölter, E. J. R., and van den Berg, A. (2014). Lactate biosensors: current status and outlook. *Analytical and Bioanalytical Chemistry*, 406(1):123–137.
- [121] Regtien, P. and Dertien, E. (2018). *Sensors for mechatronics*. Elsevier.
- [122] Reijenga, J., Van Hoof, A., Van Loon, A., and Teunissen, B. (2013). Development of Methods for the Determination of pKa Values. *Analytical Chemistry Insights*, pages 8–53.
- [123] RF Wireless World (2021). Advantages Disadvantages temperature sensor-thermocouple,RTD,thermistor,IC sensor.
- [124] Robergs, R. A., McNulty, C. R., Minett, G. M., Holland, J., and Trajano, G. (2018). Lactate, not lactic acid, is produced by cellular cytosolic energy catabolism.
- [125] Schreml, S., Meier, R., Wolfbeis, O., Landthaler, M., Szeimies, R.-M., and Babilas, P. (2011). 2D luminescence imaging of pH in vivo. *Proceedings of the National Academy of Sciences of the United States of America*, 108(6):2432–2437.
- [126] Sef, D., Szavits-Nossan, J., Predrijevac, M., Golubic, R., Sipic, T., Stambuk, K., Korda, Z., Meier, P., and Turina, M. I. (2019). Management of perioperative myocardial ischaemia after isolated coronary artery bypass graft surgery. *Open Heart*, 6(1):1027.
- [127] Sensors, P. (1856). Special Lecture Series Biosensors and Instrumentation. pages 1–9.
- [128] Senst, B., Goyal, A., and Diaz, R. R. (2020). *Cardiac Surgery*. StatPearls Publishing.
- [129] Sha, R., Komori, K., and Badhulika, S. (2017). Amperometric pH Sensor Based on Graphene-Polyaniline Composite. *IEEE Sensors Journal*, 17(16):5038–5043.
- [130] Shamsipur, M., Barati, A., and Nematifar, Z. (2019). Fluorescent pH nanosensors: Design strategies and applications.

- [131] Sharma, M. and Khurana, S. M. (2018). Biomedical engineering: The recent trends. In *Omics Technologies and Bio-engineering: Volume 2: Towards Improving Quality of Life*, pages 323–336. Elsevier.
- [132] Sharma, N. K., Nain, A., Singh, K., Rani, N., and Singal, A. (2019a). Impedimetric sensors: Principles, applications and recent trends. *International Journal of Innovative Technology and Exploring Engineering*, 8(10):4015–4025.
- [133] Sharma, P., Semwal, V., and Gupta, B. D. (2019b). Fiber optic surface plasmon resonance based lactate sensor using co-immobilization of lactate dehydrogenase and NAD<sup>+</sup>. *Optical Fiber Technology*, 49:22–27.
- [134] Shavanova, K., Bakakina, Y., Burkova, I., Shteplyuk, I., Viter, R., Ubelis, A., Beni, V., Starodub, N., Yakimova, R., and Khranovskyy, V. (2016). Application of 2D Non-Graphene Materials and 2D Oxide Nanostructures for Biosensing Technology. *Sensors*, 16(2):223.
- [135] Singh, P., Pandey, S. K., Singh, J., Srivastava, S., Sachan, S., and Singh, S. K. (2016). Biomedical Perspective of Electrochemical Nanobiosensor.
- [136] Stanley, W. C. (2001). Changes in cardiac metabolism: A critical step from stable angina to ischaemic cardiomyopathy. In *European Heart Journal, Supplement*, volume 3, pages 02–07. W.B. Saunders Ltd.
- [137] Stanley, W. C., Recchia, F. A., and Lopaschuk, G. D. (2005). Myocardial substrate metabolism in the normal and failing heart. *Physiological Reviews*, 85(3):1093–1129.
- [138] Steenbergen, C. and Frangogiannis, N. G. (2012). Ischemic heart disease. In *Muscle*, volume 1, pages 495–521. Elsevier Inc., first edit edition.
- [139] Steinegger, A., Wolfbeis, O. S., and Borisov, S. M. (2020). Optical Sensing and Imaging of pH Values: Spectroscopies, Materials, and Applications.
- [140] Stockert, J. C. and Blazquez-Castro, A. (2017). *Fluorescence Microscopy in Life Sciences*. BENTHAM SCIENCE PUBLISHERS.
- [141] Sunny, J. C., Kumar, D., Kotekar, N., and Desai, N. (2018). Incidence and predictors of perioperative myocardial infarction in patients undergoing non-cardiac surgery in a tertiary care hospital. *Indian Heart Journal*, 70(3):335–340.
- [142] Tam, E., Feigenbaum, A., Addis, J., Blaser, S., MacKay, N., Al-Dosary, M., Taylor, R., Ackerley, C., Cameron, J., and Robinson, B. (2008). A novel mitochondrial DNA mutation in COX1 leads to strokes, seizures, and lactic acidosis. *Neuropediatrics*, 39(6):328–334.
- [143] Tamayol, A., Akbari, M., Zilberman, Y., Comotto, M., Lesha, E., Serex, L., Bagherifard, S., Chen, Y., Fu, G., Ameri, S. K., Ruan, W., Miller, E. L., Dokmeci, M. R., Sonkusale, S., and Khademhosseini, A. (2016). Flexible pH-Sensing Hydrogel Fibers for Epidermal Applications. *Advanced Healthcare Materials*, 5(6):711–719.
- [144] Tønnessen, T. I. (1997). Biological basis for PCO<sub>2</sub> as a detector of ischemia. *Acta Anaesthesiologica Scandinavica*, 41(6):659–669.
- [145] Tou, Z. Q., Chan, C. C., and Leong, S. (2014). A fiber-optic pH sensor based on polyelectrolyte multilayers embedded with gold nanoparticles. *Measurement Science and Technology*, 25(7):075102.
- [146] Tronstad, C. (2012). *Developments in biomedical sensors based on electrical impedance*. PhD thesis, Oslo University Hospital.
- [147] TU Graz (2021). fluorophores.org.
- [148] Turer, A. T. and Hill, J. A. (2010). Pathogenesis of myocardial ischemia-reperfusion injury and rationale for therapy.

- [149] Vivaldi, F., Salvo, P., Poma, N., Bonini, A., Biagini, D., Del Noce, L., Melai, B., Lisi, F., and Francesco, F. D. (2021). Recent Advances in Optical, Electrochemical and Field Effect pH Sensors. *Chemosensors*, 9(2):33.
- [150] Vleugels, L. F. W., Ricois, S., Voets, I. K., and Tuinier, R. (2018). Determination of the 'apparent pK a ' of selected food hydrocolloids using ortho-toluidine blue.
- [151] Vreugdenhil, S., Freire Jorge, P. J., van Driel, M. F., and Nijsten, M. W. (2019). Ischemic priapism as a model of exhausted metabolism. *Physiological Reports*, 7(6):e13999.
- [152] Walters, F. J., Wilson, G. J., Steward, D. J., Domenech, R. J., and MacGregor, D. C. (1979). Intramyocardial pH as an index of myocardial metabolism during cardiac surgery. *Journal of Thoracic and Cardiovascular Surgery*, 78(3):319–330.
- [153] Wang, H.-S. (2014). Critical role of bicarbonate and bicarbonate transporters in cardiac function. *World Journal of Biological Chemistry*, 5(3):334.
- [154] Weidgans, B. M. (2004). New Fluorescent Optical pH Sensors with Minimal Effects of Ionic Strength. Technical report.
- [155] Weizhong Jin, Lingxiang Wu, Yuanlin Song, Jinjun Jiang, Xiaodan Zhu, Dawei Yang, and Chunxue Bai (2011). Continuous Intra-Arterial Blood pH Monitoring by a Fiber-Optic Fluorosensor. *IEEE Transactions on Biomedical Engineering*, 58(5):1232–1238.
- [156] Wencel, D., Abel, T., and McDonagh, C. (2014). Optical Chemical pH Sensors. *Analytical Chemistry*, 86(1):15–29.
- [157] Wencel, D., Kaworek, A., Abel, T., Efremov, V., Bradford, A., Carthy, D., Coady, G., McMorrow, R. C. N. R., and McDonagh, C. (2018). Optical Sensor for Real-Time pH Monitoring in Human Tissue. *Small*, 14(51):1803627.
- [158] Wikipedia (2018). Fluorescence spectroscopy.
- [159] Wikipedia (2021a). Coronary artery bypass surgery - Wikipedia.
- [160] Wikipedia (2021b). HOMO and LUMO - Wikipedia.
- [161] Wikipedia (2021c). Thermodynamic activity - Wikipedia.
- [162] Wilson and Walkers (2018). *Wilson and Walker's Principles and Techniques of Biochemistry and Molecular Biology*. Cambridge University Press.
- [163] Wolfbeis, O. S. (1997). Chemical Sensing Using Indicator Dyes. Technical Report 8.
- [164] Wolfbeis, O. S. (2013). Editorial: Probes, Sensors, and Labels: Why is Real Progress Slow? *Angewandte Chemie International Edition*, 52(38):9864–9865.
- [165] Wong, E. (2013). Physiology of cardiac conduction and contractility | McMaster Pathophysiology Review.
- [166] Xia, Z., Li, H., and Irwin, M. G. (2016). Myocardial ischaemia reperfusion injury: the challenge of translating ischaemic and anaesthetic protection from animal models to humans. *British Journal of Anaesthesia*, 117:ii44–ii62.
- [167] Yeow, J. T. (2006). Biomedical Sensors. In *Wiley Encyclopedia of Biomedical Engineering*. John Wiley & Sons, Inc., Hoboken, NJ, USA.
- [168] You, Y. H., Nagaraja, A. T., Biswas, A., Hwang, J. H., Cote, G. L., and McShane, M. J. (2017). SERS-Active Smart Hydrogels with Modular Microdomains: From pH to Glucose Sensing. In *IEEE Sensors Journal*, volume 17, pages 941–950. Institute of Electrical and Electronics Engineers Inc.
- [169] Zajíc, J. (2015). Optical pH Detection with U-Shaped Fiber-Optic Probes and Absorption Transducers. *Conference Papers in Science*, 2015:1–8.

- [170] Zhao, Y., Lei, M., Liu, S. X., and Zhao, Q. (2018a). Smart hydrogel-based optical fiber SPR sensor for pH measurements. *Sensors and Actuators, B: Chemical*, 261:226–232.
- [171] Zhao, Y., Zhang, Z., Zou, Y., and Yang, Y. (2018b). Visualization of Nicotine Adenine Dinucleotide Redox Homeostasis with Genetically Encoded Fluorescent Sensors. *Antioxidants and Redox Signaling*, 28(3):213–229.
- [172] Zheng, X. T., Yang, H. B., and Li, C. M. (2010). Optical detection of single cell lactate release for cancer metabolic analysis. *Analytical Chemistry*, 82(12):5082–5087.
- [173] Zhou, G., Wang, Y., and Cui, L. (2015). Biomedical Sensor, Device and Measurement Systems. In *Advances in Bioengineering*. InTech.



# Appendixes

## A.1. Comparison table of different type of sensor

Type of sensor	Electrochemical				Physical			Optical	
	Amperometric/ Voltametric	Potentiometric	Impedimetric/ Conductometric	Piezoelectric	Thermometric	Absorbance	Reflectance	Luminescent	
<b>Measuring Principle Possible</b>	Yes	Yes	Yes	No	No	Yes	Yes	Yes	
<b>Ischaemia sensor</b>									
<b>Example pH sensor in literature</b>	Sha et al. [129]	Park et al. [109]	Awasthi et al. [12]	-	-	Zajic [169]	Zhao et al. [171]	Wencel et al. [157]	
<b>Advantages</b>	<ul style="list-style-type: none"> <li>- High selectivity</li> <li>- Reproducible</li> <li>- Inexpensive</li> <li>- On-site measurement</li> </ul>	<ul style="list-style-type: none"> <li>- Rapid response</li> <li>- Reproducible</li> <li>- Simple technique</li> </ul>	<ul style="list-style-type: none"> <li>- No ref. electrode</li> <li>- Inexpensive</li> <li>- Miniaturisation</li> </ul>	<ul style="list-style-type: none"> <li>- High sensitivity</li> <li>- Simple structure</li> <li>- Reliable</li> </ul>	<ul style="list-style-type: none"> <li>- Wide range</li> <li>- No external power needed</li> </ul>	<ul style="list-style-type: none"> <li>- No electric interference</li> <li>- No reference electrode</li> <li>- Reagent no contact with optical fibre</li> <li>- Multiple measurements</li> <li>- Higher information</li> </ul>	<ul style="list-style-type: none"> <li>- Fast measurement</li> <li>- Great ranges</li> <li>- No dyes needed</li> </ul>	<ul style="list-style-type: none"> <li>- Simple instrumentation, low detection limits</li> <li>- wide dynamic range.</li> <li>- Fluor: high sensitivity and selectivity.</li> <li>- Benefiting from mild hydrogel formation and sol-gel switching.</li> </ul>	<ul style="list-style-type: none"> <li>- Chemiluminescence: lacks selectivity</li> <li>- Fluorescence: photobleaching</li> <li>- Loss of bio activity</li> </ul>
<b>Disadvantages</b>	<ul style="list-style-type: none"> <li>- Interference</li> <li>- Small range</li> </ul>	<ul style="list-style-type: none"> <li>- Unable to detect lower limit ions</li> </ul>	<ul style="list-style-type: none"> <li>- Sensitivity decreases by non-reacting ions</li> <li>- Low specificity</li> </ul>	<ul style="list-style-type: none"> <li>- No truly static measurements</li> <li>- Not suitable for pH and lactate sensing</li> </ul>	<ul style="list-style-type: none"> <li>- Reference</li> <li>- Not possible for ph or lactate</li> </ul>	<ul style="list-style-type: none"> <li>- Costly equipment</li> <li>- Susceptible to damage</li> <li>- Difficult modification</li> </ul>	<ul style="list-style-type: none"> <li>- Continuous fibre</li> <li>- Removal of cladding</li> <li>- Needs fluid</li> </ul>		
<b>Reference</b>	[99] [127]	[99] [127]	[99] [127]	[114]	[123]				

Table A.1. Comparison of different types of sensors for their potential to measure pH or Lactate with examples

## A.2. Comparison table of different techniques sensor

Technique	Working principle	Advantages	Disadvantages	Handling interferences	Costs	Difficulty	Material/ Devices needed	Planar/Fibre	Ref
<b>Steady State Measurements</b>									
Absorptiometry	Light is sent through material with absorption dye. The transmission of the light through the material is sensed. Problem of optical clear material and sensor can be circumvented by making use of evanescent wave absorptiometry. Where a thin film (typically <math>2 \mu\text{m}</math>) of a pH sensitive material is placed on an optical waveguide. The light is totally reflected at the interface between fibre and coating, and the attenuation of the light is determined by the pH.	Relatively simple Commonly used technique Can be used for optical fibre cladding	Need for clear sensor material Clear sample to prevent scattering Not used for fluorescence Sensitive for interferences	-	++	++	+	Both, fibre only as ATR	
Reflectometry	Light is sent at a surface or interface and the reflection of this interface is detected by a sensor. In the most common form two light sources are used. One which is emitting a wavelength that is absorbed by the indicator and the other on a wavelength which is not absorbed by the indicator. The reflection of the light in the indicator material is detected by PD or RGB imaging. Measuring the intensity of the fluorescence of excited fluorescent indicators. Continuously excitation of the indicator at certain wavelength, cause emission in a higher wavelength which can be detected. Mostly measured with spectrometers PD. Affected by many factors, but relatively simple. Quite easy to measure and therefore used a lot in research. same as above but using two dyes and two wavelengths. One carrying the signal information and the other used to normalise the intensity. Multiple configurations possible (see section 2.5.1)	Simple Ratiometric sensing Commonly used sensing	Optical isolation layer advisable Weak signal Scattering particles advisable	-	++	++	+	Both	
Luminescence intensity	excitation of the indicator at certain wavelength, cause emission in a higher wavelength which can be detected. Mostly measured with spectrometers PD. Affected by many factors, but relatively simple. Quite easy to measure and therefore used a lot in research. same as above but using two dyes and two wavelengths. One carrying the signal information and the other used to normalise the intensity. Multiple configurations possible (see section 2.5.1)	Used a lot in research. Known principle. Commercially available	Influenced by a lot of factors not only the concentration (see Section ??) Indicators with high quantum yield needed	-	+	++	+	Both	
ratiometric intensity	excitation of the indicator at certain wavelength, cause emission in a higher wavelength which can be detected. Mostly measured with spectrometers PD. Affected by many factors, but relatively simple. Quite easy to measure and therefore used a lot in research. same as above but using two dyes and two wavelengths. One carrying the signal information and the other used to normalise the intensity. Multiple configurations possible (see section 2.5.1)	Less scattering Less instrumental drift Less optical alignment interferences=	Still interferences of optical components Background fluorescence and dye bleaching More difficult than luminescence intensity	+	+	+	+	Both	
<b>Time-Resolved Measurements</b>									
Luminescence decay time (TD-FD)	Measurement of luminescence decay of the pH indicator after the light source is turned off. This kind of sensing is independent of intensity fluctuations. It makes use of the difference in the decay time of the acidic and basic form. Sensing can be done in time or in frequency domain. DLR works by adding an inert luminescent reference dye with overlapping excitation and emission spectra to the pH indicator. This reference dye has overlapping excitation and emission spectra but a decay time that is much longer of the fluorescent indicator. In frequency domain the intensity difference can be measured by a phase shift. Thanks to that inexpensive optoelectronics can be used. Almost no disadvantages from interference.	Independent of intensity fluctuations. Very good in handling interferences. Self referencing and sensitive	Expensive. Need for long life indicators. Complex	++	-	-	-	Both	
Dual Lifetime Referencing (TD-FD)	DLR works by adding an inert luminescent reference dye with overlapping excitation and emission spectra to the pH indicator. This reference dye has overlapping excitation and emission spectra but a decay time that is much longer of the fluorescent indicator. In frequency domain the intensity difference can be measured by a phase shift. Thanks to that inexpensive optoelectronics can be used. Almost no disadvantages from interference.	Almost no interferences Time or domain frequency. Simple calibration. Precise	Dyes needed with different lifetimes More complex Metal Ligand Complex needed	++	+	-	+	Both	
<b>Energy Transfers</b>									
FRET	Exists of two different type of dyes. One dye is pH responsive while the other normally not (can be possible). Photonic energy can be transferred from the first to the second dye. The emission band of the first dye overlaps with the excitation band of the second and as reaction the second dye will have an emission occurring, the ratio between these peaks can indicate the level of pH.	Low cost instrumentation	Two dyes needed in close proximity of each other.	+	+	-	-	Both	
Inner Filter Effect	Adding an extra dye which is pH independent which during photoexcitation emit fluorescence which interacts with the fluorophore. This working is often found with upconversion nanoparticles and quantum dots. No effect on decay time.	No need for close proximity. No influence on decay time Used in extreme sensing	Not much information available. Mostly seen as unwanted effect of fluorescence spectroscopy.	n.a.	-	-	-	n.a.	
Fluorescence Quenching	A quencher, quenches the fluorescence of a fluorophore or a particle. In other words, photonic energy is no longer emitted by the quencher. Quenching may be static or dynamic. In the former case, the decay time remains unaffected, the latter case, it is reduced	Speed and simplicity	Inadequate detection levels More chemistry based	n.a.	+	-	-	n.a.	
PET	PET is an excited state electron transfer process where a photoexcited electron is transferred from the donor (receptor group) to the fluorophore. Therefore, PET efficiency is high if the PET group is easily oxidized (readily loses an electron in the excited state) and the fluorophore is easily reduced.	Fast and reversible. Thermodynamically favorable	Inefficient for long wavelengths. More chemistry based	n.a.	+	-	-	n.a.	

\* FIXME

Table A.2: Overview of the different optical techniques and their (dis)advantages. Compared on four different aspects

## A.3. Protocol of producing phosphate buffers

### Steps pH buffer PBS with different Ionic Strengths

Equipment needed:

- $\text{NaH}_2\text{PO}_4$  (Sodium Dihydrogen Phosphate) (2 gram)
- $\text{NaCl}$  (background electrolyte) (10 gram)
- HCl 37% (1mL)
- NaOH 98% (1mL)
- Scale
- Demineralized Water (2L)
- Magnetic stirrer
- 40 x 50 ml Plastic containers/bottles
- 2 x 1 L beaker
- 1 x 150mL glass beakers

#### Step 1: Produce Phosphate buffer stock solution.

Location: Wet Benches MEMS-Lab

- Dissolve 1.2g  $\text{NaH}_2\text{PO}_4$  per 1L Pure Water → Solution A

#### Step 3: Produce Dissolved HCl (0.01M) and NaOH (0.01M)

Location: Wet Benches MEMS-Lab

HCl:

- Slowly dissolve 0.082 ml of 37% HCl in 25 ml water
- Adjust final solution to 100ml

NaOH:

- Slowly dissolve 0.027 ml of 98% NaOH in 25 ml water
- Adjust final solution to 100ml

#### Step 3: Produce Phosphate buffer different IS and pH

Location: Wet Benches MEMS-Lab

- Put 45 ml of Solution A in beaker
- Add magnetic stirrer
- Add pH sensor
- Add Salt according to table
- Pipet HCl and NaOH to adjust pH
- Add DM Water to 50 ml
- Label plastic container with IS, pH and Temp

IS/pH	50 mL	6.2	6.6	7	7.4	7.8	8.2
50 mM	$\text{NaH}_2\text{PO}_4$ (g)	0.06	0.06	0.06	0.06	0.06	0.06
	$\text{NaCl}$ (g)	0.1079	0.0985	0.0856	0.0734	0.0655	0.0615
	Water (mL)	45	45	45	45	45	45
100 mM	$\text{NaH}_2\text{PO}_4$ (g)	0.06	0.06	0.06	0.06	0.06	0.06
	$\text{NaCl}$ (g)	0.2529	0.2427	0.2295	0.218	0.2109	0.2074
	Water (mL)	45	45	45	45	45	45
150 mM	$\text{NaH}_2\text{PO}_4$ (g)	0.06	0.06	0.06	0.06	0.06	0.06
	$\text{NaCl}$ (g)	0.3984	0.3877	0.3744	0.3634	0.3568	0.3536
	Water (mL)	45	45	45	45	45	45
200 mM	$\text{NaH}_2\text{PO}_4$ (g)	0.06	0.06	0.06	0.06	0.06	0.06
	$\text{NaCl}$ (g)	0.5441	0.5331	0.5198	0.5091	0.5028	0.4998
	Water (mL)	45	45	45	45	45	45

## A.4. Protocol of producing HPTS loaded microbeads

Steps MEMSlab First production of HPTS loaded Microbeads

Equipment needed:

- |   |   |
|---|---|
| <input type="checkbox"/> 1 glass beakers of 50-150mL  | <input type="checkbox"/> Magnetic Stirrer |
| <input type="checkbox"/> DM Water 20 mL               | <input type="checkbox"/> Centrifuge       |
| <input type="checkbox"/> HPTS 35 mg                   | <input type="checkbox"/> Pipet            |
| <input type="checkbox"/> AmberChrom 1x8 microbeads 1g | <input type="checkbox"/> Dark storage box |

Goal of steps:

- Make first HPTS microbeads and learn processing steps.
- Look for problems.

### Step 1: Prepare HPTS

*Needed: Glass beaker, HPTS, DM Water*

*Location: MEMS Lab*

Flowchart: Mix solution of HPTS and Demineralized water with concentration of 350mg/l

1. Prepare: 100 mL DM Water
2. Prepare: 35 mg HPTS
3. Pour together and mix → Compound 1.

### Step 2: Prepare Microbeads

*Needed: Glass beaker, Microbeads*

*Location: MEMS Lab*

Flowchart: Dispersing AmberChrom 1X8 200-400 microbeads in demineralized water

1. Prepare: 10 g of AmberChrom microbeads
2. Prepare: 10 mL of DM Water
3. Pour together and mix → Compound 2.

### Step 3: Make HPTS Microbeads

*Needed: Glass beaker, Compound 1 and 2, Magnetic stirrer*

*Location: MEMS Lab*

Flowchart: Using magnetic stirrer to mix the Microbeads and HPTS. 4h – 24h of stirring.

1. Mix Compound 2 and 3 → Compound 3.
2. Use magnetic stirrer and stir for one day.

### Step 4: Centrifuge HPTS-Microbeads

*Needed: Benchtop Centrifuge, Compound 3*

*Location: EW1*

Flowchart: disperse the microbeads and use a centrifuge to separate the microspheres.

1. Put compound in centrifuge.
2. Centrifuge for 5 minutes @ 2000 rpm
3. Resulting loaded microspheres → Compound 5.

### Step 5: Store the Microbeads

*Needed: Dark storage box, DM Water, ambient temperature*

*Location: MEMS Lab*

1. Keep HPTS loaded microbeads in water solution in dark location.

## A.5. Overview different optical detection schemes by Steinegger et al. [139]

method	advantages	disadvantages	compensation of interferences by										
			optical components (e.g., filters, optical gratings)	instrumental drift	optical misalignment	background fluorescence from samples	light scattered by sensor materials	intrinsic color of samples	dye leaching and bleaching	inhomogeneous dye loading	temperature		
absorption; reflectance	simple instrumentation; low-cost; portable	moderate sensitivity; many interferences (such as ambient and background light)	-	-	-	-	-	-	-	-	-	-	-
luminescence intensity	sensitive; low-cost; portable devices; enables imaging	interfered by many parameters	-	-	-	-	-	-	-	-	-	-	-
luminescence decay time	sensitive; precise; self-referenced; enables imaging; 1-point calibration	relatively expensive; works best in case of OSPs with long lifetime showing oxygen cross-talk	++	++	++	++ <sup>b</sup>	++	++	++	++	++	++	-
two-wavelength referencing	good precision	two dyes needed; photodecomposition and leaching of the dyes may be different	-	+	++	-	+	-	-	-	-	-	+ <sup>c</sup>
dual lifetime referencing (DLR)	sensitive; precise; enables imaging; simple calibration	two dyes needed with different excited-state lifetimes; more complex	++ <sup>d</sup>	++	++	-	++	++	++	++	++	++	+ <sup>c</sup>
Förster resonance energy transfer	low-cost instrumentation	two dyes (donor and acceptor dye) needed that have to be in close proximity; and to spectrally overlap	-	+	+	-	+	-	-	-	-	-	-

<sup>a</sup> ++: Efficient compensation. +: Partial compensation. -: No compensation. 0: No effect. n.a.: Not applicable. <sup>b</sup>In the time domain only. <sup>c</sup>If both components are thermally quenched to a similar extent. <sup>d</sup>Provided there is excellent spectral overlap.

Figure A.1: Advantages and Disadvantages of the Various Optical Detection Schemes and How Well They Can Compensate for Various Kinds of Undesired Interferences by Steinegger et al. [139]

## A.6. Protocol of producing the hydrogel

Steps MEMSlab First production of hydrogel with HPTS loaded microbeads.

Equipment needed:

- |  |   |
|--|---|
| <input type="checkbox"/> 1 glass beakers of 50-150mL | <input type="checkbox"/> Ethanol 10 mL          |
| <input type="checkbox"/> DM Water 20 mL              | <input type="checkbox"/> Microscope glass slide |
| <input type="checkbox"/> HPTS loaded microbeads 20mL | <input type="checkbox"/> Container              |
| <input type="checkbox"/> Magnetic Stirrer            | <input type="checkbox"/> Pipet                  |
| <input type="checkbox"/> HydroMed D4 1g              | <input type="checkbox"/> Dark storage box       |

Goal of steps:

- Make first HPTS microbeads hydrogels and learn processing steps.
- Look for problems.

### Step 1: Prepare hydrogel

*Needed: Glass beaker of 150 mL, Ethanol (min. 10mL), DM Water (min. 10mL), Hydromed D4 (1g)*

*Location: MEMS Lab*

1. Prepare: 1 g Hydromed D4
2. Prepare: 9 mL EtOH and 1 mL DM Water (9:1)
3. Pour together and dissolve for 6 hours → Compound 1

### Step 2: Mixing HPTS-Microbeads with Hydromed D4 and deposition on membranes

*Needed: Pipet, microscope glass slides*

*Location: MEMS Lab*

Flowchart: Mix 1 ml of Hydrogel with 350 mg of microbeads and Knife coating hydrogel on glass slides.

1. Prepare: 1 mL of Compound 1
2. Prepare: 350 mg of HPTS loaded microbeads (Compound 2)
3. Mix Compound 1 and 2 for 4 hours
4. Pipet mixture on glass slides (0.1 mL)
5. Dry sensors.

### Step 3: Store the Microbeads

*Needed: Dark storage box, ambient temperature*

*Location: MEMS Lab*

1. Keep the sensors in a dark location.

### A.7. CMOS Data

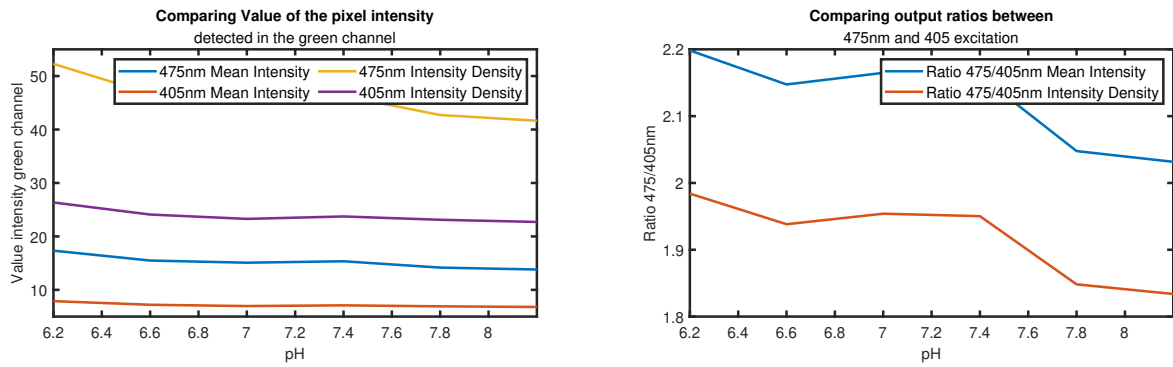


Figure A.2: The scaled output of the green channel of the thorlabs CMOS camera of Sample C

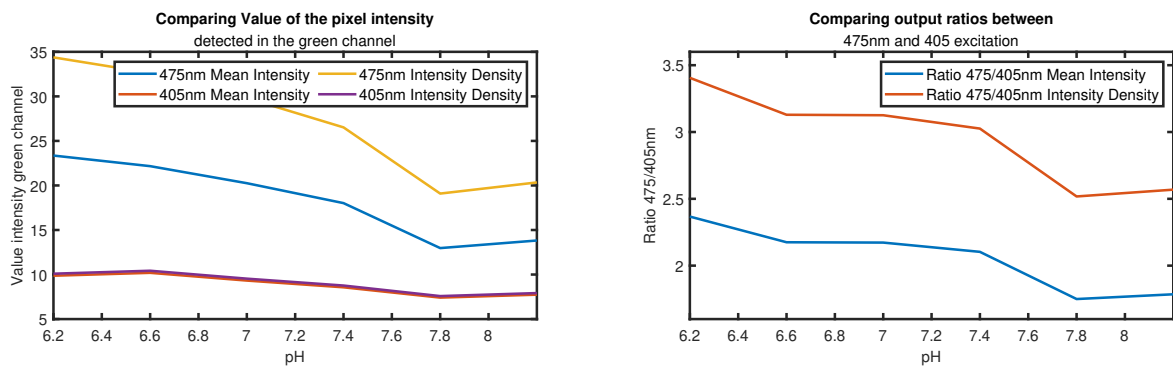


Figure A.3: The scaled output of the green channel of the thorlabs CMOS camera of Sample G

### A.8. (Un)scaled Reflection Data for Perkin Elmer

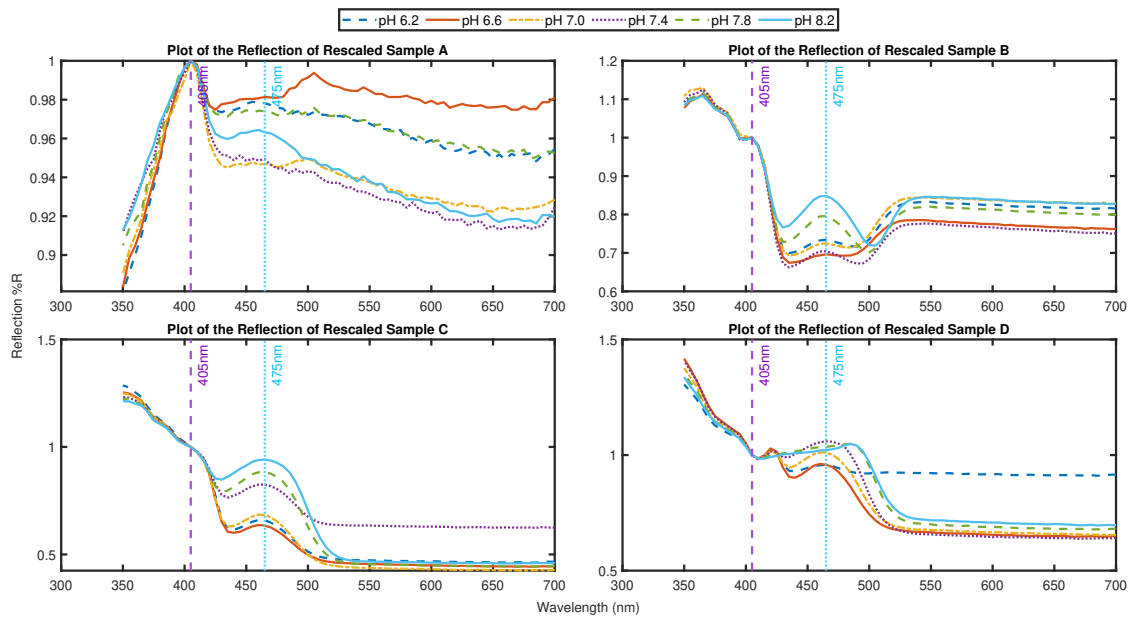


Figure A.4: Scaled Reflection of samples A-D

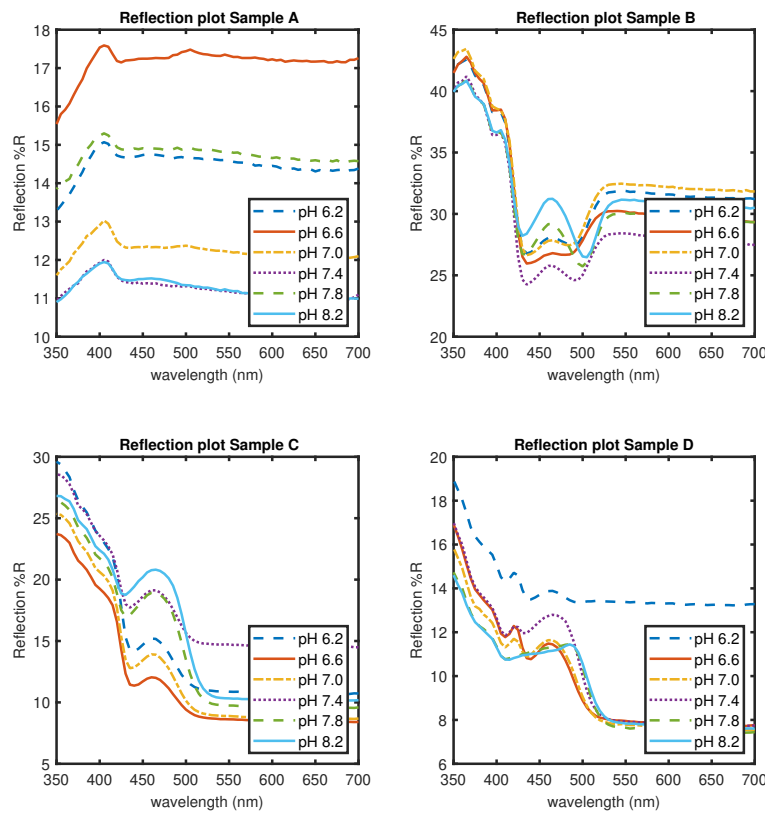


Figure A.5: Reflection of samples A - D

### A.9. (Un)scaled Transmission Data for Perkin Elmer Lambda 1050

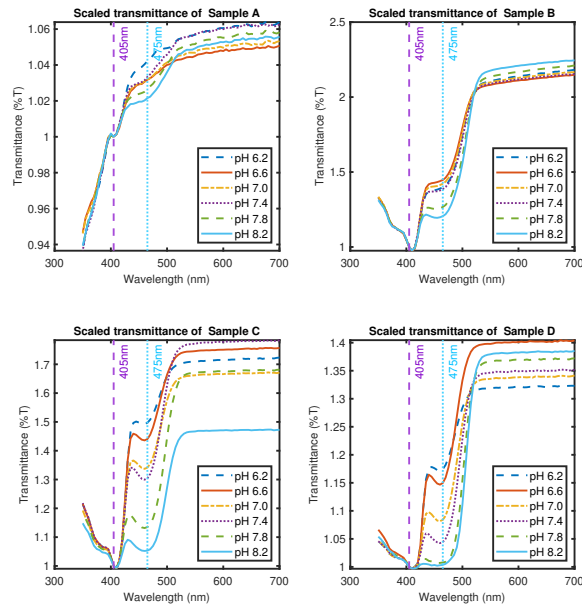


Figure A.6: Scaled Transmission of samples A-D

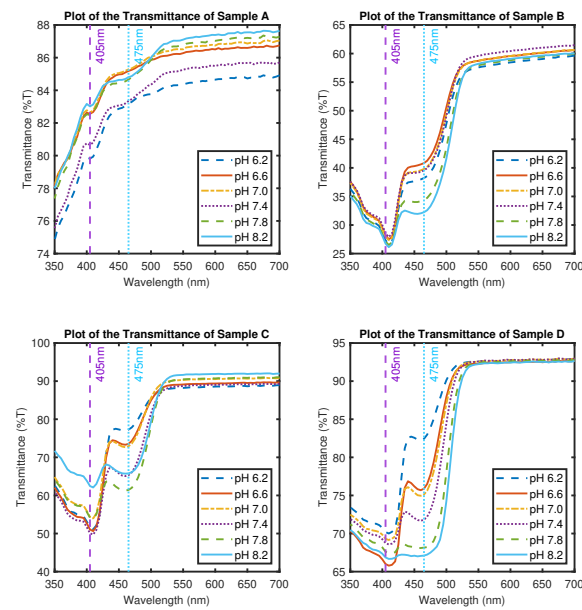


Figure A.7: Transmission of samples A-D

## A.10. (Un)scaled Absorbance Data

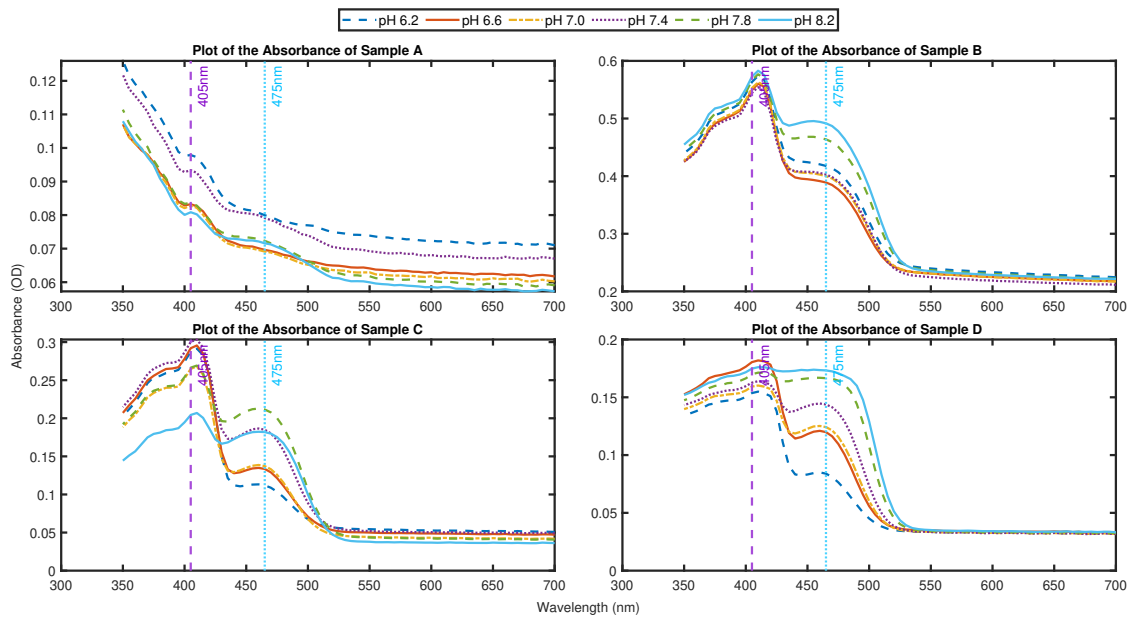


Figure A.8: Absorbance of samples A-D

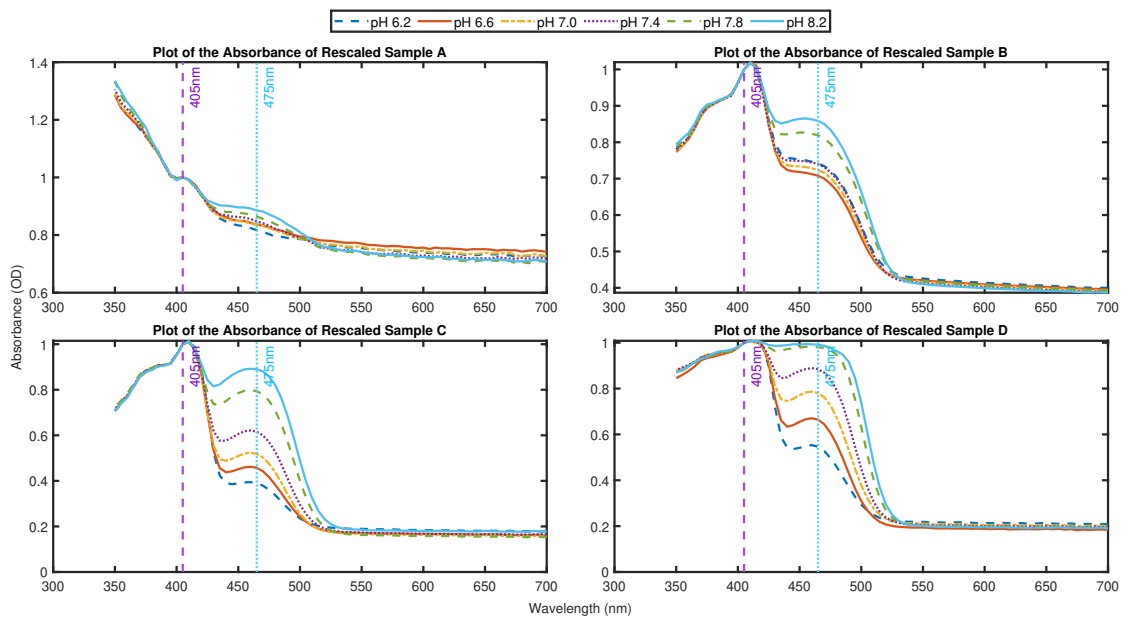


Figure A.9: Scaled Absorbance of samples A - D



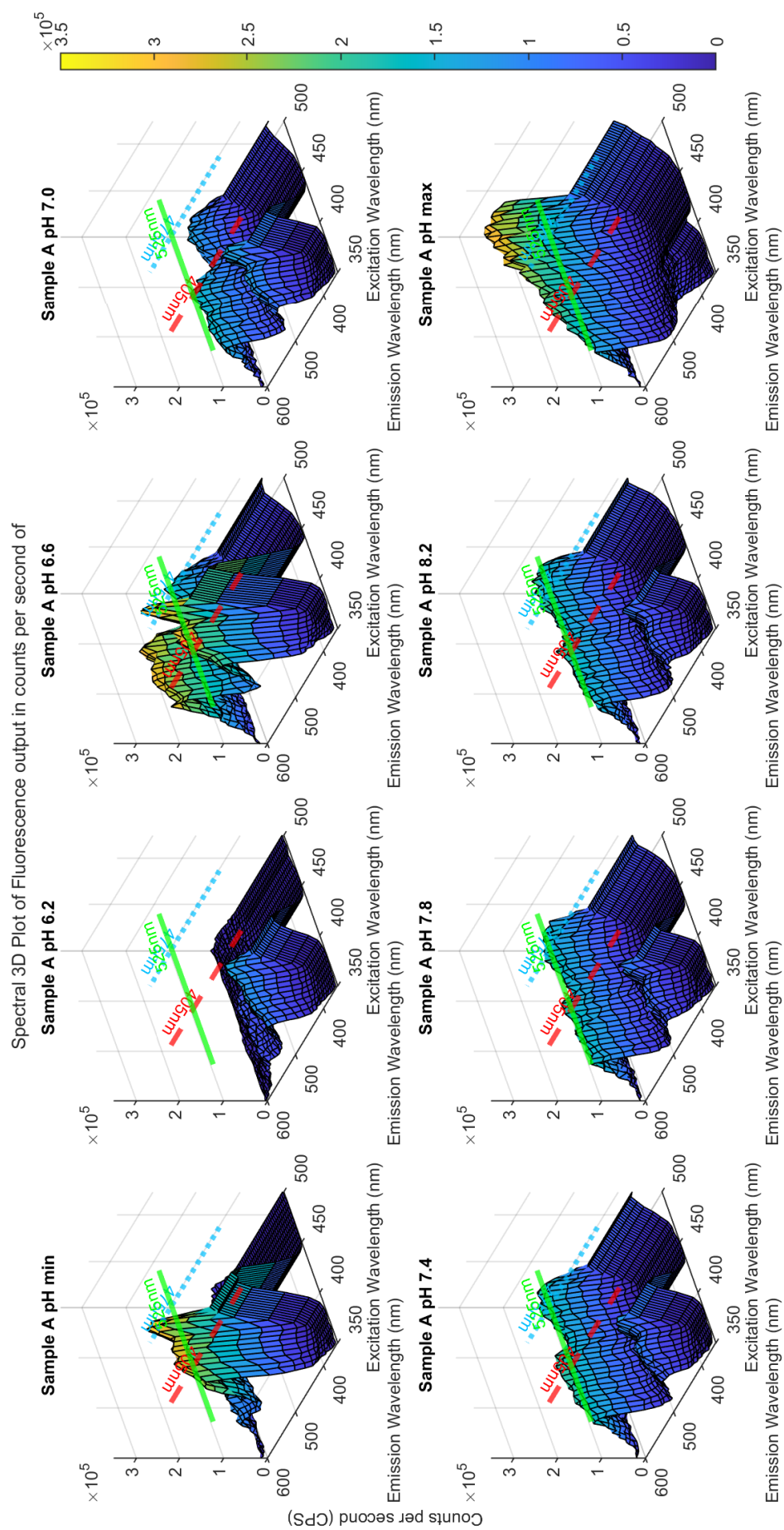


Figure A.11: Top view of fluorescence output measured by flourlog 3





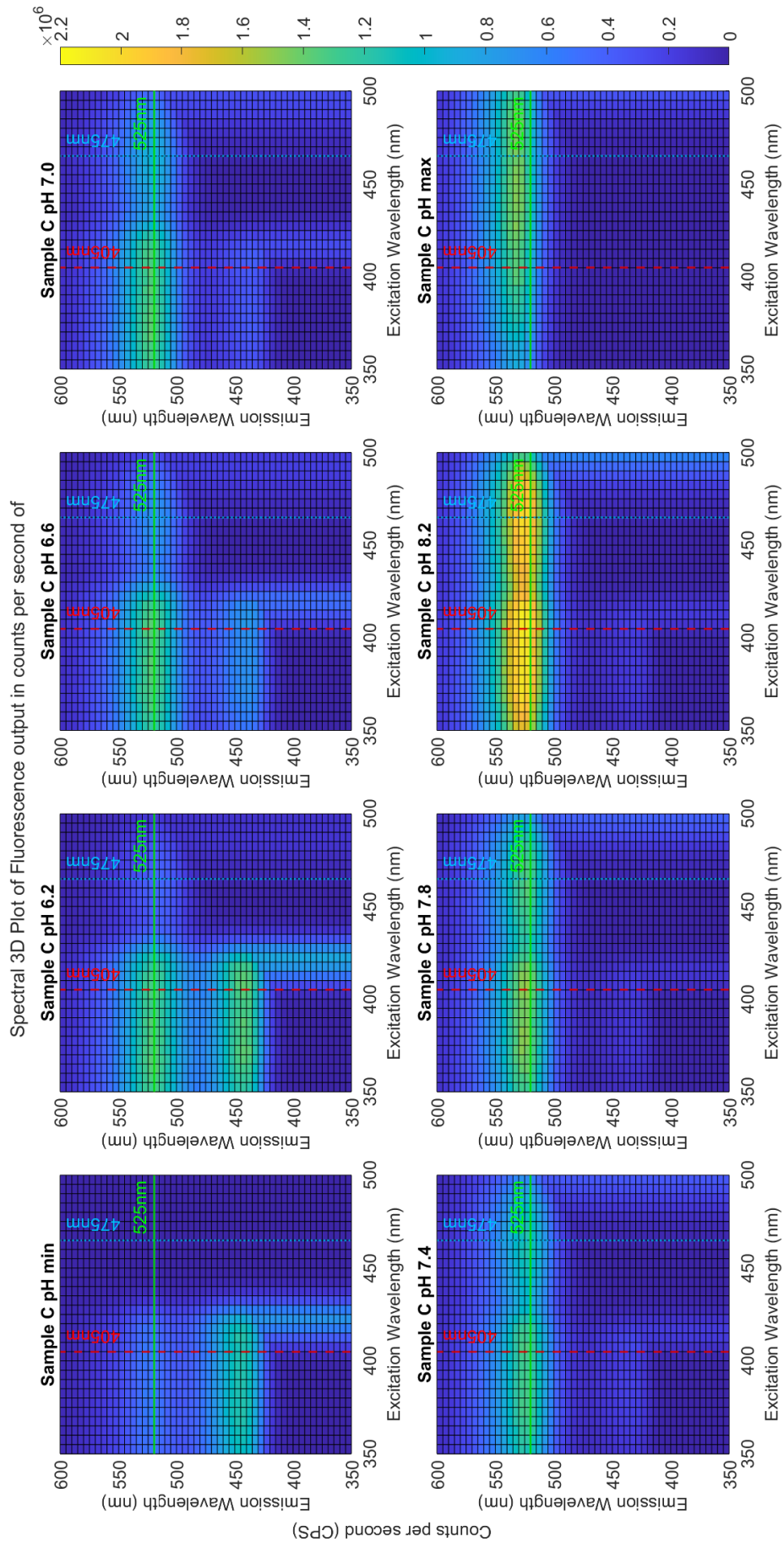


Figure A.14: Top view of fluorescence output measured by flourlog 3



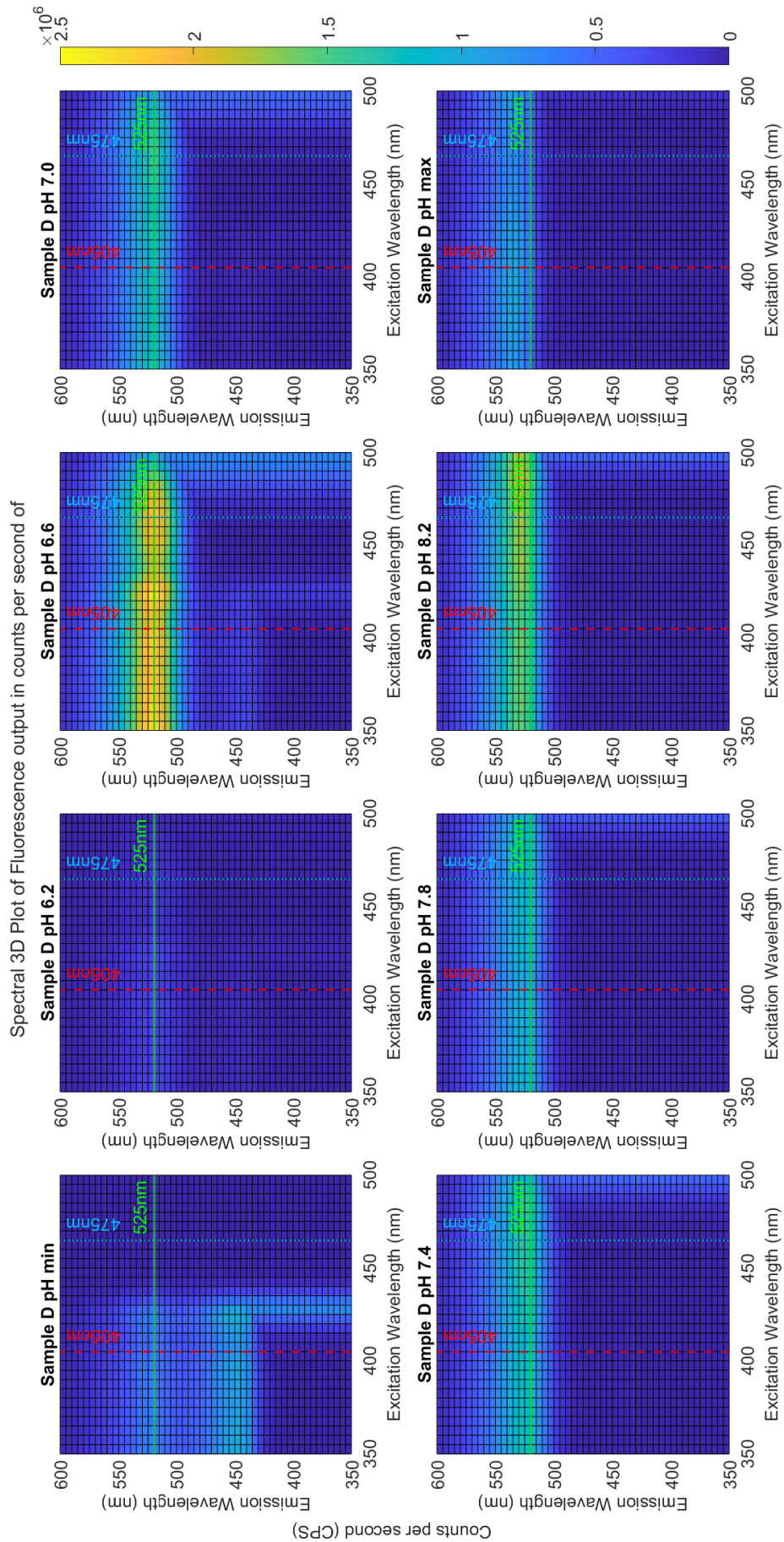
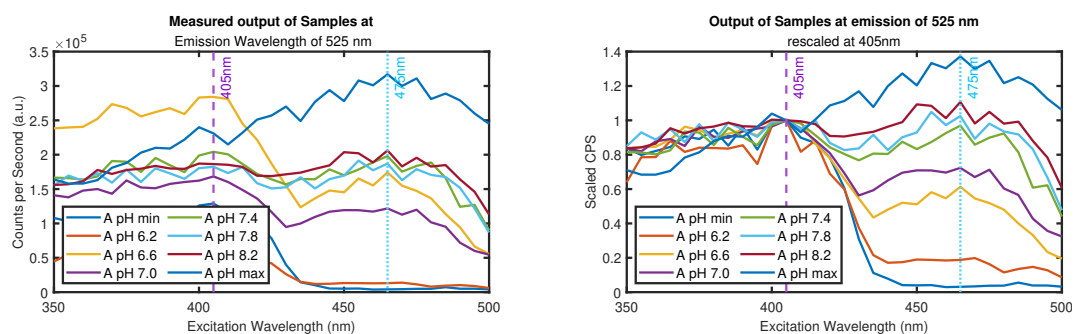


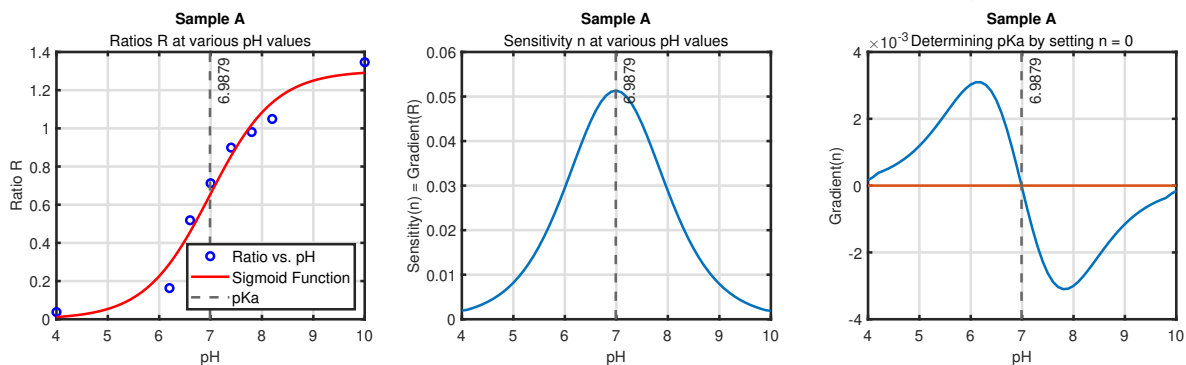
Figure A.16: Top view of fluorescence output measured by flourlog 3



### A.12. Fluorlog Sensitivity Samples A, B and D

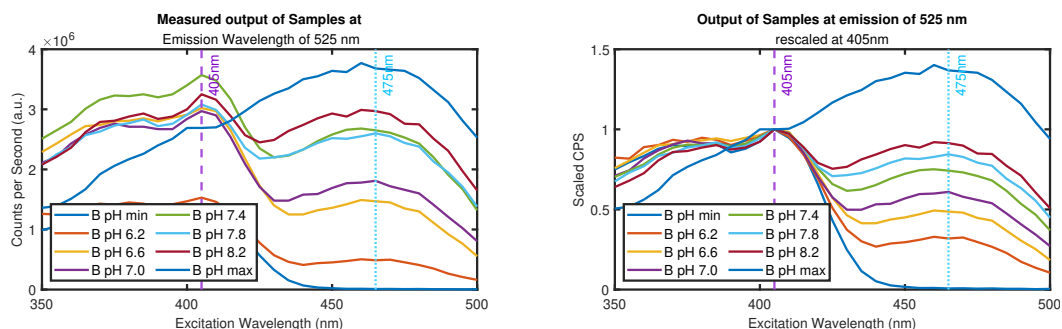


(a) Fluorescent Output in Count per Seconds of Sample A and scaled Output of Sample A at emission wavelength of 525nm

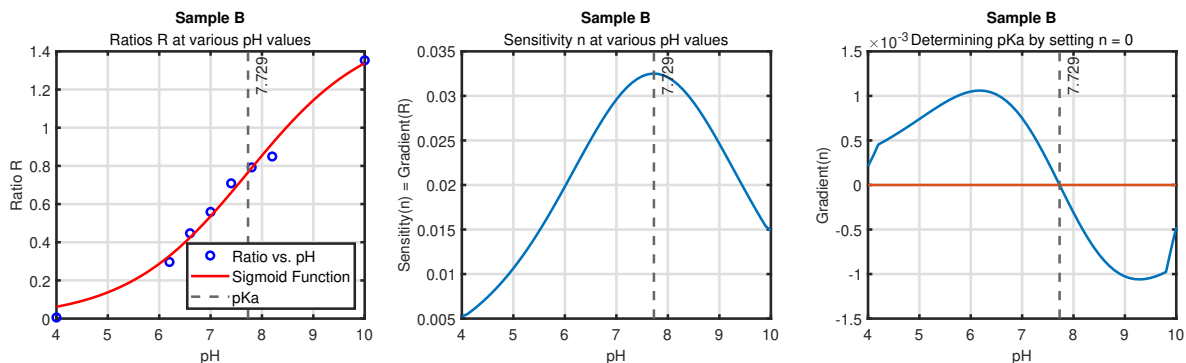


(b) Ratios, sensitivity and pKa determination for Sample A

Figure A.18: Determining the pKa of Sample A at a emission wavelength of 525nm and excitation wavelengths 475/405nm

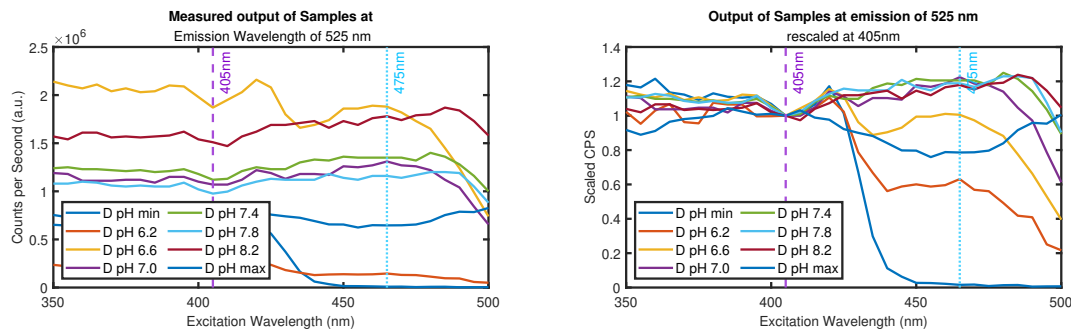


(a) Fluorescent Output in Count per Seconds of Sample B and scaled Output of Sample B

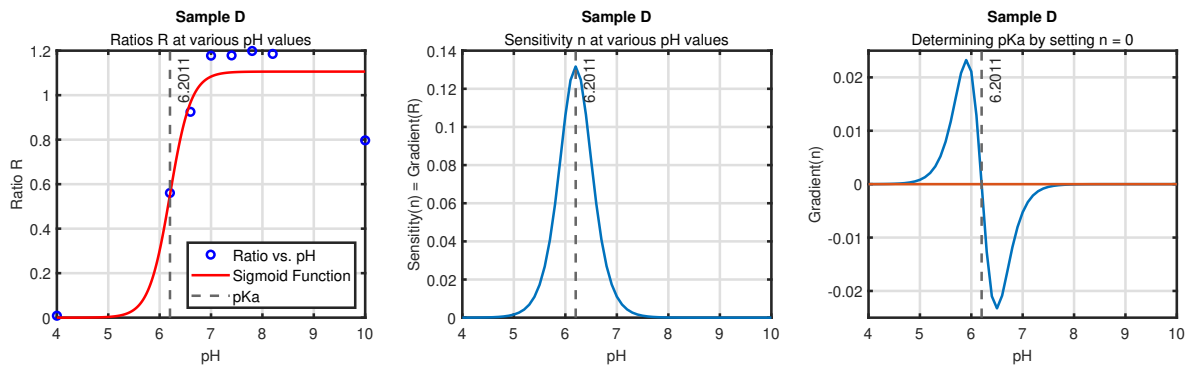


(b) Ratios, sensitivity and pKa determination for Sample B

Figure A.19: Determining the pKa of Sample B at a emission wavelength of 525nm and excitation wavelengths 475/405nm



(a) Fluorescent Output in Count per Seconds of Sample D and scaled Output of Sample D



(b) Ratios, sensitivity and pKa determination for Sample D

Figure A.20: Determining the pKa of Sample D at a emission wavelength of 525nm and excitation wavelengths 475/405nm

## A.13. Extra Results Reflection Probe

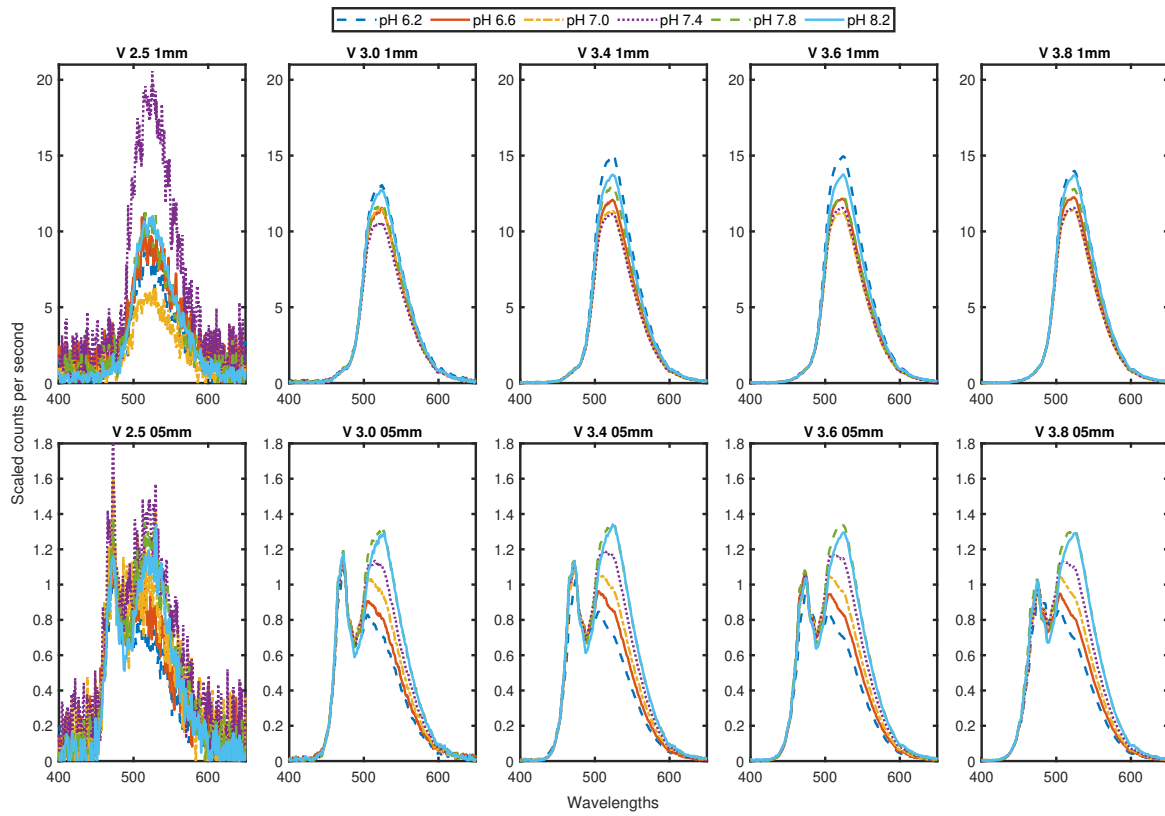
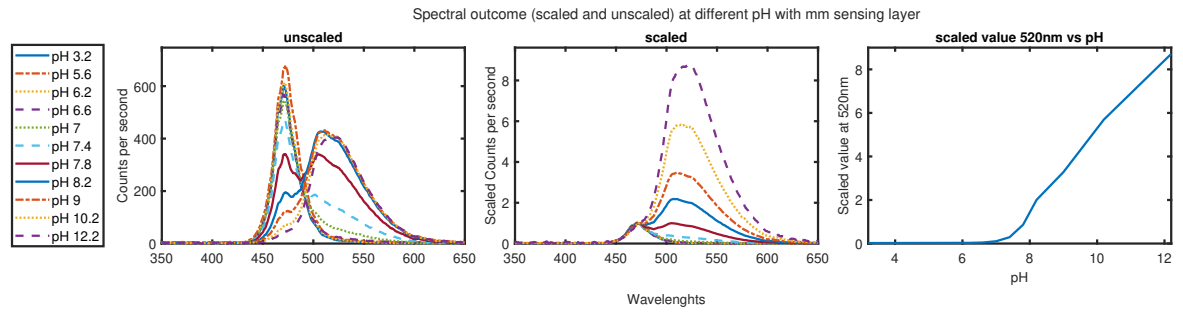
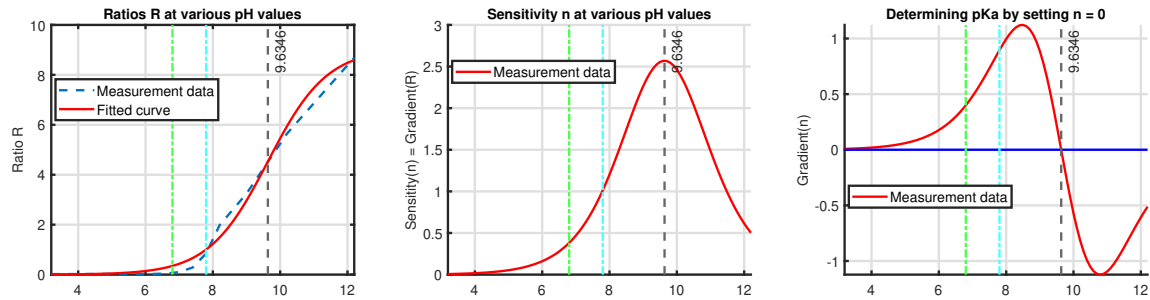


Figure A.21: Spectral output measured by Avantes Starline in counts per second, scaled to the value of 475nm for the two layer thicknesses and at different voltages and with different pH. Measured in 100mM buffer solutions

### A.14. Results of the 1mm layer of the reflection probe measurements



(a) Full range of 1mm sensing layer and relation between output and pH

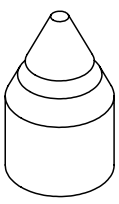
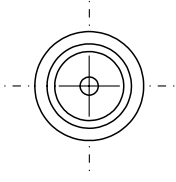
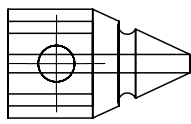
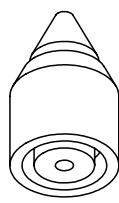
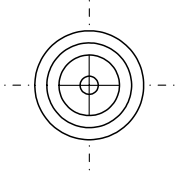
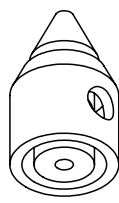
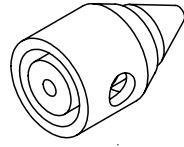
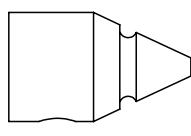
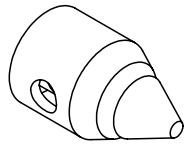
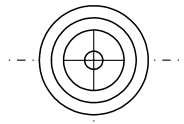
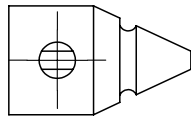
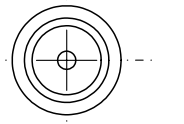
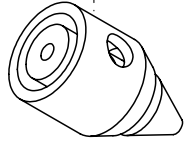
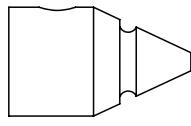
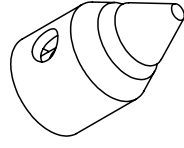


(b) Sensitivity, pKa of 0.5mm layer

Figure A.22: Outcome of the full range of the 1mm sample after submerging for 20 minutes in 150mM buffer solutions

# A.15. SOLIDWORK drawings

4	3	2	1
F	F	F	F
E	E	E	E
D	D	D	D
C	C	C	C
B	B	B	B
UNLESS OTHERWISE SPECIFIED: DIMENSIONS ARE IN MILLIMETERS SURFACE FINISH: TOLERANCES: LINEAR: ANGULAR:		FINISH:	DEBURR AND BREAK SHARP EDGES
		DO NOT SCALE DRAWING	REVISION
DRAWN	NAME	SIGNATURE	DATE
CHK'D			
APP'VD			
MFG			
Q.A			
		MATERIAL:	TITLE:
		WEIGHT:	DWG NO. <b>20degree_addon</b> <sup>A4</sup>
		SCALE:2:1	SHEET 1 OF 1
4	3	2	1

	4	3	2	1
F				
E				
D				
C				
B				
A				
UNLESS OTHERWISE SPECIFIED: DIMENSIONS ARE IN MILLIMETERS SURFACE FINISH: TOLERANCES: LINEAR: ANGULAR:		FINISH:	DEBURR AND BREAK SHARP EDGES	DO NOT SCALE DRAWING
				REVISION
	NAME	SIGNATURE	DATE	TITLE:
DRAWN				
CHK'D				
APP'VD				
MFG				
Q.A				
			MATERIAL:	DWG NO.
				<b>25degree_addon</b> <sup>A4</sup>
			WEIGHT:	SCALE:2:1
				SHEET 1 OF 1

## A.16. Results of ionic strength measurement proof-of-concept sensor

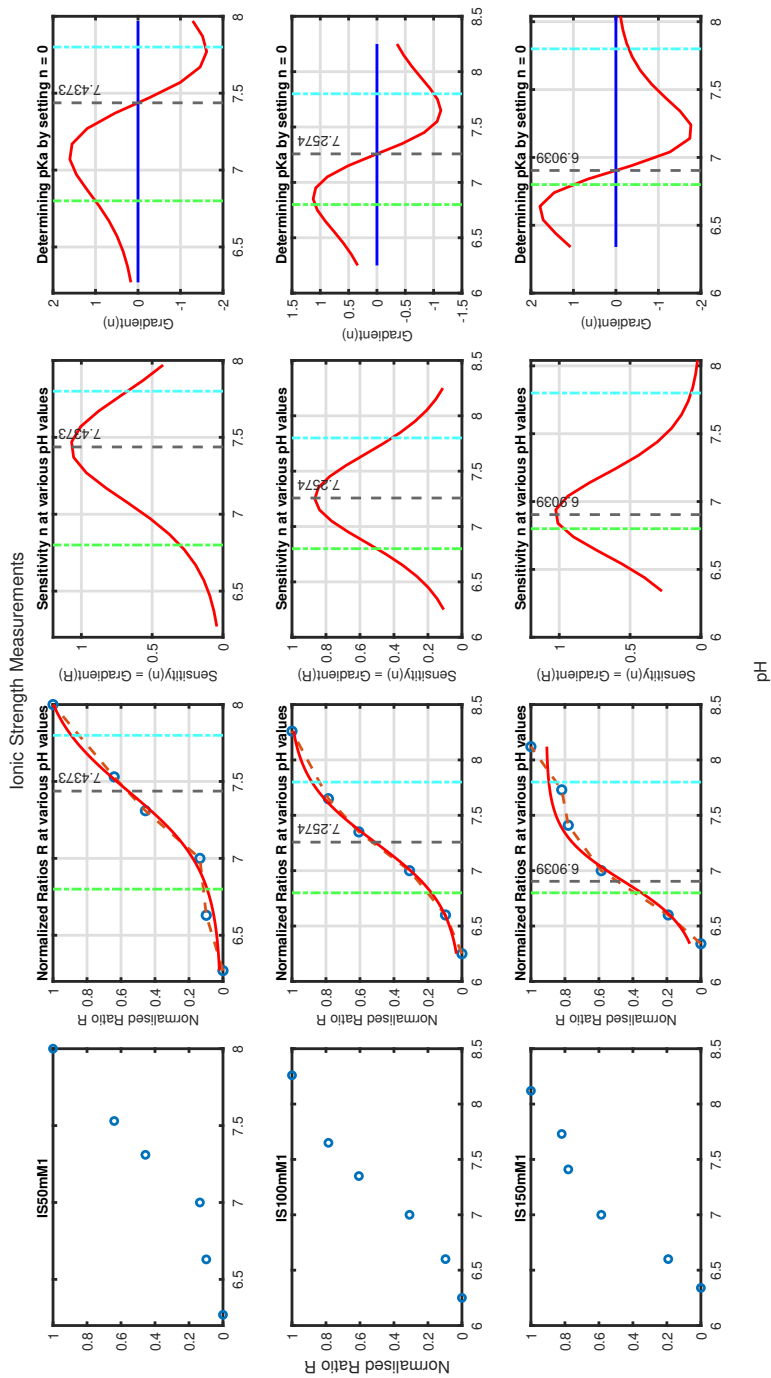


Figure A.23: Full results of Ionic Strength measurements

## A.17. Results of reproducibility measurement proof-of-concept sensor

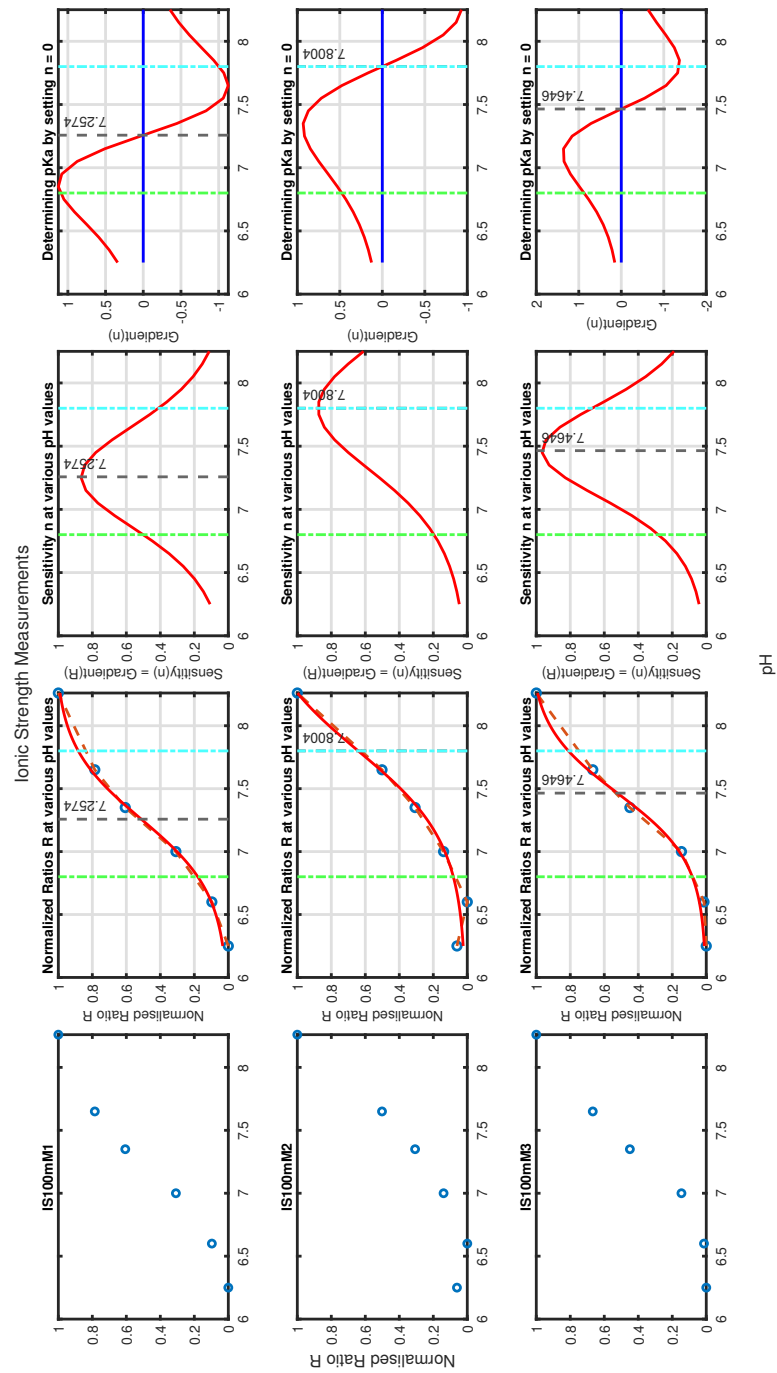


Figure A.24: Full results of reproducibility measurements

## A.18. Matlabcodes used in thesis

### A.18.1. Scripts

Listing A.1: Matlab script for the absorption data

```

1 %% Close all
2
3 clc
4 clear all
5 close all
6
7 %% Load Data
8 fds = fileDatastore('C:\Users\mauri\Documents\MATLAB\afstuderen\Absorptiemetingen\', 'ReadFcn', @load, "FileExtensions", '.csv');
9 fullFileNames = fds.Files;
10 FileNames = string(fullFileNames);
11 % correction files
12 Sample_Glass = importfileAbsorption(FileNames(5));
13 Sample_100_begin = importfileAbsorption(FileNames(3));
14 Sample_100_end = importfileAbsorption(FileNames(4));
15 Sample_0_begin = importfileAbsorption(FileNames(1));
16
17
18 %Sample A
19 FirstFile_SampleA = 7;
20 SampleA_62 = importfileAbsorption(FileNames(FirstFile_SampleA));
21 SampleA_66 = importfileAbsorption(FileNames(FirstFile_SampleA+1));
22 SampleA_70 = importfileAbsorption(FileNames(FirstFile_SampleA+2));
23 SampleA_74 = importfileAbsorption(FileNames(FirstFile_SampleA+3));
24 SampleA_78 = importfileAbsorption(FileNames(FirstFile_SampleA+4));
25 SampleA_82 = importfileAbsorption(FileNames(FirstFile_SampleA+5));
26
27 %Sample B
28 FirstFile_SampleB = 14;
29 SampleB_62 = importfileAbsorption(FileNames(FirstFile_SampleB));
30 SampleB_66 = importfileAbsorption(FileNames(FirstFile_SampleB+1));
31 SampleB_70 = importfileAbsorption(FileNames(FirstFile_SampleB+2));
32 SampleB_74 = importfileAbsorption(FileNames(FirstFile_SampleB+3));
33 SampleB_78 = importfileAbsorption(FileNames(FirstFile_SampleB+4));
34 SampleB_82 = importfileAbsorption(FileNames(FirstFile_SampleB+5));
35
36 %Sample C
37 FirstFile_SampleC = 20;
38 SampleC_62 = importfileAbsorption(FileNames(FirstFile_SampleC));
39 SampleC_66 = importfileAbsorption(FileNames(FirstFile_SampleC+1));
40 SampleC_70 = importfileAbsorption(FileNames(FirstFile_SampleC+2));
41 SampleC_74 = importfileAbsorption(FileNames(FirstFile_SampleC+3));
42 SampleC_78 = importfileAbsorption(FileNames(FirstFile_SampleC+4));
43 SampleC_82 = importfileAbsorption(FileNames(FirstFile_SampleC+5));
44
45 %Sample D
46 FirstFile_SampleD = 26;
47 SampleD_62 = importfileAbsorption(FileNames(FirstFile_SampleD));
48 SampleD_66 = importfileAbsorption(FileNames(FirstFile_SampleD+1));
49 SampleD_70 = importfileAbsorption(FileNames(FirstFile_SampleD+2));
50 SampleD_74 = importfileAbsorption(FileNames(FirstFile_SampleD+3));
51 SampleD_78 = importfileAbsorption(FileNames(FirstFile_SampleD+4));
52 SampleD_82 = importfileAbsorption(FileNames(FirstFile_SampleD+5));
53 %% Converting Transmittance to Absorbance
54 % A = 2 - log10 %T
55 % correction files
56 Sample_Glass.x_T = 2 - log10(Sample_Glass.x_T);
57 Sample_100_begin.x_T = 2 - log10(Sample_100_begin.x_T);
58 Sample_100_end.x_T = 2 - log10(Sample_100_end.x_T);
59 Sample_0_begin.x_T = 2 - log10(Sample_0_begin.x_T);
60
61 %Sample A
62 SampleA_62.x_T = 2 - log10(SampleA_62.x_T);
63 SampleA_66.x_T = 2 - log10(SampleA_66.x_T);
64 SampleA_70.x_T = 2 - log10(SampleA_70.x_T);
65 SampleA_74.x_T = 2 - log10(SampleA_74.x_T);
66 SampleA_78.x_T = 2 - log10(SampleA_78.x_T);
67 SampleA_82.x_T = 2 - log10(SampleA_82.x_T);
68
69 %Sample B
70 SampleB_62.x_T = 2 - log10(SampleB_62.x_T);
71 SampleB_66.x_T = 2 - log10(SampleB_66.x_T);
72 SampleB_70.x_T = 2 - log10(SampleB_70.x_T);
73 SampleB_74.x_T = 2 - log10(SampleB_74.x_T);
74 SampleB_78.x_T = 2 - log10(SampleB_78.x_T);
75 SampleB_82.x_T = 2 - log10(SampleB_82.x_T);
76
77 %Sample C
78 SampleC_62.x_T = 2 - log10(SampleC_62.x_T);
79 SampleC_66.x_T = 2 - log10(SampleC_66.x_T);
80 SampleC_70.x_T = 2 - log10(SampleC_70.x_T);
81 SampleC_74.x_T = 2 - log10(SampleC_74.x_T);
82 SampleC_78.x_T = 2 - log10(SampleC_78.x_T);
83 SampleC_82.x_T = 2 - log10(SampleC_82.x_T);
84
85 %Sample D
86 SampleD_62.x_T = 2 - log10(SampleD_62.x_T);
87 SampleD_66.x_T = 2 - log10(SampleD_66.x_T);
88 SampleD_70.x_T = 2 - log10(SampleD_70.x_T);
89 SampleD_74.x_T = 2 - log10(SampleD_74.x_T);
90 SampleD_78.x_T = 2 - log10(SampleD_78.x_T);
91 SampleD_82.x_T = 2 - log10(SampleD_82.x_T);
92
93 %% Plot Transmittance
94 figure
95 t = tiledlayout(2,3,'TileSpacing','compact');
96 ttl = 'Plot of the Absorbance of ';
97 nexttile
98 plot(Sample_Glass.nm,Sample_Glass.x_T)
99 legend({'Glass slide'},'Location','northeast')
100 xlabel('wavelength (nm)')
101 ylabel('Absorbance (OD)')
102 title('Plot of the Absorbance of Glass slide')
103 nexttile
104 plot(Sample_100_begin.nm,Sample_100_begin.x_T,Sample_100_end.nm,Sample_100_end.x_T,Sample_0_begin.nm,Sample_0_begin.x_T)
105 legend({'100% begin','100% end','0%Begin'},'Location','northeast')
106 xlabel('wavelength (nm)')
107 ylabel('Absorbance (OD)')
108 title('Plot of the Absorbance of Baseline Measurements')
109 tableplot(SampleA_62, SampleA_66, SampleA_70, SampleA_74, SampleA_78, SampleA_82, 'Sample A', ttl)
110 legend({'pH 6.2','pH 6.6','pH 7.0','pH 7.4','pH 7.8','pH 8.2'},'Location','northeast')
111 tableplot(SampleB_62, SampleB_66, SampleB_70, SampleB_74, SampleB_78, SampleB_82, 'Sample B', ttl)
112 legend({'pH 6.2','pH 6.6','pH 7.0','pH 7.4','pH 7.8','pH 8.2'},'Location','northeast')
113 tableplot(SampleC_62, SampleC_66, SampleC_70, SampleC_74, SampleC_78, SampleC_82, 'Sample C', ttl)
114 legend({'pH 6.2','pH 6.6','pH 7.0','pH 7.4','pH 7.8','pH 8.2'},'Location','northeast')
115 tableplot(SampleD_62, SampleD_66, SampleD_70, SampleD_74, SampleD_78, SampleD_82, 'Sample D', ttl)
116 legend({'pH 6.2','pH 6.6','pH 7.0','pH 7.4','pH 7.8','pH 8.2'},'Location','northeast')
117 xlabel(t,'Wavelength (nm)')
118 ylabel(t,'Absorbance (OD)')
119 lgd = legend({'pH 6.2','pH 6.6','pH 7.0','pH 7.4','pH 7.8','pH 8.2'});
120 lgd.NumColumns = 6;

```

```

120 lgd.Layout.Tile = 'north';
121
122 % New figure
123 figure
124 t = tiledlayout(2,2,'TileSpacing','compact');
125 ttl = 'Plot of the Absorbance of ';
126 tableplot(SampleA_62, SampleA_66, SampleA_70, SampleA_74, SampleA_78, SampleA_82, 'Sample A', ttl)
127 tableplot(SampleB_62, SampleB_66, SampleB_70, SampleB_74, SampleB_78, SampleB_82, 'Sample B', ttl)
128 tableplot(SampleC_62, SampleC_66, SampleC_70, SampleC_74, SampleC_78, SampleC_82, 'Sample C', ttl)
129 tableplot(SampleD_62, SampleD_66, SampleD_70, SampleD_74, SampleD_78, SampleD_82, 'Sample D', ttl)
130 xlabel(t, 'Wavelength (nm)')
131 ylabel(t, 'Absorbance (OD)')
132 lgd = legend({'pH 6.2','pH 6.6','pH 7.0','pH 7.4','pH 7.8','pH 8.2'});
133 lgd.NumColumns = 6;
134 lgd.Layout.Tile = 'north';
135
136 %% Glasscorrected
137 % Sample A
138 SampleA_62_corr = array2table([SampleA_62.nm, Sample_Glass.x T-SampleA_62.x T], 'VariableNames', {'nm','x T'});
139 SampleA_66_corr = array2table([SampleA_66.nm, Sample_Glass.x T-SampleA_66.x T], 'VariableNames', {'nm','x T'});
140 SampleA_70_corr = array2table([SampleA_70.nm, Sample_Glass.x T-SampleA_70.x T], 'VariableNames', {'nm','x T'});
141 SampleA_74_corr = array2table([SampleA_74.nm, Sample_Glass.x T-SampleA_74.x T], 'VariableNames', {'nm','x T'});
142 SampleA_78_corr = array2table([SampleA_78.nm, Sample_Glass.x T-SampleA_78.x T], 'VariableNames', {'nm','x T'});
143 SampleA_82_corr = array2table([SampleA_82.nm, Sample_Glass.x T-SampleA_82.x T], 'VariableNames', {'nm','x T'});
144 % Sample B
145 SampleB_62_corr = array2table([SampleB_62.nm, Sample_Glass.x T-SampleB_62.x T], 'VariableNames', {'nm','x T'});
146 SampleB_66_corr = array2table([SampleB_66.nm, Sample_Glass.x T-SampleB_66.x T], 'VariableNames', {'nm','x T'});
147 SampleB_70_corr = array2table([SampleB_70.nm, Sample_Glass.x T-SampleB_70.x T], 'VariableNames', {'nm','x T'});
148 SampleB_74_corr = array2table([SampleB_74.nm, Sample_Glass.x T-SampleB_74.x T], 'VariableNames', {'nm','x T'});
149 SampleB_78_corr = array2table([SampleB_78.nm, Sample_Glass.x T-SampleB_78.x T], 'VariableNames', {'nm','x T'});
150 SampleB_82_corr = array2table([SampleB_82.nm, Sample_Glass.x T-SampleB_82.x T], 'VariableNames', {'nm','x T'});
151 % Sample C
152 SampleC_62_corr = array2table([SampleC_62.nm, Sample_Glass.x T-SampleC_62.x T], 'VariableNames', {'nm','x T'});
153 SampleC_66_corr = array2table([SampleC_66.nm, Sample_Glass.x T-SampleC_66.x T], 'VariableNames', {'nm','x T'});
154 SampleC_70_corr = array2table([SampleC_70.nm, Sample_Glass.x T-SampleC_70.x T], 'VariableNames', {'nm','x T'});
155 SampleC_74_corr = array2table([SampleC_74.nm, Sample_Glass.x T-SampleC_74.x T], 'VariableNames', {'nm','x T'});
156 SampleC_78_corr = array2table([SampleC_78.nm, Sample_Glass.x T-SampleC_78.x T], 'VariableNames', {'nm','x T'});
157 SampleC_82_corr = array2table([SampleC_82.nm, Sample_Glass.x T-SampleC_82.x T], 'VariableNames', {'nm','x T'});
158 % Sample D
159 SampleD_62_corr = array2table([SampleD_62.nm, Sample_Glass.x T-SampleD_62.x T], 'VariableNames', {'nm','x T'});
160 SampleD_66_corr = array2table([SampleD_66.nm, Sample_Glass.x T-SampleD_66.x T], 'VariableNames', {'nm','x T'});
161 SampleD_70_corr = array2table([SampleD_70.nm, Sample_Glass.x T-SampleD_70.x T], 'VariableNames', {'nm','x T'});
162 SampleD_74_corr = array2table([SampleD_74.nm, Sample_Glass.x T-SampleD_74.x T], 'VariableNames', {'nm','x T'});
163 SampleD_78_corr = array2table([SampleD_78.nm, Sample_Glass.x T-SampleD_78.x T], 'VariableNames', {'nm','x T'});
164 SampleD_82_corr = array2table([SampleD_82.nm, Sample_Glass.x T-SampleD_82.x T], 'VariableNames', {'nm','x T'});
165 %% plot Glass corrected
166 figure
167 xlabel = 'Wavelength (nm)';
168 ylabel = 'Absorbance (OD)';
169 ttl = 'Plot of the Absorbance of Glassslide - ';
170 tableplot(SampleA_62_corr, SampleA_66_corr, SampleA_70_corr, SampleA_74_corr, SampleA_78_corr, SampleA_82_corr, 'Sample A', ttl)
171 legend({'pH 6.2','pH 6.6','pH 7.0','pH 7.4','pH 7.8','pH 8.2'}, 'Location','northeast')
172 tableplot(SampleB_62_corr, SampleB_66_corr, SampleB_70_corr, SampleB_74_corr, SampleB_78_corr, SampleB_82_corr, 'Sample B', ttl)
173 legend({'pH 6.2','pH 6.6','pH 7.0','pH 7.4','pH 7.8','pH 8.2'}, 'Location','northeast')
174 tableplot(SampleC_62_corr, SampleC_66_corr, SampleC_70_corr, SampleC_74_corr, SampleC_78_corr, SampleC_82_corr, 'Sample C', ttl)
175 legend({'pH 6.2','pH 6.6','pH 7.0','pH 7.4','pH 7.8','pH 8.2'}, 'Location','northeast')
176 tableplot(SampleD_62_corr, SampleD_66_corr, SampleD_70_corr, SampleD_74_corr, SampleD_78_corr, SampleD_82_corr, 'Sample D', ttl)
177 legend({'pH 6.2','pH 6.6','pH 7.0','pH 7.4','pH 7.8','pH 8.2'}, 'Location','northeast')
178
179 %% Samples - Sample A
180 % Sample B
181 SampleB_62_minSampleA = array2table([SampleB_62.nm, SampleB_62.x T-SampleA_62.x T], 'VariableNames', {'nm','x T'});
182 SampleB_66_minSampleA = array2table([SampleB_66.nm, SampleB_66.x T-SampleA_66.x T], 'VariableNames', {'nm','x T'});
183 SampleB_70_minSampleA = array2table([SampleB_70.nm, SampleB_70.x T-SampleA_70.x T], 'VariableNames', {'nm','x T'});
184 SampleB_74_minSampleA = array2table([SampleB_74.nm, SampleB_74.x T-SampleA_74.x T], 'VariableNames', {'nm','x T'});
185 SampleB_78_minSampleA = array2table([SampleB_78.nm, SampleB_78.x T-SampleA_78.x T], 'VariableNames', {'nm','x T'});
186 SampleB_82_minSampleA = array2table([SampleB_82.nm, SampleB_82.x T-SampleA_82.x T], 'VariableNames', {'nm','x T'});
187 % Sample C
188 SampleC_62_minSampleA = array2table([SampleC_62.nm, SampleC_62.x T-SampleA_62.x T], 'VariableNames', {'nm','x T'});
189 SampleC_66_minSampleA = array2table([SampleC_66.nm, SampleC_66.x T-SampleA_66.x T], 'VariableNames', {'nm','x T'});
190 SampleC_70_minSampleA = array2table([SampleC_70.nm, SampleC_70.x T-SampleA_70.x T], 'VariableNames', {'nm','x T'});
191 SampleC_74_minSampleA = array2table([SampleC_74.nm, SampleC_74.x T-SampleA_74.x T], 'VariableNames', {'nm','x T'});
192 SampleC_78_minSampleA = array2table([SampleC_78.nm, SampleC_78.x T-SampleA_78.x T], 'VariableNames', {'nm','x T'});
193 SampleC_82_minSampleA = array2table([SampleC_82.nm, SampleC_82.x T-SampleA_82.x T], 'VariableNames', {'nm','x T'});
194 % Sample D
195 SampleD_62_minSampleA = array2table([SampleD_62.nm, SampleD_62.x T-SampleA_62.x T], 'VariableNames', {'nm','x T'});
196 SampleD_66_minSampleA = array2table([SampleD_66.nm, SampleD_66.x T-SampleA_66.x T], 'VariableNames', {'nm','x T'});
197 SampleD_70_minSampleA = array2table([SampleD_70.nm, SampleD_70.x T-SampleA_70.x T], 'VariableNames', {'nm','x T'});
198 SampleD_74_minSampleA = array2table([SampleD_74.nm, SampleD_74.x T-SampleA_74.x T], 'VariableNames', {'nm','x T'});
199 SampleD_78_minSampleA = array2table([SampleD_78.nm, SampleD_78.x T-SampleA_78.x T], 'VariableNames', {'nm','x T'});
200 SampleD_82_minSampleA = array2table([SampleD_82.nm, SampleD_82.x T-SampleA_82.x T], 'VariableNames', {'nm','x T'});
201
202 %%
203 figure
204 t = tiledlayout(2,2,'TileSpacing','compact');
205 ttl = 'Plot of the Absorbance of ';
206 tableplot(SampleA_62, SampleA_66, SampleA_70, SampleA_74, SampleA_78, SampleA_82, 'Sample A', ttl)
207 tableplot(SampleB_62_minSampleA, SampleB_66_minSampleA, SampleB_70_minSampleA, SampleB_74_minSampleA, SampleB_78_minSampleA, SampleB_82_minSampleA, 'Sample B - Sample A', ttl)
208 tableplot(SampleC_62_minSampleA, SampleC_66_minSampleA, SampleC_70_minSampleA, SampleC_74_minSampleA, SampleC_78_minSampleA, SampleC_82_minSampleA, 'Sample C - Sample A', ttl)
209 tableplot(SampleD_62_minSampleA, SampleD_66_minSampleA, SampleD_70_minSampleA, SampleD_74_minSampleA, SampleD_78_minSampleA, SampleD_82_minSampleA, 'Sample D - Sample A', ttl)
210 xlabel(t, 'Wavelength (nm)')
211 ylabel(t, 'Absorbance (OD)')
212 lgd = legend({'pH 6.2','pH 6.6','pH 7.0','pH 7.4','pH 7.8','pH 8.2'});
213 lgd.NumColumns = 6;
214 lgd.Layout.Tile = 'north';
215
216 %% Calculate ratios
217 AbsorptionSamples = [SampleA_62.x T SampleA_66.x T SampleA_70.x T SampleA_74.x T SampleA_78.x T SampleA_82.x T SampleB_62.x T SampleB_66.x T ...
SampleB_70.x T SampleB_74.x T SampleB_78.x T SampleB_82.x T SampleC_62.x T SampleC_66.x T SampleC_70.x T SampleC_74.x T ...
SampleC_78.x T SampleC_82.x T SampleD_62.x T SampleD_66.x T SampleD_70.x T SampleD_74.x T SampleD_78.x T SampleD_82.x T];
218 Ratios = zeros(24,12);
219 for i = 1:12
220 Ratios(i,1) = AbsorptionSamples(i,i);
221 Ratios(i,2) = AbsorptionSamples(71,i);
222 Ratios(i,3) = Ratios(i,1) - Ratios(i,2);
223 Ratios(i,4) = ((Ratios(i,2) - Ratios(i,1))/Ratios(i,1))*100;
224 Ratios(i,5) = max(AbsorptionSamples(:,i));
225 Ratios(i,6) = min(AbsorptionSamples(:,i));
226 Ratios(i,7) = Ratios(i,5) - Ratios(i,6);
227 Ratios(i,8) = ((Ratios(i,6) - Ratios(i,5))/Ratios(i,5))*100;
228 Ratios(i,9) = AbsorptionSamples(48,i);
229 Ratios(i,10) = AbsorptionSamples(59,i);
230 Ratios(i,11) = Ratios(i,9) - Ratios(i,10);
231 Ratios(i,12) = ((Ratios(i,10) - Ratios(i,9))/Ratios(i,9))*100;
232 end
233 Ratios = array2table(Ratios, 'VariableNames', {'%T 700nm', '%T 350 nm', 'Difference 700-350', '%Decrease 700-350', 'Max %T', 'Min %T', 'Difference ...
Max%', 'ST at 465nm', 'ST at 405nm', 'Difference 465/405', '%Decrease 465/405'}, 'RowNames', {'Sample A pH 6.2', 'Sample A pH 6.6', 'Sample A pH 7.0', 'Sample A pH 7.4', 'Sample A pH 7.8', 'Sample A pH 8.2', 'Sample B pH 6.2', 'Sample B pH 6.6', 'Sample B pH 7.0', 'Sample B pH 7.4', 'Sample B pH 7.8', 'Sample B pH 8.2', 'Sample C pH 6.2', 'Sample C pH 6.6', 'Sample C pH 7.0', 'Sample C pH 7.4', 'Sample C pH 7.8', 'Sample C pH 8.2', 'Sample D pH 6.2', 'Sample D pH 6.6', 'Sample D pH 7.0', 'Sample D pH 7.4', 'Sample D pH 7.8', 'Sample D pH 8.2'});
234 RatiosSampleA = Ratios(1:6,1:12);
235 RatiosSampleB = Ratios(7:12,1:12);
236 RatiosSampleC = Ratios(13:18,1:12);
237 RatiosSampleD = Ratios(19:24,1:12);
238 writetable(Ratios, 'Ratios Absorption.csv', 'WriteRowNames', true);
239
240 %% Make rescale values

```

```

241
242 %Sample A
243 SampleA_62_rescale = rescaletable(SampleA_62);
244 SampleA_66_rescale = rescaletable(SampleA_66);
245 SampleA_70_rescale = rescaletable(SampleA_70);
246 SampleA_74_rescale = rescaletable(SampleA_74);
247 SampleA_78_rescale = rescaletable(SampleA_78);
248 SampleA_82_rescale = rescaletable(SampleA_82);
249
250 %Sample B
251 SampleB_62_rescale = rescaletable(SampleB_62);
252 SampleB_66_rescale = rescaletable(SampleB_66);
253 SampleB_70_rescale = rescaletable(SampleB_70);
254 SampleB_74_rescale = rescaletable(SampleB_74);
255 SampleB_78_rescale = rescaletable(SampleB_78);
256 SampleB_82_rescale = rescaletable(SampleB_82);
257
258 %Sample C
259 SampleC_62_rescale = rescaletable(SampleC_62);
260 SampleC_66_rescale = rescaletable(SampleC_66);
261 SampleC_70_rescale = rescaletable(SampleC_70);
262 SampleC_74_rescale = rescaletable(SampleC_74);
263 SampleC_78_rescale = rescaletable(SampleC_78);
264 SampleC_82_rescale = rescaletable(SampleC_82);
265
266 %Sample D
267 SampleD_62_rescale = rescaletable(SampleD_62);
268 SampleD_66_rescale = rescaletable(SampleD_66);
269 SampleD_70_rescale = rescaletable(SampleD_70);
270 SampleD_74_rescale = rescaletable(SampleD_74);
271 SampleD_78_rescale = rescaletable(SampleD_78);
272 SampleD_82_rescale = rescaletable(SampleD_82);
273 %% plotS_rescale
274 figure(5)
275 figure
276 t = tiledlayout(2,2,'TileSpacing','compact');
277 absorpplot(SampleA_62_rescale,SampleA_66_rescale,SampleA_70_rescale,SampleA_74_rescale,SampleA_78_rescale,SampleA_82_rescale,'Sample A')
278 absorpplot(SampleB_62_rescale,SampleB_66_rescale,SampleB_70_rescale,SampleB_74_rescale,SampleB_78_rescale,SampleB_82_rescale,'Sample B')
279 absorpplot(SampleC_62_rescale,SampleC_66_rescale,SampleC_70_rescale,SampleC_74_rescale,SampleC_78_rescale,SampleC_82_rescale,'Sample C')
280 absorpplot(SampleD_62_rescale,SampleD_66_rescale,SampleD_70_rescale,SampleD_74_rescale,SampleD_78_rescale,SampleD_82_rescale,'Sample D')
281
282 xlabel(t,'Wavelength (nm)')
283 ylabel(t,'Absorbance (OD)')
284 lgd = legend({'pH 6.2','pH 6.6','pH 7.0','pH 7.4','pH 7.8','pH 8.2'});
285 lgd.NumColumns = 6;
286 lgd.Layout.Tile = 'north';
287
288
289 %%
290 pH = [6.2 6.6 7.0 7.4 7.8 8.2];
291 SampleA_rescaled_at_475nm = [SampleA_62_rescale(46,2) SampleA_66_rescale(46,2) SampleA_70_rescale(46,2) SampleA_74_rescale(46,2) ...
292   SampleA_78_rescale(46,2) SampleA_82_rescale(46,2)];
293 SampleB_rescaled_at_475nm = [SampleB_62_rescale(46,2) SampleB_66_rescale(46,2) SampleB_70_rescale(46,2) SampleB_74_rescale(46,2) ...
294   SampleB_78_rescale(46,2) SampleB_82_rescale(46,2)];
295 SampleC_rescaled_at_475nm = [SampleC_62_rescale(46,2) SampleC_66_rescale(46,2) SampleC_70_rescale(46,2) SampleC_74_rescale(46,2) ...
296   SampleC_78_rescale(46,2) SampleC_82_rescale(46,2)];
297 SampleD_rescaled_at_475nm = [SampleD_62_rescale(46,2) SampleD_66_rescale(46,2) SampleD_70_rescale(46,2) SampleD_74_rescale(46,2) ...
298   SampleD_78_rescale(46,2) SampleD_82_rescale(46,2)];
299
300 figure
301 plot(pH,SampleA_rescaled_at_475nm,pH,SampleB_rescaled_at_475nm,pH,SampleC_rescaled_at_475nm ,pH,SampleD_rescaled_at_475nm)
302 xlabel('pH')
303 ylabel('Value 475 nm rescaled')
304 legend('Sample A','Sample B','Sample C','Sample D')
305 title('Plot of pH and rescaled values at 475 nm ')
306
307 %%
308
309 figure
310 t = tiledlayout(1,3,'TileSpacing','compact');
311 tableplot(SampleD_62, SampleD_66, SampleD_70, SampleD_74, SampleD_78, SampleD_82, 'Sample D', tt1)
312 title('Absorbance unscaled sample D')
313 xlabel('Wavelength (nm)')
314 ylabel('Absorbance (OD)')
315 legend({'pH 6.2','pH 6.6','pH 7.0','pH 7.4','pH 7.8','pH 8.2'},'Location','best')
316 absorpplot(SampleD_62_rescale,SampleD_66_rescale,SampleD_70_rescale,SampleD_74_rescale,SampleD_78_rescale,SampleD_82_rescale,'Sample D')
317 xlabel('Wavelength (nm)')
318 ylabel('Scaled Absorbance (OD)')
319 legend({'pH 6.2','pH 6.6','pH 7.0','pH 7.4','pH 7.8','pH 8.2'},'Location','best')
320 nexttile
321 %%
322 figure
323 plot(pH,SampleA_rescaled_at_475nm,pH,SampleB_rescaled_at_475nm,pH,SampleC_rescaled_at_475nm ,pH,SampleD_rescaled_at_475nm)
324 xlabel('pH')
325 ylabel('Value 475 nm scaled')
326 legend('Sample A','Sample B','Sample C','Sample D'),'Location','best')
327 title('Plot of pH and scaled values at 475 nm ')
328 title(t, 'Absorbance Measurements')
329 %%
330 figure(6)
331 t = tiledlayout(2,3,'TileSpacing','compact');
332 tsample = 'Fitted Curve, pKa and Sensitivity of the Absorbance of Sample C and D';
333 title(t, tsample)
334 xlabel(t, 'pH')
335 estimatepKa(pH,SampleC_rescaled_at_475nm)
336 estimatepKa(pH,SampleD_rescaled_at_475nm)

```

Listing A.2: Matlab script for the full pH range Avantes data

```

1 clear all
2 clc
3
4 path = 'C:\Users\mauri\Avantes\AvaSoft8\Metingen 24 juni\32 naar 11 5 minuten rusten laag 1\Matlab.xlsx';
5 tijdfpH = 2; %1 = tijd
6 pH = [ 3.2 5.6 6.2 6.6 7.0 7.4 7.8 8.2 9 10.2 12.2];
7
8 T = readtable(path);
9 A = table2array(T);
10 %%
11 wavelenghts = A(:,1);
12 Ascaled = A;
13 Alength = length(A(1,:));
14 time = (2:1:Alength)*10;
15 timestep = 1
16
17 names = cell(1,Alength);
18 for k = 1:1:Alength-1
19     names{k} = {'pH ' num2str(pH(k))};
20 end
21
22 names = string(names(1:k));
23 %pH = [ 6.2 6.6 7.0 7.4 7.8 8.2];
24 for j=2:1:Alength
25     Ascaled(:,j) = A(:,j) ./ (A(329,j));
26 end

```

```

27 Amax = max(A(:,2:Alength));
28 Amax = 1.1*max(Amax);
29 Amax_scaled = max(Ascaled(:,2:Alength));
30 Amax_scaled = 1.1*max(Amax_scaled);
31
32
33 figure
34 t = tiledlayout(1,3,'TileSpacing','compact');
35 for i=2:timestep:Alength
36     nexttile(1)
37     plot(wavelengths,A(:,i),'DisplayName',names{i-1})
38     hold on
39     title('unscaled')
40     ylabel('Counts per second')
41     lgd = legend;
42     ylim([0,Amax])
43     xlim([350,650])
44     nexttile(2)
45     plot(wavelengths,Ascaled(:,i),'DisplayName',names{i-1})
46     hold on
47     title('scaled')
48     ylabel('Scaled Counts per second')
49     ylim([0,Amax_scaled])
50     xlim([350,650])
51 end
52 lgd.NumColumns = 1;
53 lgd.Layout.Tile = 'west';
54 title(t, 'Spectral outcome (scaled and unscaled) at different pH with mm sensing layer')
55
56 xlabel(t,'Wavelengths')
57
58 %% Plot tegeen pH
59
60 A_520 = Ascaled(420,2:timestep:Alength);
61 nexttile
62 plot(pH, A_520)
63 title('scaled value 520nm vs pH')
64 ylabel('Scaled value at 520nm')
65 xlabel('pH')
66 figure(20)
67 estimatepKa(pH, A_520)

```

Listing A.3: Matlab script for the Avantes transition time data

```

1 clear all
2 clc
3
4 %% 11 to 3 05mm
5 path = {'C:\Users\mauri\Avantes\AvaSoft8\Metingen 24 juni\transitiontimemetingen\11to32met3Vlaag05\Matlab.xlsx'
6         'C:\Users\mauri\Avantes\AvaSoft8\Metingen 24 juni\transitiontimemetingen\32tol1met3Vlaag05mm\Matlab.xlsx'
7         'C:\Users\mauri\Avantes\AvaSoft8\Metingen 24 juni\transitiontimemetingen\11to32met3Vlaag1mm\Matlab.xlsx'
8         'C:\Users\mauri\Avantes\AvaSoft8\Metingen 24 juni\transitiontimemetingen\32tol1met3Vlaag1mm\Matlab.xlsx'};
9 namesplot={'pH 11.2 to 3.2 0.5mm' 'pH 3.2 to 11.2 0.5mm' 'pH 11.2 to 3.2 1mm' 'pH 3.2 to 11.2 1mm'};
10 figure(1)
11 t = tiledlayout('flow','TileSpacing','compact');
12 for ii=1:4
13     timestep = 5;
14     timebetweenmeasurement = 10;
15     T = readtable(path{ii});
16     A = table2array(T);
17     wavelengths = A(:,1);
18     Ascaled = A;
19     Alength = length(A(1,:));
20     time = (2:timestep:Alength)*timebetweenmeasurement;
21     names = cell(1,Alength);
22     for k = 1:1:Alength-1
23         names{k} = {[num2str((k*10)-9) ' sec']};
24     end
25     names = string(names(1:k));
26     Amax = max(A(:,2:Alength));
27     Amax = 1.1*max(Amax);
28     nexttile
29     for i=2:timestep:Alength
30         plot(wavelengths,A(:,i),'DisplayName',names{i-1})
31         hold on
32         title(namesplot{ii})
33         ylim([0,Amax])
34         xlim([400,650])
35     end
36     lgd = legend;
37     lgd.NumColumns = 1;
38     lgd.Layout.Tile = 'east';
39     ylabel(t,'Counts per second')
40     xlabel(t,'Wavelengths')
41     %%
42     figure(2)
43     t = tiledlayout('flow','TileSpacing','compact');
44     for ii=1:4
45         timestep = 5;
46         timebetweenmeasurement = 10;
47         T = readtable(path{ii});
48         A = table2array(T);
49         wavelengths = A(:,1);
50         Ascaled = A;
51         Alength = length(A(1,:));
52         time = (2:timestep:Alength)*timebetweenmeasurement;
53         names = cell(1,Alength);
54         for k = 1:1:Alength-1
55             names{k} = {[num2str((k*10)-9) ' sec']};
56         end
57         names = string(names(1:k));
58         for j=2:1:Alength
59             Ascaled(:,j) = A(:,j)./(A(329,j));
60         end
61         Amax_scaled = max(Ascaled(:,2:Alength));
62         Amax_scaled = 1.1*max(Amax_scaled);
63         nexttile
64         for i=2:timestep:Alength
65             plot(wavelengths,Ascaled(:,i),'DisplayName',names{i-1})
66             hold on
67             title(namesplot{ii})
68             ylim([0,Amax_scaled])
69             xlim([400,650])
70         end
71     end
72     lgd = legend;
73     lgd.NumColumns = 9;
74     lgd.Layout.Tile = 'north';
75     ylabel(t,'Counts per second')
76     xlabel(t,'Wavelengths')
77     %%
78
79
80
81 %% Plot tegeen tijd

```

```

82 figure
83 t = tiledlayout(1,4,'TileSpacing','compact');
84 for ii=1:4
85     timestep = 5;
86     timebetweenmeasurement = 10;
87     T = readtable(path(ii));
88     A = table2array(T);
89     wavelenghts = A(:,1);
90     Ascaled = A;
91     Alength = length(A(1,:));
92     time = (2:timestep:Alength)*timebetweenmeasurement;
93     names = cell(1,Alength);
94     for k = 1:1:Alength-1
95         names(k) = {num2str((k*10)-9) ' sec'};
96     end
97     names = string(names(1:k));
98     for j=2:1:Alength
99         Ascaled(:,j) = A(:,j)./(A(329,j));
100    end
101    Amax_scaled = max(Ascaled(:,2:Alength));
102    Amax_scaled = 1.1*Amax_scaled;
103
104    A_520 = Ascaled(420,2:timestep:Alength);
105    rextitle
106    plot(time, A_520)
107    title(namesplot(ii))
108
109 end
110 ylabel(t,'Scaled value at 520nm')
111 xlabel(t,'Tijd')

```

Listing A.4: Matlab script for calculating pKa Values from data

```

1 %% import Data
2 clear all
3 clc
4 close all
5
6 %% Importing Data and Decisions
7 figpath = 'C:\Users\mauri\Documents\MATLAB\Afstuderen\Figures\Fluorlog';
8 Sample_names = {'Sample A','Sample B','Sample C','Sample D'};
9 pKa_values = zeros(1,length(Sample_names));
10 Ratios_Samples = zeros(1,8);
11 for i = 1:length(Sample_names)
12     whichsample = i; %1=4=ABCD 5-10=6.2/6.6/7.0/7.4/7.8/8.2 11=Min 12=Max 13=Background
13     [SampleData, names, names_forplot, figSample, Excitationwavelenghts, Emissionwavelenghts] = importflourlogssampleddata(whichsample);
14     Samples_525em = zeros(31,length(names));
15     Samples_525em_scaled405 = zeros(31,length(names));
16     wavelenghts525 = 36;
17     for k = 1:length(names)
18         Samples_525em(:,k) = SampleData.(names(k))(wavelength525,:);
19         value405 = Samples_525em(12,k);
20         Samples_525em_scaled405(:,k) = Samples_525em(:,k)/value405;
21     end
22     % Samples_525em_scaled405 sorted = [Samples_525em_scaled405(:,8), Samples_525em_scaled405(:,1:7)];
23     % Samples_525em_sorted = [Samples_525em(:,8), Samples_525em(:,1:7)];
24
25     pH = [ 6.2 6.6 7.0 7.4 7.8 8.2 ];
26     pHminmax = [ 4 6.2 6.6 7.0 7.4 7.8 8.2 10];
27
28     for kk = 1:length(names)
29         Ratios_Samples(i,kk) = Samples_525em_scaled405(26,kk)/Samples_525em_scaled405(12,kk);
30     end
31     [pKa_values(i), param, stats] = sigmoid_pKa(pHminmax,Ratios_Samples(i,:),Sample_names(i));
32     param
33     stats
34 end
35 T = array2table(pKa_values,'VariableNames',{'Sample A','Sample B','Sample C','Sample D'},'RowNames', {'pKa Value'})
36
37 %%
38 lmin = Samples_525em(26,1);
39 lmax = Samples_525em(26,8);
40 lmin_scaled = Samples_525em_scaled405(26,1);
41 lmax_scaled = Samples_525em_scaled405(26,8);
42 k=2;
43 pHminmax(k);
44 Ratio_SampleA = Ratios_Samples(1,:);
45 Ratio_SampleB = Ratios_Samples(2,:);
46 Ratio_SampleC = Ratios_Samples(3,:);
47 Ratio_SampleD = Ratios_Samples(4,:);
48 %%
49 figure
50 t = tiledlayout(4,3,'TileSpacing','compact');
51 title(t, 'Ratios, sensitivity and pKa of Sample A')
52 xlabel(t, 'pH');
53 [fitresult, pKa_valueA] = estimatepKa(pHminmax, Ratio_SampleA);
54 title(t, 'Ratios, sensitivity and pKa of Sample B')
55 xlabel(t, 'pH');
56 [fitresult, pKa_valueB] = estimatepKa(pHminmax, Ratio_SampleB);
57 title(t, 'Ratios, sensitivity and pKa of Sample C')
58 xlabel(t, 'pH');
59 [fitresult, pKa_valueC] = estimatepKa(pHminmax, Ratio_SampleC);
60 title(t, 'Ratios, sensitivity and pKa of Sample A, B, C, D')
61 xlabel(t, 'pH');
62 [fitresult, pKa_valueD] = estimatepKa(pHminmax, Ratio_SampleD);

```

Listing A.5: Matlab script for the full data obtained by flourlog

```

1 %% import Data
2 clear all
3 clc
4 close all
5
6 %% Importing Data and Decisions
7 for i = 3
8
9     whichsample = i; %1=4=ABCD 5-12=Min/6.2/6.6/7.0/7.4/7.8/8.2/Max 13=Background
10
11     [SampleData, names, names_forplot, figSample, Excitationwavelenghts, Emissionwavelenghts] = importflourlogssampleddata(whichsample);
12
13     figpath = 'C:\Users\mauri\Documents\MATLAB\Afstuderen\Figures\Fluorlog';
14     savefigures = 0;
15     spectralimages = 0; % 1=spectral images
16     type = 4; % 1 = surface, 2 = contour, 3 = contour3, 4 = surfacetopview
17     plots500600 = 1; % 1=plots ranging 500/600
18     comparefigures = 1; %
19     plots515530 = 1;
20     plot525 = 1;
21     plots525scaled = 1; %plots of 525 emission

```

```

22 plot525scaled = 1; %plots of 525 emission
23
24
25 %% Surface, Contour plots
26 xlabel('Excitation Wavelength (nm)');
27 ylabel('Emission Wavelength (nm)');
28 ttl = 'Sample ';
29 ylimit = 2500000;
30 colorscale = ([0 ylimit]);
31 figure
32 t = tiledlayout(2,4,'TileSpacing','compact');
33 if spectralimages == 1
34 fluorlogplot(Excitationwavelengths, Emissionwavelengths, SampleData, names, xlabel, ylabel, ttl, type, names_forplot, ylimit, colorscale);
35 cb = colorbar;
36 cb.Layout.Tile = 'east';
37 title(t, 'Spectral 3D Plot of Fluorescence output in counts per second of')
38 ylabel(t, 'Counts per second (CPS)')
39 elseif plots500600 == 1
40 startwavelength = 31; %500 nm
41 endwavelength = 51; % 600 nm
42 startexcitation = 12; % 405 nm
43 endexcitation = 26; % 475 nm
44 firstsample = 1; % A 6.2
45 lastsample = length(names); % A 6.6
46 Max_Ratio405_475_Samples = cell((lastsample-firstsample),3);
47 for l = firstsample:1:lastsample
48 [Ratios_Sample.(names{l}), Max_Emissionwavelength.(names{l})] = plotemissions2(SampleData, names, l, startwavelength, endwavelength,...
49 Emissionwavelengths, Excitationwavelengths, startexcitation, endexcitation, names_forplot);
50 Max_Ratio405_475_Samples{l,1} = (names{l});
51 Max_Ratio405_475_Samples{l,2} = max(Ratios_Sample.(names{l}).(2));
52 Max_Ratio405_475_Samples{l,3} = Max_Emissionwavelength.(names{l});
53 end
54 Max_Ratio405_475_Samples = cell2table(Max_Ratio405_475_Samples(firstsample:lastsample,:), 'VariableNames', {'Sample' 'Difference 405/475' ...
55 'Wavelength'});
56 end
57
58 %%
59 figure
60 ylimit = 1600000;
61 colorscale = ([0 ylimit]);
62 t = tiledlayout(2,3,'TileSpacing','compact');
63 xlabel('Excitation Wavelength (nm)');
64 ylabel('Emission Wavelength (nm)');
65 ttl = 'Sample ';
66 plots = [1 4 8];
67 for k = 1:3
68 fulltitle = [sprintf('%s', ttl) names_forplot(plots(k))];
69 nexttile(k)
70 surf(Excitationwavelengths, Emissionwavelengths, SampleData.(names(plots(k))))
71 caxis(colorscale)
72 xline(405,'--r','405nm','LineWidth',2);
73 xline(465,':','475nm','Color','#00c0ff','LineWidth',2);
74 yline(520,'-g','525nm','LineWidth',2);
75 xlabel(sprintf('%s',xlabel))
76 ylabel(sprintf('%s',ylabel))
77 title(fulltitle);
78 hold on
79 nexttile(k+3)
80 surf(Excitationwavelengths, Emissionwavelengths, SampleData.(names(plots(k))))
81 caxis(colorscale)
82 view(2)
83 xline(405,'--r','405nm','LineWidth',2);
84 xline(465,':','475nm','Color','#00c0ff','LineWidth',2);
85 yline(520,'-g','525nm','LineWidth',2);
86 xlabel(sprintf('%s',xlabel))
87 ylabel(sprintf('%s',ylabel))
88 title(fulltitle);
89 xlim([350 500]);
90 ylim([350 600]);
91 hold on
92 end
93
94
95
96
97
98 cb = colorbar;
99 cb.Layout.Tile = 'west';
100 title(t, 'Spectral 3D Plot of Fluorescence output in counts per second of')
101 ylabel(t, 'Counts per second (CPS)')
102 %% Output of Excitations at Emission 515 - 530
103 Samples_515em = zeros(31,length(names));
104 Samples_520em = zeros(31,length(names));
105 Samples_525em = zeros(31,length(names));
106 Samples_530em = zeros(31,length(names));
107 % Emission
108 wavelength515 = 34; % 34 is 515
109 wavelength520 = 35; % 34 is 515
110 wavelength525 = 36; % 34 is 515
111 wavelength530 = 37; % 34 is 515
112 if plots515530 == 1
113 figure('WindowState','maximized')
114 subplot(2,2,1)
115 for k = 1:length(names) %vanaf 3 want geen glas of leeg sample meenemen
116 Samples_515em(:,k) = SampleData.(names{k})(wavelength515,:);
117 plot(Excitationwavelengths,Samples_515em(:,k),'DisplayName', names_forplot(k))
118 hold on
119 if k == length(names)
120 xlabel('Excitation Wavelength (nm)')
121 ylabel('Counts per Second (a.u.)')
122 title('Measured output of Samples at', ' Emission Wavelength of 515 nm')
123 legend('-DynamicLegend','AutoUpdate','off','Location','best');
124 xline(405,'--','405nm','Color','#8200c8');
125 xline(465,':','475nm','Color','#00c0ff');
126 else
127 end
128 end
129 subplot(2,2,2)
130 for k = 1:length(names) %vanaf 3 want geen glas of leeg sample meenemen
131 Samples_520em(:,k) = SampleData.(names{k})(wavelength520,:);
132 plot(Excitationwavelengths,Samples_520em(:,k),'DisplayName', names_forplot(k))
133 xlabel('Excitation Wavelength (nm)')
134 hold on
135 if k == length(names)
136 legend('-DynamicLegend','AutoUpdate','off','Location','best');
137 xlabel('Excitation Wavelength (nm)')
138 ylabel('Counts per Second (a.u.)')
139 title('Measured output of Samples at', ' Emission Wavelength of 520 nm')
140 xline(405,'--','405nm','Color','#8200c8');
141 xline(465,':','475nm','Color','#00c0ff');
142 else
143 end
144 end
145 subplot(2,2,3)
146 for k = 1:length(names) %vanaf 3 want geen glas of leeg sample meenemen
147 Samples_525em(:,k) = SampleData.(names{k})(wavelength525,:);
148 plot(Excitationwavelengths,Samples_525em(:,k),'DisplayName', names_forplot(k))
149 hold on
150 if k == length(names)

```

```

151 xlabel('Excitation Wavelength (nm)')
152 ylabel('Counts per Second (a.u.)')
153 title('Measured output of Samples at', ' Emission Wavelength of 525 nm')
154 legend('-DynamicLegend','AutoUpdate','off','Location','best');
155 xline(405,'--','405nm','Color','#8200c8');
156 xline(465,':','475nm','Color','#00c0ff');
157 else
158 end
159 end
160 subplot(2,2,4)
161 for k = 1:length(names) %vanaf 3 want geen glas of leeg sample meenemen
162 Samples_530em(:,k) = SampleData.(names(k))(wavelength530,:);
163 plot(Excitationwavelengths,Samples_530em(:,k),'DisplayName', names_forplot(k))
164 hold on
165 if k == length(names)
166 xlabel('Excitation Wavelength (nm)')
167 ylabel('Counts per Second (a.u.)')
168 title('Measured output of Samples at', ' Emission Wavelength of 530 nm')
169 legend('-DynamicLegend','AutoUpdate','off','Location','best');
170 xline(405,'--','405nm','Color','#8200c8');
171 xline(465,':','475nm','Color','#00c0ff');
172 else
173 end
174 end
175 else
176 end
177
178 figure
179 subplot(1,2,1)
180 for k = 1:length(names) %vanaf 3 want geen glas of leeg sample meenemen
181 Samples_525em(:,k) = SampleData.(names(k))(wavelength525,:);
182 if plot525 == 1
183 plot(Excitationwavelengths,Samples_525em(:,k),'DisplayName', names_forplot(k))
184 hold on
185 if k == length(names)
186 xlabel('Excitation Wavelength (nm)')
187 ylabel('Counts per Second (a.u.)')
188 title('Measured output of Samples at', ' Emission Wavelength of 525 nm')
189 lgd = legend('-DynamicLegend','AutoUpdate','off','Location','best');
190 lgd.NumColumns = 2;
191 xline(405,'--','405nm','Color','#8200c8');
192 xline(465,':','475nm','Color','#00c0ff');
193 else
194 end
195 else
196 end
197 end
198
199
200 %% Rescaling
201 Samples_525em_scaled405 = zeros(31,length(names));
202
203 subplot(1,2,2)
204 for o = 1:length(names)
205 value405 = Samples_525em(12,o);
206 Samples_525em_scaled405(:,o) = Samples_525em(:,o)/value405;
207 if plot525scaled == 1
208 plot(Excitationwavelengths,Samples_525em_scaled405(:,o),'DisplayName', names_forplot(o))
209 hold on
210 if o == length(names)
211 xlabel('Excitation Wavelength (nm)')
212 ylabel('Scaled CPS')
213 title('Output of Samples at emission of 525 nm','rescaled at 405nm')
214 lgd = legend('-DynamicLegend','AutoUpdate','off','Location','best');
215 lgd.NumColumns = 2;
216 xline(405,'--','405nm','Color','#8200c8');
217 xline(465,':','475nm','Color','#00c0ff');
218 else
219 end
220 else
221 end
222 end
223
224
225 %% All scaled figure
226 figure(100)
227 if (whichsample ≤ 4) && (comparefigures == 1)
228 subplot(2,2,whichsample)
229 elseif whichsample ≥ 5
230 place = whichsample-4;
231 subplot(2,4,place)
232 end
233
234 for o = 1:length(names)
235 value405 = Samples_525em(12,o);
236 Samples_525em_scaled405(:,o) = Samples_525em(:,o)/value405;
237 if plot525scaled == 1
238 plot(Excitationwavelengths,Samples_525em_scaled405(:,o),'DisplayName', names_forplot(o))
239 hold on
240 if o == length(names)
241 xlabel('Excitation Wavelength (nm)')
242 ylabel('Scaled CPS')
243 title('Output of Samples at emission of 525 nm','rescaled at 405nm')
244 legend('-DynamicLegend','AutoUpdate','off','Location','best');
245 xline(405,'--','405nm','Color','#8200c8');
246 xline(465,':','475nm','Color','#00c0ff');
247 else
248 end
249 else
250 end
251 end
252
253
254 %% Saving all unscaled figures
255 figure(90)
256 if (whichsample ≤ 4) && (comparefigures == 1)
257 subplot(2,2,whichsample)
258 elseif whichsample ≥ 5
259 place = whichsample-4;
260 subplot(2,4,place)
261 end
262
263 for k = 1:length(names) %vanaf 3 want geen glas of leeg sample meenemen
264 Samples_525em(:,k) = SampleData.(names(k))(wavelength525,:);
265 plot(Excitationwavelengths,Samples_525em(:,k),'DisplayName', names_forplot(k))
266 hold on
267 if k == length(names)
268 xlabel('Excitation Wavelength (nm)')
269 ylabel('Counts per Second (a.u.)')
270 title('Measured output of Samples at', ' Emission Wavelength of 525 nm')
271 legend('-DynamicLegend','AutoUpdate','off','Location','best');
272 xline(405,'--','405nm','Color','#8200c8');
273 xline(465,':','475nm','Color','#00c0ff');
274 ylim([0 4000000])
275 else
276 end
277 end
278
279 % saving
280 if whichsample == 4 && comparefigures == 1 && savefigures == 1
281 filename = fullfile(figpath, 'Emissions525AllSamples.png');
282 exportgraphics(gcf,filename)

```

```

282     filename = fullfile(figpath, 'Emissions525AllSamples.fig');
283     saveas(gcf,filename)
284 else
285 end
286 end

```

Listing A.6: Matlab script for processing the CMOS data in imageJ

```

1  close all
2  clc
3  clear all
4
5  %%
6  fds = fileDatastore('C:\Users\mauri\Documents\MATLAB\Afstuderen\First Batch', 'ReadFcn', @load, 'FileExtensions','.csv','IncludeSubfolders'...
7  true);
8  fullFileNames = fds.Files;
9  FileNames = string(fullFileNames);
10 names = {'C_405_green' 'C_475_green' 'D_405_green' 'D_475_green' 'E_405_green' 'E_475_green' 'F_405_green' 'F_475_green' 'G_405_green' '...
11         'G_475_green' 'H_405_green' 'H_475_green'};
12 beginsample = 1;
13 pH = {[6.2 6.6 7.0 7.4 7.8 8.2]};
14
15 for j = 1:length(names)
16     i = j+beginsample-1;
17     k = j+1;
18     Samples.(names{j}) = readtable(FileNames{i});
19     L.(names{j}) = table2array([Samples.(names{j}) (1:6, [4 8])]);
20 end
21 R_C_large_mean = L.C_475_green(:,1)./L.C_405_green(:,1)
22 R_C_large_InDens = L.C_475_green(:,2)./L.C_405_green(:,2)
23
24 figure
25 subplot(1,2,1)
26 plot(pH,L_C_475_green(:,1),'DisplayName','475nm Mean Intensity')
27 hold on
28 plot(pH,L_C_405_green(:,1),'DisplayName','405nm Mean Intensity')
29 hold on
30 plot(pH,L_C_475_green(:,2),'DisplayName','475nm Intensity Density')
31 hold on
32 plot(pH,L_C_405_green(:,2),'DisplayName','405nm Intensity Density')
33 hold on
34 xlabel('pH')
35 ylabel('Value intensity green channel')
36 title('Comparing Value of the pixel intensity', 'detected in the green channel')
37 legend
38 xlim([6.2 8.2])
39 subplot(1,2,2)
40 plot(pH, R_C_large_mean,'DisplayName','Ratio 475/405nm Mean Intensity')
41 hold on
42 plot(pH, R_C_large_InDens,'DisplayName','Ratio 475/405nm Intensity Density')
43 xlabel('pH')
44 ylabel('Ratio 475/405nm Intensity green channel')
45 title('Comparing Ratios the intensity', 'detected in the green channel')
46 legend
47 %%
48 plotintensities(pH, L_C_475_green,L_C_405_green)
49
50 plotintensities(pH, L_E_475_green,L_E_405_green)
51
52 plotintensities(pH, L_G_475_green,L_G_405_green)

```

Listing A.7: Matlab script for the Avantes data

```

1  clear all
2  clc
3
4  path = 'C:\Users\mauri\Avantes\AvaSoft8\Metingen 24 juni\32 naar 11 5 minuten rusten laag 1\Matlab.xlsx';
5  timestep = 1;
6  tijdoefpH = 2; %1 = tijd
7  pH = [ 3.2 5.6 6.2 6.6 7.0 7.4 7.8 8.2 9 10.2 12.2];
8
9  T = readtable(path);
10 A = table2array(T);
11 %%
12 wavelengths = A(:,1);
13 Ascaled = A;
14 Alength = length(A(1,:));
15 time = (2:timestep:Alength)*10;
16
17 names = cell(1,Alength);
18 if tijdoefpH==1
19     for k = 1:Alength-1
20         names(k) = {[num2str((k*10)-9) ' sec']};
21     end
22 elseif tijdoefpH==2
23     for k = 1:Alength-1
24         names(k) = {'pH ' num2str(pH(k))};
25     end
26 end
27
28 names = string(names(1:k));
29 spH = [ 6.2 6.6 7.0 7.4 7.8 8.2];
30 for j=2:Alength
31     Ascaled(:,j) = A(:,j) ./ (A(329,j));
32 end
33
34 Amax = max(A(:,2:Alength));
35 Amax_scaled = 1.1*max(Amax);
36 Amax_scaled = max(Ascaled(:,2:Alength));
37 Amax_scaled = 1.1*max(Amax_scaled);
38
39 figure
40 t = tiledlayout(1,3,'TileSpacing','compact');
41 for i=2:timestep:Alength
42     nexttile(1)
43     plot(wavelengths,A(:,i),'DisplayName',names{i-1})
44     hold on
45     title('unscaled')
46     ylabel('Counts per second')
47     lgd = legend;
48     ylim([0,Amax])
49     xlim([350,650])
50     nexttile(2)
51     plot(wavelengths,Ascaled(:,i),'DisplayName',names{i-1})
52     hold on
53     title('scaled')
54     ylabel('Scaled Counts per second')

```

```

55     ylim([0,Amax_scaled])
56     xlim([350,650])
57 end
58 lgd.NumColumns = 1;
59 lgd.Layout.Tile = 'west';
60 title(t, 'Spectral outcome (scaled and unscaled) at different pH with nm sensing layer')
61
62 xlabel(t,'Wavelengths')
63
64 %% Plot tegen tijd
65 if tijdofpH == 1
66     A_520 = Ascaled(420,2:timestep:Alength);
67     nexttile
68     plot(time, A_520)
69     title('Scaled value 520nm vs pH')
70     ylabel('Scaled value at 520nm')
71     xlabel('Tijd')
72 elseif tijdofpH == 2
73     A_520 = Ascaled(420,2:timestep:Alength);
74     nexttile
75     plot(pH, A_520)
76     title('scaled value 520nm vs pH')
77     ylabel('Scaled value at 520nm')
78     xlabel('pH')
79 elseif tijdofpH ≤ 3
80     print('no time or pH selected')
81 end

```

Listing A.8: Matlab script for the reflection data

```

1 %% Close all
2
3 clc
4 clear all
5 close all
6
7 %% Load Data
8
9 fds = fileDatastore('C:\Users\mauri\Documents\MATLAB\Afstuderen\Reflectiemetingen\', 'ReadFcn', @load, "FileExtensions", '.csv');
10 fullFileNames = fds.Files;
11 FileNames = string(fullFileNames);
12 % correction files
13 Sample_Glass = importfileAbsorption(FileNames(4));
14 Sample_100_end = importfileAbsorption(FileNames(3));
15 Sample_0_begin = importfileAbsorption(FileNames(1));
16
17 %Sample A
18 FirstFile_SampleA = 6;
19 SampleA_62 = importfileAbsorption(FileNames(FirstFile_SampleA));
20 SampleA_66 = importfileAbsorption(FileNames(FirstFile_SampleA+1));
21 SampleA_70 = importfileAbsorption(FileNames(FirstFile_SampleA+2));
22 SampleA_74 = importfileAbsorption(FileNames(FirstFile_SampleA+3));
23 SampleA_78 = importfileAbsorption(FileNames(FirstFile_SampleA+4));
24 SampleA_82 = importfileAbsorption(FileNames(FirstFile_SampleA+5));
25
26 %Sample B
27 FirstFile_SampleB = 12;
28 SampleB_62 = importfileAbsorption(FileNames(FirstFile_SampleB));
29 SampleB_66 = importfileAbsorption(FileNames(FirstFile_SampleB+1));
30 SampleB_70 = importfileAbsorption(FileNames(FirstFile_SampleB+2));
31 SampleB_74 = importfileAbsorption(FileNames(FirstFile_SampleB+3));
32 SampleB_78 = importfileAbsorption(FileNames(FirstFile_SampleB+4));
33 SampleB_82 = importfileAbsorption(FileNames(FirstFile_SampleB+5));
34
35 %Sample C
36 FirstFile_SampleC = 18;
37 SampleC_62 = importfileAbsorption(FileNames(FirstFile_SampleC));
38 SampleC_66 = importfileAbsorption(FileNames(FirstFile_SampleC+1));
39 SampleC_70 = importfileAbsorption(FileNames(FirstFile_SampleC+2));
40 SampleC_74 = importfileAbsorption(FileNames(FirstFile_SampleC+3));
41 SampleC_78 = importfileAbsorption(FileNames(FirstFile_SampleC+4));
42 SampleC_82 = importfileAbsorption(FileNames(FirstFile_SampleC+5));
43
44 %Sample D
45 FirstFile_SampleD = 24;
46 SampleD_62 = importfileAbsorption(FileNames(FirstFile_SampleD));
47 SampleD_66 = importfileAbsorption(FileNames(FirstFile_SampleD+1));
48 SampleD_70 = importfileAbsorption(FileNames(FirstFile_SampleD+2));
49 SampleD_74 = importfileAbsorption(FileNames(FirstFile_SampleD+3));
50 SampleD_78 = importfileAbsorption(FileNames(FirstFile_SampleD+4));
51 SampleD_82 = importfileAbsorption(FileNames(FirstFile_SampleD+5));
52
53 %% Plot Reflection
54 figure
55 t = tiledlayout(2,3,'TileSpacing','compact');
56 nexttile
57 plot(Sample_Glass.nm,Sample_Glass.x_T)
58 legend({'Glass slide','Location','Southeast'})
59 title('Reflection plot Glass slide')
60 hold on
61 nexttile
62 plot(Sample_100_end.nm,Sample_100_end.x_T,Sample_0_begin.nm,Sample_0_begin.x_T)
63 legend({'100% end','0%begin','Location','southeast'})
64 title('Reflection plot Baseline Measurements')
65 nexttile
66 plot(SampleA_62.nm,SampleA_62.x_T,SampleA_66.nm,SampleA_66.x_T,SampleA_70.nm,SampleA_70.x_T,SampleA_74.nm,SampleA_74.x_T,SampleA_78.nm,...
67     SampleA_78.x_T,SampleA_82.nm,SampleA_82.x_T)
68 title('Reflection plot Sample A')
69 nexttile
70 plot(SampleB_62.nm,SampleB_62.x_T,SampleB_66.nm,SampleB_66.x_T,SampleB_70.nm,SampleB_70.x_T,SampleB_74.nm,SampleB_74.x_T,SampleB_78.nm,...
71     SampleB_78.x_T,SampleB_82.nm,SampleB_82.x_T)
72 title('Reflection plot Sample B')
73 nexttile
74 plot(SampleC_62.nm,SampleC_62.x_T,SampleC_66.nm,SampleC_66.x_T,SampleC_70.nm,SampleC_70.x_T,SampleC_74.nm,SampleC_74.x_T,SampleC_78.nm,...
75     SampleC_78.x_T,SampleC_82.nm,SampleC_82.x_T)
76 title('Reflection plot Sample C')
77 nexttile
78 plot(SampleD_62.nm,SampleD_62.x_T,SampleD_66.nm,SampleD_66.x_T,SampleD_70.nm,SampleD_70.x_T,SampleD_74.nm,SampleD_74.x_T,SampleD_78.nm,...
79     SampleD_78.x_T,SampleD_82.nm,SampleD_82.x_T)
80 title('Reflection plot Sample D')
81 xlabel(t,'Wavelength (nm)')
82 ylabel(t,'Reflection %')
83 lgd = legend({'pH 6.2','pH 6.6','pH 7.0','pH 7.4','pH 7.8','pH 8.2'});
84 lgd.NumColumns = 6;
85 lgd.Layout.Tile = 'north';
86 %% New figure
87 figure
88 t = tiledlayout(2,2,'TileSpacing','compact');
89 nexttile
90 plot(SampleA_62.nm,SampleA_62.x_T,SampleA_66.nm,SampleA_66.x_T,SampleA_70.nm,SampleA_70.x_T,SampleA_74.nm,SampleA_74.x_T,SampleA_78.nm,...
91     SampleA_78.x_T,SampleA_82.nm,SampleA_82.x_T)
92 title('Reflection plot Sample A')
93 nexttile
94 plot(SampleB_62.nm,SampleB_62.x_T,SampleB_66.nm,SampleB_66.x_T,SampleB_70.nm,SampleB_70.x_T,SampleB_74.nm,SampleB_74.x_T,SampleB_78.nm,...
95     SampleB_78.x_T,SampleB_82.nm,SampleB_82.x_T)

```

```

90 title(' Reflection plot Sample B')
91 nexttile
92 plot(SampleC_62_nm,SampleC_62_x_T,SampleC_66_nm,SampleC_66_x_T,SampleC_70_nm,SampleC_70_x_T,SampleC_74_nm,SampleC_74_x_T,SampleC_78_nm,...
93 title(' Reflection plot Sample C')
94 nexttile
95 plot(SampleD_62_nm,SampleD_62_x_T,SampleD_66_nm,SampleD_66_x_T,SampleD_70_nm,SampleD_70_x_T,SampleD_74_nm,SampleD_74_x_T,SampleD_78_nm,...
96 SampleD_78_x_T,SampleD_82_nm,SampleD_82_x_T)
97 lgd = legend({'pH 6.2','pH 6.6','pH 7.0','pH 7.4','pH 7.8','pH 8.2'});
98 title('Reflection plot Sample D')
99
100 lgd.NumColumns = 6;
101 lgd.Layout.Tile = 'north';
102 xlabel(t,'Wavelength (nm)')
103 ylabel(t,'Reflection %R')
104 %% Glasscorrected
105 % Sample A
106 SampleA_62_corr = array2table([SampleA_62_nm, SampleA_62_x_T-Sample_Glass_x_T],'VariableNames',{'nm','x_T'});
107 SampleA_66_corr = array2table([SampleA_66_nm, SampleA_66_x_T-Sample_Glass_x_T],'VariableNames',{'nm','x_T'});
108 SampleA_70_corr = array2table([SampleA_70_nm, SampleA_70_x_T-Sample_Glass_x_T],'VariableNames',{'nm','x_T'});
109 SampleA_74_corr = array2table([SampleA_74_nm, SampleA_74_x_T-Sample_Glass_x_T],'VariableNames',{'nm','x_T'});
110 SampleA_78_corr = array2table([SampleA_78_nm, SampleA_78_x_T-Sample_Glass_x_T],'VariableNames',{'nm','x_T'});
111 SampleA_82_corr = array2table([SampleA_82_nm, SampleA_82_x_T-Sample_Glass_x_T],'VariableNames',{'nm','x_T'});
112 % Sample B
113 SampleB_62_corr = array2table([SampleB_62_nm, SampleB_62_x_T-Sample_Glass_x_T],'VariableNames',{'nm','x_T'});
114 SampleB_66_corr = array2table([SampleB_66_nm, SampleB_66_x_T-Sample_Glass_x_T],'VariableNames',{'nm','x_T'});
115 SampleB_70_corr = array2table([SampleB_70_nm, SampleB_70_x_T-Sample_Glass_x_T],'VariableNames',{'nm','x_T'});
116 SampleB_74_corr = array2table([SampleB_74_nm, SampleB_74_x_T-Sample_Glass_x_T],'VariableNames',{'nm','x_T'});
117 SampleB_78_corr = array2table([SampleB_78_nm, SampleB_78_x_T-Sample_Glass_x_T],'VariableNames',{'nm','x_T'});
118 SampleB_82_corr = array2table([SampleB_82_nm, SampleB_82_x_T-Sample_Glass_x_T],'VariableNames',{'nm','x_T'});
119 % Sample C
120 SampleC_62_corr = array2table([SampleC_62_nm, SampleC_62_x_T-Sample_Glass_x_T],'VariableNames',{'nm','x_T'});
121 SampleC_66_corr = array2table([SampleC_66_nm, SampleC_66_x_T-Sample_Glass_x_T],'VariableNames',{'nm','x_T'});
122 SampleC_70_corr = array2table([SampleC_70_nm, SampleC_70_x_T-Sample_Glass_x_T],'VariableNames',{'nm','x_T'});
123 SampleC_74_corr = array2table([SampleC_74_nm, SampleC_74_x_T-Sample_Glass_x_T],'VariableNames',{'nm','x_T'});
124 SampleC_78_corr = array2table([SampleC_78_nm, SampleC_78_x_T-Sample_Glass_x_T],'VariableNames',{'nm','x_T'});
125 SampleC_82_corr = array2table([SampleC_82_nm, SampleC_82_x_T-Sample_Glass_x_T],'VariableNames',{'nm','x_T'});
126 % Sample D
127 SampleD_62_corr = array2table([SampleD_62_nm, SampleD_62_x_T-Sample_Glass_x_T],'VariableNames',{'nm','x_T'});
128 SampleD_66_corr = array2table([SampleD_66_nm, SampleD_66_x_T-Sample_Glass_x_T],'VariableNames',{'nm','x_T'});
129 SampleD_70_corr = array2table([SampleD_70_nm, SampleD_70_x_T-Sample_Glass_x_T],'VariableNames',{'nm','x_T'});
130 SampleD_74_corr = array2table([SampleD_74_nm, SampleD_74_x_T-Sample_Glass_x_T],'VariableNames',{'nm','x_T'});
131 SampleD_78_corr = array2table([SampleD_78_nm, SampleD_78_x_T-Sample_Glass_x_T],'VariableNames',{'nm','x_T'});
132 SampleD_82_corr = array2table([SampleD_82_nm, SampleD_82_x_T-Sample_Glass_x_T],'VariableNames',{'nm','x_T'});
133 %% plot Glass corrected
134 figure
135 t = tiledlayout(2,2,'TileSpacing','compact');
136 nexttile
137 plot(SampleA_62_corr_nm,SampleA_62_corr_x_T,SampleA_66_corr_nm,SampleA_66_corr_x_T,SampleA_70_corr_nm,SampleA_70_corr_x_T,SampleA_74_corr_nm,...
138 SampleA_74_corr_x_T,SampleA_78_corr_nm,SampleA_78_corr_x_T,SampleA_82_corr_nm,SampleA_82_corr_x_T)
139 title(' Reflection plot Sample A - Glass slide')
140 nexttile
141 plot(SampleB_62_corr_nm,SampleB_62_corr_x_T,SampleB_66_corr_nm,SampleB_66_corr_x_T,SampleB_70_corr_nm,SampleB_70_corr_x_T,SampleB_74_corr_nm,...
142 SampleB_74_corr_x_T,SampleB_78_corr_nm,SampleB_78_corr_x_T,SampleB_82_corr_nm,SampleB_82_corr_x_T)
143 title(' Reflection plot Sample B - Glass slide')
144 nexttile
145 plot(SampleC_62_corr_nm,SampleC_62_corr_x_T,SampleC_66_corr_nm,SampleC_66_corr_x_T,SampleC_70_corr_nm,SampleC_70_corr_x_T,SampleC_74_corr_nm,...
146 SampleC_74_corr_x_T,SampleC_78_corr_nm,SampleC_78_corr_x_T,SampleC_82_corr_nm,SampleC_82_corr_x_T)
147 title(' Reflection plot Sample C - Glass slide')
148 nexttile
149 plot(SampleD_62_corr_nm,SampleD_62_corr_x_T,SampleD_66_corr_nm,SampleD_66_corr_x_T,SampleD_70_corr_nm,SampleD_70_corr_x_T,SampleD_74_corr_nm,...
150 SampleD_74_corr_x_T,SampleD_78_corr_nm,SampleD_78_corr_x_T,SampleD_82_corr_nm,SampleD_82_corr_x_T)
151 title(' Reflection plot Sample D - Glass slide')
152 xlabel(t,'Wavelength (nm)')
153 ylabel(t,'Reflection %R')
154 lgd = legend({'pH 6.2','pH 6.6','pH 7.0','pH 7.4','pH 7.8','pH 8.2'});
155 lgd.NumColumns = 6;
156 lgd.Layout.Tile = 'north';
157 %% Samples Sample A
158 % Sample B
159 SampleB_62_minSampleA = array2table([SampleB_62_nm, SampleA_62_x_T-SampleB_62_x_T],'VariableNames',{'nm','x_T'});
160 SampleB_66_minSampleA = array2table([SampleB_66_nm, SampleA_66_x_T-SampleB_66_x_T],'VariableNames',{'nm','x_T'});
161 SampleB_70_minSampleA = array2table([SampleB_70_nm, SampleA_70_x_T-SampleB_70_x_T],'VariableNames',{'nm','x_T'});
162 SampleB_74_minSampleA = array2table([SampleB_74_nm, SampleA_74_x_T-SampleB_74_x_T],'VariableNames',{'nm','x_T'});
163 SampleB_78_minSampleA = array2table([SampleB_78_nm, SampleA_78_x_T-SampleB_78_x_T],'VariableNames',{'nm','x_T'});
164 SampleB_82_minSampleA = array2table([SampleB_82_nm, SampleA_82_x_T-SampleB_82_x_T],'VariableNames',{'nm','x_T'});
165 % Sample C
166 SampleC_62_minSampleA = array2table([SampleC_62_nm, SampleA_62_x_T-SampleC_62_x_T],'VariableNames',{'nm','x_T'});
167 SampleC_66_minSampleA = array2table([SampleC_66_nm, SampleA_66_x_T-SampleC_66_x_T],'VariableNames',{'nm','x_T'});
168 SampleC_70_minSampleA = array2table([SampleC_70_nm, SampleA_70_x_T-SampleC_70_x_T],'VariableNames',{'nm','x_T'});
169 SampleC_74_minSampleA = array2table([SampleC_74_nm, SampleA_74_x_T-SampleC_74_x_T],'VariableNames',{'nm','x_T'});
170 SampleC_78_minSampleA = array2table([SampleC_78_nm, SampleA_78_x_T-SampleC_78_x_T],'VariableNames',{'nm','x_T'});
171 SampleC_82_minSampleA = array2table([SampleC_82_nm, SampleA_82_x_T-SampleC_82_x_T],'VariableNames',{'nm','x_T'});
172 % Sample D
173 SampleD_62_minSampleA = array2table([SampleD_62_nm, SampleA_62_x_T-SampleD_62_x_T],'VariableNames',{'nm','x_T'});
174 SampleD_66_minSampleA = array2table([SampleD_66_nm, SampleA_66_x_T-SampleD_66_x_T],'VariableNames',{'nm','x_T'});
175 SampleD_70_minSampleA = array2table([SampleD_70_nm, SampleA_70_x_T-SampleD_70_x_T],'VariableNames',{'nm','x_T'});
176 SampleD_74_minSampleA = array2table([SampleD_74_nm, SampleA_74_x_T-SampleD_74_x_T],'VariableNames',{'nm','x_T'});
177 SampleD_78_minSampleA = array2table([SampleD_78_nm, SampleA_78_x_T-SampleD_78_x_T],'VariableNames',{'nm','x_T'});
178 SampleD_82_minSampleA = array2table([SampleD_82_nm, SampleA_82_x_T-SampleD_82_x_T],'VariableNames',{'nm','x_T'});
179 title('Reflection plot Sample A - Sample B')
180 nexttile
181 plot(SampleC_62_minSampleA_nm,SampleC_62_minSampleA_x_T,SampleC_66_minSampleA_nm,SampleC_66_minSampleA_x_T,SampleC_70_minSampleA_nm,...
182 SampleC_70_minSampleA_x_T,SampleC_74_minSampleA_nm,SampleC_74_minSampleA_x_T,SampleC_78_minSampleA_nm,SampleC_78_minSampleA_x_T,...
183 SampleC_82_minSampleA_nm,SampleC_82_minSampleA_x_T)
184 title('Reflection plot Sample A - Sample C')
185 nexttile
186 plot(SampleD_62_minSampleA_nm,SampleD_62_minSampleA_x_T,SampleD_66_minSampleA_nm,SampleD_66_minSampleA_x_T,SampleD_70_minSampleA_nm,...
187 SampleD_70_minSampleA_x_T,SampleD_74_minSampleA_nm,SampleD_74_minSampleA_x_T,SampleD_78_minSampleA_nm,SampleD_78_minSampleA_x_T,...
188 SampleD_82_minSampleA_nm,SampleD_82_minSampleA_x_T)
189 title('Reflection plot Sample A - Sample D')
190 xlabel(t,'Wavelength (nm)')
191 ylabel(t,'Reflection %R')
192 lgd = legend({'pH 6.2','pH 6.6','pH 7.0','pH 7.4','pH 7.8','pH 8.2'});
193 lgd.NumColumns = 6;
194 lgd.Layout.Tile = 'north';
195 %% Calculate ratios
196 AbsorptionSamples = [SampleA_62_x_T SampleA_66_x_T SampleA_70_x_T SampleA_74_x_T SampleA_78_x_T SampleA_82_x_T SampleB_62_x_T SampleB_66_x_T...
197 SampleB_70_x_T SampleB_74_x_T SampleB_78_x_T SampleB_82_x_T SampleC_62_x_T SampleC_66_x_T SampleC_70_x_T SampleC_74_x_T...
198 SampleC_78_x_T SampleC_82_x_T SampleD_62_x_T SampleD_66_x_T SampleD_70_x_T SampleD_74_x_T SampleD_78_x_T SampleD_82_x_T];
199 Ratios = zeros(24,12);
200 for
201 Ratios(i,1) = AbsorptionSamples(1,i);
202 Ratios(i,2) = AbsorptionSamples(71,i);
203 Ratios(i,3) = Ratios(i,1) - Ratios(i,2);
204 Ratios(i,4) = ((Ratios(i,2) - Ratios(i,1))/Ratios(i,1))*100;
205 Ratios(i,5) = max(AbsorptionSamples(:,i));
206 Ratios(i,6) = min(AbsorptionSamples(:,i));
207 Ratios(i,7) = Ratios(i,5) - Ratios(i,6);
208 Ratios(i,8) = ((Ratios(i,6) - Ratios(i,5))/Ratios(i,5))*100;
209 Ratios(i,9) = AbsorptionSamples(48,i);
210 Ratios(i,10) = AbsorptionSamples(59,i);
211 Ratios(i,11) = Ratios(i,9) - Ratios(i,10);
212 Ratios(i,12) = ((Ratios(i,10) - Ratios(i,9))/Ratios(i,9))*100;
213 end

```

```

208 Ratios = array2table(Ratios,'VariableNames',{'%R 700nm','%R 350 nm','Difference 700-350','%Decrease 700-350','%Max %R','%Min %R','Difference ...
    Max/Min','%Decrease Max/Min', '%R at 465nm','%R at 405nm','Difference 465/405','%Decrease 465/405'},'RowNames',{'Sample A pH 6.2','...
    Sample A pH 6.6', 'Sample A pH 7.0', 'Sample A pH 7.4', 'Sample A pH 7.8', 'Sample A pH 8.2','Sample B pH 6.2','Sample B pH 6.6', '...
    Sample B pH 7.0', 'Sample B pH 7.4', 'Sample B pH 7.8', 'Sample B pH 8.2','Sample C pH 6.2','Sample C pH 6.6', 'Sample C pH 7.0', '...
    Sample C pH 7.4', 'Sample C pH 7.8', 'Sample C pH 8.2','Sample D pH 6.2','Sample D pH 6.6', 'Sample D pH 7.0', 'Sample D pH 7.4', '...
    Sample D pH 7.8', 'Sample D pH 8.2'});
209 RatiosSampleA = Ratios(1:6,1:12);
210 RatiosSampleB = Ratios(7:12,1:12);
211 RatiosSampleC = Ratios(13:18,1:12);
212 RatiosSampleD = Ratios(19:24,1:12);
213 writetable(Ratios,'Ratios_Reflection.csv','WriteRowNames',true);
214
215 %% Make rescale values
216
217 %Sample A
218 SampleA_62_rescale = rescaletable(SampleA_62);
219 SampleA_66_rescale = rescaletable(SampleA_66);
220 SampleA_70_rescale = rescaletable(SampleA_70);
221 SampleA_74_rescale = rescaletable(SampleA_74);
222 SampleA_78_rescale = rescaletable(SampleA_78);
223 SampleA_82_rescale = rescaletable(SampleA_82);
224
225 %Sample B
226 SampleB_62_rescale = rescaletable(SampleB_62);
227 SampleB_66_rescale = rescaletable(SampleB_66);
228 SampleB_70_rescale = rescaletable(SampleB_70);
229 SampleB_74_rescale = rescaletable(SampleB_74);
230 SampleB_78_rescale = rescaletable(SampleB_78);
231 SampleB_82_rescale = rescaletable(SampleB_82);
232
233 %Sample C
234 SampleC_62_rescale = rescaletable(SampleC_62);
235 SampleC_66_rescale = rescaletable(SampleC_66);
236 SampleC_70_rescale = rescaletable(SampleC_70);
237 SampleC_74_rescale = rescaletable(SampleC_74);
238 SampleC_78_rescale = rescaletable(SampleC_78);
239 SampleC_82_rescale = rescaletable(SampleC_82);
240
241 %Sample D
242 SampleD_62_rescale = rescaletable(SampleD_62);
243 SampleD_66_rescale = rescaletable(SampleD_66);
244 SampleD_70_rescale = rescaletable(SampleD_70);
245 SampleD_74_rescale = rescaletable(SampleD_74);
246 SampleD_78_rescale = rescaletable(SampleD_78);
247 SampleD_82_rescale = rescaletable(SampleD_82);
248
249 %% plotS rescale
250 figure
251 t = tiledlayout(2,2,'TileSpacing','compact');
252 absorpplot(SampleA_62_rescale,SampleA_66_rescale,SampleA_70_rescale,SampleA_74_rescale,SampleA_78_rescale,SampleA_82_rescale,'Sample A')
253 absorpplot(SampleB_62_rescale,SampleB_66_rescale,SampleB_70_rescale,SampleB_74_rescale,SampleB_78_rescale,SampleB_82_rescale,'Sample B')
254 absorpplot(SampleC_62_rescale,SampleC_66_rescale,SampleC_70_rescale,SampleC_74_rescale,SampleC_78_rescale,SampleC_82_rescale,'Sample C')
255 absorpplot(SampleD_62_rescale,SampleD_66_rescale,SampleD_70_rescale,SampleD_74_rescale,SampleD_78_rescale,SampleD_82_rescale,'Sample D')
256
257 xlabel(t,'Wavelength (nm)')
258 ylabel(t,'Reflection %R')
259 lgd = legend({'pH 6.2','pH 6.6','pH 7.0','pH 7.4','pH 7.8','pH 8.2'});
260 lgd.NumColumns = 6;
261 lgd.Layout.Tile = 'north';
262
263 %%
264 pH = [6.2 6.6 7.0 7.4 7.8 8.2];
265 SampleA_rescaled_at_475nm = [SampleA_62_rescale(46,2) SampleA_66_rescale(46,2) SampleA_70_rescale(46,2) SampleA_74_rescale(46,2) ...
    SampleA_78_rescale(46,2) SampleA_82_rescale(46,2)];
266 SampleB_rescaled_at_475nm = [SampleB_62_rescale(46,2) SampleB_66_rescale(46,2) SampleB_70_rescale(46,2) SampleB_74_rescale(46,2) ...
    SampleB_78_rescale(46,2) SampleB_82_rescale(46,2)];
267 SampleC_rescaled_at_475nm = [SampleC_62_rescale(46,2) SampleC_66_rescale(46,2) SampleC_70_rescale(46,2) SampleC_74_rescale(46,2) ...
    SampleC_78_rescale(46,2) SampleC_82_rescale(46,2)];
268 SampleD_rescaled_at_475nm = [SampleD_62_rescale(46,2) SampleD_66_rescale(46,2) SampleD_70_rescale(46,2) SampleD_74_rescale(46,2) ...
    SampleD_78_rescale(46,2) SampleD_82_rescale(46,2)];
269
270 figure
271 plot(pH,SampleA_rescaled_at_475nm,pH,SampleB_rescaled_at_475nm,pH,SampleC_rescaled_at_475nm ,pH,SampleD_rescaled_at_475nm)
272 xlabel('pH')
273 ylabel('Value 475 nm scaled')
274 legend({'Sample A', 'Sample B', 'Sample C', 'Sample D'},'Location','best')
275 title('Plot of pH and scaled values at 475 nm ')
276
277 %%
278 figure
279 t = tiledlayout(1,3,'TileSpacing','compact');
280 plot(SampleC_62_corr_nm,SampleC_62_corr_x_T,SampleC_66_corr_nm,SampleC_66_corr_x_T,SampleC_70_corr_nm,SampleC_70_corr_x_T,SampleC_74_corr_nm...
    ,SampleC_74_corr_x_T,SampleC_78_corr_nm,SampleC_78_corr_x_T,SampleC_82_corr_nm,SampleC_82_corr_x_T)
281 title(' Reflection plot Sample C - Glass slide')
282 xlabel('Wavelength (nm)')
283 ylabel('Reflection %R')
284 legend({'pH 6.2','pH 6.6','pH 7.0','pH 7.4','pH 7.8','pH 8.2'},'Location','best')
285 absorpplot(SampleC_62_rescale,SampleC_66_rescale,SampleC_70_rescale,SampleC_74_rescale,SampleC_78_rescale,SampleC_82_rescale,'Sample C')
286 xlabel('Wavelength (nm)')
287 ylabel('Scaled Reflection %R')
288 legend({'pH 6.2','pH 6.6','pH 7.0','pH 7.4','pH 7.8','pH 8.2'},'Location','best')
289 nexttile
290 plot(pH,SampleA_rescaled_at_475nm,pH,SampleB_rescaled_at_475nm,pH,SampleC_rescaled_at_475nm ,pH,SampleD_rescaled_at_475nm)
291 xlabel('pH')
292 ylabel('Value 475 nm scaled')
293 legend({'Sample A', 'Sample B', 'Sample C', 'Sample D'},'Location','best')
294 title('Plot of pH and scaled values at 475 nm ')
295 title(t, 'Reflection Measurements' )

```

Listing A.9: Matlab script for the Transmission data

```

1 %% Close all
2
3 clc
4 clear all
5 close all
6
7 %% Load Data
8 fds = fileDatastore('C:\Users\mauri\Documents\MATLAB\Afstuderen\Absorptiemetingen','ReadFcn',@load,'FileExtensions','.csv');
9 fullFileNames = fds.Files;
10 FileNames = string(fullFileNames);
11 % correction files
12 Sample_Glass = importfileAbsorption(FileNames(5));
13 Sample_100_begin = importfileAbsorption(FileNames(3));
14 Sample_100_end = importfileAbsorption(FileNames(4));
15 Sample_0_begin = importfileAbsorption(FileNames(1));
16
17 %Sample A
18 FirstFile_SampleA = 7;
19 SampleA_62 = importfileAbsorption(FileNames(FirstFile_SampleA));
20 SampleA_66 = importfileAbsorption(FileNames(FirstFile_SampleA+1));
21 SampleA_70 = importfileAbsorption(FileNames(FirstFile_SampleA+2));
22 SampleA_74 = importfileAbsorption(FileNames(FirstFile_SampleA+3));
23 SampleA_78 = importfileAbsorption(FileNames(FirstFile_SampleA+4));
24 SampleA_82 = importfileAbsorption(FileNames(FirstFile_SampleA+5));
25 %Sample B

```

```

25 FirstFile SampleB = 14;
26 SampleB_62 = importfileAbsorption(FileNames(FirstFile_SampleB));
27 SampleB_66 = importfileAbsorption(FileNames(FirstFile_SampleB+1));
28 SampleB_70 = importfileAbsorption(FileNames(FirstFile_SampleB+2));
29 SampleB_74 = importfileAbsorption(FileNames(FirstFile_SampleB+3));
30 SampleB_78 = importfileAbsorption(FileNames(FirstFile_SampleB+4));
31 SampleB_82 = importfileAbsorption(FileNames(FirstFile_SampleB+5));
32 %Sample C
33 FirstFile SampleC = 20;
34 SampleC_62 = importfileAbsorption(FileNames(FirstFile_SampleC));
35 SampleC_66 = importfileAbsorption(FileNames(FirstFile_SampleC+1));
36 SampleC_70 = importfileAbsorption(FileNames(FirstFile_SampleC+2));
37 SampleC_74 = importfileAbsorption(FileNames(FirstFile_SampleC+3));
38 SampleC_78 = importfileAbsorption(FileNames(FirstFile_SampleC+4));
39 SampleC_82 = importfileAbsorption(FileNames(FirstFile_SampleC+5));
40 %Sample D
41 FirstFile SampleD = 26;
42 SampleD_62 = importfileAbsorption(FileNames(FirstFile_SampleD));
43 SampleD_66 = importfileAbsorption(FileNames(FirstFile_SampleD+1));
44 SampleD_70 = importfileAbsorption(FileNames(FirstFile_SampleD+2));
45 SampleD_74 = importfileAbsorption(FileNames(FirstFile_SampleD+3));
46 SampleD_78 = importfileAbsorption(FileNames(FirstFile_SampleD+4));
47 SampleD_82 = importfileAbsorption(FileNames(FirstFile_SampleD+5));
48
49 %% Plot Transmittance
50 figure
51 t = tiledlayout(2,3,'TileSpacing','compact');
52 ttl = 'Plot of the Transmission of ';
53 nexttile
54 plot(SampleGlass_nm,SampleGlass_x_T)
55 legend({'Glass slide'},'Location','northeast')
56 title('Plot of the Transmission of Glass slide')
57 nexttile
58 plot(Sample_100_begin_nm,Sample_100_begin_x_T,Sample_100_end_nm,Sample_100_end_x_T,Sample_0_begin_nm,Sample_0_begin_x_T)
59 legend({'100% begin','100% end','0%Begin'},'Location','northeast')
60 title('Plot of the Transmission of Baseline Measurements')
61 tableplot(SampleA_62, SampleA_66, SampleA_70, SampleA_74, SampleA_78, SampleA_82, 'Sample A', ttl)
62 legend({'pH 6.2','pH 6.6','pH 7.0','pH 7.4','pH 7.8','pH 8.2'},'Location','northeast')
63 tableplot(SampleB_62, SampleB_66, SampleB_70, SampleB_74, SampleB_78, SampleB_82, 'Sample B', ttl)
64 legend({'pH 6.2','pH 6.6','pH 7.0','pH 7.4','pH 7.8','pH 8.2'},'Location','northeast')
65 tableplot(SampleC_62, SampleC_66, SampleC_70, SampleC_74, SampleC_78, SampleC_82, 'Sample C', ttl)
66 legend({'pH 6.2','pH 6.6','pH 7.0','pH 7.4','pH 7.8','pH 8.2'},'Location','northeast')
67 tableplot(SampleD_62, SampleD_66, SampleD_70, SampleD_74, SampleD_78, SampleD_82, 'Sample D', ttl)
68 legend({'pH 6.2','pH 6.6','pH 7.0','pH 7.4','pH 7.8','pH 8.2'},'Location','northeast')
69 xlabel(t,'Wavelength (nm)')
70 ylabel(t,'Transmission (%T)')
71 lgd = legend({'pH 6.2','pH 6.6','pH 7.0','pH 7.4','pH 7.8','pH 8.2'});
72 lgd.NumColumns = 6;
73 lgd.Layout.Tile = 'north';
74
75 %% New figure
76 figure
77 t = tiledlayout(2,2,'TileSpacing','compact');
78 ttl = 'Plot of the Transmission of ';
79 tableplot(SampleA_62, SampleA_66, SampleA_70, SampleA_74, SampleA_78, SampleA_82, 'Sample A', ttl)
80 tableplot(SampleB_62, SampleB_66, SampleB_70, SampleB_74, SampleB_78, SampleB_82, 'Sample B', ttl)
81 tableplot(SampleC_62, SampleC_66, SampleC_70, SampleC_74, SampleC_78, SampleC_82, 'Sample C', ttl)
82 tableplot(SampleD_62, SampleD_66, SampleD_70, SampleD_74, SampleD_78, SampleD_82, 'Sample D', ttl)
83 xlabel(t,'Wavelength (nm)')
84 ylabel(t,'Transmission (%T)')
85 lgd = legend({'pH 6.2','pH 6.6','pH 7.0','pH 7.4','pH 7.8','pH 8.2'});
86 lgd.NumColumns = 6;
87 lgd.Layout.Tile = 'north';
88
89 %% Glasscorrected
90 % Sample A
91 SampleA_62_corr = array2table([SampleA_62_nm, SampleGlass_x_T-SampleA_62_x_T],'VariableNames',{'nm','x_T'});
92 SampleA_66_corr = array2table([SampleA_66_nm, SampleGlass_x_T-SampleA_66_x_T],'VariableNames',{'nm','x_T'});
93 SampleA_70_corr = array2table([SampleA_70_nm, SampleGlass_x_T-SampleA_70_x_T],'VariableNames',{'nm','x_T'});
94 SampleA_74_corr = array2table([SampleA_74_nm, SampleGlass_x_T-SampleA_74_x_T],'VariableNames',{'nm','x_T'});
95 SampleA_78_corr = array2table([SampleA_78_nm, SampleGlass_x_T-SampleA_78_x_T],'VariableNames',{'nm','x_T'});
96 SampleA_82_corr = array2table([SampleA_82_nm, SampleGlass_x_T-SampleA_82_x_T],'VariableNames',{'nm','x_T'});
97
98 % Sample B
99 SampleB_62_corr = array2table([SampleB_62_nm, SampleGlass_x_T-SampleB_62_x_T],'VariableNames',{'nm','x_T'});
100 SampleB_66_corr = array2table([SampleB_66_nm, SampleGlass_x_T-SampleB_66_x_T],'VariableNames',{'nm','x_T'});
101 SampleB_70_corr = array2table([SampleB_70_nm, SampleGlass_x_T-SampleB_70_x_T],'VariableNames',{'nm','x_T'});
102 SampleB_74_corr = array2table([SampleB_74_nm, SampleGlass_x_T-SampleB_74_x_T],'VariableNames',{'nm','x_T'});
103 SampleB_78_corr = array2table([SampleB_78_nm, SampleGlass_x_T-SampleB_78_x_T],'VariableNames',{'nm','x_T'});
104 SampleB_82_corr = array2table([SampleB_82_nm, SampleGlass_x_T-SampleB_82_x_T],'VariableNames',{'nm','x_T'});
105
106 % Sample C
107 SampleC_62_corr = array2table([SampleC_62_nm, SampleGlass_x_T-SampleC_62_x_T],'VariableNames',{'nm','x_T'});
108 SampleC_66_corr = array2table([SampleC_66_nm, SampleGlass_x_T-SampleC_66_x_T],'VariableNames',{'nm','x_T'});
109 SampleC_70_corr = array2table([SampleC_70_nm, SampleGlass_x_T-SampleC_70_x_T],'VariableNames',{'nm','x_T'});
110 SampleC_74_corr = array2table([SampleC_74_nm, SampleGlass_x_T-SampleC_74_x_T],'VariableNames',{'nm','x_T'});
111 SampleC_78_corr = array2table([SampleC_78_nm, SampleGlass_x_T-SampleC_78_x_T],'VariableNames',{'nm','x_T'});
112 SampleC_82_corr = array2table([SampleC_82_nm, SampleGlass_x_T-SampleC_82_x_T],'VariableNames',{'nm','x_T'});
113
114 % Sample D
115 SampleD_62_corr = array2table([SampleD_62_nm, SampleGlass_x_T-SampleD_62_x_T],'VariableNames',{'nm','x_T'});
116 SampleD_66_corr = array2table([SampleD_66_nm, SampleGlass_x_T-SampleD_66_x_T],'VariableNames',{'nm','x_T'});
117 SampleD_70_corr = array2table([SampleD_70_nm, SampleGlass_x_T-SampleD_70_x_T],'VariableNames',{'nm','x_T'});
118 SampleD_74_corr = array2table([SampleD_74_nm, SampleGlass_x_T-SampleD_74_x_T],'VariableNames',{'nm','x_T'});
119 SampleD_78_corr = array2table([SampleD_78_nm, SampleGlass_x_T-SampleD_78_x_T],'VariableNames',{'nm','x_T'});
120 SampleD_82_corr = array2table([SampleD_82_nm, SampleGlass_x_T-SampleD_82_x_T],'VariableNames',{'nm','x_T'});
121
122 %% plot glass corrected
123 figure
124 t = tiledlayout(2,2,'TileSpacing','compact');
125 ttl = 'Transmittance of Glassslide - ';
126 tableplot(SampleA_62_corr, SampleA_66_corr, SampleA_70_corr, SampleA_74_corr, SampleA_78_corr, SampleA_82_corr, 'Sample A', ttl)
127 tableplot(SampleB_62_corr, SampleB_66_corr, SampleB_70_corr, SampleB_74_corr, SampleB_78_corr, SampleB_82_corr, 'Sample B', ttl)
128 tableplot(SampleC_62_corr, SampleC_66_corr, SampleC_70_corr, SampleC_74_corr, SampleC_78_corr, SampleC_82_corr, 'Sample C', ttl)
129 tableplot(SampleD_62_corr, SampleD_66_corr, SampleD_70_corr, SampleD_74_corr, SampleD_78_corr, SampleD_82_corr, 'Sample D', ttl)
130 xlabel(t,'Wavelength (nm)')
131 ylabel(t,'Transmission (%T)')
132 lgd = legend({'pH 6.2','pH 6.6','pH 7.0','pH 7.4','pH 7.8','pH 8.2'});
133 lgd.NumColumns = 6;
134 lgd.Layout.Tile = 'north';
135
136 %% Samples - Sample A
137 % Sample B
138 SampleB_62_minSampleA = array2table([SampleB_62_nm, SampleA_62_x_T-SampleB_62_x_T],'VariableNames',{'nm','x_T'});
139 SampleB_66_minSampleA = array2table([SampleB_66_nm, SampleA_66_x_T-SampleB_66_x_T],'VariableNames',{'nm','x_T'});
140 SampleB_70_minSampleA = array2table([SampleB_70_nm, SampleA_70_x_T-SampleB_70_x_T],'VariableNames',{'nm','x_T'});
141 SampleB_74_minSampleA = array2table([SampleB_74_nm, SampleA_74_x_T-SampleB_74_x_T],'VariableNames',{'nm','x_T'});
142 SampleB_78_minSampleA = array2table([SampleB_78_nm, SampleA_78_x_T-SampleB_78_x_T],'VariableNames',{'nm','x_T'});
143 SampleB_82_minSampleA = array2table([SampleB_82_nm, SampleA_82_x_T-SampleB_82_x_T],'VariableNames',{'nm','x_T'});
144
145 % Sample C
146 SampleC_62_minSampleA = array2table([SampleC_62_nm, SampleA_62_x_T-SampleC_62_x_T],'VariableNames',{'nm','x_T'});
147 SampleC_66_minSampleA = array2table([SampleC_66_nm, SampleA_66_x_T-SampleC_66_x_T],'VariableNames',{'nm','x_T'});
148 SampleC_70_minSampleA = array2table([SampleC_70_nm, SampleA_70_x_T-SampleC_70_x_T],'VariableNames',{'nm','x_T'});
149 SampleC_74_minSampleA = array2table([SampleC_74_nm, SampleA_74_x_T-SampleC_74_x_T],'VariableNames',{'nm','x_T'});
150 SampleC_78_minSampleA = array2table([SampleC_78_nm, SampleA_78_x_T-SampleC_78_x_T],'VariableNames',{'nm','x_T'});
151 SampleC_82_minSampleA = array2table([SampleC_82_nm, SampleA_82_x_T-SampleC_82_x_T],'VariableNames',{'nm','x_T'});
152
153 % Sample D
154 SampleD_62_minSampleA = array2table([SampleD_62_nm, SampleA_62_x_T-SampleD_62_x_T],'VariableNames',{'nm','x_T'});
155 SampleD_66_minSampleA = array2table([SampleD_66_nm, SampleA_66_x_T-SampleD_66_x_T],'VariableNames',{'nm','x_T'});
156 SampleD_70_minSampleA = array2table([SampleD_70_nm, SampleA_70_x_T-SampleD_70_x_T],'VariableNames',{'nm','x_T'});
157 SampleD_74_minSampleA = array2table([SampleD_74_nm, SampleA_74_x_T-SampleD_74_x_T],'VariableNames',{'nm','x_T'});
158 SampleD_78_minSampleA = array2table([SampleD_78_nm, SampleA_78_x_T-SampleD_78_x_T],'VariableNames',{'nm','x_T'});
159 SampleD_82_minSampleA = array2table([SampleD_82_nm, SampleA_82_x_T-SampleD_82_x_T],'VariableNames',{'nm','x_T'});

```

```

156 %%
157 figure
158 t = tiledlayout(2,2,'TileSpacing','compact');
159 t1 = "Transmittance of ";
160 tableplot(SampleA_62, SampleA_66, SampleA_70, SampleA_74, SampleA_78, SampleA_82, 'Sample A', t1)
161 tableplot(SampleB_62_minSampleA, SampleB_66_minSampleA, SampleB_70_minSampleA, SampleB_74_minSampleA, SampleB_78_minSampleA, ...
162 SampleB_82_minSampleA, 'Sample B', t1)
163 tableplot(SampleC_62_minSampleA, SampleC_66_minSampleA, SampleC_70_minSampleA, SampleC_74_minSampleA, SampleC_78_minSampleA, ...
164 SampleC_82_minSampleA, 'Sample C', t1)
165 tableplot(SampleD_62_minSampleA, SampleD_66_minSampleA, SampleD_70_minSampleA, SampleD_74_minSampleA, SampleD_78_minSampleA, ...
166 SampleD_82_minSampleA, 'Sample D', t1)
167 xlabel(t,'Wavelength (nm)')
168 ylabel(t,'Transmission (%T)')
169 lgd = legend({'pH 6.2','pH 6.6','pH 7.0','pH 7.4','pH 7.8','pH 8.2'});
170 lgd.NumColumns = 6;
171 lgd.Layout.Tile = 'north';
172
173 %% Calculate ratios
174 AbsorptionSamples = [SampleA_62.x T SampleA_66.x T SampleA_70.x T SampleA_74.x T SampleA_78.x T SampleA_82.x T SampleB_62.x T SampleB_66.x T ...
175 SampleB_70.x T SampleB_74.x T SampleB_78.x T SampleB_82.x T SampleC_62.x T SampleC_66.x T SampleC_70.x T SampleC_74.x T ...
176 SampleC_78.x T SampleC_82.x T SampleD_62.x T SampleD_66.x T SampleD_70.x T SampleD_74.x T SampleD_78.x T SampleD_82.x T];
177 Ratios = zeros(24,12);
178 for i = 1:12;
179 Ratios(i,1) = AbsorptionSamples(i,1);
180 Ratios(i,2) = AbsorptionSamples(71,i);
181 Ratios(i,3) = Ratios(i,1) - Ratios(i,2);
182 Ratios(i,4) = ((Ratios(i,2) - Ratios(i,1))/Ratios(i,1))*100;
183 Ratios(i,5) = max(AbsorptionSamples(:,i));
184 Ratios(i,6) = min(AbsorptionSamples(:,i));
185 Ratios(i,7) = Ratios(i,5) - Ratios(i,6);
186 Ratios(i,8) = ((Ratios(i,6) - Ratios(i,5))/Ratios(i,5))*100;
187 Ratios(i,9) = AbsorptionSamples(48,i);
188 Ratios(i,10) = AbsorptionSamples(59,i);
189 Ratios(i,11) = Ratios(i,9) - Ratios(i,10);
190 Ratios(i,12) = ((Ratios(i,10) - Ratios(i,9))/Ratios(i,9))*100;
191 end
192 Ratios = array2table(Ratios,'VariableNames',{'T 700nm','T 350 nm','Difference 700-350','%Decrease 700-350','Max %T','Min %T','Difference ...
193 Max/Min','%Decrease Max/Min','T at 465nm','T at 405nm','Difference 465/405','%Decrease 465/405','RowNames',{'Sample A pH 6.2','...
194 Sample A pH 6.6',' Sample A pH 7.0',' Sample A pH 7.4',' Sample A pH 7.8',' Sample A pH 8.2',' Sample B pH 6.2',' Sample B pH 6.6',' ...
195 Sample B pH 7.0',' Sample B pH 7.4',' Sample B pH 7.8',' Sample B pH 8.2',' Sample C pH 6.2',' Sample C pH 6.6',' Sample C pH 7.0',' ...
196 Sample C pH 7.4',' Sample C pH 7.8',' Sample C pH 8.2',' Sample D pH 6.2',' Sample D pH 6.6',' Sample D pH 7.0',' Sample D pH 7.4',' ...
197 Sample D pH 7.8',' Sample D pH 8.2'});
198 RatiosSampleA = Ratios(1:6,1:12);
199 RatiosSampleB = Ratios(7:12,1:12);
200 RatiosSampleC = Ratios(13:18,1:12);
201 RatiosSampleD = Ratios(19:24,1:12);
202 writetable(Ratios,"Ratios_Absorption.csv","WriteRowNames",true);
203
204 %%
205 % Sample A
206 SampleA_62_scaled = array2table([SampleA_62.nm, SampleA_62.x T/SampleA_62.x T(60)],'VariableNames',{'nm','x T'});
207 SampleA_66_scaled = array2table([SampleA_66.nm, SampleA_66.x T/SampleA_66.x T(60)],'VariableNames',{'nm','x T'});
208 SampleA_70_scaled = array2table([SampleA_70.nm, SampleA_70.x T/SampleA_70.x T(60)],'VariableNames',{'nm','x T'});
209 SampleA_74_scaled = array2table([SampleA_74.nm, SampleA_74.x T/SampleA_74.x T(60)],'VariableNames',{'nm','x T'});
210 SampleA_78_scaled = array2table([SampleA_78.nm, SampleA_78.x T/SampleA_78.x T(60)],'VariableNames',{'nm','x T'});
211 SampleA_82_scaled = array2table([SampleA_82.nm, SampleA_82.x T/SampleA_82.x T(60)],'VariableNames',{'nm','x T'});
212
213 % Sample B
214 SampleB_62_scaled = array2table([SampleB_62.nm, SampleB_62.x T/SampleB_62.x T(60)],'VariableNames',{'nm','x T'});
215 SampleB_66_scaled = array2table([SampleB_66.nm, SampleB_66.x T/SampleB_66.x T(60)],'VariableNames',{'nm','x T'});
216 SampleB_70_scaled = array2table([SampleB_70.nm, SampleB_70.x T/SampleB_70.x T(60)],'VariableNames',{'nm','x T'});
217 SampleB_74_scaled = array2table([SampleB_74.nm, SampleB_74.x T/SampleB_74.x T(60)],'VariableNames',{'nm','x T'});
218 SampleB_78_scaled = array2table([SampleB_78.nm, SampleB_78.x T/SampleB_78.x T(60)],'VariableNames',{'nm','x T'});
219 SampleB_82_scaled = array2table([SampleB_82.nm, SampleB_82.x T/SampleB_82.x T(60)],'VariableNames',{'nm','x T'});
220
221 % Sample C
222 SampleC_62_scaled = array2table([SampleC_62.nm, SampleC_62.x T/SampleC_62.x T(60)],'VariableNames',{'nm','x T'});
223 SampleC_66_scaled = array2table([SampleC_66.nm, SampleC_66.x T/SampleC_66.x T(60)],'VariableNames',{'nm','x T'});
224 SampleC_70_scaled = array2table([SampleC_70.nm, SampleC_70.x T/SampleC_70.x T(60)],'VariableNames',{'nm','x T'});
225 SampleC_74_scaled = array2table([SampleC_74.nm, SampleC_74.x T/SampleC_74.x T(60)],'VariableNames',{'nm','x T'});
226 SampleC_78_scaled = array2table([SampleC_78.nm, SampleC_78.x T/SampleC_78.x T(60)],'VariableNames',{'nm','x T'});
227 SampleC_82_scaled = array2table([SampleC_82.nm, SampleC_82.x T/SampleC_82.x T(60)],'VariableNames',{'nm','x T'});
228
229 % Sample D
230 SampleD_62_scaled = array2table([SampleD_62.nm, SampleD_62.x T/SampleD_62.x T(60)],'VariableNames',{'nm','x T'});
231 SampleD_66_scaled = array2table([SampleD_66.nm, SampleD_66.x T/SampleD_66.x T(60)],'VariableNames',{'nm','x T'});
232 SampleD_70_scaled = array2table([SampleD_70.nm, SampleD_70.x T/SampleD_70.x T(60)],'VariableNames',{'nm','x T'});
233 SampleD_74_scaled = array2table([SampleD_74.nm, SampleD_74.x T/SampleD_74.x T(60)],'VariableNames',{'nm','x T'});
234 SampleD_78_scaled = array2table([SampleD_78.nm, SampleD_78.x T/SampleD_78.x T(60)],'VariableNames',{'nm','x T'});
235 SampleD_82_scaled = array2table([SampleD_82.nm, SampleD_82.x T/SampleD_82.x T(60)],'VariableNames',{'nm','x T'});
236
237 figure
238 t = tiledlayout(2,2,'TileSpacing','compact');
239 t1 = "Scaled Transmittance of ";
240 tableplot(SampleA_62_scaled, SampleA_66_scaled, SampleA_70_scaled, SampleA_74_scaled, SampleA_78_scaled, SampleA_82_scaled, 'Sample A', ...
241 t1)
242 tableplot(SampleB_62_scaled, SampleB_66_scaled, SampleB_70_scaled, SampleB_74_scaled, SampleB_78_scaled, SampleB_82_scaled, 'Sample B', t1)
243 tableplot(SampleC_62_scaled, SampleC_66_scaled, SampleC_70_scaled, SampleC_74_scaled, SampleC_78_scaled, SampleC_82_scaled, 'Sample C', t1)
244 tableplot(SampleD_62_scaled, SampleD_66_scaled, SampleD_70_scaled, SampleD_74_scaled, SampleD_78_scaled, SampleD_82_scaled, 'Sample D', t1)
245
246 xlabel(t,'Wavelength (nm)')
247 ylabel(t,'Scaled Transmission (%T)')
248 lgd = legend({'pH 6.2','pH 6.6','pH 7.0','pH 7.4','pH 7.8','pH 8.2'});
249 lgd.NumColumns = 6;
250 lgd.Layout.Tile = 'north';
251
252 %%
253 pH = [6.2 6.6 7.0 7.4 7.8 8.2];
254 SampleA_rescaled_at_475nm = [SampleA_62_scaled.x T(46) SampleA_66_scaled.x T(46) SampleA_70_scaled.x T(46) SampleA_74_scaled.x T(46) ...
255 SampleA_78_scaled.x T(46) SampleA_82_scaled.x T(46)];
256 SampleB_rescaled_at_475nm = [SampleB_62_scaled.x T(46) SampleB_66_scaled.x T(46) SampleB_70_scaled.x T(46) SampleB_74_scaled.x T(46) ...
257 SampleB_78_scaled.x T(46) SampleB_82_scaled.x T(46)];
258 SampleC_rescaled_at_475nm = [SampleC_62_scaled.x T(46) SampleC_66_scaled.x T(46) SampleC_70_scaled.x T(46) SampleC_74_scaled.x T(46) ...
259 SampleC_78_scaled.x T(46) SampleC_82_scaled.x T(46)];
260 SampleD_rescaled_at_475nm = [SampleD_62_scaled.x T(46) SampleD_66_scaled.x T(46) SampleD_70_scaled.x T(46) SampleD_74_scaled.x T(46) ...
261 SampleD_78_scaled.x T(46) SampleD_82_scaled.x T(46)];
262
263 figure
264 plot(pH, SampleA_rescaled_at_475nm, pH, SampleB_rescaled_at_475nm, pH, SampleC_rescaled_at_475nm, pH, SampleD_rescaled_at_475nm)
265 xlabel('pH')
266 ylabel('Value 475 nm rescaled')
267 legend('Sample A', 'Sample B', 'Sample C', 'Sample D')
268 title('Plot of pH and rescaled values at 475 nm')
269
270 %%
271 figure
272 t = tiledlayout(1,3,'TileSpacing','compact');
273 t1 = "Transmittance of ";
274 tableplot(SampleC_62, SampleC_66, SampleC_70, SampleC_74, SampleC_78, SampleC_82, 'Sample C', t1)

```

```

271 legend({'pH 6.2','pH 6.6' , 'pH 7.0','pH 7.4','pH 7.8','pH 8.2'},'Location','best')
272 ylabel('Transmission (%T)')
273 xlabel('Wavelength (nm)')
274 ttl = 'Scaled Transmittance of ';
275 tableplot(SampleC_62_scaled, SampleC_70_scaled, SampleC_74_scaled, SampleC_78_scaled, SampleC_82_scaled, 'Sample C', ttl)
276 xlabel('Wavelength (nm)')
277 ylabel('Scaled Transmission (%T)')
278 legend({'pH 6.2','pH 6.6' , 'pH 7.0','pH 7.4','pH 7.8','pH 8.2'},'Location','best')
279 nexttile
280 plot(pH,SampleA_rescaled_at_475nm,pH,SampleB_rescaled_at_475nm,pH,SampleC_rescaled_at_475nm ,pH,SampleD_rescaled_at_475nm)
281 xlabel('pH')
282 ylabel('Value 475 nm scaled')
283 legend({'Sample A', 'Sample B', 'Sample C', 'Sample D'},'Location','best')
284 title('Plot of pH and scaled values at 475 nm ')
285 title(t, 'Transmission Measurements' )

```

Listing A.10: Matlab script for plotting the voltages of the Avantes Data

```

1 %% open voltages
2
3 clear all
4 close all
5 clc
6
7 %% Datafile
8
9 path = 'C:\Users\mauri\Avantes\AvaSoft8\Metingen 25Juni\1mm voltages\';
10 % Import the data
11 [wavelengths, names, Voltages100mM1mm, Voltages150mM1mm, Voltages200mM1mm, Voltages100mMscaled1mm, Voltages150mMscaled1mm, ...
    Voltages200mMscaled1mm]= avantesvoltages(path);
12
13 path = 'C:\Users\mauri\Avantes\AvaSoft8\Metingen 25Juni\05mm voltages\';
14
15 [wavelengths, names, Voltages100mM05mm, Voltages150mM05mm, Voltages200mM05mm, Voltages100mMscaled05mm, Voltages150mMscaled05mm, ...
    Voltages200mMscaled05mm]= avantesvoltages(path);
16 names1 = {'1mm pH 6.2' '1mm pH 6.6' '1mm pH 7.0' '1mm pH 7.4' '1mm pH 7.8' '1mm pH 8.2' '100 mA' '150 mA' '300mA' '350mA' '450 mA'};
17 names05 = {'05mm pH 6.2' '05mm pH 6.6' '05mm pH 7.0' '05mm pH 7.4' '05mm pH 7.8' '05mm pH 8.2' '100 mA' '150 mA' '300mA' '350mA' '450 mA'};
18 namespH = {'pH 6.2' 'pH 6.6' 'pH 7.0' 'pH 7.4' 'pH 7.8' 'pH 8.2'};
19
20 figure
21 t = tiledlayout(2,6,'TileSpacing','compact');
22 for i=1:6
23 nexttile
24 plot(wavelengths,Voltages100mM1mm.(names{i}))
25 xlim([400, 650])
26 ylim([0,1200])
27 title(names1{i})
28 end
29 lgd = legend(names1{7:11});
30 lgd.NumColumns = 5;
31 lgd.Layout.Tile = 'north';
32 for i=1:6
33 nexttile(6+i)
34 plot(wavelengths,Voltages100mM05mm.(names{i}))
35 xlim([400, 650])
36 ylim([0,1200])
37 title(names05{i})
38 end
39 ylabel(t,'Counts per second')
40 xlabel(t,'Wavelengths')
41
42
43
44 %%
45 figure
46 t = tiledlayout(2,6,'TileSpacing','compact');
47 for i=1:6
48 nexttile
49 plot(wavelengths,Voltages100mMscaled1mm.(names{i}))
50 xlim([400, 650])
51 ylim([0,21])
52 title(names1{i})
53 end
54 lgd = legend(names1{7:11});
55 lgd.NumColumns = 5;
56 lgd.Layout.Tile = 'north';
57 for i=1:6
58 nexttile(6+i)
59 plot(wavelengths,Voltages100mMscaled05mm.(names{i}))
60 xlim([400, 650])
61 ylim([0,1.8])
62 title(names05{i})
63 end
64 ylabel(t,'Scaled counts per second')
65 xlabel(t,'Wavelengths')
66
67 %%
68 figure
69 t = tiledlayout(2,5,'TileSpacing','compact');
70 for i=7:11
71 nexttile
72 plot(wavelengths,Voltages100mM1mm.(names{i}))
73 xlim([400, 650])
74 title([names1{i} ' 1mm'])
75 end
76 lgd = legend(namespH{1:6});
77 lgd.NumColumns = 6;
78 lgd.Layout.Tile = 'north';
79 for i=7:11
80 nexttile(i-1)
81 plot(wavelengths,Voltages100mM05mm.(names{i}))
82 xlim([400, 650])
83 title([names05{i} ' 05mm'])
84 end
85 ylabel(t,'Counts per second')
86 xlabel(t,'Wavelengths')
87
88 figure
89 t = tiledlayout(2,5,'TileSpacing','compact');
90 for i=7:11
91 nexttile
92 plot(wavelengths,Voltages100mMscaled1mm.(names{i}))
93 xlim([400, 650])
94 ylim([0,21])
95 title([names1{i} ' 1mm'])
96 end
97 lgd = legend(namespH{1:6});
98 lgd.NumColumns = 6;
99 lgd.Layout.Tile = 'north';
100 for i=7:11
101 nexttile(i-1)
102 plot(wavelengths,Voltages100mMscaled05mm.(names{i}))
103 xlim([400, 650])
104 ylim([0,1.8])
105 title([names05{i} ' 05mm'])

```

```

106 end
107 ylabel(t,'Scaled counts per second')
108 xlabel(t,'Wavelengths')
109
110 %% Value
111 for i = 1:11
112 Value100mM_525em1mm.(names{i}) = Voltages100mM1mm.(names{i})(420,:);
113 Value100mMscaled_525em1mm.(names{i}) = Voltages100mMscaled1mm.(names{i})(420,:);
114 Value150mM_525em1mm.(names{i}) = Voltages150mM1mm.(names{i})(420,:);
115 Value150mMscaled_525em1mm.(names{i}) = Voltages150mMscaled1mm.(names{i})(420,:);
116 Value200mM_525em1mm.(names{i}) = Voltages200mM1mm.(names{i})(420,:);
117 Value200mMscaled_525em1mm.(names{i}) = Voltages200mMscaled1mm.(names{i})(420,:);
118 Value100mM_525em05mm.(names{i}) = Voltages100mM05mm.(names{i})(420,:);
119 Value100mMscaled_525em05mm.(names{i}) = Voltages100mMscaled05mm.(names{i})(420,:);
120 Value150mM_525em05mm.(names{i}) = Voltages150mM05mm.(names{i})(420,:);
121 Value150mMscaled_525em05mm.(names{i}) = Voltages150mMscaled05mm.(names{i})(420,:);
122 Value200mM_525em05mm.(names{i}) = Voltages200mM05mm.(names{i})(420,:);
123 Value200mMscaled_525em05mm.(names{i}) = Voltages200mMscaled05mm.(names{i})(420,:);
124
125 end
126 pH = [6.2 6.6 7.0 7.4 7.8 8.2];
127 Voltage = [2.5 3.0 3.4 3.6 3.8];
128 %%
129
130 figure
131 t = tiledlayout(2,5,'TileSpacing','compact');
132 for i = 1:5
133 nexttile
134 plot(pH,Value100mMscaled_525em1mm.(names{i+6}))
135 hold on
136 plot(pH,Value150mMscaled_525em1mm.(names{i+6}))
137 hold on
138 plot(pH,Value200mMscaled_525em1mm.(names{i+6}))
139 ylim([0,21])
140 title([names1{i+6} ' 1mm'])
141 end
142 lgd = legend({'100mM','150mM','200mM'});
143 lgd.NumColumns = 3;
144 lgd.Layout.Tile = 'north';
145 for i = 1:5
146 nexttile(i+5)
147 plot(pH,Value100mMscaled_525em05mm.(names{i+6}))
148 hold on
149 plot(pH,Value150mMscaled_525em05mm.(names{i+6}))
150 hold on
151 plot(pH,Value200mMscaled_525em05mm.(names{i+6}))
152 ylim([0,1.8])
153 title([names05{i+6} ' 05mm'])
154 end
155 ylabel(t,'Scaled counts per second')
156 xlabel(t,'pH value')
157
158 figure
159 i = 3
160 t = tiledlayout(1,2,'TileSpacing','compact');
161 nexttile
162 plot(pH,Value100mMscaled_525em1mm.(names{i+6}))
163 hold on
164 plot(pH,Value150mMscaled_525em1mm.(names{i+6}))
165 hold on
166 plot(pH,Value200mMscaled_525em1mm.(names{i+6}))
167 ylim([0,21])
168 title(['350nA 1mm'])
169
170 lgd = legend({'100mM','150mM','200mM'});
171 lgd.NumColumns = 3;
172 lgd.Layout.Tile = 'north';
173 nexttile
174 plot(pH,Value100mMscaled_525em05mm.(names{i+6}))
175 hold on
176 plot(pH,Value150mMscaled_525em05mm.(names{i+6}))
177 hold on
178 plot(pH,Value200mMscaled_525em05mm.(names{i+6}))
179 ylim([0,1.8])
180 title(['350 nA 05mm'])
181 ylabel(t,'Scaled counts per second')
182 xlabel(t,'pH value')
183 %%
184 figure
185 [fitresult, pKa_value100] = estimatepKa(pH,Value100mMscaled_525em05mm.(names{10}));
186 [fitresult, pKa_value150] = estimatepKa(pH,Value150mMscaled_525em05mm.(names{10}));
187 [fitresult, pKa_value200] = estimatepKa(pH,Value200mMscaled_525em05mm.(names{10}));
188
189 %%
190 % figure
191 % for i = 1:5
192 % subplot(2,3,i)
193 % plot(pH,Value100mM_525em05mm.(names{i+6}),'DisplayName','100mM')
194 % hold on
195 % plot(pH,Value150mM_525em05mm.(names{i+6}),'DisplayName','150mM')
196 % hold on
197 % plot(pH,Value200mM_525em05mm.(names{i+6}),'DisplayName','200mM')
198 % title(names{i+6})
199 % xlabel('pH')
200 % ylabel('counts per second')
201 % legend
202 % end
203
204 figure
205 t = tiledlayout(1,4,'TileSpacing','compact');
206 for i = 5
207 nexttile
208 plot(wavelengths,Voltages100mMscaled1mm.(names{i}))
209 xlim([400, 650])
210 ylim([0,21])
211 title(names1{i})
212 end
213 lgd = legend(names1{7:11});
214
215 for i = 5
216 nexttile
217 plot(wavelengths,Voltages100mMscaled05mm.(names{i}))
218 xlim([400, 650])
219 ylim([0,1.8])
220 title(names05{i})
221 end
222 lgd = legend(names1{7:11});
223
224 for i = 9
225 nexttile
226 plot(wavelengths,Voltages100mMscaled1mm.(names{i}))
227 xlim([400, 650])
228 ylim([0,21])
229 title([names1{i} ' 1mm'])
230 end
231 lgd = legend(namespH{1:6});
232
233 for i = 9
234 nexttile
235 plot(wavelengths,Voltages100mMscaled05mm.(names{i}))
236 xlim([400, 650])

```

```

237 ylim([0,1.8])
238 title([names05{i} ' 05nm'])
239 end
240 lgd = legend(namespH{1:6});
241
242 ylabel(t,'Scaled counts per second')
243 xlabel(t,'Wavelengths')

```

Listing A.11: Matlab script for plotting data of the proof of concept sensor

```

1  clc
2  close all
3  clear all
4  %%
5  path = 'C:\Users\mauri\Google Drive\Stude\Master BME\Afstuderen\04_Thesis\Experiments\27_Juli\Nieuwe Opstelling\';
6  %%
7  tablenames = { 'IS100mM1' 'IS100mM2' 'IS100mM3'};% 'IS100mM1' 'IS150mM1' };% 'IS100mMLaag2'};% 'IS150mM1'};%
8  %Import data
9  for i = 1:length(tablenames)
10     [S.(tablenames{i})]= dualwavelengthpH(path,tablenames{i});
11 end
12 %1 = 'pH'; 2 = 'IntensitiesMeasured'; 3 = 'Intensities405nm'; 4 = 'Intensities475nm'; 5 = 'Intensities405nmScaled'; 6 = '...
13     Intensities475nmScaled'; 7 = 'Intensity525_405'; 8 = 'Intensity525_475';
14 % 9 = 'Ratio525_405_475';
15 %%
16 figure
17 t = tiledlayout('flow')
18 nexttile(1)
19 plot(S.(tablenames{j}).pH,S.(tablenames{j}).Ratio525_405_475,'o','MarkerSize',5)
20 hold on
21 %plot(S.(tablenames{j}).pH,S.(tablenames{j}).Intensity525_405)
22 %plot(S.(tablenames{j}).pH,S.(tablenames{j}).Intensity525_475)
23 title(tablenames{j})
24
25 legend({'Ratios 525 405/475nm', 'Peak emission 525 at excitation 405 nm', 'Peak emission 525 at excitation 475 nm'})
26 [fitresult, pKa_value] = estimatepKa_final(S.(tablenames{j}).pH, S.(tablenames{j}).Ratio525_405_475)
27 end
28 pH = S.(tablenames{j}).pH
29 values = S.(tablenames{j}).Ratio525_405_475
30 %%
31 figure
32 t = tiledlayout(3,4,'TileSpacing','compact')
33 for jj = 1:length(tablenames)
34     nexttile
35     normalizedratios = S.(tablenames{jj}).Ratio525_405_475./(max(S.(tablenames{jj}).Ratio525_405_475))
36     rescaledratios = rescale(S.(tablenames{jj}).Ratio525_405_475)
37     %plot(S.(tablenames{jj}).pH,normalizedratios,'o','MarkerSize',5)
38     plot(S.(tablenames{jj}).pH,rescaledratios,'o','MarkerSize',5)
39     hold on
40     %plot(S.(tablenames{jj}).pH,S.(tablenames{jj}).Intensity525_405)
41     %plot(S.(tablenames{jj}).pH,S.(tablenames{jj}).Intensity525_475)
42     title(tablenames{jj})
43     ylabel(t,'Normalised Ratio R')
44     % legend({'Ratios 525 405/475nm 50mM', 'Ratios 525 405/475nm 100mM', 'Ratios 525 405/475nm 150mM'})
45     title(t,'Ionic Strength Measurements')
46     xlabel(t,'pH')
47     [fitresult, pKa_value] = estimatepKa_final(S.(tablenames{jj}).pH, rescaledratios)
48 end
49 %%
50 path = 'C:\Users\mauri\Google Drive\Stude\Master BME\Afstuderen\04_Thesis\Experiments\27_Juli\Nieuwe Opstelling\TransitionTime\';
51 tablenames = {'TT100mM8262' 'TT100mM6282' 'TT100mMLaag8262' 'TT100mMLaag6282'} %'TT100mM6662' 'TT100mM7066' 'TT100mM7470' 'TT100mM7874...
52     'TT100mM8278';
53 %Import data
54 figure
55 t = tiledlayout('flow')
56 for i = 1:length(tablenames)
57     [S.(tablenames{i})]= dualwavelengthTime(path,tablenames{i});
58 end
59 %1 = 'pH'; 2 = 'IntensitiesMeasured'; 3 = 'Intensities405nm'; 4 = 'Intensities475nm'; 5 = 'Intensities405nmScaled'; 6 = '...
60     Intensities475nmScaled'; 7 = 'Intensity525_405'; 8 = 'Intensity525_475';
61 %%
62 figure
63 t = tiledlayout('flow')
64 for j = 1:length(tablenames)
65     nexttile
66     Time = S.(tablenames{j}).Time;
67     Ratio = S.(tablenames{j}).Ratio525_405_475;
68     hold on
69     ResponseTime(Time,Ratio)
70     legend
71     xlabel('Seconds [s]')
72     ylabel('Ratio Emission 405/475')
73     title('Transition Time 100mM (8.2 to 6.2)')
74     legend({'Measurement Data', 'Fitted Curve'})
75 end
76 %% Fittedline
77 figure
78 t = tiledlayout(2,2,'TileSpacing','compact')
79 title(t,'Response Time Two layers')
80 xlabel(t,'Time [sec]')
81 ylabel(t,'Ratios R')
82 nexttile
83 % Fit TT100mM8262
84 Time_TT100mM8262 = S.TT100mM8262.Time;
85 Ratio_TT100mM8262 = S.TT100mM8262.Ratio525_405_475;
86 a = 0.4271 ;
87 b = -0.002875 ;
88 c = 0.1161 ;
89 T_TT100mM8262 = 1/-b;
90 ResponseTime_TT100mM8262 = num2str(round(T_TT100mM8262))
91 Fit_TT100mM8262 = c+a*exp(b*Time_TT100mM8262) ;
92 plot(Time_TT100mM8262,Ratio_TT100mM8262,'o')
93 hold on
94 xline(T_TT100mM8262, 'r.-', {'Response Time ' ResponseTime_TT100mM8262})
95 plot(Time_TT100mM8262,Fit_TT100mM8262)
96 title('Layer 0.5 mm')
97 xlim([0 1500])
98
99 % Fit TT100mM6282
100 nexttile
101 Time_TT100mM6282 = S.TT100mM6282.Time;
102 Ratio_TT100mM6282 = S.TT100mM6282.Ratio525_405_475;
103 a = -0.2968 ;
104 b = -0.001916 ;
105 c = 0.9 ;
106 T_TT100mM6282 = 1/-b;
107 ResponseTime_TT100mM6282 = num2str(round(T_TT100mM6282))
108 Fit_TT100mM6282 = c+a*exp(b*Time_TT100mM6282) ;
109 plot(Time_TT100mM6282,Ratio_TT100mM6282,'o')
110 hold on
111 xline(T_TT100mM6282, 'r.-', {'Response Time ' ResponseTime_TT100mM6282})
112 plot(Time_TT100mM6282,Fit_TT100mM6282)

```

```

113 title('Layer 0.5 mm')
114 xlim([0 1500])
115 % Fit TT100mMLaag8262
116 nexttitle
117 Time_TT100mMLaag8262 = S.TT100mMLaag8262.Time;
118 Ratio_TT100mMLaag8262 = S.TT100mMLaag8262.Ratio525_405_475;
119 a = 1.023 ;
120 b = -0.002609 ;
121 c = 0.4398 ;
122 T_TT100mMLaag8262 = 1/-b
123 ResponseTime_TT100mMLaag8262 = num2str(round(T_TT100mMLaag8262))
124 Fit_TT100mMLaag8262 = c+a*exp(b*Time_TT100mMLaag8262) ;
125 plot(Time_TT100mMLaag8262,Ratio_TT100mMLaag8262,'o')
126 hold on
127 xline(T_TT100mMLaag8262, 'r.-',{'Response Time ' ResponseTime_TT100mMLaag8262})
128 plot(Time_TT100mMLaag8262,Fit_TT100mMLaag8262)
129 title('Layer 1mm')
130 xlim([0 1500])
131
132
133 % Fit TT100mMLaag6282
134 nexttitle
135 Time_TT100mMLaag6282 = S.TT100mMLaag6282.Time;
136 Ratio_TT100mMLaag6282 = S.TT100mMLaag6282.Ratio525_405_475;
137 a = -1.56 ;
138 b = -0.001311 ;
139 c = 1.6 ;
140 T_TT100mMLaag6282 = 1/-b
141 ResponseTime_TT100mMLaag6282 = num2str(round(T_TT100mMLaag6282))
142 Fit_TT100mMLaag6282 = c+a*exp(b*Time_TT100mMLaag6282) ;
143 plot(Time_TT100mMLaag6282,Ratio_TT100mMLaag6282,'o')
144 hold on
145 xline(T_TT100mMLaag6282, 'r.-',{'Response Time ' ResponseTime_TT100mMLaag6282})
146 plot(Time_TT100mMLaag6282,Fit_TT100mMLaag6282)
147 title('Layer 1mm')
148 xlim([0 1500])

```

## A.18.2. Functions

Listing A.12: Matlab function to plot absorption data plots

```

1 function absorpplot(Sample1, Sample2, Sample3, Sample4, Sample5, Sample6, samplename)
2 %UNTITLED Summary of this function goes here
3 % Detailed explanation goes here
4 nexttitle
5 samplename = samplename;
6 plot(Sample1(:,1), Sample1(:,2), Sample2(:,1), Sample2(:,2), Sample3(:,1), Sample3(:,2), Sample4(:,1), Sample4(:,2), Sample5(:,1), Sample5(:,2), ...
7 Sample6(:,1), Sample6(:,2))
8 xline(405, '--', '405nm', 'Color', '#8200c8');
9 xline(465, ':', '475nm', 'Color', '#00c0ff');
10 title(sprintf('Plot of the Absorbance of Rescaled %s', samplename));
11 end

```

Listing A.13: Matlab function for voltage per pH Avantes data

```

1 function [wavelengths, names, Voltages100mM, Voltages150mM, Voltages200mM, Voltages100mMscaled, Voltages150mMscaled, Voltages200mMscaled]= ...
2 avantesvoltages(path)
3 %% 100mM
4 tablenames = '100mM.xlsx';
5 paths = string([path tablenames]);
6 T = readtable(paths);
7 A = table2array(T);
8 wavelengths = A(3:end,1);
9 wavelengthscale = 337;
10 names = {'pH62' 'pH66' 'pH70' 'pH74' 'pH78' 'pH82' 'V25' 'V30' 'V34' 'V36' 'V38'};
11 Ascaled = A;
12 for k=2:1:31
13     Ascaled(:,k) = A(:,k) ./ (A(wavelengthscale,k));
14 end
15
16 for i = 1:6
17     Voltages100mM.(names{i}) = A(3:end,1+(i*5-4):1+(i*5));
18     Voltages100mMscaled.(names{i}) = Ascaled(3:end,1+(i*5-4):1+(i*5));
19     if i ≤ 6
20         Voltages100mM.(names{i+5}) = A(3:end,i:5:26+i);
21         Voltages100mMscaled.(names{i+5}) = Ascaled(3:end,i:5:26+i);
22     end
23 end
24 %% 150mM
25 tablenames = '150mM.xlsx';
26 paths = string([path tablenames]);
27 T = readtable(paths);
28 A = table2array(T);
29 names = {'pH62' 'pH66' 'pH70' 'pH74' 'pH78' 'pH82' 'V25' 'V30' 'V34' 'V36' 'V38'};
30 Ascaled = A;
31 for k=2:1:31
32     Ascaled(:,k) = A(:,k) ./ (A(wavelengthscale,k));
33 end
34
35 for i = 1:6
36     Voltages150mM.(names{i}) = A(3:end,1+(i*5-4):1+(i*5));
37     Voltages150mMscaled.(names{i}) = Ascaled(3:end,1+(i*5-4):1+(i*5));
38     if i ≤ 6
39         Voltages150mM.(names{i+5}) = A(3:end,i:5:26+i);
40         Voltages150mMscaled.(names{i+5}) = Ascaled(3:end,i:5:26+i);
41     end
42 end
43 %% 200mM
44 tablenames = '200mM.xlsx';
45 paths = string([path tablenames]);
46 T = readtable(paths);
47 A = table2array(T);
48 names = {'pH62' 'pH66' 'pH70' 'pH74' 'pH78' 'pH82' 'V25' 'V30' 'V34' 'V36' 'V38'};
49 Ascaled = A;
50 for k=2:1:31
51     Ascaled(:,k) = A(:,k) ./ (A(wavelengthscale,k));
52 end
53
54 for i = 1:6
55     Voltages200mM.(names{i}) = A(3:end,1+(i*5-4):1+(i*5));
56     Voltages200mMscaled.(names{i}) = Ascaled(3:end,1+(i*5-4):1+(i*5));
57     if i ≤ 6
58         Voltages200mM.(names{i+5}) = A(3:end,i:5:26+i);
59         Voltages200mMscaled.(names{i+5}) = Ascaled(3:end,i:5:26+i);
60     end
61 end

```

Listing A.14: Matlab function for plots of the full data obtained by flourlog

```

1 function fluorloopplo(exwl, emwl, S1c_Samples, names, xlabel, ylabel, ttl, type, namesforplot, ylim, colorscale)
2 %UNTITLED3 Summary of this function goes here
3 % Detailed explanation goes here
4 S = S1c_Samples;
5
6 for k = 1:length(names)
7     fulltitle = [sprintf('%s', ttl) namesforplot{k}];
8     nexttile
9     if type == 1
10        names(k) = surf(exwl, emwl, S.(names{k}))
11        caxis(colorscale)
12    elseif type == 2
13        contour(exwl, emwl, S.(names{k}))
14        colorbar
15    elseif type == 3
16        contour3(exwl, emwl, S.(names{k}))
17        colorbar
18    elseif type == 4
19        surf(exwl, emwl, S.(names{k}))
20        caxis(colorscale)
21        view(2)
22    else
23        print('Type Unknown')
24    end
25    xline(405, '-r', '405nm', 'LineWidth', 2);
26    xline(465, ':', '475nm', 'Color', '#00c0ff', 'LineWidth', 2);
27    yline(520, '-g', '525nm', 'LineWidth', 2);
28    xlabel(sprintf('%s', xlabel))
29    ylabel(sprintf('%s', ylabel))
30    title(fulltitle);
31    hold on
32    ylim(ylim)
33 end

```

Listing A.15: Matlab function for importing fluorlog data

```

1 function [SampleData, names, names_forplot, figSample, Excitationwavelengths, Emissionwavelengths] = importflourlogsampleddata(whichsample)
2 fds = fileDatastore('C:\Users\mauri\Documents\MATLAB\Afstuderen\DataFluorlog2', 'ReadFcn', @load);
3 fullFileNames = fds.Files;
4 FileNames = string(fullFileNames);
5
6 %%
7 names_S1c = {'A pH62' 'A pH66' 'A pH70' 'A pH74' 'A pH78' 'A pH82' 'A pHmax' 'A pHmin' 'B pH62' 'B pH66' 'B pH70' 'B pH74' 'B pH78' 'B pH82'...
8             'B pHmax' 'B pHmin' 'C pH62' 'C pH66' 'C pH70' 'C pH74' 'C pH78' 'C pH82' 'C pHmax' 'C pHmin' 'D pH62' 'D pH66' 'D pH70' 'D pH74' '...
9             'D pH78' 'D pH82' 'D pHmax' 'D pHmin' 'Glass' 'Leeg'};
10 names_S1c_forplot = {'A pH 6.2' 'A pH 6.6' 'A pH 7.0' 'A pH 7.4' 'A pH 7.8' 'A pH 8.2' 'A pH max' 'A pH min' 'B pH 6.2' 'B pH 6.6' 'B pH 7...
11             'B pH 7.4' 'B pH 7.8' 'B pH 8.2' 'B pH max' 'B pH min' 'C pH 6.2' 'C pH 6.6' 'C pH 7.0' 'C pH 7.4' 'C pH 7.8' 'C pH 8.2' 'C pH ...
12             'max' 'C pH min' 'D pH 6.2' 'D pH 6.6' 'D pH 7.0' 'D pH 7.4' 'D pH 7.8' 'D pH 8.2' 'D pH max' 'D pH min' 'Glass' 'Leeg'};
13
14 names_R1c_forplot = names_S1c_forplot;
15 names_S1c_R1c_forplot = names_S1c_forplot;
16 %Importing S1c Files
17 beginsample = 35; % eerste S1c Sample
18 for j = 1:length(names_S1c)
19     i = j+beginsample-1;
20     S1c_Samples.(names_S1c{j}) = ImportFluorlogData(FileNames(i));
21 end
22 %Importing R1c Files
23 beginsample = 1;
24 endsample = 34;
25 for j = 1:length(names_R1c)
26     i = j+beginsample-1;
27     R1c_Samples.(names_R1c{j}) = ImportFluorlogData(FileNames(i));
28 end
29 %Importing S1c_R1c Files
30 beginsample = 69;
31 for j = 1:length(names_S1c_R1c)
32     i = j+beginsample-1;
33     T = readtable(FileNames(i));
34     S1c_R1c_Samples.(names_S1c_R1c{j}) = table2array(T(2:52,2:32));
35 end
36 % creating excitation wavelengths
37 N=30;
38 Excitationwavelengths = zeros(N+1,1);
39 for n = 0:N
40     z = 350+(5*n);
41     Excitationwavelengths(n+1) = z;
42 end
43 % creating emission wavelengths
44 N2=50;
45 Emissionwavelengths = zeros(N2+1,1);
46 for n = 0:N2
47     z = 350+(5*n);
48     Emissionwavelengths(n+1) = z;
49 end
50 %%
51 % for k = 4:length(names_S1c)
52 %     if 4 ≤ k ≤ 6
53 %         S1c_Samples_corrected.(names_S1c(k)) = S1c_Samples.(names_S1c(k))-S1c_Samples.(names_S1c(1))-S1c_Samples.(names_S1c(2))-S1c_Samples.(...
54 %         names_S1c(3));
55 %     elseif 8 ≤ k ≤ 10
56 %         S1c_Samples_corrected.(names_S1c(k)) = S1c_Samples.(names_S1c(k))-S1c_Samples.(names_S1c(1))-S1c_Samples.(names_S1c(2))-S1c_Samples.(...
57 %         names_S1c(7));
58 %     end
59 %%
60 SamplesA = {'A pHmin' 'A pH62' 'A pH66' 'A pH70' 'A pH74' 'A pH78' 'A pH82' 'A pHmax'};
61 SamplesB = {'B pHmin' 'B pH62' 'B pH66' 'B pH70' 'B pH74' 'B pH78' 'B pH82' 'B pHmax'};
62 SamplesC = {'C pHmin' 'C pH62' 'C pH66' 'C pH70' 'C pH74' 'C pH78' 'C pH82' 'C pHmax'};
63 SamplesD = {'D pHmin' 'D pH62' 'D pH66' 'D pH70' 'D pH74' 'D pH78' 'D pH82' 'D pHmax'};
64 Samples62 = {'A pH62' 'B pH62' 'C pH62' 'D pH62'};
65 Samples66 = {'A pH66' 'B pH66' 'C pH66' 'D pH66'};
66 Samples70 = {'A pH70' 'B pH70' 'C pH70' 'D pH70'};
67 Samples74 = {'A pH74' 'B pH74' 'C pH74' 'D pH74'};
68 Samples78 = {'A pH78' 'B pH78' 'C pH78' 'D pH78'};
69 Samples82 = {'A pH82' 'B pH82' 'C pH82' 'D pH82'};
70 SamplesMin = {'A pHmin' 'B pHmin' 'C pHmin' 'D pHmin'};
71 SamplesMax = {'A pHmax' 'B pHmax' 'C pHmax' 'D pHmax'};
72 SamplesBackground = {'Leeg' 'Glass'};
73
74 SamplesA_forplot = {'A pH min' 'A pH 6.2' 'A pH 6.6' 'A pH 7.0' 'A pH 7.4' 'A pH 7.8' 'A pH 8.2' 'A pH max'};
75 SamplesB_forplot = {'B pH min' 'B pH 6.2' 'B pH 6.6' 'B pH 7.0' 'B pH 7.4' 'B pH 7.8' 'B pH 8.2' 'B pH max'};
76 SamplesC_forplot = {'C pH min' 'C pH 6.2' 'C pH 6.6' 'C pH 7.0' 'C pH 7.4' 'C pH 7.8' 'C pH 8.2' 'C pH max'};
77 SamplesD_forplot = {'D pH min' 'D pH 6.2' 'D pH 6.6' 'D pH 7.0' 'D pH 7.4' 'D pH 7.8' 'D pH 8.2' 'D pH max'};
78 Samples62_forplot = {'A pH 6.2' 'B pH 6.2' 'C pH 6.2' 'D pH 6.2'};
79 Samples66_forplot = {'A pH 6.6' 'B pH 6.6' 'C pH 6.6' 'D pH 6.6'};
80 Samples70_forplot = {'A pH 7.0' 'B pH 7.0' 'C pH 7.0' 'D pH 7.0'};
81 Samples74_forplot = {'A pH 7.4' 'B pH 7.4' 'C pH 7.4' 'D pH 7.4'};
82 Samples78_forplot = {'A pH 7.8' 'B pH 7.8' 'C pH 7.8' 'D pH 7.8'};
83 Samples82_forplot = {'A pH 8.2' 'B pH 8.2' 'C pH 8.2' 'D pH 8.2'};
84 SamplesMin_forplot = {'A pH min' 'B pH min' 'C pH min' 'D pH min'};
85 SamplesMax_forplot = {'A pH max' 'B pH max' 'C pH max' 'D pH max'};

```

```

82 SamplesBackground_forplot = {'Leeg' 'Glass'};
83
84 %% selecting Samples
85 if whichtsample == 1
86 names = SamplesA;
87 names_forplot = SamplesA_forplot;
88 figSample = 'SampleA';
89 elseif whichtsample == 2
90 names = SamplesB;
91 names_forplot = SamplesB_forplot;
92 figSample = 'SampleB';
93 elseif whichtsample == 3
94 names = SamplesC;
95 names_forplot = SamplesC_forplot;
96 figSample = 'SampleC';
97 elseif whichtsample == 4
98 names = SamplesD;
99 names_forplot = SamplesD_forplot;
100 figSample = 'SampleD';
101 elseif whichtsample == 5
102 names = SamplesMin;
103 names_forplot = SamplesMin_forplot;
104 figSample = 'SampleMin';
105 elseif whichtsample == 6
106 names = Samples62;
107 names_forplot = Samples62_forplot;
108 figSample = 'Sample62';
109 elseif whichtsample == 7
110 names = Samples66;
111 names_forplot = Samples66_forplot;
112 figSample = 'Sample66';
113 elseif whichtsample == 8
114 names = Samples70;
115 names_forplot = Samples70_forplot;
116 figSample = 'Sample70';
117 elseif whichtsample == 9
118 names = Samples74;
119 names_forplot = Samples74_forplot;
120 figSample = 'Sample74';
121 elseif whichtsample == 10
122 names = Samples78;
123 names_forplot = Samples78_forplot;
124 figSample = 'Sample78';
125 elseif whichtsample == 11
126 names = Samples82;
127 names_forplot = Samples82_forplot;
128 figSample = 'Sample82';
129 elseif whichtsample == 12
130 names = SamplesMax;
131 names_forplot = SamplesMax_forplot;
132 figSample = 'SampleMax';
133 elseif whichtsample == 13
134 names = SamplesBackground;
135 names_forplot = SamplesBackground_forplot;
136 figSample = 'SampleBackground';
137 else
138 end
139 SampleData = S1c_R1c_Samples; % S1c_Samples R1c_Samples S1c_R1c_Samples

```

Listing A.16: Matlab function for plotting data from a table

```

1 function tableplot(Sample1, Sample2, Sample3, Sample4, Sample5, Sample6, samplename, ttl)
2 %UNTITLED3 Summary of this function goes here
3 % Detailed explanation goes here
4 fulltitle = [sprintf('%s', ttl) sprintf('%s', samplename)];
5 nextTitle
6 plot(Sample1.nm, Sample1.x_T, Sample2.nm, Sample2.x_T, Sample3.nm, Sample3.x_T, Sample4.nm, Sample4.x_T, Sample5.nm, Sample5.x_T, Sample6.nm, ...
7 Sample6.x_T)
8 xline(405, '--', '405nm', 'Color', '#8200c8');
9 xline(465, ':', '475nm', 'Color', '#00c0ff');
10 title(fulltitle);

```

Listing A.17: Matlab function for estimating pKa values

```

1 function [fitresult, pKa_value] = estimatepKa(pHrange, values)
2 %CREATEFIT(PHMINMAX,RATIO_SAMPLED)
3 % Create a fit.
4
5 % Data for 'untitled fit 1' fit:
6 % X Input : pHminmax
7 % Y Output: Ratio_SampleD
8 % Output:
9 % fitresult : a fit object representing the fit.
10 % gof : structure with goodness-of fit info.
11
12 % See also FIT, CPIT, SPIT.
13
14 % Auto-generated by MATLAB on 15-Jul-2021 09:37:35
15
16
17 %% Fit: 'untitled fit 1'.
18 [xData, yData] = prepareCurveData( pHrange, values );
19
20 % Set up fittype and options.
21 ft = fittype( '(a-b)/(1+exp((x-c)/d))+b', 'independent', 'x', 'dependent', 'y' );
22 opts = fitoptions( 'Method', 'NonlinearLeastSquares' );
23 opts.Display = 'Off';
24 opts.Lower = [0 1 6.5 -Inf];
25 opts.Upper = [Inf Inf 15 5];
26 opts.MaxFunEvals = 99999999;
27 opts.MaxIter = 99999999;
28 opts.StartPoint = [0.706046088019609 0.0318328463774207 0.27692298496089 0.0461713906311539];
29
30 % Fit model to data.
31 fitresult = fit( xData, yData, ft, opts );
32
33 % Plot fit with data.
34 % figure( 'Name', 'untitled fit 1' );
35 % sh = plot( fitresult, xData, yData );
36 % legend( h, 'Ratio_SampleD vs. pHminmax', 'untitled fit 1', 'Location', 'NorthEast', 'Interpreter', 'none' );
37
38 % Label axes
39 % xlabel( 'pHminmax', 'Interpreter', 'none' );
40 % ylabel( 'Ratio_SampleD', 'Interpreter', 'none' );
41 % grid on
42 % Plot data self
43 a = fitresult.a;
44 b = fitresult.b;
45 c = fitresult.c;

```

```

45 d = fitresult.d;
46 xfit = xData(1):0.1:xData(length(xData));
47 yfit = ((a-b)./(1+exp((xfit-c)./d))+b);
48 [xxData, yyData] = prepareCurveData(xfit, yfit);
49 [fitresult2] = fit(xxData, yyData, ft, opts);
50 [dl, dd2] = differentiate(fitresult, xData);
51 [ddl, dd2] = differentiate(fitresult2, xxData);
52 yln = zeros(1, length(xfit));
53 pKa_value = polyxpoly(xfit, yln, xfit, dd2);
54 name = num2str(pKa_value);
55
56
57
58 nexttile
59 %plot(pHrange, values, '--') % cfit plot method
60 hold on
61 p = plot(fitresult, xData, yData, '--');
62 p(1).LineWidth = 1;
63 p(2).LineWidth = 1;
64 xlabel(' ')
65 box on
66 grid on
67 xline(pKa_value, '--', name, 'LineWidth', 1)
68 xline(6.8, 'g-', 'LineWidth', 1)
69 xline(7.8, 'c-', 'LineWidth', 1)
70
71 legend({'Measurement data', 'Fitted curve'}, 'Location', 'best')
72 ylabel('Ratio R')
73 title('Ratios R at various pH values')
74 nexttile
75 %plot(xData, dl, '--', 'LineWidth', 1) % double plot method
76 hold on
77 plot(xfit, ddl, 'r-', 'LineWidth', 1) % cfit plot method
78 grid on
79 xline(pKa_value, '--', name, 'LineWidth', 1)
80 xline(6.8, 'g-', 'LineWidth', 1)
81 xline(7.8, 'c-', 'LineWidth', 1)
82
83 legend({'Measurement data'}, 'Location', 'best')
84 ylabel('Sensitivity (n = Gradient(R))')
85 title('Sensitivity n at various pH values')
86 nexttile
87 %plot(xData, dd2, '--', 'LineWidth', 1) % double plot method
88 hold on
89 plot(xfit, dd2, 'r-', 'LineWidth', 1)
90 plot(xfit, yln, 'b', 'LineWidth', 1)
91 xline(pKa_value, '--', name, 'LineWidth', 1)
92 xline(6.8, 'g-', 'LineWidth', 1)
93 xline(7.8, 'c-', 'LineWidth', 1)
94
95 legend({'Measurement data'}, 'Location', 'best')
96 ylabel('Gradient (n)')
97 title('Determining pKa by setting n = 0')
98 grid on

```

Listing A.18: Matlab function for opening data of the proof of concept sensor

```

1 function [S]= dualwavelengthpH(path, tablename)
2 %% 50mM
3 paths = string({[path tablename '.xlsx']});
4 T = readtable(paths);
5 A = table2array(T);
6 wavelengths = A(3:end,1);
7 pH = A(2,2:end);
8 I = A(3:end,1:end);
9 w1405 = 90; %90 is 400 98 is 405nm
10 w1475 = 218; %218 is 475 nm
11 w1525 = 304; %304 is 525nm 288 is 515 nm
12
13 names50mM = num2cell(zeros(1, length(pH)));
14 for i = 1:length(pH)
15     names50mM{i} = num2str(pH(i));
16 end
17
18 I_405 = zeros(length(I), length(pH));
19 I_475 = zeros(length(I), length(pH));
20 I_525_405 = zeros(1, length(pH));
21 I_525_475 = zeros(1, length(pH));
22 Ratio_405_475 = zeros(1, length(pH));
23 I_405scaled = zeros(length(I), length(pH));
24 I_475scaled = zeros(length(I), length(pH));
25 for k=2:2:length(I(1,:))
26     j= k/2;
27     I_405(:, j) = I(:,k);
28     I_475(:, j) = I(:,k+1);
29     Peak_405nm(:, j) = find(I_405(:,j))==max(I_405(60:120,j));
30     Peak_475nm(:, j) = find(I_475(:,j))==max(I_475(201:235,j));
31     Peak_emission_405nm(:, j) = find(I_405(:,j))==max(I_405(270:340,j));
32     Peak_emission_475nm(:, j) = find(I_475(:,j))==max(I_475(270:340,j));
33     I_405scaled(:, j) = (I_405(:,j))./(I_405(Peak_405nm(j),j));
34     I_475scaled(:, j) = (I_475(:,j))./(I_475(Peak_475nm(j),j));
35     I_525_405(j) = I_405scaled(Peak_emission_405nm(j),j);
36     I_525_475(j) = I_475scaled(Peak_emission_475nm(j),j);
37     Ratio_405_475(j) = (I_525_475(j))/(I_525_405(j))
38 end
39 % Create Structure with all information
40 field1 = 'pH';
41 field2 = 'IntensitiesMeasured';
42 field3 = 'Intensities405nm';
43 field4 = 'Intensities475nm';
44 field5 = 'Intensities405nmScaled';
45 field6 = 'Intensities475nmScaled';
46 field7 = 'Intensity525_405';
47 field8 = 'Intensity525_475';
48 field9 = 'Ratio525_405_475';
49
50 S = struct(field1, pH, field2, I, field3, I_405, field4, I_475, field5, I_405scaled, field6, I_475scaled, field7, I_525_405, field8, I_525_475, field9, ...
51     Ratio_405_475)
52 figure
53 t = tiledlayout(2, length(pH), 'TileSpacing', 'compact');
54 for l = 1:length(pH)
55     nexttile
56     plot(wavelengths, I_405(:,l))
57     title(names50mM{l})
58     nexttile(1+length(pH))
59     plot(wavelengths, I_475(:,l))
60     title(names50mM{l})
61 end
62 figure
63 t = tiledlayout(2, length(pH), 'TileSpacing', 'compact');
64 for l = 1:length(pH)
65     nexttile
66     plot(wavelengths, I_405scaled(:,l))
67     title(names50mM{l})

```

```

68 nexttile(1+length(pH))
69 plot(wavelengths,I_475scaled(:,1))
70 title(names50mM{1})
71 end
72 figure(3)
73 t = tiledlayout('flow')
74 nexttile
75 plot(pH,Ratio_405_475,'DisplayName','Ratio 405/475')
76 hold on
77 plot(pH,I_525_405,'DisplayName','Scaled Intensity 405nm')
78 plot(pH,I_525_475,'DisplayName','Scaled Intensity 475nm')
79 legend
80 title('Intensity Ratio at 525nm_(475/405nm)')

```

Listing A.19: Matlab function for opening the reponse time data of the proof of concept sensor

```

1 function [S]= dualwavelengthTime(path, tablename)
2 %% Time
3 paths = string([path tablename '.xlsx']);
4 T = readtable(paths);
5 A = table2array(T);
6 wavelengths = A(3:end,1);
7 Time = A(2,2:end);
8 realtime = datetime(Time,'ConvertFrom','excel');
9 realtime.Format = 'HH:mm:ss';
10 realtime = seconds(realtime-realtime(1));
11 I = A(3:end,1:end);
12 wl405 = 90; %90 is 400 98 is 405nm
13 wl475 = 218; %218 is 475 nm
14 wl525 = 304; %304 is 525nm 288 is 515 nm
15
16 names50mM = num2cell(zeros(1,length(realtime)));
17 for i = 1:length(realtime)
18     names50mM{i} = (realtime(i));
19 end
20
21 I_405 = zeros(length(I),length(realtime));
22 I_475 = zeros(length(I),length(realtime));
23 I_525_405 = zeros(1,length(realtime));
24 I_525_475 = zeros(1,length(realtime));
25 Ratio_405_475 = zeros(1,length(realtime));
26 I_405scaled = zeros(length(I),length(realtime));
27 I_475scaled = zeros(length(I),length(realtime));
28 for k=2:2:length(I(1,:))
29     j= k/2;
30     I_405(:, j) = I(:,k);
31     I_475(:, j) = I(:,k+1);
32     Peak_405nm(:, j) = find(I_405(:,j))==max(I_405(60:120,j));
33     Peak_475nm(:, j) = find(I_475(:,j))==max(I_475(201:235,j));
34     Peak_emission_405nm(:, j) = find(I_405(:,j))==max(I_405(270:340,j));
35     Peak_emission_475nm(:, j) = find(I_475(:,j))==max(I_475(270:340,j));
36     I_405scaled(:, j) = (I_405(:,j))./(I_405(Peak_405nm(j),j));
37     I_475scaled(:, j) = (I_475(:,j))./(I_475(Peak_475nm(j),j));
38     I_525_405(j) = I_405scaled(Peak_emission_405nm(j),j);
39     I_525_475(j) = I_475scaled(Peak_emission_475nm(j),j);
40     Ratio_405_475(j) = (I_525_475(j))/(I_525_405(j));
41 end
42 % Create Structure with all information
43 field1 = 'Time';
44 field2 = 'IntensitiesMeasured';
45 field3 = 'Intensities405nm';
46 field4 = 'Intensities475nm';
47 field5 = 'Intensities405nmScaled';
48 field6 = 'Intensities475nmScaled';
49 field7 = 'Intensity525_405';
50 field8 = 'Intensity525_475';
51 field9 = 'Ratio525_405_475';
52
53 S = struct(field1,realtime,field2,I,field3,I_405,field4,I_475,field5,I_405scaled,field6,I_475scaled,field7,I_525_405,field8,I_525_475,field9...
54     ,Ratio_405_475)
55
56 nexttile
57 plot(realtime,Ratio_405_475,'DisplayName','Ratio 405/475')
58 hold on
59 %plot(realtime,I_525_405,'DisplayName','Scaled Intensity 405nm')
60 %plot(realtime,I_525_475,'DisplayName','Scaled Intensity 475nm')
61 hAx=gca; % get the axes handle
62 hAx.XTickLabel=hAx.XTickLabel; % overwrite the existing tick labels with present values
63 legend
64 xlabel('Seconds [s]')
65 ylabel('Ratio Emission 405/475')
66 title('Transition Time 100mM ')

```

## A.19. Literature Review

---

# Feasible methods to detect myocardial ischaemia during cardioplegia-induced arrest

---

### A literature review

**Maurits F. Vriesendorp**

Department of BioMedical Engineering  
Delft University of Technology  
Delft, 2628 CD  
mauritsvriesendorp@gmail.com

### ABSTRACT

**Background:** Myocardial ischaemia induced by cardioplegia is the most prominent risk during open-heart surgery. To achieve adequate protection of the cardiomyocytes during surgery, the cardioplegia must arrive at all the cardiomyocytes. Local obstruction can lead to regional ischaemia. Different methods can monitor parameters related to this ischaemia. The goal of the literature review is to lay the groundwork for developing a sensor which can help the physician with monitoring the condition of the heart during cardiac surgery.

**Methods:** A search method was performed to find literature that developed feasible methods to monitor this local ischaemia. First, the different parameters related to the ischaemia of the cardiomyocytes are discussed. Followed by the selection of a type of sensor on which the literature will focus. The existing literature was reviewed on optical methods which can detect pH and lactate in the physiological range.

**Results:** After analysing 1,050 articles, thirty-seven different methods were assessed on their feasibility to monitor ischaemia. Seven articles found were designed to measure lactate levels. Thirteen articles are absorption-based optical sensors, fourteen are fluorescent-based sensors, and five are sensors based on the reflection.

**Conclusion:** There are many different techniques to monitor the physical parameters. All these techniques have different (dis)advantages which can be significant depending on your requirements. The fluorescent pH sensors show the most potential to be used as an ischaemia sensor for the heart. While the manufacturability of the sensors will be the biggest obstacle for future work

**Keywords** Ischaemia, Optical, Sensing, Fluorescence, Monitoring

# Contents

<b>1</b>	<b>Introduction</b>	<b>1</b>
<b>I</b>	<b>Background</b>	<b>3</b>
<b>2</b>	<b>Myocardial Ischaemia</b>	<b>4</b>
2.1	Parameter related to myocardial ischaemia . . . . .	4
2.2	Metabolism of the cell . . . . .	4
2.2.1	Normal metabolism . . . . .	4
2.2.2	Metabolism during ischaemia . . . . .	5
2.2.3	Early parameters of myocardial ischaemia . . . . .	6
2.3	Cardioplegia and Cardioplegia induced Cardiac Arrest. . . . .	7
2.4	Selection of parameters . . . . .	8
<b>3</b>	<b>Type of Technologies</b>	<b>9</b>
3.1	Sensing ischaemia . . . . .	9
3.2	Sensors and Transducers . . . . .	9
3.2.1	Types of sensors used in biomedical sensors. . . . .	10
3.2.2	Selection of sensor . . . . .	11
3.3	Optical Sensor . . . . .	11
3.3.1	Light interaction. . . . .	11
3.3.2	Measuring of light. . . . .	13
3.3.3	Optical sensing platforms . . . . .	15
3.3.4	Materials used in optical sensors . . . . .	16
<b>II</b>	<b>Literature study</b>	<b>17</b>
<b>4</b>	<b>Literature search</b>	<b>18</b>
4.1	Finding the best optical ischaemia sensor . . . . .	18
4.2	Method of literature search. . . . .	18
4.2.1	Identifying gaps in the current literature . . . . .	18
4.2.2	Search strategy. . . . .	19
4.2.3	Selection criteria . . . . .	19
4.3	Results of Literature Search . . . . .	20
4.3.1	Outcome of the literature scan. . . . .	20
4.3.2	Optical lactate sensors . . . . .	20
4.3.3	Absorption based sensor. . . . .	23
4.3.4	Fluorescent based sensors . . . . .	25
4.3.5	Reflection based sensor . . . . .	28
4.4	Discussion of the literature . . . . .	29
4.4.1	Search for a potential sensor . . . . .	29
4.4.2	Lactate based ischaemia sensor . . . . .	30
4.4.3	Absorption based ischaemia sensor. . . . .	30
4.4.4	Fluorescent based ischaemia sensor . . . . .	30
4.4.5	Reflection based ischaemia sensor . . . . .	31
4.4.6	Possible sensor. . . . .	31
4.4.7	Limitations of study . . . . .	33
4.4.8	Recommendation for further work . . . . .	34
4.5	Conclusion . . . . .	34
<b>A</b>	<b>Relation PtCO<sub>2</sub>, pH and lactate with decreased bloodflow</b>	<b>35</b>
	<b>Bibliography</b>	<b>36</b>

## 1

# Introduction

Cardiac surgery is the field of medicine involved in the surgical treatment of the heart. With a variety of procedures, surgeons can treat acquired cardiovascular diseases and congenital malformations of the coronary arteries and/or heart valves. Although there are some exceptions (i.e. off-pump bypass surgery), the heart is usually arrested to enable surgeons to operate [100]. Before the heart can be arrested during such an operation, a heart-lung machine is first connected to the major blood vessels of the patient. This machine takes over the function of the heart and lungs during cardiac arrest; blood is drained from the vena cava/right atrium, oxygenated and then returned to the aorta. After connecting the heart-lung machine, the aorta is clamped, and cardioplegia is injected into the coronary artery to induce cardiac arrest [75].

Cardioplegia is the universal term used for pharmacological solutions that are administered during cardiac surgery to arrest the heart temporarily [28]. While there are many different types of cardioplegia solutions, they are all primarily based on potassium chloride (KCl). KCl prevents repolarisation in the cardiomyocyte. The resulting diastolic cardiac arrest reduces the metabolism of the cardiomyocyte, preserving it without blood supply. Cardioplegia can reduce the oxygen demand by ten-fold; in combination with lowering the temperature, this can be even twenty-fold [13].

The standard method to administer cardioplegia is through antegrade perfusion in the aortic root or the ostia of the coronary arteries for around two minutes. This process must be repeated multiple times throughout the procedure. This is when electrical activity begins to appear again due to diffusion of the cardioplegia and washout of its components along with products of anaerobic cellular metabolism. Although the quantity of the administered cardioplegia solution can be measured at its entry point, the exact distribution of cardioplegia through the coronary system is unknown. To achieve adequate protection of the cardiomyocytes during the procedure, the cardioplegia must arrive at all the cardiomyocytes. However, occlusion or stenosis of a distal coronary artery may obstruct the distribution of cardioplegia, resulting in regional ischaemia. This narrowing can be the result of pre-existing conditions as coronary artery disease or left ventricular hypertrophy, but also iatrogenic complications (i.e. misplaced sutures, loose calcification's).

Ischaemia occurs as a consequence of an imbalance between oxygen supply and oxygen demand [110]. Local ischaemia will lead to myocardial damage. Myocardial damage is one of the most common causes of morbidity and mortality after heart surgery. These reasons are why the field of cardiac surgery is continuously looking for improvements of techniques to better preserve the cardiomyocytes during open-heart surgery [39]. As a result of that, there is no blood flow, normal parameters that are used to detect ischaemia are not applicable. These parameters include proteins like Troponin and Creatine Kinase MB (CK-MB) or mechanical such as cardiac output [38]. The absence of tools or parameters to monitor the myocardium during cardiac arrest makes the administration of cardioplegia a black box. Only when the heart starts beating again, clinicians become aware whether cardioplegia was distributed well enough to preserve the myocardium. By then, the process of ischaemia is irreversible and myocardial function is lost.

Perioperative myocardial infarction (MI) is one of the most severe complications following cardiac surgery, especially coronary artery bypass graft (CABG) surgery with a reported incidence of around 5% [36, 55]. In-hospital mortality rates are around 12%-40% after perioperative myocardial ischaemia [112]. After a CABG, the 30-day mortality is five times higher for patients with myocardial infarction than without [99]. In the Netherlands, around 13.000 patient received open-heart surgery in 2018 of which 6835 CABG's. Around 340 CABG patients are experiencing adverse effects from their heart surgery in the form of myocardial ischaemia. This number does not include patients who have aortic valve replacements, which are related to an even higher incidence of myocardial ischaemia after surgery. In some cases, this can be around 29% of patients [69]. In the USA, around 224,000 open-heart surgeries

were performed in 2016 [35]. This shows the scale of patients who are at risk. Next to the short-term effects, myocardial ischaemia is associated with an increased risk of progressive heart failure in the years following the operation [80]. An additional downside of myocardial ischaemia is that it uses valuable healthcare resources and has a high economic impact [68]. The cost of a CABG in the USA can go up to \$ 151,886 (average \$75,345), while in the Netherlands this is around \$ 15,742 [3]. These numbers show the relevance of ischaemia monitoring during cardiac surgery. When clinicians would be able to detect the ischaemic response of the cardiomyocyte during cardiac arrest, this would improve outcomes, bypass time and costs through detection of (regional) ischaemia at a reversible stage and through tailor-made administration of cardioplegia.

The goal of the literature review is to lay the groundwork for developing a sensor which can help the physician with monitoring the condition of the heart during cardiac surgery. This groundwork consists of multiple parts. First of all, background information is needed to understand what is happening to a heart during cardioplegia induced cardiac arrest. It is essential to understand the normal metabolism of the cardiomyocyte, myocardial ischaemia and parameters which can be detected during cardioplegia induced cardiac arrest. Selecting interesting parameters is not sufficient; it is needed that the relations of these parameters with cardioplegia are fully understood. Secondly, background information is needed about the sensing of biomedical parameters. What are the types of sensors being used in biomedical applications and which sensor has the most potential to monitor the parameters related to myocardial ischaemia? There is no golden standard in monitoring myocardial ischaemia. Therefore, different potential types of sensing platforms and materials should be investigated before comparing different sensors discussed in the literature.

Positioning this literature review in comparison to recent literature it is combining the latest techniques found with a different focus than other reviews. Thanks to this approach, multiple different techniques are evaluated, and the (dis)advantages can be well compared. This literature review differs from global trends in reviewing the literature. Most reviews are getting more and more specialised as more research in converging to specialisation. Therefore, most literature reviews are focused on one type of material, one type of measuring, one type of transducing, one type of phenomena or one type of tissue. While this makes perfect sense, this review indicates that there is also a need for overarching reviews that merge different fields of research for a larger purpose.

To prevent this literature review from becoming too broad, several choices have been made in the background information to narrow the scope of this literature review. These decisions impact the approach of the literature search to find potential ischaemia sensors. This literature review will give an overview of all kinds of different type of sensors which can be used to measure parameters related to ischaemia. Before this overview is made, the current literature reviews regarding this subject will be discussed. This will be important because sufficient articles describe parts which can be relevant for ischaemia monitoring, but there are no reviews found which compares the different types of sensing mechanisms related to ischaemia. To make sure this literature review gives the insight needed to develop a sensor capable of ischaemia monitoring, this review tries to answer the following research question:

*What are feasible methods to detect myocardial ischaemia during a cardioplegia-induced arrest?*

To answer this research question, it is divided into the following three sub-questions.

*Which physical parameters are related to myocardial ischaemia during a cardioplegia-induced arrest?*

*Which types of technologies are capable of measuring these parameters during a cardioplegia-induced arrest?*

*What is the best technique of the chosen technology that can be used to measure the parameters during a cardioplegia-induced arrest?*

First of all, background information is needed. This will be in the first part of the literature review. Chapter 2 will revolve around answering the first subquestion. The second subquestion will be the focus of Chapter 3. The second part of this literature review is the main focus of this review and will be centred around answering the third subquestion. In Chapter 4, a systematic literature search is described to compare all different types of sensors. In total, thirty-seven different types of sensing mechanism will be evaluated, and in the discussion, the main potential sensors will be elaborated.

# I Background

## 2

## Myocardial Ischaemia

## 2.1. Parameter related to myocardial ischaemia

In this chapter, the processes and parameters related to myocardial ischaemia are specified. Furthermore, cardioplegia and the cardioplegia induced cardiac arrest are described, and a decision is made on which parameters the literature review will focus. This chapter will focus on the first subquestion of this literature review:

*A: Which physical parameters are related to myocardial ischaemia during a cardioplegia-induced arrest?*

This question will be answered by first explaining the metabolism of the cardiomyocyte during normal condition. This metabolism will be compared with the metabolism during ischaemia. Afterwards, the first parameters indicating myocardial ischaemia will be described. Subsequently, a short description of cardioplegia and cardioplegia induced cardiac arrest will be given. At last, the parameters on which the continuation of this research will be conducted are chosen.

## 2.2. Metabolism of the cell

## 2.2.1. Normal metabolism

A cardiomyocyte is a heart muscle cell. It is different from a normal cell because it has multiple mitochondria. These mitochondria are important for the production of Adenosine triphosphate (ATP). ATP is the organic compound that is used for intracellular energy transfer. ATP provides energy and is used in almost all forms of life [66, 109]. The energy (ATP) demand of the cardiomyocyte is determined by the contractile state, the heart rate, the cardiac output, the sympathetic/parasympathetic balance, and the temperature. In normal conditions, 95% of all the ATP is produced by oxidative phosphorylation in the mitochondria [110, 127]. As illustrated in Figure 2.1 ATP is formed from  $\text{ADP} + \text{P}_i$  by using oxygen to

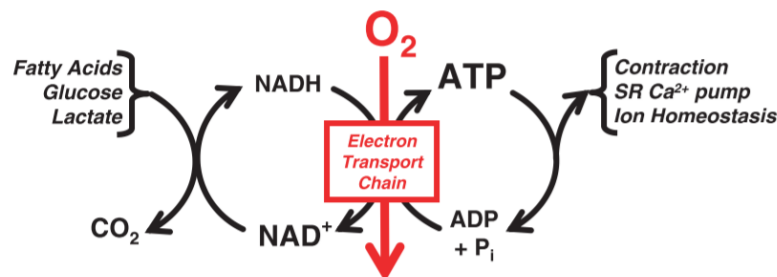


Figure 2.1: Linkages between cardiac power, ATP hydrolysis, oxidative phosphorylation, and NADH generation by dehydrogenase in metabolism. Reprinted from Stanley et al. [109]

transfer an electron from NADH. This transfer produces water ( $\text{H}_2\text{O}$ ) as a by-product. The hydrogen is added to  $\text{NAD}^+$  by the dehydrogenation of carbon fuels in the mitochondria. These carbon fuels are fatty acids, glucose and lactate. In Figure 2.2, the pathways of cardiomyocyte metabolism are illustrated. This figure shows that Acetyl-CoA is needed to produce NADH in the mitochondria. The distribution between Acetyl-CoA formed by fatty acids and pyruvate is between 90:10% and 60:40%. The distribution of glucose and lactate contributing to pyruvate is approximately equal [109]. When the heart is functioning normally, it uses more lactate than it produces. So the cardiomyocyte absorbs lactate from the blood. The concentration of lactate in the cardiomyocyte will increase when the (anaerobic) glycolysis is producing more pyruvate than is being oxidated by the pyruvate dehydrogenase (PDH).

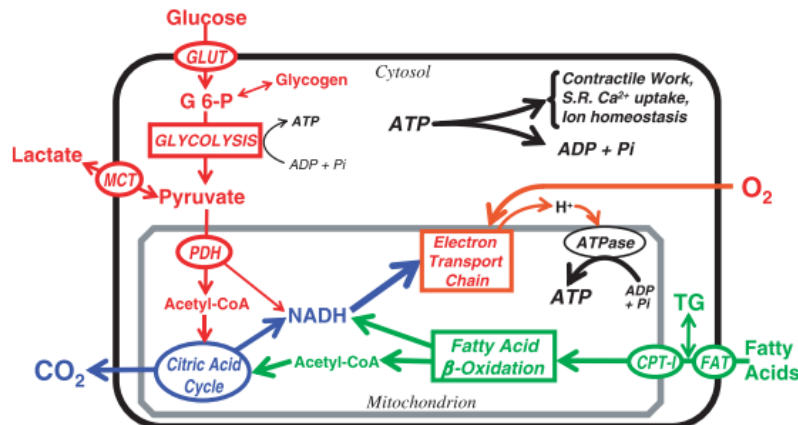


Figure 2.2: The pathways and regulatory points of myocardial substrate metabolism. Reprinted from Stanley et al. [109]

### 2.2.2. Metabolism during ischaemia

Ischaemia occurs as a consequence of an imbalance between oxygen supply and oxygen demand [110]. Ischaemia is besides an insufficient oxygen supply also associated with reduced availability of nutrients and the inadequate removal of metabolic waste products [110]. During ischaemia, the effects of oxygen deprivation cannot be separated from the effects of accumulating waste products. When the mitochondria of the cardiomyocyte cannot produce enough energy, because of a lack of oxygen, it switches to anaerobic glycolysis to produce energy. However, anaerobic glycolysis is less efficient than the aerobic process. The anaerobic produces only two ATP per glucose, while the optimised aerobic respiration produces thirty-two ATP per glucose. The anaerobic glycolysis only produces 6% of what the aerobic process can produce [77]. This change of metabolism causes a negative energy balance in the cardiomyocyte, and thus anaerobic glycolysis uses high energy reserves. Besides the use of these reserves, it also causes an increase in lactic acid, which will immediately break down into lactate and hydrogen atoms because of the pH level in the cardiomyocyte [98]. The increase of the acid in the cardiomyocyte causes the pH to drop. Figure 2.3 illustrates how the cardiomyocyte tries to compensate for this drop of pH by exchanging  $H^+$  for  $Na^+$ . This increase of  $Na^+$  in the cardiomyocyte is compensated by the exchanging it for  $Ca^{2+}$ . This increase of  $Ca^{2+}$  damages the membrane of the mitochondrion and reduces the contractility of the cardiomyocyte [127]. After 1 minute of full ischaemia there, is almost no contractility of the cardiomyocyte left [110]. After reperfusion of the heart, this damage can

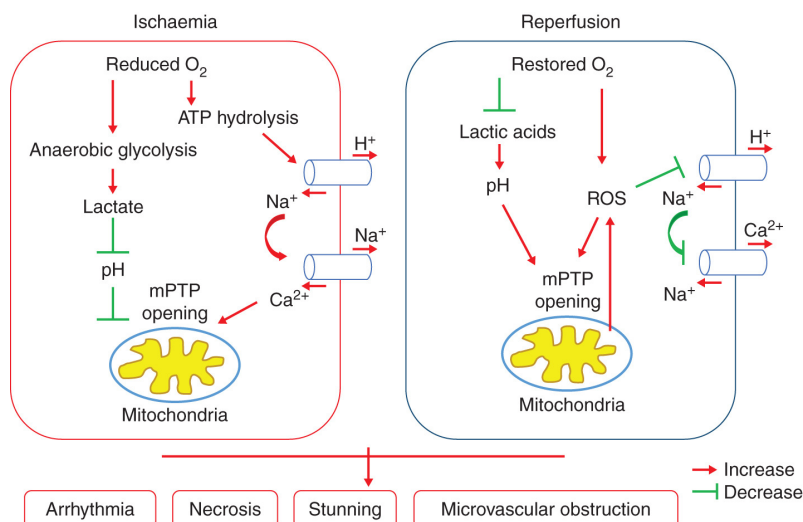


Figure 2.3: Changes in the cardiomyocyte during ischaemia and reperfusion. Reprinted from Xia et al. [127]

be further worsened [110]. This is because when the heart is suddenly reperfused with oxygenated

blood, the cardiomyocytes are exposed to extremes. This sudden change has a significant effect on the processes in the cell. Figure 2.3 shows that the  $\text{Na}^+/\text{H}^+$  pumps are inhibited, and the pH in the cardiomyocyte increases. Around 25%–45% of patients who die after CABG have histological evidence of the ischaemia/reperfusion injury [119]. When the condition of the heart is better monitored on ischaemia symptoms, the degree of the injury caused by the reperfusion can be decreased. Myocardial damage is one of the most common causes of morbidity and mortality after heart surgery [39]. The numbers of patients with myocardial damage after cardiac surgery can vary between 2–10% after CABG [119] and 29 % of AVR [69].

### 2.2.3. Early parameters of myocardial ischaemia

The simplified metabolism overviews of figure 2.1 & 2.2 and the ischaemic processes illustrated in figure 2.3 give a few interesting parameters to look into. These parameters will be discussed and the most promising parameters will be chosen to be further investigated in the second part of the literature study.

#### Lactate

First of all lactate, when the cardiomyocyte changes from aerobic process to an anaerobic process, the metabolism of lactate changes. Lactate originates from the breakdown of lactic acid in lactate and a hydrogen ion, see equation 2.1



As described in section 2.2.2, the cardiomyocyte uses lactate from outside of the cell to produce ATP during normal conditions. However, during the anaerobic process more lactate is being produced than used [108]. This is called hyperlactatemia [67], and it causes an increase of lactate in the cell. This increase of lactate causes a drop of pH in the cell because of the acidity of lactate [67]. When the cell pH drops below 7.35, and the lactate levels are higher than 5mmol/L, it is called lactic acidosis [113]. Another marker of lactic acidosis is a bicarbonate level of lower than 20 mmol/L in blood. Bicarbonate ( $\text{HCO}_3^-$ ) levels can be measured in the blood because it is a buffer of  $\text{CO}_2$  and pH [122]. There are two different types of lactic acidosis. Type A is caused by impairment of tissue oxygenation, hypoperfusion, hypoxia while type B is caused by toxin-induced impairment of the cellular metabolism [78]. In this review, the focus will be on the type A lactic acidosis. The disadvantage of the acidosis is that it stimulates cell apoptosis (cell death) when a cell is hypoxic. Lactate is not a physical parameter which is easy to measure [96]. Most lactate sensors that are being developed to measure lactate, measure lactate in sweat and tear fluid [48].

#### pH

The acidity of a cell is described by the measured pH. pH indicates the concentration of hydrogen ions in a solution inversely. It is the negative base 10 logarithm of the molar concentration of hydrogen ions. A pH of 7 is neutral at a temperature of 25°C. A pH of lower than 7 indicates acidity and greater than 7 indicate a basic solution. The pH of blood usually is between 7.34–7.45, while the cytosol of the cell usually has a pH of 7.2. Intracellular pH (pHi) is vital in the intracellular processes and for the membrane transport. The pH is lower intracellular than extracellular because there are fewer bicarbonates in the cell [116]. Cells use  $\text{CO}_2$  and  $\text{HCO}_3^-$  and phosphate buffers ( $\text{H}_2\text{PO}_4^-$  and  $\text{HPO}_4^{2-}$ ) to keep the pHi at an optimal level [27]. Figure 2.3 shows the role of pH during ischemia. The increase of the  $\text{H}^+$  activates the  $\text{Na}^+/\text{H}^+$  ion exchangers. This causes problems with the contraction capabilities of the cell, as described in 2.2.2. The body is continuously working to keep the pH level constant. Therefore, the interaction between the cell and the blood is essential. During ischaemia red blood cell in the intravascular space are used to accept protons. This can partially delay the decrease of the pHi and results in that the intracellular acidification is less compared with the extracellular pH [129]. This protects the cell against hypoxic, ischaemic and toxic injuries [70]. El Banani et al. [42] show that the drop of pHi immediately starts after ischaemia occurs. Both the drop of extracellular pH and intracellular pH have the potential to be a parameter which can be measured. In 1985 [64] showed the potential of measuring pH during cardiac surgery and Khabbaz et al. [63] proved that it was possible to measure the drop in pH caused by occlusion during surgery. In this study, three Khuri sensors were placed on the heart to monitor the pH level during cardioplegia. They showed a clear drop of pH of the posterior tissue in comparison with

## 2.3. Cardioplegia and Cardioplegia induced Cardiac Arrest

7

the anterior tissue. This indicates that there was a problem with the cardioplegia. This study showed that pH has a high potential to monitor the ischaemia in the heart.

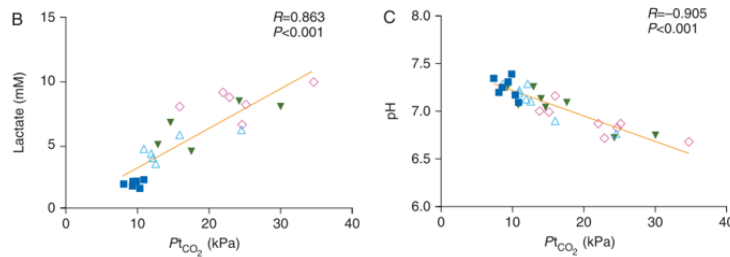
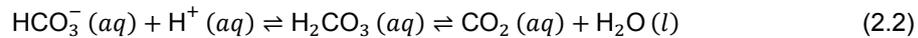


Figure 2.4: Pearson correlation revealed a significant correlation between myocardial PtCO<sub>2</sub> and tissue lactate (B) and tissue pH (C). Single values displayed as baseline (squares), blood flow 75% (open triangles), 50% (filled triangles), and 25% (diamonds). Reprinted from Pischke et al. [88]

### PCO<sub>2</sub>

PCO<sub>2</sub> stands for the partial pressure of carbon dioxide (CO<sub>2</sub>). Protons formed by the increase of lactate during anaerobic metabolism will react with HCO<sub>3</sub><sup>-</sup> to form water and CO<sub>2</sub> (see equation 2.2). Because there is no blood flow, the CO<sub>2</sub> will not be transported away and will accumulate in the cell. Pischke et al. [88] showed in their research that there is a correlation between the tissue CO<sub>2</sub> (P<sub>t</sub>CO<sub>2</sub>) and the tissue lactate and tissue pH. This can be seen in Figure 2.4. In Figure A.1 in Appendix A, the reaction of the pH, P<sub>t</sub>CO<sub>2</sub> and P<sub>t</sub>O<sub>2</sub> on a decreased blood flow is illustrated. Walters et al. [121] showed that it is possible to calculate PCO<sub>2</sub> from measured pH in a cardiomyocyte and vice versa. Tønnessen [116] started investigating in 1997 the possibilities of detecting PCO<sub>2</sub> as ischaemia detection, which led to the creation of the sensor tested by Pischke et al. [88]. This creation shows the potential of using CO<sub>2</sub> to measure myocardial ischaemia.



### O<sub>2</sub>

Oxygen is needed for the metabolism of the cardiomyocyte. StO<sub>2</sub> stands for the oxygen saturation of muscle tissue. During cardioplegia, the oxygen consumption of the cardiac cells can reduce up to 97% [50]. This means there is still a residual uptake of oxygen in the cell. This is slowly decreasing the oxygen level around the cardiomyocyte. Putnam et al. [92] showed that the StO<sub>2</sub> could detect regional changes before the change in lactate levels during CPB. On average, the lowest StO<sub>2</sub> was recorded 90 minutes before the highest lactate peak. Tissue oxygen saturation has the potential to be measured real-time, which makes it an interesting parameter. Most of the development of oxygen sensors are skin sensors. These type of sensors measure the oxygenation of a muscle or tissue by using Near Infra-Red and the absorption difference between oxygenated and deoxygenated blood cell. These type of sensors are getting more advanced such as the Humon Hex [7] or Moxy Monitor [10].

## 2.3. Cardioplegia and Cardioplegia induced Cardiac Arrest

As stated in the problem description in the introduction, cardioplegia is a common term used for pharmacological solutions. With cardioplegia, the heart can be arrested temporally. Dr Melrose was the first to discover that a high level of potassium citrate (K<sub>3</sub>C<sub>6</sub>H<sub>5</sub>O<sub>7</sub>) causes a temporal cardiac arrest [28]. A normal cardiomyocyte has a resting membrane potential of -85mV. The influx of sodium (Na<sup>+</sup>) leads to depolarisation of the membrane potential causing the cardiomyocyte to contract. The goal of cardioplegia is to target voltage-gated channels. The presence of potassium reduces the membrane potential making sure that the cardiomyocyte will not repolarise again. The resting potential is around -50mV when the voltage-gated channel will close, and the heart will go into a diastolic cardiac arrest. [20]. Figure 2.5 gives an overview of the influence of potassium on the membrane potential and the various channels. There are many different types of cardioplegia; there is no clear consensus on what is the best practice. Many similarities are found between different solutions [20]. All solutions have high levels of potassium chloride (KCl) (15-35mEq/L) and other electrolytes such as Mg<sup>2+</sup>, Ca<sup>2+</sup>, Cl<sup>-</sup>,

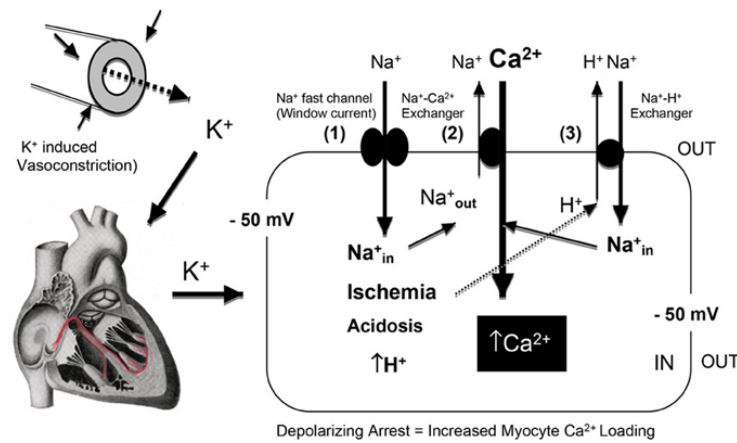


Figure 2.5: A schematic of the effect of hyperkalemia and prolonged myocardial membrane depolarization on  $\text{Na}^+$  entry through the "window current" and the net influx of  $\text{Ca}^{2+}$  into the cardiomyocyte via the reversal of the  $\text{Na}^+/\text{Ca}^{2+}$  exchanger. Reprinted from Dobson et al. [37]

$\text{Na}^+$  and Bicarbonates are added just before administration [28]. Cardioplegia can be administered in a single dose or with multiple doses. Single is more used in minimally invasive cardiac surgery and basic CABG because it reduces time and interruptions during the procedure. However, in more complex surgery, the multiple-dose cardioplegia achieves better myocardial protection [28]. The use of electrolytes in cardioplegia can interfere with measurements if the sensor would be based on measuring the electrolyte concentration in and around a cell. That is why the focus of this research will be on the physical parameters and not on electrolytes concentrations.

### 2.4. Selection of parameters

All four parameters discussed in 2.2.3 are interconnected with each other. A decrease of  $\text{O}_2$  causes an increase of the lactate in the cell. This increase of lactate causes a decrease of pH as well the increase of  $\text{CO}_2$ . The goal of this sensor is to measure cardiomyocyte ischaemia, mainly the lack of oxygen in the cardiomyocyte. Lactate has a direct influence on pH because lactic acid disintegrates in lactate and a hydrogen ion ( $\text{H}^+$ ) (eq. 2.1). However, pH is not only dependent on lactate. pH has multiple buffers (phosphate and bicarbonates) in the cell which try to keep the cellular environment at the same concentration. An increase of  $\text{CO}_2$  also influences the pH (eq. 2.2).  $\text{PCO}_2$  is measured in blood because it diffuses out of the cell into the bloodstream. At last, the  $\text{O}_2$  saturation can be measured in the tissue, but it says less about the acidosis inside of the cell.

Parameter	Advantages	Disadvantages	Depended on	Used to measure ischaemia
Lactate	Direct product of anaerobic glycolysis	Enzyme needed to measure lactate	pH	only in sport Payne et al. [85]
pH	Direct information about acidity in the cell	Buffer system in cell try to keep pH steady	Lactate Various buffers ( $\text{CO}_2$ , phosphate)	Khuri and Marston [64] Khabbaz et al. [63]
$\text{PCO}_2$	Measures the pH and the accumulation of $\text{CO}_2$	Influenced by the buffer system of pH	pH	Pischke et al. [88]
$\text{O}_2$	Oxygen is used by the cell and a decrease indicates a cell using too much oxygen	Only partial pressure or oxygen in haemoglobin can be measured easily	Oxygen uptake cell	Nichols et al. [81]

Table 2.1: Comparison of different parameters with the (dis)advantages of measuring them to monitor myocardial ischaemia

The (dis)advantages of the parameters are shown in table 2.1 and show performed studies to measure the ischaemia of tissue. Focusing on all four parameters will make this review long and exhaustive. Therefore a decision is made to focus on only two of the four parameters. These parameters are pH and Lactate. Although lactate is challenging to measure, lactate is chosen because it is the direct product of the ischaemia. pH is chosen as the second parameter because multiple studies show the direct correlation between pH and lactate [76, 88, 120] and Khabbaz et al. [63] already showed the capability to monitor ischaemia in the heart with pH. Therefore the second subquestions will focus on the different types of sensors which can detect lactate and pH.

## 3

## Type of Technologies

### 3.1. Sensing ischaemia

In this chapter, an introduction on sensors is given, and it will review different types of sensors used in the biomedical world. After this, a selection is made on which type of sensor this literature review will focus on. More information will be given on this type of sensing and techniques used to read-out the information. This chapter will finish with an elaboration on which type of sensing platforms and materials are used. The goal of this chapter is to answer the second subquestion:

*B: Which types of technologies are capable of measuring these parameters during a cardioplegia-induced arrest?*

In Chapter 2, these parameters were discussed, and eventually, pH and lactate were chosen as the parameter on which this literature review will focus. That is why the research question can be restated as:

*B: Which types of technologies are capable of measuring pH or lactate during a cardioplegia-induced arrest?*

To answer this question, it is essential to look at the concepts and types related to measuring biomedical signals.

### 3.2. Sensors and Transducers

A sensor is described as; *a device that responds to a physical stimulus (such as heat, light, sound, pressure, magnetism, or a particular motion) and transmits a resulting impulse (as for measurement or operating a control)* by Merriam and Webster Dictionary [11]. Yeow [130] states that "biomedical sensors are a subset of specialised sensors responsible for sensing physiological or biological measurands." Most biomedical sensors measure a physical property which they translate in a property which can be used in diagnostics or therapeutics. Figure 3.1 illustrates that to extract the information from the body a transducer is needed. This part converts the output of the body to a signal which can be handled and quantified. When a transducer is not working correctly, the information will be useless [118]. The second part of a sensor is the instrumentation. This is where the measurement is controlled. The output of the instrumentation will be processed into a signal which can be used and read. The definitions of sensors and transducers are often used interchangeably. Although the definitions are not the same, this literature review will use the term sensor in the continuation of this review. This is done because there is no agreement on the use of these terms in the literature. For the reason that the designation of these definitions makes little difference to the review, sensor will be used to avoid confusion.

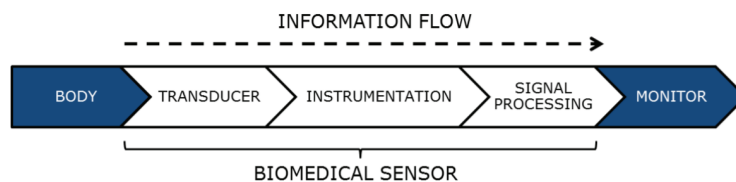


Figure 3.1: Information flow from the body to the monitor provided by the biomedical sensor. As found in Tronstad [118]

Two other definitions that are often used interchangeably; "biosensor" and "biomedical sensor". This is wrong because a biosensor is a type of biomedical sensor. It is a type of sensor which senses biological signals like enzyme, antigen, antibody, hormone, DNA, RNA and microbes. While a biomedical sensor is the umbrella term for all the sensors used in the biomedical field [137]. For this literature review, the focus will be on the biomedical sensor. The goal is to create an overview of all the sensor which are capable of measuring the parameters described in 2.2.3 and are capable of *in-vivo* measurements

### 3.2.1. Types of sensors used in biomedical sensors

There are different methods of classifying biomedical sensors. It is possible to categorise all the biomedical sensors in physical or chemical sensors [137]. Physical sensors can be split up into electrodes, measuring electrical changes or optrodes, where light is used as measurand. The chemical sensors include electrochemical, biosensors and chemiluminescence. This classification is not optimally for this research, because physical sensing can be more than only electrical or optical. Therefore, in this review, the classification as described by Shavanova et al. [104] Sharma and Khurana [102], Hajian et al. [53] and Singh et al. [106] will be combined into the following classification in figure 3.2.

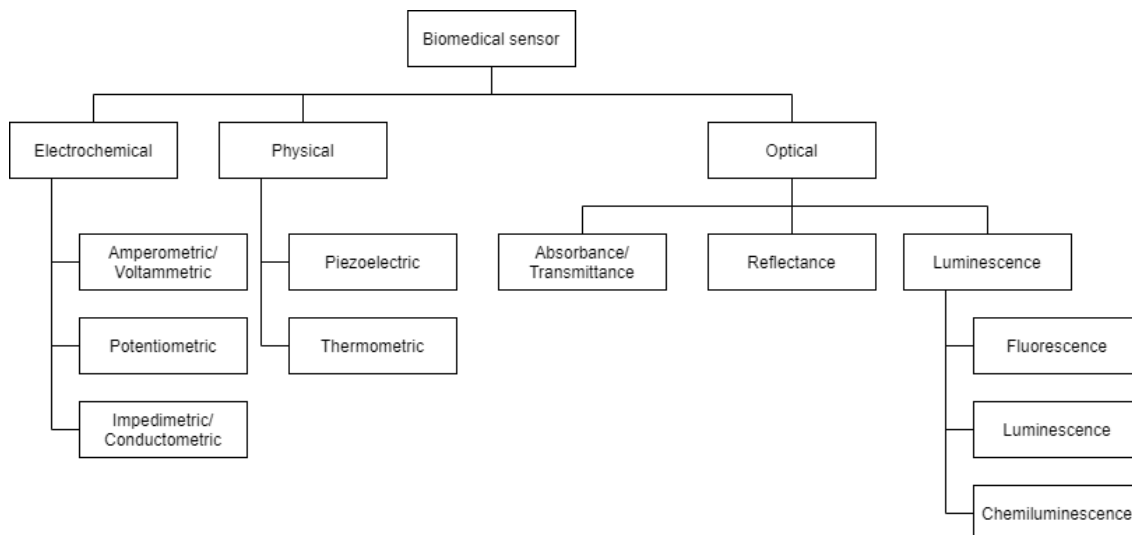


Figure 3.2: Classification of Biomedical sensor developed for this literature review by combining classifications of Shavanova et al. [104], Sharma and Khurana [102], Hajian et al. [53] Singh et al. [106]

#### Electrochemical

Electrochemical sensors are biosensors that make use of the electrical charge which is made by chemical reaction with the biological element. This reaction comes from a chemically selective layer which is called the recognition element [24]. Most electrochemical sensors are based on the potentiometric and amperometric principle. Potentiometric sensors measure the electrical potential with a high impedance meter and do not need an external source. Potentiometric sensors always need a reference electrode to measure the potential current [86]. Amperometric also need a reference electrode, but it measures the current generated by enzymatic or bio-affinity reaction at the surface of the electrode. A constant working potential is given on the working electrode. A redox reaction is always occurring at amperometric sensors [58]. Voltammetric have a similar working principle but measures the current as the potential is varied and is less used in the biosensing. Impedimetric sensors are less used, and conductometric sensors are a subset of impedimetric sensors [9]. Amperometric sensors are most successfully commercialised devices [104].

#### Physical

Physical sensors are based on their type of signal. This signal can be from a mechanical sensor which is measured by a piezoelectric principle. Piezoelectric sensors can be used to measure pressure, acceleration, strain or force [97]. Thermal sensor measures, for example, temperature by the thermometric principle. In thermometric sensing, the heat that occurs when a recognition element interacts with an enzyme is measured [104]. Other types of physical sensors like magnetic or radiant sensors are not relevant for this literature review [15].

#### Optical

Optical sensors are sensors that measure a change of light. This change can come from the absorption, the reflection or the scattering of the light. Absorption is related to transmission and therefore combined. The last light principle is luminescence; this is the emission of light of matter after excitation[14]. The

## 3.3. Optical Sensor

11

differences will be explained in section 3.3.1. Absorption based sensors measure the change in light by absorption of the tissue or solution [74]. Reflection based sensors measure the change of reflected light of the tissue or solution. Figure 3.3 shows the differences between the light principles. Section 3.3.1 will further elaborate light interaction with tissue.

## 3.2.2. Selection of sensor

Table 3.1 shows an overview of the sensors discussed in figure 3.2 with the (dis)advantages per sensor type. Of course, there are many different types of sensor per measuring principle, but it gives a good indication of which type of sensors are capable of measuring the pH or lactate of tissue or solutions. It is clear that the physical sensors are not capable of measuring pH or lactate, and for all the other type of sensors, there are already sensors made in the research field. Because the electrochemical sensors are more related to chemistry, can interfere with the oxidation and have lower specificity; this research will focus on optical sensors. Optical sensors in overall have no problems with electrical interference, do not need a reference electrode and can have higher information content in the signal. The higher information content is because the whole optical range can be used and an expensive spectrometer is used the interpret the signal out of the optical sensor. In section 3.3, an elaboration is given on the different types of sensors and the light interaction phenomena.

Type of sensor	Electrochemical			Physical			Optical	
Measuring Principle	Amperometric/Voltammetric	Potentiometric	Impedimetric/Conductometric	Piezoelectric	Thermometric	Absorbance	Reflectance	Luminescent
Possible ischaemia sensor	Yes	Yes	Yes	No	No	Yes	Yes	Yes
Example pH sensor in literature	Sha et al. [101]	Park et al. [84]	Awasthi et al. [22]	-	-	Zajic [132]	Zhao et al. [134]	Wencel et al. [124]
Example lactate sensor in literature	Payne et al. [85]	Onor et al. [83]	Zaryanov et al. [133]	-	-	Andrus et al. [21]	Sharma et al. [103]	Biswas et al. [26]
Advantages	<ul style="list-style-type: none"> <li>- High selectivity</li> <li>- Reproducible</li> <li>- Inexpensive</li> <li>- On-site measurement</li> </ul>	<ul style="list-style-type: none"> <li>- Rapid response</li> <li>- Reproducible</li> <li>- Simple technique</li> </ul>	<ul style="list-style-type: none"> <li>- No ref. electrode</li> <li>- Inexpensive</li> <li>- Miniaturisation</li> </ul>	<ul style="list-style-type: none"> <li>- High sensitivity</li> <li>- Simple structure</li> <li>- Reliable</li> </ul>	<ul style="list-style-type: none"> <li>- Wide range</li> <li>- No external power needed</li> </ul>	<ul style="list-style-type: none"> <li>- No electric interference</li> <li>- No reference electrode</li> <li>- Reagent no contact with optical fibre</li> <li>- Multiple measurements</li> <li>- Higher information</li> </ul>	<ul style="list-style-type: none"> <li>- Fast measurement</li> <li>- Great ranges</li> <li>- No dyes needed</li> </ul>	<ul style="list-style-type: none"> <li>- Chemilumi: simple instrumentation, low detection limits wide dynamic range.</li> <li>- Fluor: high sensitivity and selectivity.</li> <li>- Benefiting from mild hydrogel formation and sol-gel switching.</li> <li>- Chemiluminesce: lacks selectivity</li> <li>- Fluorescence: photobleaching</li> <li>- Loss of bio activity</li> </ul>
Disadvantages	<ul style="list-style-type: none"> <li>- Interference</li> <li>- Small range</li> </ul>	<ul style="list-style-type: none"> <li>- Unable to detect lower limit ions</li> </ul>	<ul style="list-style-type: none"> <li>- Sensitivity decreases by non-reacting ions</li> <li>- Low specificity</li> </ul>	<ul style="list-style-type: none"> <li>- No truly static measurements</li> <li>- Not suitable for pH and lactate sensing</li> </ul>	<ul style="list-style-type: none"> <li>- Reference</li> <li>- Not possible for pH or lactate</li> </ul>	<ul style="list-style-type: none"> <li>- Costly equipment</li> <li>- Susceptible to damage</li> <li>- Difficult modification</li> </ul>	<ul style="list-style-type: none"> <li>- Continuous fibre</li> <li>- Removal of cladding</li> <li>- Needs fluid</li> </ul>	
Reference	[78] [107]	[78] [107]	[78] [107]	[90]	[2]			

Table 3.1: Comparison of different types of sensors for their potential to measure pH or Lactate with examples

## 3.3. Optical Sensor

## 3.3.1. Light interaction

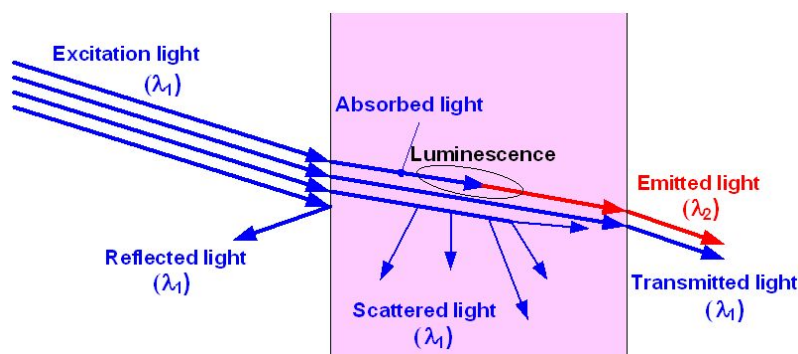


Figure 3.3: Interaction between light and matter. Different phenomena and their wavelengths. Reprinted from A. et al. [14]

There are several phenomena caused when light and matter interact. Light is defined by  $\lambda$  and the unit nm is used for the size of the wavelength. When the light gets reflected, scattered or transmitted, it keeps the same wavelength as the excitation light has ( $\lambda_1$ ). However, different wavelength ( $\lambda_2$ ) can be

emitted after absorbed light interacts with electron or molecules. When light hits matter, it can be absorbed, reflected or transmitted. For example, if light passes through a colour filter, some wavelengths will be absorbed while others will be transmitted. During absorption, the frequency of the light is around the energy level of the electrons in the matter. This causes the electrons to absorb the energy of the wavelength. This absorption causes a change in energy state. When the excitation light exists of multiple wavelengths, the wavelength corresponding to the energy level of the matter will be absorbed. Absorbance and transmittance are closely related in transparent matter because in a transparent material, there is always transmitted light. In opaque material, there is no transmitted light and therefore no relation between absorbance and transmittance [14]. In figure 3.4, this difference between absorbance and reflection is illustrated with the different denominations.

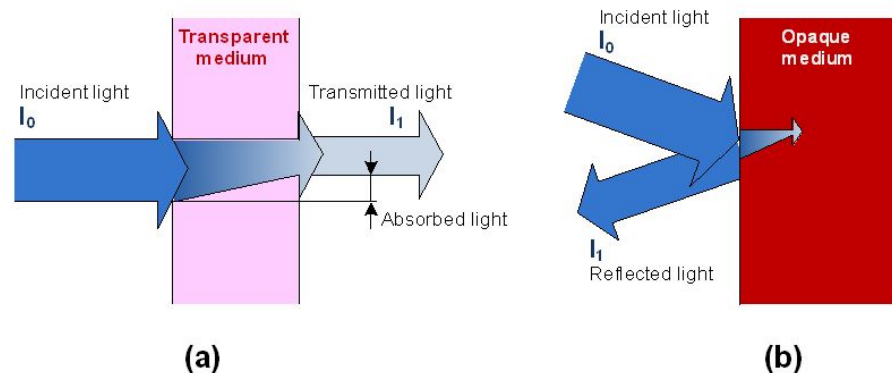


Figure 3.4: Absorption, transmission and reflection performance of the light: (a) in a transparent medium; (b) to face opaque medium. Reprinted from A. et al. [14]

When analysing light after absorption, a dip is seen in the transmission spectra, and a peak is seen in the absorption spectra. Absorbance has a logarithmic relationship with transmittance, see equation 3.1; with an absorbance of 0 corresponding to a transmittance of 100% and an absorbance of 1 corresponding to 10% transmittance.

$$A_{\lambda} = \ln \frac{I_0}{I_1} \quad (3.1)$$

$A_{\lambda}$  is the absorption coefficient, and it is possible to measure the change of intensity to relate this to the matter. Analysing the spectral distribution of light gives information about the matter the light has passed through. Reflection is a different light phenomena. In an optical fibre reflectance is the main factor of the functioning of an optical fibre. The internal reflection is almost 100% in optical fibres, and this makes it a excellent media to transfer information. If the cladding is removed of a fibre, this can change the internal reflection. Equation 3.2 shows the formula to calculate the coefficient of reflectance ( $\rho_{\lambda}$ ). This equation shows a one-to-one relationship between the incident light and the reflected light.

$$\rho_{\lambda} = \frac{I_0}{I_1} \quad (3.2)$$

Figure 3.3 shows two other light phenomena when matter is excited by light. Scattered light cannot be used to measure properties of matter because it is random and hard to detect. Scattered light is mostly seen as noise or loss of information. The last phenomenon is luminescence. This phenomenon causes a different wavelength to be returned than the excitation light [14]. There are three types of luminescence: fluorescence, phosphorescence and chemiluminescence. Fluorescence is based on the absorption of light and emitting a longer wavelength with lower energy. The release of a photon after an excited electrons falls back to a lower energy state. Phosphorescence can absorb the energy of a wavelength and store it for a time and release this later as an afterglow. The difference between fluorescence and phosphorescence are illustrated in figure 3.5. Chemiluminescence is luminescence caused by a chemical reaction. The chemical reaction causes the electron to get excited, and when the electron falls back to its ground state, it releases light [12].

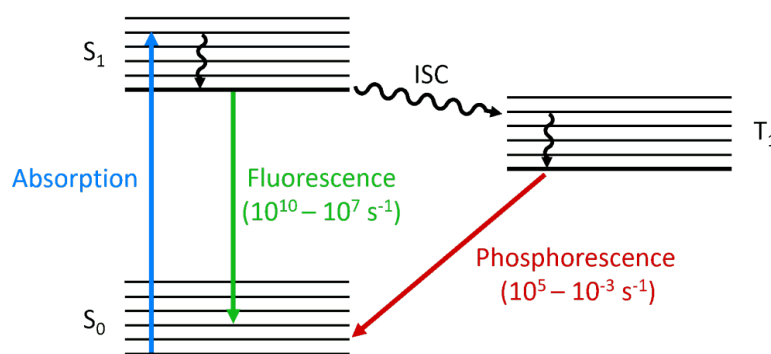


Figure 3.5: Jablonski diagram of fluorescence and phosphorescence processes and their typical rate constants. Reprinted from Flu [5]

### 3.3.2. Measuring of light

Pirzada and Altintas [87] did an extensive review of the different types of measuring techniques used in optical sensors in the field of bio-sensing and are shown in figure 3.6. This section will give a brief description per type of measuring technique, and the feasibility of in-vivo testing is taken into consideration. Changes in light intensities are measured by photodetectors and the most common instrument used to detect light intensities is an optical spectrometer. It exists of a wavelength splitter and photodetectors. In the early days a prism was used to split the wavelengths. Nowadays, a diffraction grating and movable slits are used to split the wavelengths.

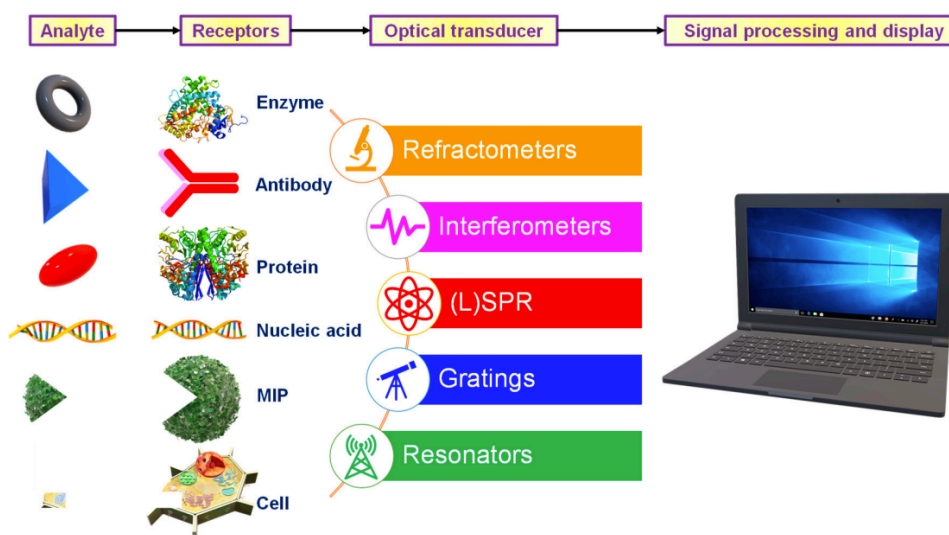


Figure 3.6: Construction of different optical sensors. Reprinted from Pirzada and Altintas [87]

#### Refractometers

Refractometers are based on the different refractive index of different materials, the light that goes through an optical fibre. It is mostly used to analyse samples when the light transfers from air to liquid the light will slow down and will bend following Snell's Law. This bending can be measured and related to the substance of the analyte. This method is not suitable for in vivo testing.

#### Interferometers

Interferometry measures the difference of interference of light beams. Usually, the light comes from a single source and is split up into different beams which follow different paths. This path difference will change the phase of the light. When the beams come together, the phase difference will cause an intermediate intensity pattern. For example, in biosensors, the interference can be caused by the difference of two surfaces, a layer on the tip of the sensor, which can bind with a ligand, and an internal

reference layer. Figure 3.7 shows an example of binding molecules on the tip changes the interference between the two layers [126]. This difference of interference is visible by a spectrometer or photodetector. Interferometry is a suitable method for in vivo testing.

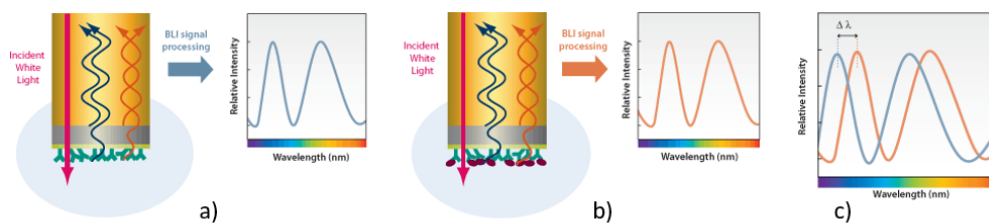


Figure 3.7: This figure shows the working mechanism of biointerferometer. a) layer of immobilised protein on the biosensor tip, and an internal reference layer result in a specific wavelength intensity. b) when a ligand binds to the surface tip the properties change and a different interference is observed. c) the difference of wavelength contains information about the measurand. Modified and Reprinted from Wikipedia [126]

### Resonators and Surface Plasmon Resonance

Resonators are techniques which are based on the change of resonance when a molecule binds to a ligand. The most common type of resonator is the Surface Plasmon Resonator. Another type of resonator used in biosensing is an optical ring resonator. The optical ring resonators are not suitable for in vivo sensing on tissue [111]. Surface Plasmon Resonators work by sending light against a metal film. This metal film is connected to ligands which can connect with biomolecules. The light reflected from this metal film is measured while the excitation light changes its angle. At a certain resonance angle, the plasmons resonate with light; this causes an absorption of the light in that angle. This absorption will develop a dark line in the read-out. SPR can use a spectrometer or a single photodetector, and figure 3.8 shows the working principle of SPR. SPR can be suitable for in vivo testing, but this can be difficult as there are light angle changes needed for the measurements [25].

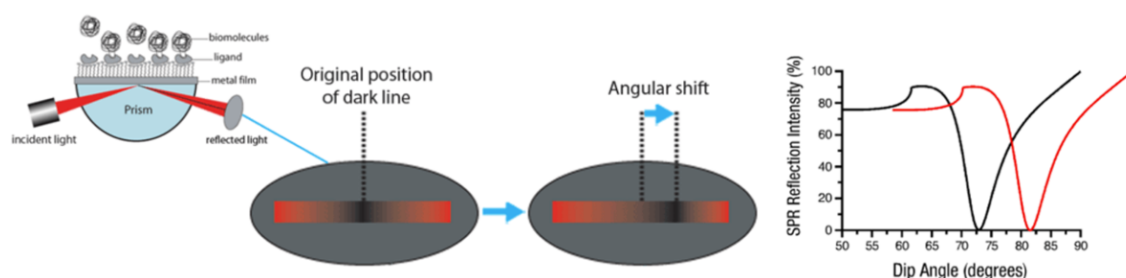


Figure 3.8: The excitation of surface plasmons results in a dark line in the reflected beam, and the angular position of the dark line shifts as a molecule binding event takes place. SPR causes an intensity dip in the reflected light at the sensor surface. A shift in the curve represents molecular binding. Modified and Reprinted from Biosensin Instruments [25]

### Gratings

Gratings are techniques based on the periodic structure that splits and diffracts light into several beams travelling in different directions. The most common type of grating used in optical sensing is the fibre Bragg grating. It is the grating of an optical fibre with periodic variation of the refractive index of the core. This change of refractiveness generates an optical filter which can be specified for specific wavelengths [57]. Figure 3.9 shows how the core refractive index changes the spectral response. Gratings can be a suitable method for measuring in vivo, but it is challenging because of the fabrication method and the need for a continuous fibre.

### Raman Scattering and FTIR

The last type of technique is Raman Scattering or Fourier Transform Infrared spectroscopy. These types are not taken into consideration by Pirzada and Altintas [87] but still are often used to measure properties of materials or fluids. The difference between Raman scattering and FTIR is that Raman

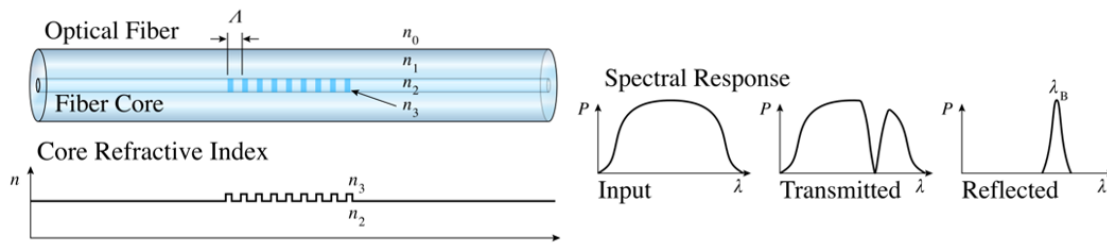


Figure 3.9: A Fiber Bragg Grating structure, with refractive index profile and spectral response. Modified and reprinted from [4]

Scattering is based on the scattering of light while FTIR is based on the absorption of light. The light used with these methods is usually a monochromatic laser. This laser interacts with molecular vibrations and phonons. It causes a change in the laser energy, and the light is scattered. When measuring the Raman scattering, a filter is needed to eliminate the stronger Rayleigh scattering. In biosensing, the Surface Enhanced Raman Scattering is used more often because it can detect single molecules [82].

### 3.3.3. Optical sensing platforms

There are two main types of optical sensors platform, a planar sensor or an optical fibre sensor [125]. The planar sensor has some advantages over the optical fibre; it is more robust, better compatibility for microfabrication techniques, better integration with lab-on-a-chip systems. It is optimal for integrated optical sensor and can be used for multi-analyte sensing. [125].

An optical fibre gives the possibility to measure in locations which are otherwise hard to access. It allows the equipment to be further away from the tissue or substance. When the light passes through the fibre, it only has very low attenuation, and noise from other sources are reduced [14]. Optical fibre also allows for combining multiple fibres for an optical network. In optical fibre sensing, there are two types of sensing. Intrinsic or extrinsic are depended on the interaction between the measurand and the light.

An intrinsic sensor measures the changes that happen inside of the optical fibre. The optical fibre is the sensor itself and measures changes in the characteristics of the fibre such as intensity, phase, wavelength and transit time [19]. An extrinsic sensor uses the optical fibre to transfer the light to and from the sensing area. The optical fibre remains unchanged, and the change is outside of the fibre. The light that is sent in is recollected for the detection [19]. Both intrinsic and extrinsic sensors are capable of measuring in-vivo.

There are three types of planar sensors. There are two types of nonwaveguiding planar sensors. In the particle planar nonwaveguiding sensors light is send at particles which interact with the material. This light interacts with the particle, and a detector measures the response. In the planar nonwaveguiding sensor, a gel matrix is used to trap the particles. In these gel matrices, fluid can interact with the particles, and a detector can measure the response. It allows for better control of the measurements and better reproducibility of the sensors. Waveguiding planar sensors work differently, using a medium

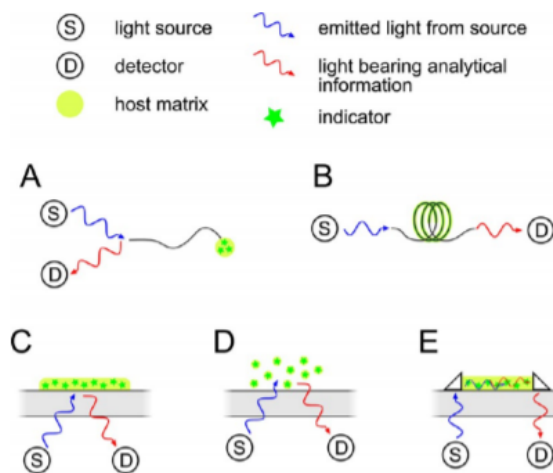


Figure 3.10: Schematic representation of different sensor platforms: (A) fiber-optic tip sensor, (B) fiber-optic evanescent field sensor, (C) planar nonwaveguiding sensor, (D) planar nonwaveguiding sensor particles, and (E) planar waveguide sensor. Reprinted from Wencel et al. [125]

they guide the light through a material which interacts, with the environment and the light. The response of this interaction is again guided to the detector. This type of sensing gives even more control over the measurements. Another variation of the waveguiding sensor is a medium which is non-transmissive in specific concentrations and becomes more transmissive when the environment changes. This increase in transmission can result in more response from the detector. Waveguiding planar sensors are the most promising for in vivo sensing because of the increased control and trapped particles in gel-matrix.

#### **3.3.4. Materials used in optical sensors**

There are multiple materials used to improve the measurements of optical sensors. It varies from gel matrices which trap particles or interact with the environment themselves, to particles made to interact with the environment like fluorophores and dyes. Each type of material will be discussed briefly, and their advantages will be mentioned. The matrix which interacts with the environment is an essential part of the in-vivo sensor. A good transfer of information is needed, and no biological reaction is wanted (bio-inert). So the matrix has to be bio-compatible, accurate and reproducible. Most optical sensors make use of a gel matrix. Often hydrogels/sol-gels are used. A sol-gel is a gel-like material made from inorganic substances. A hydrogel is a type of sol-gel. It is a super-absorbent gel made from natural or synthetic polymers. Up to 99.5% water by volume is retained between the polymer network of the gel [8].

Fluorophores, dyes, probes and quantum dots are all compounds that are used with fluorescent optical sensing. All these compound emit a higher wavelength light when they are excited by light. These terms are often used interchangeably, but this is not always correct. Fluorescent dyes can be grouped into organic dyes, biological fluorophores and quantum dots [6]. Dyes can be absorption or fluorescent-based. When a dye is fluorescent-based it is a reactive dye. Probes are a substitute term for fluorophores.

Quantum dots are different, they are semiconductor nanoparticles ranging in size from 1nm to 10nm, and these particles can be used as fluorophores. Quantum dots can have a wide range of optical properties not present in organic fluorophores. Quantum dots have a brighter emission and a higher signal to noise ratio compared with organic dyes. However, the toxicity of quantum dots to cells is a significant issue and therefore not often used for in-vivo sensing [1]



## Literature study

## 4

## Literature search

### 4.1. Finding the best optical ischaemia sensor

In the following chapter, the central part of the literature review is discussed. First of all, the method of the literature search is elaborated. From analysing multiple reviews, a search strategy is shaped with additional selection criteria. The various designs from this literature search are discussed to give an overview of all the techniques currently being used. All three different types of optical sensors are reviewed. Following this, all sensors are assessed on their potential to be an ischaemia sensor during a cardioplegia induced arrest. Ultimately, the limitations of this review will be discussed, and a recommendation for further work will be made. The goal of the literature review is to answer the last subquestion:

*C: What is the most feasible technique of the chosen technology that can be used to measure the parameters during a cardioplegia-induced arrest?*

Chapter 3 describes why this research will focus on optical sensing, while the decision to focus on pH and lactate is described in Chapter 2. This is why the research subquestion can be reformulated as the following:

*C: What is the most feasible optical sensing technique for measuring pH or lactate during a cardioplegia-induced arrest?*

By answering this last subquestion, the general research question can be answered.

## 4.2. Method of literature search

### 4.2.1. Identifying gaps in the current literature

The search for small pH and lactate sensors is not new. The first pH sensor was the glass electrode and was invented in 1920 by Duncan McInnes and Malcolm Dole [49], and the first pH sensor was tested in the heart in 1976 [44]. In 1985 a pH sensor developed by dr. Khuri was used during cardiac surgery [64] as described in 2.2.3. All of these sensors are electrochemical, while this is still the most used type of biosensors the optical sensors are emerging. In the field of pH and lactate sensing, multiple reviews have been written. These reviews are the basis on which this review builds, but these reviews do not cover the full aim of this review. This review will look into the development of metabolic optical sensors which are capable of measuring the physiological range of the indicators described in 2.2.3.

At first, a literature scan was performed to find all the latest reviews about the subject. Only PubMed was used for this scan, to focus more on the medical orientated journals instead of the chemistry orientated journals. For this scan the following search term was used: (*"pH" OR lactate*) AND ( *\*sensor\** ) AND ( *\*optic\* OR \*chemical\** ) NOT (*\*drugs\* OR glucose*). The results were filtered on **review, 2010-2020** and language **English**. Optic and chemical were added to the search term to include all reviews about optical sensor and chemical, to make sure that the optical sensors which used chemical parts in their sensor were included. A decision was made to exclude glucose and drug-based sensors. These terms resulted in many more results and were determined not to be essential. The search term in Scopus gave 230 results, of which 132 in chemistry journals. The PubMed search resulted in 132 reviews. These reviews were evaluated, and of these 132, 13 were found useful for the first scan. After evaluating these papers, three more additional reviews were found useful to determine the search strategy. Alam et al. [18], Pundir et al. [91], Sigaeva et al. [105] gave useful insights into; Point-of-Care, lactate (bio)sensors and the optical detection of molecules. After thoroughly examining the reviews, the following gaps were identified.

Current reviews:

1. Are focused on pH or Lactate, not ischaemia
2. Are focused on a smaller theme such as the type of technique, in vitro, POC, electrochemical or nanotechnology
3. Are focused on a broader theme (biosensors, biomedical application)
4. Which are about a fluorescent sensor, are often just about different types of dyes
5. show that the last extensive reviews about optical pH, lactate sensing are from before 2015

Therefore this literature review should focus on sensors which; measure lactate and pH monitoring within the physiological range, are published in the last ten years (2010-2020), describe optical sensing through absorption, reflection or fluorescence and are based on an optical fibre or planar sensor.

#### 4.2.2. Search strategy

This review is interested in the potential to measure ischaemia with a sensor. In 2.4 is explained that the focus of measuring ischaemia will be on pH and Lactate. In 3.2.2 is elucidated why the focus will be on an optical sensor. Section 4.2.1 identified multiple gaps in existing reviews. To tackle these gaps and to find the best possible sensor, a search strategy was constructed. This search strategy exists of multiple parts which are shown in figure 4.1. Although the review scan was only executed in PubMed, this scan is performed in Scopus. It was done to include all possible sensors which show potential to be able to measure within the physiological range. The reviews discussed in section 4.2.1 showed more than enough progress in the development of sensors in the last ten years, so the literature scan only included articles from 2010-2020.

AND					
	<i>Parameter</i>	<i>Transducer</i>	<i>Type of sensing</i>	<i>Tissue</i>	<i>NOT</i>
<b>OR</b>	"pH"	*sensor*	*optic*	"in vivo"	nerve
	lactate*	*transducer*	*fibre*	myocyte*	kinematics
	*lactic*		*luminescent*	cardiomyocyte*	
			*fiber*	myocard*	
			*fluorescent*	tissue	
				blood*	
			*muscle*		

Figure 4.1: Search terms used in literature search in Scopus

#### 4.2.3. Selection criteria

In section 4.2.1, the focus of the review is described, and in section 4.2.2, this is translated into a search strategy. However, to compare different articles, a minimum of information is needed. Therefore, the various articles will be selected on the following criteria.

1. Not a review article
2. Set up described with an optical sensor
3. Sensing lactate or pH
4. Can measure in or around the physiological range of lactate (0-5mM) and pH (6.0-8.0)
5. Has the possibility to measure in-vivo

Articles that meet these requirements will be further elaborated in this study. After this elaboration, each article will be evaluated on five criteria to assess for the most significant potential. In this evaluation, the most important criteria are if the sensor is measuring the physiological range and the applicability for measuring in vivo. It is different from the five selected criteria above, because when a sensor has the possibility to be used in vivo, this does not mean that it will be easily applicable. The third and

fourth criteria for the most significant potential will be more specific on the capabilities of the sensor concerning the resolution/accuracy and the response time for the sensor. The resolution or accuracy should be below 0.1 for both pH and lactate. The response time should be around 1-2 minutes with the possibility to be decreased in future work. At last, the manufacturability of the devices is checked. It is done because the master thesis following this literature review is limited in time and resources. Therefore a well-considered choice must be made.

### 4.3. Results of Literature Search

#### 4.3.1. Outcome of the literature scan

A total of thirty-seven studies were identified for inclusion in this review. The search of the SCOPUS database provided a total of 1,004 articles, while 298 other records were found through other sources such as PubMed and Google Scholar. After duplicate removal 1,050 records remained eligible for screening. Succeeding the title abstract screening, 154 full-text articles were assessed for eligibility. Of these, 129 were articles were excluded for various reasons, which can be found in figure 4.2. In total, twelve more articles were found through reference checking of the remaining twenty-five articles. It resulted in thirty-seven articles which are included in this literature review. Seven articles found were designed to measure lactate levels. Thirteen articles are absorption-based optical sensors, fourteen are fluorescent-based sensors, and five are sensors based on the reflection. All thirty-seven sensors will first be described in the following section. This is done because all sensors use a different technique or a different set-up. The short description also states the most important findings of the study. Hereafter, the sensors will be discussed per type of light phenomena, and the potential of the techniques is elaborated.

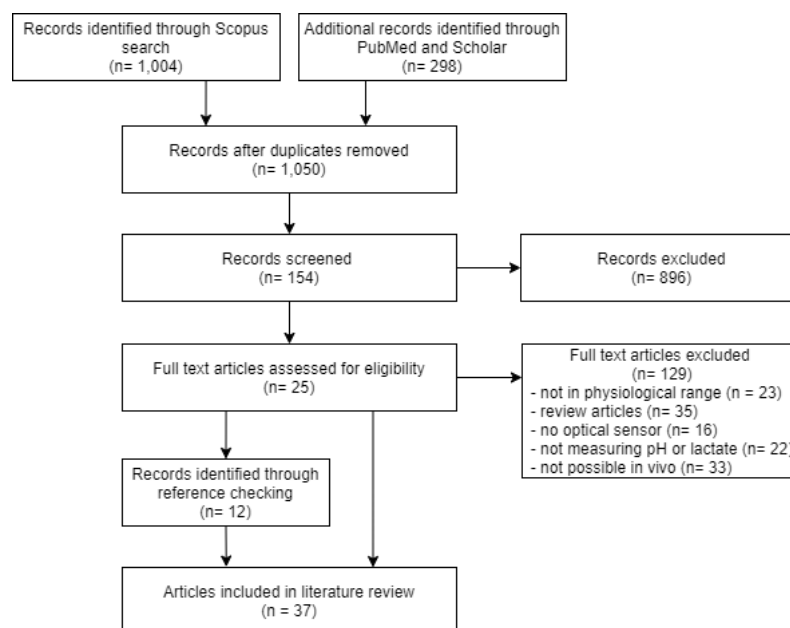


Figure 4.2: Flow diagram of records included in this literature review

#### 4.3.2. Optical lactate sensors

In table 4.1, an overview is given on the lactate sensors found in the literature. Seven different types of sensors were evaluated, five of them are optical fibres, and two are planar sensors. Most articles did not describe drift, resolution, shelf life or dry bleaching. Therefore these are not evaluated and compared. Jernelv et al. [60] combined a quantum cascade laser with a mercury-cadmium-telluride (MCT) detector to measure medical analytes. Two different sensors were tested, an attenuated total reflection spectroscope and a transmission spectroscope. The transmission spectroscope was extrinsic and worked on the absorption principle and had a range between 0-10 mM and the diameter of the fibre was 400  $\mu\text{m}$

Ref	Year	Fibre/Planar	Type sensing	AB/FL/RE	IN/EX	Measured in	Reactive material	Gel matrix	Use QD	Ratio metric	Excitation Peaks	Peaks Measured	Range	Diameter fibre	Reproducibility	Accuracy	Response Time
[60]	2019	fibre	RES	AB	EX	test sol	-	X	-	X	1200-900 cm <sup>-1</sup>	1040 cm <sup>-1</sup> 1124 cm <sup>-1</sup>	0-10 mM	400microns	-	-	10s
[23]	2020	fibre	NIR SPC	AB	EX	test sol	-	X	X	X	NIR	1233, 1710, 1750, 2205, 2319, 2341 nm	0-14 mM	-	-	-	instant
[136]	2010	fibre	-	FL	EX	in vitro (single cell)	LDH	X	X	Yes	360 nm	460 nm	0.0-1.5 nM	0.2 microns	-	-	-
[26]	2017	fibre	-	FL	EX	in vitro (flow cell)	PEM lined microparticles	YES (alginate)	X	Yes	420 nm 540 nm	710 nm	0.1-1.1 mM	-	-	-	-
[103]	2019	fibre	SPR	RE	IN	in vitro	L-LDH NAD	YES (TEMED)	X	X	-	560-620 nm	0-10 mM	600microns	good	9.50 nm/mM	1 min
[40]	2016	planar	IR SPC	AB	EX	on vivo	-	X	X	X	NIR	NIR	0-16 mM	-	good	-	-
[21]	2015	planar	-	FL	EX	in vitro	LOx	YES (pHEMA)	X	+	-	-	0.1-4.2 mM	-	-	-	15 min

Table 4.1: Overview of lactate based sensors found in the literature. RES: resonator, (N)IR SPC: (Near)InfraRed Spectroscopy, SPR: Surface Plasmon Resonance, FL: fluorescent based sensors, AB: absorption based sensors, RE: Reflection based sensor, IN: Intrinsic sensor, EX: Extrinsic sensor, \*Quantum cascade laser,

Ref	Year	Fibre/Planar	Type sensing	Measured in	Reactive material	Gel matrix	Use QD	Ratio metric	Excitation Peaks	Peaks Measured	Range	Diameter fibre	Reproducibility	Accuracy	Resolution	Response time	Dry bleaching
[47]	2012	fibre	R SPC	Test solution	polymer polyaniline	polymer polyaniline	X	X	-	605 nm 832 nm	2.0-12.0	800 microns	-	-	-	-	-
[95]	2012	fibre	SPC	Test solution	brilliant yellow	(poly(allylamine hydrochloride))	X	X	White light	497 nm	6.8-9.0	600 microns	-	4.65 nm/0.2 pH	0.2	-	-
[59]	2013	fibre	IFM	Test solution	Neutral Red	YES (TMOS, MTMS)	X	X	White light	536 nm 461 nm	6.0-9.0	600 microns	good	50 mV/pH	-	20s	-
[117]	2014	fibre	LSPR	Test solution	AuNPs with chitosan poly(sodium 4-styrenesulfonate)	NO	X	X	White light	532 nm	6.5-8.0	125 microns	-	8.67nm/pH	-	26s	none
[132]	2014	fibre	SPC	Test solution	methyl orange bromothymol blue	YES (TMOS)	X	X	halogen lamp	MR:400, 550 MO:520, 450 BB:450, 630 nm	3.0-7.6	400 microns	-	-	0.03	-	BB bleaches
[114]	2015	fibre	-	on vivo (skin)	brilliant yellow	YES (Alginate glycerol)	X	X	-	600 nm	5.0-8.0	800 microns	-	-	-	1-5 min	-
[65]	2017	fibre	SPC	tissue samples	Neutral Red PAA	X	X	X	White light	640-760 nm	6.0-8.0	300 microns	-	-	0.08	1s	-
[79]	2017	fibre	GRT	Test solution	sodium alginate	YES (TEMED)	X	X	Broadband	1530-1550 nm	2.0-12.0	-	good	0.66nm/pH	-	2s	none
[54]	2019	fibre	GRT	bio samples	anthocyanins	(polyethylene glycol diacrylate)	X	Yes	520 nm 638 nm	520 nm 638 nm	2.5-10	100 microns	-	-	-	3 min	-
[56]	2012	planar	IFM	Test solution	Congo red	YES (TREOS, TriEOS)	YES	Yes	400 nm	525 nm 605 nm	2.0-6.0	-	-	-	-	60s	-
[43]	2013	planar	IR SPC	on vivo	Basic fuchsin	-	X	X	NIR	NIR	4.0-9.0	-	-	-	0.045	2s	-
[31]	2013	planar	REF	-	Purple cabbage pigment	YES (TEOS EtOH)	X	X	632 nm	533 nm	2.0-11.0	-	good	-	0.003	2 min	-
[62]	2016	planar	-	in vitro (cell culture)	Phenol red indicator	NO	X	Yes	545 nm 680 nm	555 nm	6.5-8.1	-	good	-	0.1	-	none

Table 4.2: Overview of absorption based pH sensor found in the literature. IFM: interferometer, (IR)SPC: Infra Red Spectrometer, R SPC: Raman Spectrometer, REF: Refractometer, GRT: Grating based sensor

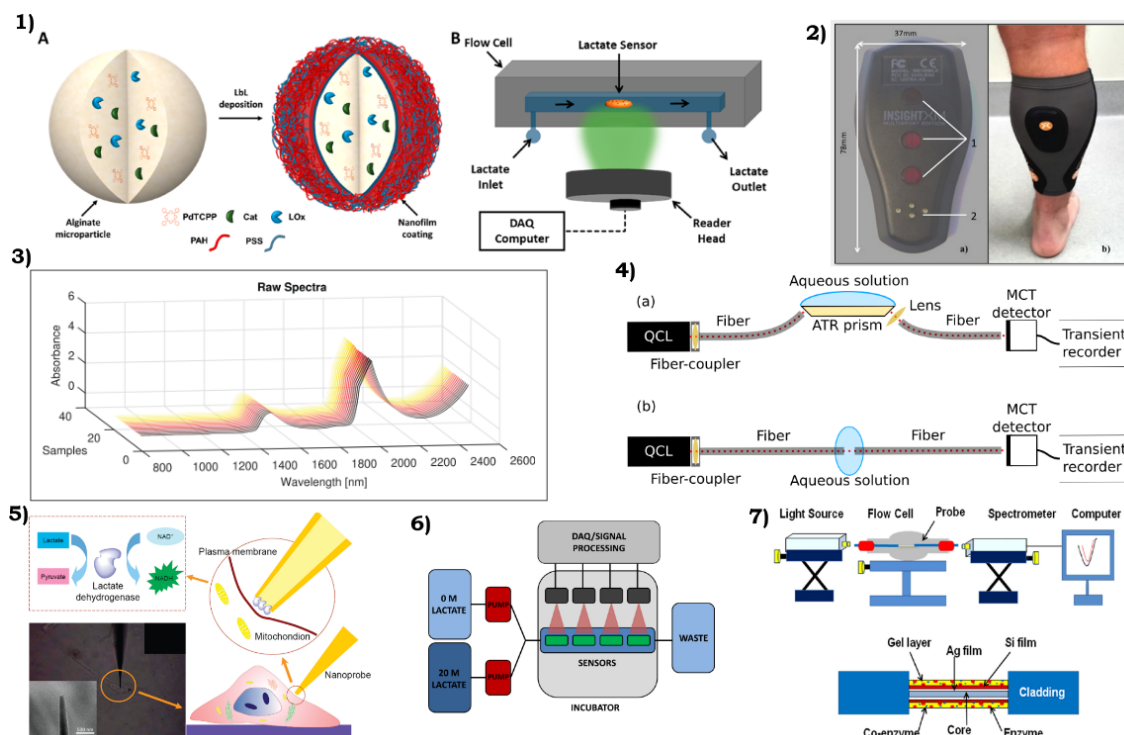


Figure 4.3: Overview of results and set-ups used in the optical lactate sensors: 1) Micro-particles and readout system of Biswas et al. [26] 2) BXInsight sensor used in Driller et al. [40] 3) the NIR spectra found by Baishya et al. [23] 4) Set-up for measuring lactate and other bio-samples of Jernelv et al. [60] 5) Overview of micro-tip used for single-cell lactate measurements of Zheng et al. [136] 6) Lactate readout of Andrus et al. [21] 7) Flow cell set-up by Sharma et al. [103]

and a fast response time. Baishya et al. [23] designed an optical fibre absorption sensor using Near-Infrared spectroscopy. This sensor measured the change in lactate extrinsic, and discovered that multiple wavelengths could be linked with lactic acidosis. A halogen tungsten lamp was used and indium gallium arsenide (InGaAs) and polycrystalline lead sulfide (PbS) as detectors. The sensor had a swift response time and a range between 0-14 mM. Zheng et al. [136] designed a fluorescent-based nanosensor which can measure a single cell in vitro. The released lactate was catalysed by LDH which produced fluorescent NADH, and this fluorescence was excited and collected by a fluorescence detection system. The sensor had a high spatial resolution, low background interference and a dynamic range (0.06-1 mM) comparable to the physiological range of the single-cell released lactate. Biswas et al. [26] designed a hydrogel-based fluorescent sensor, which included enzymatic microsensor embedded in a hydrogel matrix. In this sensor, LOx was encapsulated in an alginate micro-particle, which was coated with a phosphorescent metalloporphyrin layer. These micro-particles were excited with 530 nm, and the emission had a wavelength of 710 nm. The range of the sensor was in the range of 0.1-1.1 mM. Sharma et al. [103] was the only lactate sensor based on reflection; it was an intrinsic sensor which used Surface Plasmon Resonance to detect lactate in the range of 0-10 mM, with a sensitivity of 9.50 nm/mM. It made use of tungsten halogen lamp, an optical fibre with a uncladded part and a spectrometer. The uncladded part was coated with silver, silicon and a hydrogel filled with enzymes which react with lactate. These enzymes were lactate dehydrogenase (LDH) and NAD<sup>+</sup>. Interaction between lactate and the functional layer with the enzymes changed the refractive index of the hydrogel. Driller et al. [40] tested a non-invasive near-infrared (NIR) lactate sensor to measure the production of lactate during exercises. This extrinsic sensor measured the absorption of the near infrared light which changed with the secretion of lactate. The sensor is commercially available and designed by BSXinsight. The sensor used three NIR LED's and calculated the lactate levels in the cell by the absorption. No more details were available from this device since 2016. Andrus et al. [21] designed a planar fluorescent based lactate sensor which used a hydrogel with Lactate Oxidase (LOx). They tested the sensor in-vitro and used a red excitation source with the peak at 627 nm. They achieved a range between 0.1-4.2 mM. The response time was around 15 minutes, and the signal retention after 20 cycles was 70-81%.

### 4.3.3. Absorption based sensor

All absorption based sensors found in the literature which meet the requirements are extrinsic. All the absorption based sensors are not reporting any drift or shelf life, so this information is left out of table 4.2. Figure 4.4 shows all optic fibre-based absorption sensors, and figure 4.5 shows all the planar sensors found in the literature.

#### Optical Fibre

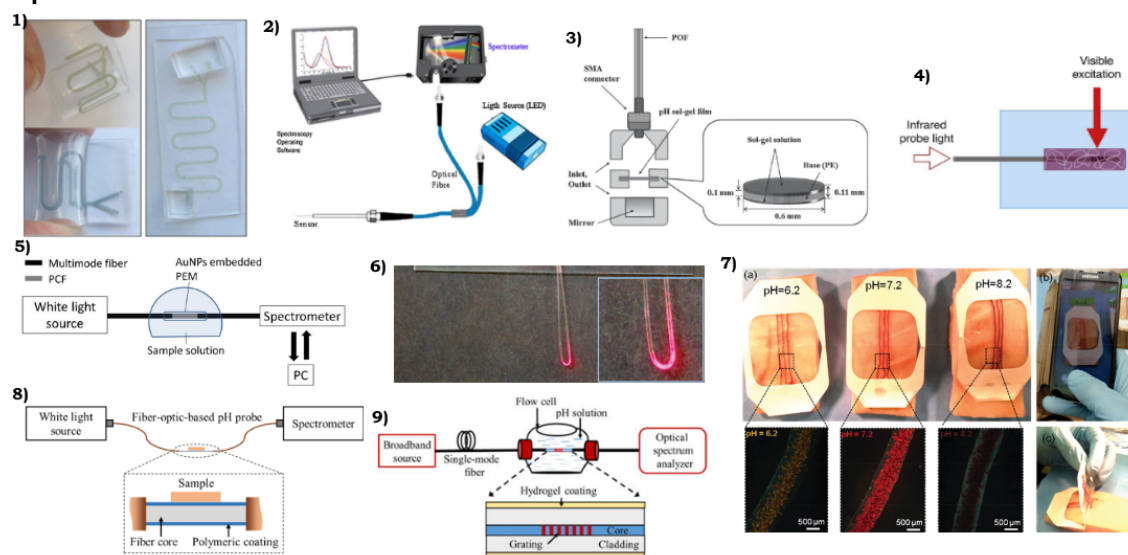


Figure 4.4: Overview of fibre-based absorption sensors: 1) Polymer polyaniline microfluidic channels of Florea et al. [47] 2) Sensor set up of Raoufi et al. [95] 3) Sol-gel film with neutral red of Jeon et al. [59] 4) Infrared probe with chromophores by Hartings et al. [54] 5) Continuous optical fibre set up with gold nanoparticles by Tou et al. [117] 6) U shaped optical fiber with the spectroscopy outcome of bromothymol blue of Zajic [132] 7) Flexible Hydrogel fibers for epidermal application by Tamayol et al. [114] 8) Fibre optic pH probe by Kim et al. [65] 9) Optical fibre coated with a hydrogel with a long period fibre grating and the corresponding transmission dip of Mishra et al. [79]

Florea et al. [47] designed a fast microfluidic photometric device which measured pH through a polyaniline (PAni) coating. This extrinsic sensor reacted on the absorption of PAni, which caused the light to change. A pH test solution was fed through micro-fluidic channels. The UV-VIS spectra were measured with an optical fibre with the diameter of 800 $\mu$ m and a mini spectrometer. The pH-sensitive peaks were 605 and 832 nm, and they were able to measure the range of 1.0-12.0 pH. Raoufi et al. [95] designed a optical pH sensor which was based on the absorbance of brilliant yellow. They used a layer by layer technique with as cross-linker polyallylamine hydrochloride (PAH). They found out that the sensitivity was depended on the number of layers and concluded that six double layers had the best sensitivity between 6.80-9.00. It is an extrinsic sensor because it measured the change outside of the optical fibre with a diameter of 600  $\mu$ m. They recorded a resolution of 0.20 pH. Jeon et al. [59] designed a sensor based on a sol-gel film with as the pH indicator Neutral Red (NR). The light of the optical fibre with a diameter of 600  $\mu$ m was sent through the film and reflected by a mirror. The reflected light was measured by a spectrometer. The absorbance and the intensity of light were used to determine the pH of a test solution. A white light source was used (210 - 2000 nm), this resulted in a basicidic absorbance peak between 461 nm and an acidic absorbance peak at 536 nm. The range of the sensor was between 6.0-9.0 pH. It showed a fast response time (20s). Tou et al. [117] described a sensor which used localised surface plasmon resonance to measure the response of polyelectrolyte multilayers with gold nanoparticles. This layer was placed on a photonic crystal fibre between two multi-mode fibres. White light was inserted in this fibre, and on the end of the other fibre a spectrometer was placed. The height of the absorbance peak depends on the number of bi-layers. The peak is at 532 nm and is capable of measuring a range of 6.5 and 8.0. The fibre had a diameter of 125  $\mu$ m. Zajic [132] designed a simple U shaped fibre optic sensor with a diameter of 400  $\mu$ m. They coated the fibre with three different pH indicators: methyl orange, methyl red, and bromothymol blue. With these coatings, it was possible to measure pH between 3 and 7.6 in test solutions. The sensor was made by removing the cladding of

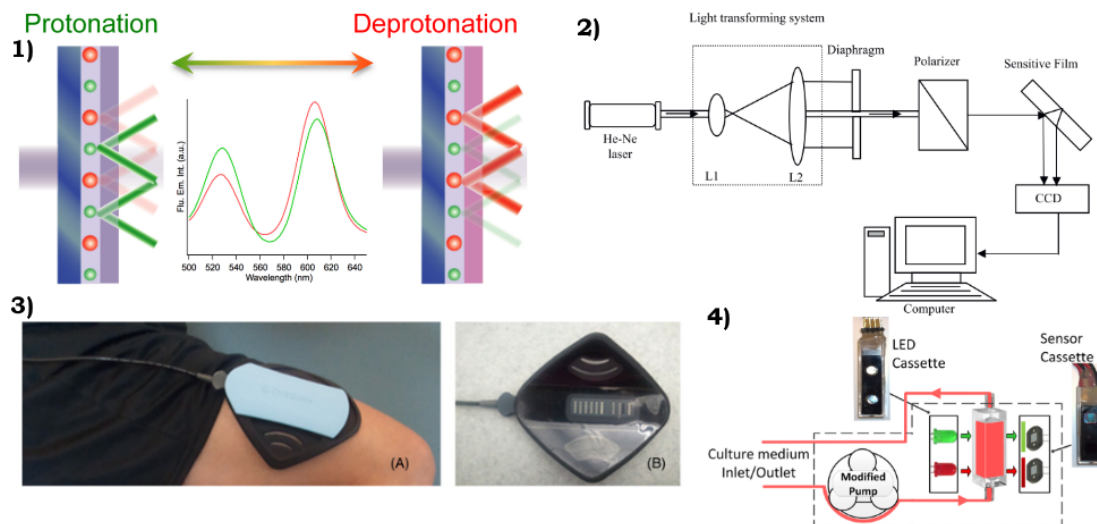


Figure 4.5: Overview of planar based absorption pH sensors set-ups: 1) Two typed of quantum dots interaction with environment in sol gel based optode by Hiruta et al. [56] 2) Experiment set-up used by Chen and Gu [31] 3) Careguide CW-NIRS Sensor used to measure pH through the skin DAby Ellerby et al. [43] 4) non contact set up with two LED's used by Kattippambil Rajan et al. [62]

a silica fibre. A halogen lamp was used to send light through the fibre, a spectrometer was used the measure the output. On this stripped part, a sol-gel with the indicators was coated. Wavelengths depended on the type of coating, as the accuracy. Tamayol et al. [114], produced flexible hydrogels which are capable of measuring pH for epidermal applications. The sensor is based absorption of beads with brilliant yellow and the fibres had a diameter of 800  $\mu\text{m}$ . A smartphone camera was enough for the readout, a range between 5.0-8.0 could be detected. The response time was relatively slow (1-5 min). Kim et al. [65] designed two different sensors. A multi-core sensor using Raman spectroscopy and a continuous transmission-based probe. The Raman spectroscopy used a laser with a wavelength of 785 nm and measured different Raman shift peaks. The transmission-based probe used white light through a polymeric coated optical fibre and a spectrometer. The diameter of the probe was 300  $\mu\text{m}$  and was capable of measuring the range between 6.0-8.0 pH. Mishra et al. [79] designed an optical fibre coated with a hydrogel with a long period fibre grating. This sensor had a broad pH range between 2.0-12.0 and a fast response time under two seconds. The optical fibre was excited by a laser with a 1540 nm wavelength. The peak at the end of the fibre shifted from 1544 to 1550 nm. It is an intrinsic sensor because the change of the light inside of the sensor is measured. Hartings et al. [54] developed a sensor which was based on fibre Bragg grating and used ratiometric measurements to determine the pH of test solutions. The optical fibre was internally illuminated by infrared light, visible excitation of green and red LED's was perpendicular on the fibre. The fibre had a diameter of 100  $\mu\text{m}$  and was capable of detecting a range between 2.0-12.0 pH and had a response time of 3 minutes.

### Planar sensor

Hiruta et al. [56] designed a film with double sol-gel layers with in the first layer two types of quantum dots and the second layer light-absorbing pH indicators (Congo red or basic fuchsin). The quantum dots have emission peaks at 525 and 605 nm. The sensor with Congo red had good repeatability in the range between 2.0-6.0 pH. This sensor made use of fluorescence, absorption and reflectance. The quantum dots can be used to fit the absorption spectra of the pH indicators, so this sensor can be used in different configurations. They also tested methyl yellow and neutral red in the second layer and had a range between 4.0-10.0 pH. Ellerby et al. [43] validated a commercially available device named CareGuide, which used continuous-wave NIRS to determine the muscle oxygenation and the muscle pH. This sensor used a chip-scale spectrometer and a multiple LED's. Each bank contains a set of 12 LEDs with six different peak wavelengths (2 LED's at each peak wavelength) that are turned on simultaneously to produce broadband, NIR illumination over the wavelength range 700–1000 nm. An algorithm calculated the pH and smO<sub>2</sub> levels. 6 LED rows are used to correct the result for tissue scattering. Chen and Gu [31] designed an optical pH sensitive film based on immobilised

## 4.3. Results of Literature Search

25

purple cabbage pigment. The PCP was entrapped in a sol-gel film and coated on glass slides. The film was examined by a UV-VIS spectrometer and had a range between 2-12 pH. The film was excited with a laser with 633 nm wavelength, the maximum absorption wavelength of the film shifted from 597 to 609 nm, while the 533 nm peak was used to determine the pH concentration of the test solutions. The response time was 2 minutes, the reproducibility was less than 0.3%. Kattippambil Rajan et al. [62] developed an optical non-contact pH sensor using green and red LEDs and photodiodes. This sensor was capable of measuring a range between 6.5 and 8.1 pH in medium cell cultures. A resolution of 0.1 pH was achieved and because there is no contact between the sensor and the cell medium no bleaching is possible.

## 4.3.4. Fluorescent based sensors

All fluorescent-based sensors found in the literature which meet the requirements are extrinsic. All the fluorescent-based sensors are not reporting any drift, so this information is left out of table 4.3. Figure 4.6 shows all fibre-based absorption sensors and figure 4.7 shows all the planar sensors found in the literature

## Optical Fibre

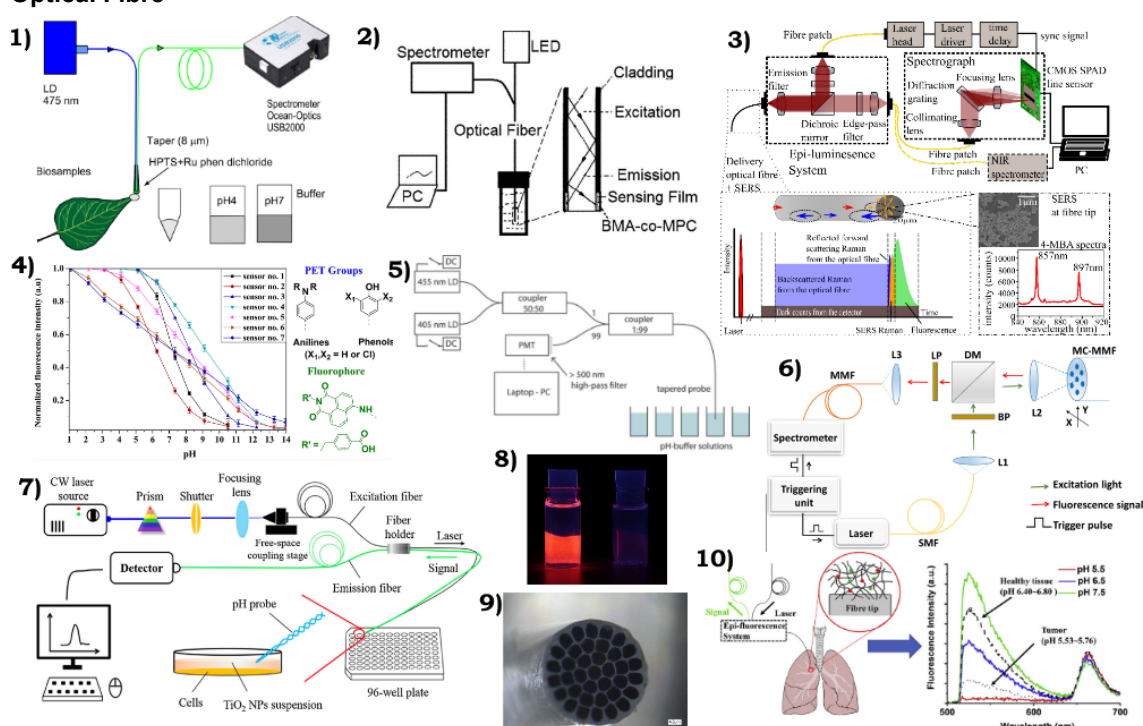


Figure 4.6: Overview of fibre-based fluorescent pH sensors set-ups and results: 1) Experimental set up by Kasik et al. [61] 2) Schematic diagram of the in vitro device for measuring fluorescence and structure of the pH sensor probe by Weizhong Jin et al. [123] 3) Optical fibre using SERS and CMOS SPAD line arrays set up by Ehrlich et al. [41] 4) Single fluorophore broad range results by Qi et al. [93] 5) Sensor set up by Cui et al. [34] 6) Optical setup to allow fibre based sensing by Choudhary et al. [32] 7) dual core micro-probe experimental set-up by Chen et al. [30] 8) image of fluorescent result by Aigner et al. [16] 9) Multicore fibre tip used by Wencel et al. [124] 10) Graphical abstract of hydrogel based pH sensor by Gong et al. [51]

Kasik et al. [61] used the pH-sensitive coating HPTS and ruthenium to design a sensor capable of detecting pH in small volumes of bio-samples. A blue LED (475 nm) was fed into a tapered and coated optic probe. Spectroscopy measured the fluorescent wavelengths and a range of 5.0-9.0 was measured through the emission peak of 560 nm. The fibres used have a diameter of 125  $\mu\text{m}$  and were tapered to a diameter of 8  $\mu\text{m}$ . The resolution was relatively low (0.2 pH) while the response time was high (10s). Weizhong Jin et al. [123] designed an intra-arterial sensor which was capable of detecting in other environment and had a fast response time. The sensor was capable of measuring the range of 6.8-8.0 pH by using an excitation wavelength of 395 nm and measured the peak at 510 nm. The resolution

Ref	Year	Fibre/planar	Type sensing	Measured in	Reactive material	Gel matrix	Use QD	Ratio metric	Excitation Peaks	Peaks Measured	Range	Diameter fibre	Shelf live	Reproducibility	Resolution	Response time	Dry bleaching
[61]	2010	fibre	SPC	biosamples in vivo (blood)	HPTS	Xerogel	X	Yes	475 nm	560 nm	5.0-9.0	125 microns	-	good	0.2	10s	-
[123]	2011	fibre	REF	Test solution	AMPN	YES (HEMA)	X	Yes	395 nm	510 nm	6.8-8.0	0.75 mm	good (5 months)	good	0.03	15s	very little
[16]	2012	fibre	SPC	Test solution	PET rhodamines	YES (pHEMA)	X	Yes	600 nm	572 nm	5.0-10.0	-	good	good	0.1	< 1min	-
[93]	2015	fibre	SPC	Test solution	multi-ionophores	YES (D4)	X	Yes	480 nm	540 nm	1.0-14.0	-	good	good	-	60s	-
[34]	2015	fibre	SPC	Test solution	HPTS-CTAB	YES (EТЕOS:GLYMCO)	X	Yes	405 nm	508 nm	5.8-7.3	25 microns	long term	good	0.07	<60 s	after 1 hour
[30]	2017	fibre	IFM	in vitro (cell culture)	BCECF	YES (OrMoSils)	X	Yes	485 nm	520 nm	6.0-8.0	80 microns	-	good	0.035	-	-
[41]	2017	fibre	SERS	-	AuNs with mercaptobenzoic acid	YES (FIXME)	X	Yes	786 nm	857 nm	5.0-9.0	50 microns	-	-	0.07	10-60 s	-
[124]	2018	fibre	-	in vivo	HPTS	YES (EТЕOS:GPTMS)	X	Yes	405 nm	520 nm	3.0-9.0	400 microns	28 weeks	very good	0.0013	<2 min	-
[32]	2019	fibre	IFM	in vivo (ovine lung)	Fluorescein	NO	YES	Yes	488 nm	520 nm	5.5-8.0	150 microns	-	Good	0.02	instant	-
[51]	2020	fibre	IFM	in vivo (ovine lung)	5(6)-FAM Porphyrin	YES (PHPMA)	X	Yes	485 nm	540 nm	5.5-8.0	200 microns	-	-	0.1	30s	only with continuous
[17]	2013	planar	SPC	Test solution	DPP Dye	YES (pHEMA)	X	Yes	450 nm	570 nm	5.0-12.0	-	Planar: short	good	-	-	-
[72]	2018	planar	R SPC	pork tissue	bromothymol blue rhodamine B	YES (TEOS and APTES)	X	Yes	980 nm	540 655 nm	4.9-8.1	-	-	-	0.1	-	absent
[29]	2020	planar	IFM	in vivo (blood)	(HPTS)	YES (polyurethane)	X	Yes	520 nm	475 nm	5.0-8.0	-	-	-	0.01	1s	-

Table 4.3: Overview of fluorescent-based sensors found in the literature. RES: resonator, (N)IR SPC: (Near)InfraRed Spectroscopy, SPR: Surface Plasmon Resonance, IFM: interferometer, R SPC: Raman Spectrometer, REF: Refractometer, GRT: Gratings, SERS: Surface Enhanced Raman Spectroscopy

Ref	Year	Fibre/planar	Type sensing	Intrinsic/Extrinsic	Measured in	Reactive material	Gel matrix	Ratio metric	Excitation Peaks	Peaks Measured	Range	Diameter fibre	Shelf live	Reprod ucibility	Accuracy	Resolution	Response time	Dry bleaching
[71]	2013	fibre	REF	Intrinsic	in vivo samples	chlorophenol red bromophenol blue	YES (TEOS)	X	-	1500 nm	1.0-13.0	125 microns	-	good	-	0.017	40 s	-
[131]	2017	fibre	SERS	Extrinsic	Test solution	MBA-AuNP	YES (alginate)	Yes	550 nm	1400 nm	4.0-8.0	-	-	good	0.065 pH-1	-	-	-
[135]	2018	fibre	SPR	Intrinsic	Test solution	Ag	(AAM, BAAM, APS, TEMED)	X	-	600 nm	1.0-12.0	125 microns	Good	good	13nm/pH	-	20-30 s	-
[45]	2019	fibre	REF	Extrinsic	Test solution	polyHEMA	YES (HEMA, EGDMA)	Yes	532 nm	RP	5.0-7.0	500 microns	-	-	-	0.1	10 s	none
[94]	2020	fibre	GRT	Intrinsic	Test solution	sodium alginate	YES (alginate)	Yes	1488 nm	1520 nm	4.0-12.5	80 microns	-	good	-0.265 nm/pH	-	<30 s	-

Table 4.4: Overview of reflectance-based sensors found in the literature. SPR: Surface Plasmon Resonance, IFM: interferometer, REF: Refractometer, GRT: Gratings, SERS: Surface Enhanced Raman Spectroscopy

was high, little dry-bleaching was detected. The fibre had a diameter of 750  $\mu\text{m}$  and the sensors made use of the differences in refraction because of the fluorescence of the coating. Aigner et al. [16] designed a fluorescent sensor which used photoinduced electron transfers of linked rhodamines. These fluorescent dyes were tested in two different types of matrices, a silica matrix and poly(HEMA) matrix. Excitation peak was measured at 600 nm and emission excited at 572 nm. The higher, the pH the lower fluorescent intensity. They achieved high pH sensitivity in the range of 5-7 pH and low cross-sensitivity. The sensor showed good reversibility between pH 3.7 and 7.5 and had a response time of less than a minute. Qi et al. [93] designed a fluorescent pH sensor based on a single fluorophore. This fluorophore was 4-amino-1,8-naphthalimide. This sensor was capable of measuring the full range of pH (1-14) and showed excellent stability, reversibility, and response time of 1 min. The excitation peak was 480 nm, the emission peak was 540nm. The sensitivity depends on the range of the sensor. Cui et al. [34] designed a sensor which was made out of a coated tapered optical fibre. The coating existed of an HTPS and hexadecyltrimethylammonium bromide (CTAB) in a sol-gel matrix. The optical fibre was excited by two sources with a 405 and a 450 nm wavelength. It resulted in an emission wavelength at 510 nm, which was higher with higher pH. This sensor achieved a resolution of 0.07 pH in test solutions in the physiological range between 5.75 and 7.25. Chen et al. [30] used interferometry to measure the local pH *in vitro* with dual-core micro-probes. This probe consisted of an emission fibre and a excitation fibre, which are twisted and burned into a tip of 80  $\mu\text{m}$ . The probe was excited by a continuous wave argon laser, the emissions were measured by a detector. With this sensor, they were capable of measuring the range between 6.0-8.0 pH and high resolution. Ehrlich et al. [41] used SERS to develop a sensors capable of measuring pH with a single fibre with a diameter of 50  $\mu\text{m}$ . The used functionalised gold shells for the SERS and excited the samples with a 786 nm laser. The intensity count of the wavelength 857 and 897 nm were used to determine the pH. They achieved a resolution of 0.07 pH and short response time (10-60s) within the range of 5.0-9.0 pH. Wencel et al. [124] designed a fibre-based ratiometric optical pH sensor. This sensor had the capabilities to measure pH in real-time and continuous in tissue. It existed out of a plastic multi-core fibre (diameter of 400  $\mu\text{m}$ ) with a sol gel matrix with entrapped HPTS. HPTS had two absorption maxima (405 nm and 450nm), a pH sensitive emission band of 520 nm. The sensor had a very high resolution of 0.00013 pH and showed good reproducibility, long-term stability, a response time of <2 min, and drift of 0.003 pH units per 22 h. The sensitivity of the sensor was optimal between 6.0-8.0 pH. Gong et al. [51] designed a hydrogel-based optical fibre fabricated by *in situ* photo-polymerisation with two pH-indicators, 5(6)-FAM and Porphyrin. Porphyrin emission was insensitive to pH and thus was a good ratiometric mean to measure pH. The diameter of the glass optical fibre was 200  $\mu\text{m}$ . The sensor showed a good linear correlation between 5.5 and 8.0 pH with a precision of 0.10 pH. The normalised intensity showed an emission peak around 530 nm while the sensor was excited with a wavelength of 485 nm. The response time of the sensor was around 30 seconds. Designed to observe lung tumour tissue acidity the sensor was tested *ex vivo* in ovine lungs. From the same group, Choudhary et al. [32], designed a high fidelity fibre sensor which used silica micro-spheres loaded with fluorophores to measure metabolic changes. These silica micro-sphere have a diameter of 10  $\mu\text{m}$  and are loaded into pits etched into the end of a multi-core fibre of 150  $\mu\text{m}$ . They used fluorescein based fluorophore for measuring pH and palladium porphyrin complex based for measuring oxygen. An excitation of 520 nm resulted in an emission of 488 nm. An accuracy of 0.02 pH and 0.6 mg/L oxygen were achieved. Response to pH and oxygen environments were both observed to be less than 1 second.

### Planar Sensors

Aigner et al. [17] designed fluorescent pH-sensitive material which they tested planar and on an optical fibre. 1,4-diketopyrrolo-[3,4-c]pyrrole dye was the fluorescent marker, it was tested on multiple hydrogel matrices. The excitation peak was 450 nm, the emission peak was 570 nm. The range was between 5 - 12 pH for both the planar sensor and the nanobeads for optical fibres. The nanobeads showed possibilities to be measured with a simple RGB camera. Liu et al. [73] developed a modularised optical sensor for pH monitoring in biological matrixes. Using upconversion nanoparticles (UCNPs) in combination with bovineserumalbumin and dyes, they were able to measure the pH difference with Raman spectroscopy. They achieved a resolution of 0.1 in the range of 4.9-8.1. The UCNPs were excited with 980 nm laser, the emission peak were 540 and 655 nm. Cattini et al. [29] designed a planar sensor for inline blood measurements, which had the potential to be used in other measurements as well. The sensor was based on interferometry and used two LED's and two photo-detectors and a disposable

sensor. In the sensors exist of a polyurethane hydrogel and pH-sensitive HPTS micro-beads. They achieved a resolution of 0.01 in the range of 5.0-8.0 with a response time of a second.

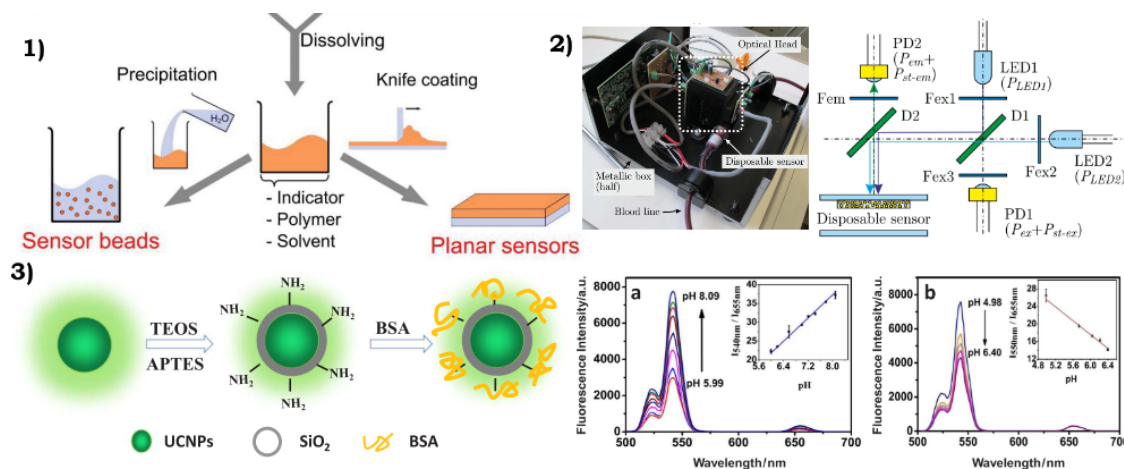


Figure 4.7: Overview of planar based fluorescent pH sensors set-ups and results: 1) Scheme for the preparation of the fluorescence pH-sensors by Aigner et al. [17] 2) Schematic of the optical layout of the optical and picture of the developed measuring system head by Cattini et al. [29] 3) Schematic illustrations for the preparation of the UCNPs@SiO<sub>2</sub>@BSA composites used for the modularised fluorescent sensor and results from the experiments by Liu et al. [73]

#### 4.3.5. Reflection based sensor

There are only five optical fibre reflection-based sensors found in the literature which meet the requirements. These sensors depend on the internal or external reflection of light with the fibre. Within these five sensors, the accuracy as well as the resolution, is described. There was no use of Quantum Dots, so this is not discussed in table 4.4. Figure 4.8 shows the set-ups of the different sensors. Li et al. [71] designed a simple optical fibre sensor with a section of no core. In this set-up, a centre part of the fibre was replaced with a sol-gel with a pH-sensitive coating which consisted of tetraethyl orthosilicate (TEOS) and multiple pH indicators. These pH indicators have different sensitive ranges and thus by combining these they achieved a simple sensor which was capable of measuring almost the full range of pH (1-13). They measured at 1550 nm and the response time was around 60 seconds. You et al. [131] designed a modular optical sensor using Surface-enhanced Raman spectroscopy (SERS). It was an extrinsic sensor which measured the scattering of a hydrogel based layer excited by an excitation laser of 780 nm. They used gold nanoparticle-based pH probes capped with 4-mercaptobenzoic acid (MBA-AuNPs) in a hydrogel. Ratiometric intensity changed at 1430 and 1078  $\text{cm}^{-1}$ . They achieved a sensitivity of  $0.07 \text{ pH}^{-1}$  in the analytical range of 4.43-8.07 pH. The sensor also showed the potential of using SERS for multiple small molecule targets. The sensor showed great potential for in-vivo measurements but was only tested in aqueous solutions. Zhao et al. [135] designed a surface plasmon resonance sensor. It was based on the change in the reflective index of a hydrogel when pH changed in the environment. This coating was placed with a silver film on a single-mode fibre between two parts of multi-mode fibres. This intrinsic sensor was tested in test solutions and had a wide range of 1-12 pH. The response time was less than 30 seconds for rise and fall. Furthermore, the sensor showed good stability, prominent sensitivity, remarkable reproducibility and simple fabrication. Elsherif et al. [46] developed an optical fibre sensor based on light-diffusing micro-lens arrays. It was an extrinsic sensor using refractometry. The sensor used a green laser with a wavelength of 532 nm. The reflected power of the laser was depended on the pH of the solution. The fibre had a diameter of 500 microns and they used asymmetric micro-lens structures. PolyHEMA was as pH-sensitive material and they achieved a range of 5.0-7.0 with a resolution of 0.1 and a swift response time. Ran et al. [94] designed a miniature pH probe using a functional microfiber Bragg grating. The sensor had a functional layer of sodium alginate gel, which reacts with pH. This layer was immobilised on the microfiber ( $<10 \mu\text{m}$ ) by electrostatic self-assembly technique. The sodium alginate gel had a higher reflective index when the pH was low. This extrinsic sensor was capable of measuring pH linearly between 4 and 12 in a test solution. The results show that the sensitivity of the sensor could be increased when, the diameter of the fibre was reduced and the diameter of the functional layer was increased.

## 4.4. Discussion of the literature

29

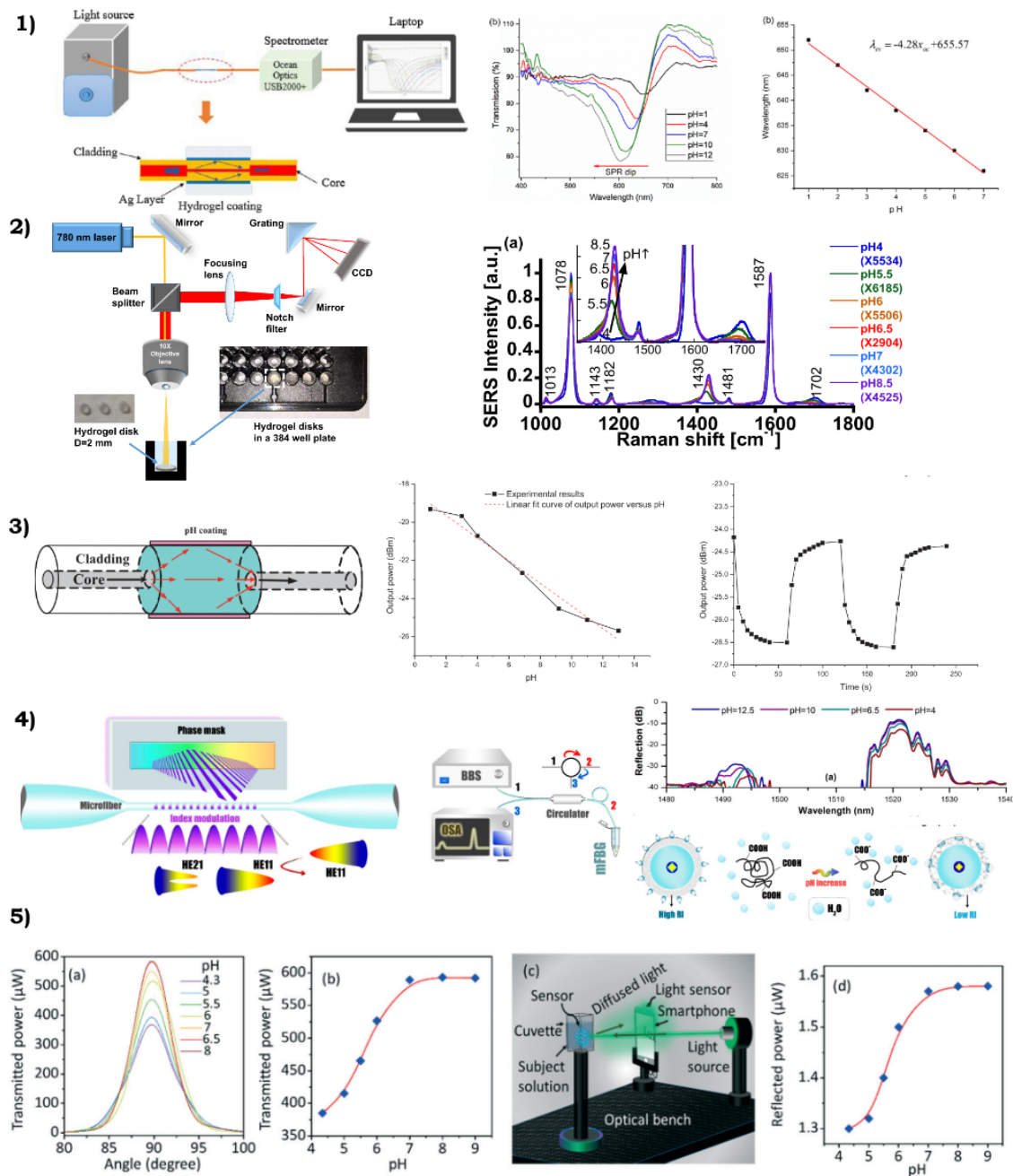


Figure 4.8: Overview of reflection based sensor set-ups with results: 1) The sensor set up of Zhao et al. [135] with the results of the measurements. 2) The SERS hydrogel set up of You et al. [131] with the corresponding SERS Scattering. 3) The design of Li et al. [71] with the results and response times. 4) The phase-mask of the sensor of Ran et al. [94] with the working principle and the measurement results. 5) Schematic of the setup utilised for testing the pH-sensor in the reflection mode and the corresponding results of Elsherif et al. [46]

## 4.4. Discussion of the literature

### 4.4.1. Search for a potential sensor

The goal of this literature study is to answer the third subquestion: What is the most feasible optical sensing technique for measuring pH or lactate during cardioplegia induced arrest? With answering the third subquestion the general research question of this literature review can be answered which was to find the feasible methods to detect myocardial ischaemia. To answer the third question, 37 different

type of sensors are compared. First, the different types of lactate sensors will be discussed, followed by the absorption, fluorescent and reflection based sensors. Per type of sensor, the sensor with the most potential will be featured. Following this, all sensors will be evaluated on their potential to be in vivo ischaemia sensor by the following criteria. The sensor should be able to measure in the physiological range; it should be applicable for in vivo measurements. The resolution, accuracy, response time and manufacturability should be acceptable as discussed in section 4.2.3. The result of these criteria can be found in table 4.6. Following the evaluation of the different type of sensors, the limitation of the study will be discussed, a recommendation will be made for further work.

#### 4.4.2. Lactate based ischaemia sensor

Biswas et al. [26], Driller et al. [40] and Baishya et al. [23] are not using a reactive material, they only use NIR, but it is used in different ways. Driller et al. [40] measures with NIR on the skin and focus on the production of lactic acid by muscle tissue during intense training. In comparison Baishya et al. [23] placed small cuvettes with solutions in a NIR spectroscope. Jernelv et al. [60] used IR spectroscopy with a quantum cascade laser. This technique is more advanced and uses continuous fibre. Further explanation of why on skin transducers like Driller et al. [40] are not suitable for in-vivo measurements will be given in the next section. Studies from Zheng et al. [136], Andrus et al. [21] and Biswas et al. [26] were tested in vitro and more focused on single-cell lactate levels. Andrus et al. [21] sensor needed 15 minutes to give the result of the lactate levels they measured. Another problem with the lactate sensors is that they work with enzymes which tend to perform less in oxygen-depleted environments [96]. Sharma et al. [103] is one of the only optical lactate sensors using the internal reflection to measure the levels of lactate. Comparing sizes, it is noticeable that Zheng et al. [136] fibre tip is tiny in comparison to all other fibres. This is because it is designed to measure the single-cell lactate levels in vitro. Table 4.6 shows that none of the found lactate sensors in the literature seems valid to use for an in vivo ischaemia sensor. It is mostly because the sensors do not seem applicable for in-vivo measurements

#### 4.4.3. Absorption based ischaemia sensor

Ellerby et al. [43] tested NIR spectroscopy to measure the levels of pH in muscles tissue during exercise. The devices which Ellerby and Driller tested, appear to be bankrupt or discontinued. Tarar et al. [115] argued in his review that the properties of the skin still limit the success of optical sensing through the skin and explains why these sensors are discontinued. The absorption-based sensor with a reactive material are better suitable for in-vivo measurements, because of their resolution and the uses of gel matrices. Gel matrices make sure that the reactive material does not leak out of the sensor. The disadvantage of these sensors is that they only have been tested in aqueous test solutions and not in-vivo. All of the absorption based sensors are extrinsic, most of the optical fibre sensors are individual fibres with a sensing area in the middle of the fibre. Only Raoufi et al. [95] and use bifurcated fibre. In the continuous fibre, different techniques have been used, such as replacing the cladding by a gel matrix with reactive material or using long period fibre grating. The reactive materials determined the peaks which were measured and the range of the sensor. An overview of the different dyes is given in 4.5. The largest ranges were achieved with the use of polymer polyaniline (2.0-12.0), sodium alginate (2.0-12.0) and purple cabbage pigment (2.0-11.0). These broad ranges are not needed for the use on the heart tissue. Not all sensors have their response time and their resolution/sensitivity reported. Therefore it is hard to decide which absorption-based sensor has the most potential to be an ischaemia sensor for the heart. Table 4.6 show that Raoufi et al. [95], Kim et al. [65] and Hiruta et al. [56] have the most potential for an ischaemia sensor. The sensor of Raoufi et al. [95] show great potential because it is bifurcated, has a good resolution between the physiological range. However, the sensor is still large, 600  $\mu\text{m}$  and the response time is not described in the paper. In the study of Kim et al. [65] it is hard to determine if the absorption-based sensor has the potential to be used in vivo; all the other criteria show good possibilities. At last Hiruta et al. [56] shows great potential, however, manufacturing the sensor can be a problem because of the complexity of manufacturing.

#### 4.4.4. Fluorescent based ischaemia sensor

In comparison with the absorption based sensors, the fluorescent-based sensors are tested ex/in vivo. Gong et al. [51], Wencel et al. [124] and Choudhary et al. [32] all tested ex vivo in animal models and Wencel et al. [124] even tested in vivo in humans. Most fluorescent material used to measure pH was excited with violet/blue light (400-500 nm) except for Aigner et al. [16] which used a yellow light to

## 4.4. Discussion of the literature

31

ref	Dye	Wavelength measured	Range
Raoufi et al. [95]	brilliant yellow	450 nm	6.80-9.00
Florea et al. [47]	polymer polyaniline	605 nm 832 nm	2.00-12.00
Hiruta et al. [56]	Congo red	525 nm	2.00-6.00
	basic fuchsin	605 nm	4.00-9.00
Jeon et al. [59]	Neutral Red	536 nm 461 nm	6.00-9.00
Chen and Gu [31]	Purple cabbage pigment	533 nm	2.00-11.00
	methyl orange	MR: 400 and 550 nm	
Zajic [132]	methyl red	MO: 520 and 450 nm	3.00-7.60
	bromothymol blue	BB: 450 and 630 nm	
Mishra et al. [79]	sodium alginate	1530-1550 nm	2.00-12.00

Table 4.5: Overview of different absorption dyes used to measure pH during experiments

excite the fluorophores in their sensor. The peaks for the pH sensors were all measured in the green range (500-570 nm). A disadvantage of the fluorescent-based technique is that the response time is overall relatively slow. Multiple sensors got response times under one minute, where Choudhary et al. [32] even got an instant result with the use of their fluorescent microspheres. Almost all sensor used a hydrogel based matrix for their fluorophores. Kasik et al. [61] had the lowest accuracy of 0.2 pH of the pH sensors while, Wencel et al. [124] achieved an accuracy of 0.0013 pH. Of the studies that reported the shelf live and reproducibility, all of them were reported as good except for the planar sensor variant of Aigner et al. [17]. Most sensors did not report problems with photobleaching or drift, which are common problems with the use of fluorophores [125]. The most used reactive material is HTPS. Combining table 4.6 and table 4.3 it shows that one of the most promising sensors is the sensor of Wencel et al. [124]. This sensor was tested in vivo and showed excellent results; the only disadvantage of this sensor is that the response time is still slow (< 2min). Now the sensor still had a diameter of 400 microns, while they aim to make a sensor below 100 microns to make it minimally invasive. Other possible sensors are Qi et al. [93], Aigner et al. [16] and Cui et al. [34], but these sensors have a lower resolution, and their applicability and complexity make it harder to use these sensors. This complexity is why Choudhary et al. [32] and Gong et al. [51] have lower potential to be the ischaemia sensor of this project. At last [29] shows great potential as a planar sensor, however, this sensor is designed as an intra-arterial sensor, so it is questionable if this sensor will work in vivo on the heart tissue.

#### 4.4.5. Reflection based ischaemia sensor

In comparison with the absorption and fluorescent-based sensor, more of the reflection-based sensors are intrinsic. It is because the interaction of the indicator with the environment changes the internal reflection of the optical fibre. Most of the sensors make use of a continuous fibre in which the transmission change is measured, only Ran et al. [94] uses a sensor with a single fibre in which the light is internally reflected. Li et al. [71] and Zhao et al. [135] all removed the cladding of the optical fibre to have interaction with the environment. Elsherif et al. [45] is a different kind of sensor and uses the reflection of light from a cuvette to measure the pH level. Thanks to the intrinsic nature, the sensors have much faster response times. It allows for great ranges because these sensors do not need fluorophores or dyes. Li et al. [71] and Ran et al. [94] measure the reflection in the infrared range, while Zhao et al. [135] measure in the yellow/orange range. As with the absorption-based sensor these reflection-based sensor are only tested in a test solution and can experience problems in vivo, because of the continuous fibre. All sensors have high resolution and reported good reproducibility. Of all sensors, Ran et al. [94] has the best potential to measure ischaemia in the heart tissue, this is because the optical fibre is minimally invasive (<10 microns) and it is not using a continuous fibre. The disadvantage is the complexity to manufacture and to read-out these fibres.

#### 4.4.6. Possible sensor

Table 4.6 gives a short overview of the sensors discussed in this literature review and evaluates the sensors by five criteria discussed in section 4.4.1. Not all studies contain enough information for a clear decision; therefore a question mark is added when it is not clear yet if the sensor meets the criteria and if it can be a valuable technique. The last column is based on the combination of the five criteria. For the continuation of this research, a decision needs to be made on which principle and type of sensing, the proof of principle will be built on. Looking at the literature found, the following deductions can be

Ref	Parameter	Principle	Type of Sensing	Physiological Range	Applicable for in vivo	Resolution/ Accuracy	Response Time	Easy to Manufacture	Potential Sensor
Jermelv et al. [60]	Lactate	AB	Fibre	✓	X	?	✓	X	X
Baishya et al. [23]	Lactate	AB	Fibre	✓	X	?	✓	X	X
Zheng et al. [136]	Lactate	FL	Fibre	X	X	?	?	X	X
Biswas et al. [26]	Lactate	FL	Fibre	X	X	?	?	X	X
Sharma et al. [103]	Lactate	RE	Fibre	✓	X	✓	✓	X	X
Driller et al. [40]	Lactate	AB	Planar	✓	X	?	?	X	X
Andrus et al. [21]	Lactate	FL	Planar	X	X	?	X	X	X
Florea et al. [47]	pH	AB	Fibre	✓	X	?	?	✓	X
Raoufi et al. [95]	pH	AB	Fibre	✓	✓	X	?	✓	✓
Jeon et al. [59]	pH	AB	Fibre	✓	?	?	?	✓	?
Tou et al. [117]	pH	AB	Fibre	✓	?	✓	✓	?	?
Zajic [132]	pH	AB	Fibre	✓	X	✓	?	✓	X
Tamayol et al. [114]	pH	AB	Fibre	✓	X	X	X	✓	X
Kim et al. [65]	pH	AB	Fibre	✓	?	✓	✓	✓	✓
Mishra et al. [79]	pH	AB	Fibre	✓	X	✓	✓	X	X
Hartings et al. [54]	pH	AB	Fibre	✓	X	?	X	✓	X
Hiruta et al. [56]	pH	AB	Planar	✓	✓	?	✓	X	✓
Ellerby et al. [43]	pH	AB	Planar	✓	X	✓	✓	✓	X
Chen and Gu [31]	pH	AB	Planar	✓	?	✓	✓	?	?
Kattiparambil Rajan et al. [62]	pH	AB	Planar	✓	X	✓	?	?	X
Kasik et al. [61]	pH	FL	Fibre	✓	?	X	✓	✓	?
Weizhong Jin et al. [123]	pH	FL	Fibre	✓	?	✓	✓	?	?
Aigner et al. [16]	pH	FL	Fibre	✓	✓	✓	✓	?	✓
Qi et al. [93]	pH	FL	Fibre	✓	✓	?	✓	?	✓
Cui et al. [34]	pH	FL	Fibre	✓	?	✓	✓	✓	✓
Chen et al. [30]	pH	FL	Fibre	✓	✓	✓	?	X	?
Ehrlich et al. [41]	pH	FL	Fibre	✓	✓	✓	✓	X	?
Wencel et al. [124]	pH	FL	Fibre	✓	✓	✓	?	?	✓
Choudhary et al. [32]	pH	FL	Fibre	✓	✓	✓	✓	X	?
Gong et al. [51]	pH	FL	Fibre	✓	✓	✓	✓	X	?
Aigner et al. [17]	pH	FL	Planar	✓	X	?	?	?	X
Liu et al. [72]	pH	FL	Planar	✓	?	✓	✓	X	?
Cattini et al. [29]	pH	FL	Planar	✓	?	✓	✓	✓	?
Li et al. [71]	pH	RE	Fibre	✓	?	✓	✓	X	?
You et al. [131]	pH	RE	Fibre	✓	?	✓	✓	X	?
Zhao et al. [135]	pH	RE	Fibre	✓	?	✓	✓	?	?
Elsherif et al. [45]	pH	RE	Fibre	?	X	✓	✓	?	X
Ran et al. [94]	pH	RE	Fibre	✓	✓	✓	✓	X	?

Table 4.6: Evaluation of all the sensors found in the literature on their capabilities to be in vivo ischaemia sensor.

made. First of all, that all the lactate based sensors found in this review are not very applicable for in vivo measurements. It has various reasons, but the need for oxygen for the enzymatic reaction to take place limits the possibilities for these type of sensors. The second problem with lactate sensors is that the manufacturability of these sensors is difficult. Another conclusion which can be made from this review is that fluorescent fibre based techniques are the most advanced. These type of sensors are already being used in-vivo and show great potential. Only one sensor by Aigner et al. [17] can certainly not be used as ischaemia sensor because of the short shelf live of the planar sensor. The applicability is the most significant uncertainty of the reflection sensors as to whether they are suitable as a potential sensor. Just as with the lactate sensor, the manufacturability is a reason why the focus of the rest of the research will not be on reflection based sensors. Absorption based sensor are considered to be the easiest to be manufactured. It is mainly because only a dye and a hydro/sol-gel matrix are needed, no fluorophores, lasers or nanoparticles have to be used to test these transducers. The main disadvantage of these sensors is that they are only tested in test solutions or bio-samples. This makes it hard to determine if they would succeed in measuring the pH on the tissue of the heart. The last hurdle which should be investigated with the absorption-based sensor is the size of the fibres used, most of them are above 300  $\mu\text{m}$ , and this is still invasive for the tissue. Fluorescent based optical fibres are smaller but have problems with dry bleaching and response time. The objective of the continuation of the research will be to make a proof of concept of a chosen method. The information available after this literature study will be a great addition to determine the direction of the research. However, more information is needed to make this decision. First of all, the manufacturability has to be further investigated to see what is possible with limited resources. Secondly, it is essential to elaborate on which risks are accompanied by using fluorophores and dyes. In the third place, further investigation into the hydrogel/sol-gel material is required. It needs to be done to make sure it does not damage the tissue of the heart. At last, the possibility to combine planar and optical fibre techniques in a sensor needs to be examined. It can be an advantage to place a hydrogel with a planar LED on the tissue and only use optical fibres to receive the information of the tissue. All in all, there is still a lot of work to be done, but this study provides a comprehensive overview of what is possible and where the focus will need to be in future work.

#### 4.4.7. Limitations of study

The goal of this literature study was to give a comprehensive overview of what type of optical technologies are being used to detect changes in physiological parameters. It was done step-by-step to make sure that no information was missed. However, some limitations should be noticed. This limitation impacts the quality of the findings and the ability to answer the hypotheses in section 4.1. First of all, because there was no clear review on comparing the different principles and sensors, a rather broad scope was selected. This decision was made to compare all different types of optical transducer along the criteria needed for an ischaemia sensor. A result of this decision is that the comparison misses profoundness compared to if only one type of technique was selected. Since it would not be apparent in advance whether a planar or an optical sensor would be better, this broadened the scope as well. Secondly, every research had a different purpose in mind while designing and testing the sensor. Therefore it is difficult to compare the results and designs; some researcher would accept results or risk which others tried to prevent. Thirdly, this missing information induces that results like table 4.6 are based on expectations and predictions instead of apparent facts. A limitation looking at the remainder of this research is that many of the sensors have been tested in liquids instead of in vivo. It led to a choice between less but more certain transducers or more but less certain transducers for tissue sensing; the latter was chosen in this review. In the fourth place, there are multiple ways of categorising the type of technology used in the transducers. Therefore other technologies or odd solutions can be overlooked by using this search strategy. At last, a limitation of this literature review which can be considered is the search strategy itself. One could debate that the search strategy should include terms like absorption, transmission or reflectance. These terms are not included in the search strategy, because adding those would significantly increase the results found in the literature. While most of the studies would include terms as which contain optic nevertheless

To achieve a comprehensive overview with all different opportunities, it could not be prevented that the search strategy would be broad. This broad scope allows that researches from all different kind of areas are included, some research has much more focus on the chemistry of the different dyes. In contrast, other research can be focused much more on experimenting on the possibilities of using optical fibres in medical applications. Although it was an informed decision, it certainly presents limitations for comparing results. Not all studies report the same outcomes and share all the information needed to make a clear choice. To compensate these differences, the transducers were evaluated per parameter, type of sensing and light principle. It made a more substantiated comparison possible and restrains the adverse effect of this limitation. In the different comparison tables, much information is missing because of this difference in designing and reporting. This missing information is insurmountable, when comparing so many different sources and technologies. A result of this is that this review will not end with a clear elaboration on what is the optimal techniques; instead, it describes interesting areas to focus on in further work. The decision to include all sensors which measure in liquids instead of in vivo was a considered one. When a sensor is capable of measuring parameters in a solution, the chances are that it will work in tissue. When this research would have decided to not take into account all sensors which have not been tested in a solution, it would only contain ten studies. Of those ten studies, multiple have published previous work which included researching the proof of principle with test solutions. So to include the latest technologies in this review, a decision was made to include all types of sensors which have the potential to be used in vivo. Determining which terms to include in the search strategy can be a significant limitation. The goal is to include as many terms as possible while not making the scan too exhaustive and time consuming. Not adding terms like absorption, planar or spectroscopy followed from a deliberate decision made concerning the resources available

Other limitations need to be addressed when the quality of the research is asses. Chapter 2 and 3 lay the groundwork for the literature study. In these chapters, decisions were made, which have a significant impact on the results of the literature study. First of all, the decision was made to focus on pH and lactate instead of  $O_2$ ,  $CO_2$  or other parameters. This decision was based on the literature and with the ultimate goal of the thesis in mind. It does not mean that the other parameters are not capable of measuring ischaemia of the heart tissue. For example, Pischke et al. [89] are already working on an ischaemia sensor based on  $CO_2$  for more than 20 years now and a first product is being certified. The same can be said about the different measurement techniques. The sensor developed by Pischke is using electrochemical sensing, just as other commercially available sensors, or are being researched right

now [49, 85, 101]. Table 3.1 show that each type of transducer has its own (dis)advantages. Choosing to focus on optical sensing is clearly explained in section 3.2.2, but still, it has a significant influence on the outcome of the literature study. At last, categorising the optical transducers as described in section 3.3.2 resulted in that these methods were the main focus of the literature studies. Not all the studies found could be categorised in this classification, which increased the complexity of the comparison and limit the methods used.

To increase the completeness of this research, future work can be done by investigating other measurement techniques on the one hand. On the other hand, future work can be focused more on one principle or type of sensing. If future work shows that one light principle would be superior, focusing on only this technology allows for better comparison like the review of Wencel et al. [125]. Focusing on one type of parameter can also be advantageous to compare the differences between measurements techniques like the review of Rassaei et al. [96]. The existence of this kind of reviews are the reasons this literature review uses a different approach, but the advantages of these types of reviews should not be neglected.

#### 4.4.8. Recommendation for further work

Besides the recommendation on future work made in the previous section regarding a different focus of comparing the literature, other recommendations can be made. These recommendations are on how to continue with the groundwork laid in this review. The first recommendation is to focus solely on pH; this literature review showed that the lactate based sensors have little potential to be used as an ischaemia sensor. pH is better suitable for this, if a reliable pH sensor is developed, this can be used for more than only ischaemia. Many researchers now are looking into the possibility to use a pH sensor in differentiating between normal and cancerous tissue [32, 51]. Adding other parameters can make the sensor more accurate and reliable, but for achieving a proof of concept, this will be an unnecessary increase in complexity. A second recommendation will be to devise a method to quickly evaluate if sensor based on test solutions are capable of measuring tissue pH. As most sensor are first being tested on test solutions and only in further work tested in other areas; a method to determine the potential will optimise the search to the best potential ischaemia sensor. A third recommendation is not to fully depreciate electrochemical sensors, because these type of sensor are much more advanced than the optical sensors. Ghoneim et al. [49] wrote a fifty-page long review on the recent progress in electrochemical pH sensing. The future work should not be blinded on the idea that optical sensing is the only potential solution to the problem. In his review, seven representative works regarding the monitoring of ischaemia are listed. The research group of John A. Rogers at Northwestern University is getting good results with flexible ischaemia sensors and are optimising the use of electrochemical sensors [33][128][52]. The fourth recommendation is to focus on the biocompatibility of the sensor regarding the heart tissue; during cardioplegia, the heart is arrested so the sensor can be easily connected with the heart. The ultimate goal of the sensor is to be used even when the heart is working. The number of forces and deformations are high during the normal contraction of the heart. With this goal in mind, a method should be chosen, which can be compatible with this interaction. Even more important is that the sensor will not damage the tissue during sensing, optimally the sensor is or completely bioinert or minimally bioactive so that during the period of sensing no interaction takes place which can interfere with the monitoring.

#### 4.5. Conclusion

This literature review evaluated thirty-seven studies which showed the potential to be an ischaemia sensor for the heart during cardioplegia induced arrest. In the background information informed decisions were made to focus solely on optical sensors which measure pH or lactate. Analysing these sensors, the following conclusions can be made. First of all, there are many different techniques to achieve sensing of physical parameters. All these techniques have different (dis)advantages which can be important depending on your requirements. Secondly, the fluorescent pH sensor shows the most potential to be used as an ischaemia sensor for the heart. At the same time, the manufacturability of the sensors is the biggest obstacle in all the different categories. The results show that several investigated sensors are feasible methods to detect myocardial ischaemia during a cardioplegia-induced cardiac arrest, but further development is necessary.

# A Relation PtCO<sub>2</sub>, pH and lactate with decreased bloodflow

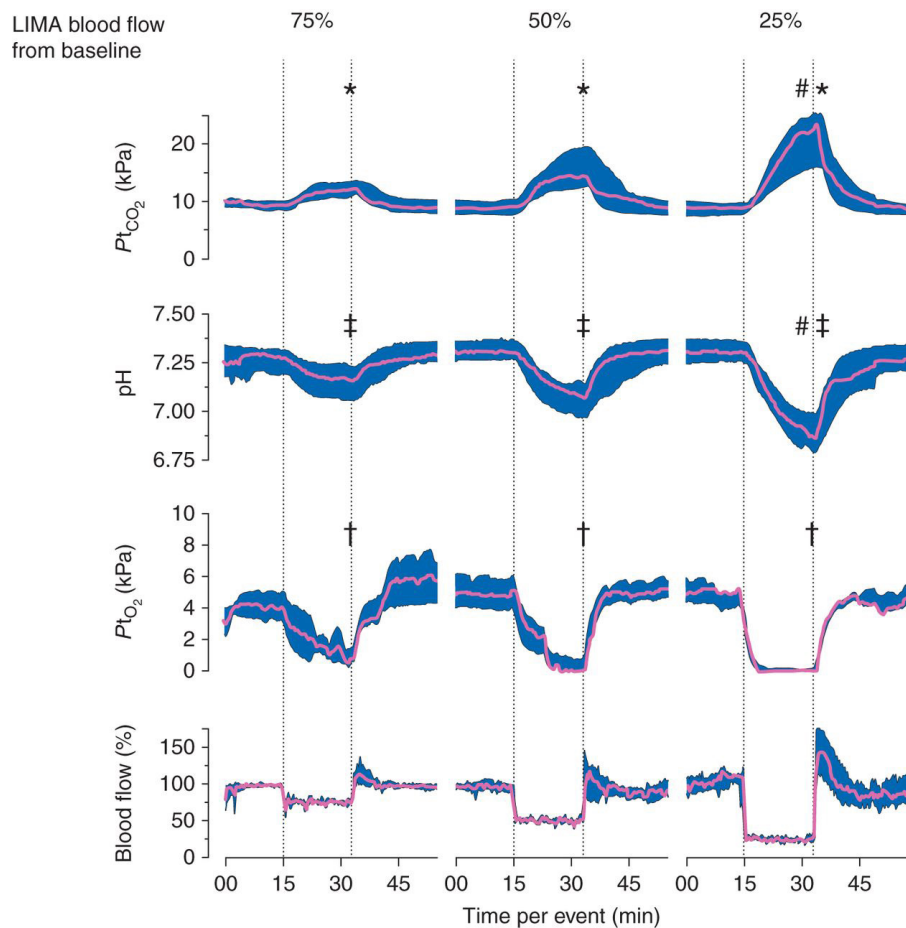


Figure A.1: Figure as found in Pischke et al. [88].” Blood flow in the LIMA graft was reliably reduced from baseline levels (100%) to 75, 50 and 25% (lowest panel). Myocardial PtCO<sub>2</sub> increased significantly (\*) and flow-dependently during all blood flow reduction events. Maximum PtCO<sub>2</sub> during 25% blood flow was significantly different from the two other occlusion intervals (#). Myocardial pH was significantly reduced during every blood flow reduction event (†) and was significantly more reduced during 25% blood flow when compared with 50 and 75% blood flow (#). Myocardial PtO<sub>2</sub> decreased significantly during every blood flow reduction (†) and reached zero during 50 and 25% blood flow. All values expressed as median (pink lines) and quartile range (blue area);”

## Bibliography

- [1] Advantages of quantum dots over, . URL <http://bme240.eng.uci.edu/students/07s/yokabe/advantages.htm>.
- [2] Advantages Disadvantages temperature sensor-thermocouple,RTD,thermistor,IC sensor, . URL <https://www.rfwireless-world.com/Terminology/Advantages-and-Disadvantages-of-temperature-Sensor.html>.
- [3] Coronary artery bypass surgery - Wikipedia. URL [https://en.wikipedia.org/wiki/Coronary\\_artery\\_bypass\\_surgery#cite\\_note-55](https://en.wikipedia.org/wiki/Coronary_artery_bypass_surgery#cite_note-55).
- [4] Fiber Bragg grating - Wikipedia. URL [https://en.wikipedia.org/wiki/Fiber\\_Bragg\\_grating](https://en.wikipedia.org/wiki/Fiber_Bragg_grating).
- [5] Fluorescence, Phosphorescence, Photoluminescence Differences, . URL <https://www.edinst.com/us/blog/photoluminescence-differences/>.
- [6] Fluorophores, Dyes & Probes | Biocompare.com, . URL <https://www.biocompare.com/7670-Fluorophores-Dyes-Probes/>.
- [7] Humon - The World's First Muscle Oxygen Sensor for Endurance Sports. URL <https://humon.io/>.
- [8] Hydrogel - Wikipedia. URL <https://nl.wikipedia.org/wiki/Hydrogel>.
- [9] Impedimetric Sensors: Principles, Applications and Recent Trends. doi: 10.35940/ijitee.J9806.0881019.
- [10] Moxy Monitor - Muscle Oxygen Monitor. URL <https://www.moxymonitor.com/>.
- [11] Sensor | Definition of Sensor by Merriam-Webster. URL <https://www.merriam-webster.com/dictionary/sensor>.
- [12] Chemiluminescence - Wikipedia, 9 2020. URL <https://en.wikipedia.org/wiki/Chemiluminescence>.
- [13] Myocardial Protection | Abdominal Key, 2020. URL <https://abdominalkey.com/myocardial-protection/>.
- [14] Miguel A., Olaya Gonzalez, and Jos R. Optical Fiber Sensors for Chemical and Biological Measurements. In *Current Developments in Optical Fiber Technology*. InTech, 6 2013. doi: 10.5772/52741. URL <http://dx.doi.org/10.5772/52741>.
- [15] Rafiq Ahmad and Khaled N. Salama. Physical Sensors for Biomedical Applications. In *Proceedings of IEEE Sensors*, volume 2018-October. Institute of Electrical and Electronics Engineers Inc., 12 2018. ISBN 9781538647073. doi: 10.1109/ICSENS.2018.8589646.
- [16] Daniel Aigner, Sergey M. Borisov, Francisco J. Orriach Fernández, Jorge F. Fernández Sánchez, Robert Saf, and Ingo Klimant. New fluorescent pH sensors based on covalently linkable PET rhodamines. *Talanta*, 99:194–201, 9 2012. ISSN 00399140. doi: 10.1016/j.talanta.2012.05.039.
- [17] Daniel Aigner, Birgit Ungerböck, Torsten Mayr, Robert Saf, Ingo Klimant, and Sergey M. Borisov. Fluorescent materials for pH sensing and imaging based on novel 1,4-diketopyrrolo-[3,4-c]pyrrole dyes. *Journal of Materials Chemistry C*, 1(36):5685–5693, 9 2013. ISSN 20507526. doi: 10.1039/c3tc31130a. URL [www.rsc.org/MaterialsC](http://www.rsc.org/MaterialsC).

- [18] Fahmida Alam, Sohini RoyChoudhury, Ahmed Hasnain Jalal, Yogeswaran Umasankar, Shahrzad Forouzanfar, Naznin Akter, Shekhar Bhansali, and Nezih Pala. Lactate biosensing: The emerging point-of-care and personal health monitoring. *Biosensors and Bioelectronics*, 117: 818–829, 2018. ISSN 18734235. doi: 10.1016/j.bios.2018.06.054.
- [19] Alan S. Morris and Reza Langari. *Measurement and Instrumentation*. Elsevier, 2016. ISBN 9780128008843. doi: 10.1016/C2013-0-15387-1. URL <https://linkinghub.elsevier.com/retrieve/pii/C20130153871>.
- [20] Jason M. Ali, Lachlan F. Miles, Yasir Abu-Omar, Carlos Galhardo, and Florian Falter. Global cardioplegia practices: Results from the global cardiopulmonary bypass survey. In *Journal of Extra-Corporeal Technology*, volume 50, pages 83–93. American Society of Extra-Corporeal Technology, 2018. URL [/pmc/articles/PMC6002645/?report=abstracthttps://www.ncbi.nlm.nih.gov/pmc/articles/PMC6002645/](https://pubmed.ncbi.nlm.nih.gov/pmc/articles/PMC6002645/).
- [21] Liam P. Andrus, Rachel Unruh, Natalie A. Wisniewski, and Michael J. McShane. Characterization of lactate sensors based on lactate oxidase and palladium benzoporphyrin immobilized in hydrogels. *Biosensors*, 5(3):398–416, 2015. ISSN 20796374. doi: 10.3390/bios5030398.
- [22] Prasoon Awasthi, Ranjan Mukherjee, Siva Prakasam O Kare, and Soumen Das. Impedimetric blood pH sensor based on MoS<sub>2</sub>-Nafion coated microelectrode. *RSC Advances*, 6(104):102088–102095, 10 2016. ISSN 20462069. doi: 10.1039/c6ra17786g. URL <https://pubs.rsc.org/en/content/articlehtml/2016/ra/c6ra17786ghttps://pubs.rsc.org/en/content/articlelanding/2016/ra/c6ra17786g>.
- [23] Nystha Baishya, Mohammad Momouei, Karthik Budidha, Meha Qassem, Pankaj Vadgama, and Panicos A Kyriacou. Near infrared spectrometric investigation of lactate in a varying pH buffer. *Journal of Near Infrared Spectroscopy*, 28(5-6):328–333, 10 2020. ISSN 0967-0335. doi: 10.1177/0967033520905374. URL <http://journals.sagepub.com/doi/10.1177/0967033520905374>.
- [24] Nikhil Bhalla, Pawan Jolly, Nello Formisano, and Pedro Estrela. Introduction to biosensors. *Essays in Biochemistry*, pages 60–61, 2016. doi: 10.1042/EBC20150001.
- [25] Biosensin Instruments. How Does Surface Plasmon Resonance Work? | Biosensing Instrument. URL <https://biosensingusa.com/technologies/surface-plasmon-resonance/surface-plasmon-resonance-work/http://biosensingusa.com/technologies/surface-plasmon-resonance/surface-plasmon-resonance-work/>.
- [26] Aniket Biswas, Lindsey R. Bornhoeft, Swayoma Banerjee, Yil Hwan You, and Michael J. McShane. Composite Hydrogels Containing Bioactive Microreactors for Optical Enzymatic Lactate Sensing. *ACS Sensors*, 2(11):1584–1588, 11 2017. ISSN 23793694. doi: 10.1021/acssensors.7b00648. URL <https://pubs.acs.org/doi/abs/10.1021/acssensors.7b00648>.
- [27] R. F. Burton. Intracellular buffering. *Respiration Physiology*, 33(1):51–58, 4 1978. ISSN 00345687. doi: 10.1016/0034-5687(78)90083-X.
- [28] Catalina Carvajal, Amandeep Goyal, and Prasanna Tadi. *Cardioplegia*. StatPearls Publishing, 3 2020. URL <http://www.ncbi.nlm.nih.gov/pubmed/32119350>.
- [29] Stefano Cattini, Stefano Cattini, Luca Accorsi, Stefano Truzzi, Luigi Rovati, and Luigi Rovati. On the development of an instrument for in-line and real-time monitoring of blood-pH in extracorporeal circulation. *IEEE Transactions on Instrumentation and Measurement*, 69(8):5640–5648, 2020. ISSN 15579662. doi: 10.1109/TIM.2019.2961499.
- [30] Sisi Chen, Qingbo Yang, Hai Xiao, Honglan Shi, and Yinfa Ma. Local pH monitoring of small cluster of cells using a fiber-optic dual-core micro-probe. *Sensors and Actuators, B: Chemical*, 241:398–405, 3 2017. ISSN 09254005. doi: 10.1016/j.snb.2016.10.079. URL <https://linkinghub.elsevier.com/retrieve/pii/S0925400516317063>.

- [31] Xin Chen and Zhengtian Gu. Absorption-type optical pH sensitive film based on immobilized purple cabbage pigment. *Sensors and Actuators, B: Chemical*, 178:207–211, 3 2013. ISSN 09254005. doi: 10.1016/j.snb.2012.12.094.
- [32] Tushar R. Choudhary, Michael G. Tanner, Alicia Megia-Fernandez, Kerriane Harrington, Harry A. Wood, Adam Marshall, Patricia Zhu, Sunay V. Chankeshwara, Debaditya Choudhury, Graham Monro, Muhammed Ucuncu, Fei Yu, Rory R. Duncan, Robert R. Thomson, Kevin Dhaliwal, and Mark Bradley. High fidelity fibre-based physiological sensing deep in tissue. *Scientific Reports*, 9(1):1–10, 2019. ISSN 20452322. doi: 10.1038/s41598-019-44077-7.
- [33] Hyun Joong Chung, Matthew S. Sulkin, Jong Seon Kim, Camille Goudeseune, Hsin Yun Chao, Joseph W. Song, Sang Yoon Yang, Yung Yu Hsu, Roozbeh Ghaffari, Igor R. Efimov, and John A. Rogers. Stretchable, multiplexed pH sensors with demonstrations on rabbit and human hearts undergoing ischemia. *Advanced Healthcare Materials*, 3(1):59–68, 2014. ISSN 21922659. doi: 10.1002/adhm.201300124.
- [34] Qingsong Cui, Ondřej Podrazký, Jan Mrázek, Jana Proboštová, and Ivan Kašík. Tapered-Fiber Optical Sensor for Physiological pH Range. *IEEE Sensors Journal*, 15(9):4967–4973, 9 2015. ISSN 1530437X. doi: 10.1109/JSEN.2015.2432091.
- [35] Richard S D’agostino, Jeffrey P Jacobs, Vinay Badhwar, Felix G Fernandez, Gaetano Paone, David W Wormuth, and David M Shahian. The Society of Thoracic Surgeons Adult Cardiac Surgery Database: 2018 Update on Outcomes and Quality. *The Annals of Thoracic Surgery*, 105:15–23, 2018. doi: 10.1016/j.athoracsur.2017.10.035. URL <https://doi.org/10.1016/j.athoracsur.2017.10.035>.
- [36] Piroze M. Davierwala, Alexander Verevkin, Sergey Leontyev, Martin Misfeld, Michael A. Borger, and Friedrich W. Mohr. Impact of expeditious management of perioperative myocardial ischemia in patients undergoing isolated coronary artery bypass surgery. *Circulation*, 128(SUPPL.1), 9 2013. ISSN 00097322. doi: 10.1161/CIRCULATIONAHA.112.000347. URL <https://pubmed.ncbi.nlm.nih.gov/24030411/><https://pubmed.ncbi.nlm.nih.gov/24030411/?dopt=Abstract>.
- [37] Geoffrey P. Dobson, Giuseppe Faggian, Francesco Onorati, and Jakob Vinten-Johansen. Hyperkalemic cardioplegia for adult and pediatric surgery: end of an era? *Frontiers in Physiology*, 4: 228, 8 2013. ISSN 1664-042X. doi: 10.3389/fphys.2013.00228. URL [www.frontiersin.org](http://www.frontiersin.org).
- [38] Schreiber Donald and Brenner Barry E. Cardiac Markers: Definition and Efficacy, Cardiac Troponins, Creatine Kinase–MB, 2018. URL <https://emedicine.medscape.com/article/811905-overview>.
- [39] Cornelia Drescher, Antje Diestel, Sonja Wollersheim, Felix Berger, and Katharina R.L. Schmitt. How does hypothermia protect cardiomyocytes during cardioplegic ischemia? *European Journal of Cardio-thoracic Surgery*, 40(2):352–359, 1 2011. ISSN 10107940. doi: 10.1016/j.ejcts.2010.12.006. URL <https://academic.oup.com/ejcts/article-lookup/doi/10.1016/j.ejcts.2010.12.006>.
- [40] Matthew Driller, Daniel Plews, and Nattai Borges. Wearable near Infrared Sensor for Determining an Athlete’s Lactate Threshold during Exercise. *NIR news*, 27(4):8–10, 6 2016. ISSN 0960-3360. doi: 10.1255/nirn.1609. URL <http://journals.sagepub.com/doi/10.1255/nirn.1609>.
- [41] K. Ehrlich, A. Kufcsák, S. McAughtrie, H. Fleming, N. Krstajic, C. J. Campbell, R. K. Henderson, K. Dhaliwal, R. R. Thomson, and M. G. Tanner. pH sensing through a single optical fibre using SERS and CMOS SPAD line arrays. *Optics Express*, 25(25):30976, 12 2017. ISSN 1094-4087. doi: 10.1364/OE.25.030976. URL <https://www.osapublishing.org/abstract.cfm?URI=oe-25-25-30976>.

- [42] Houda El Banani, Monique Bernard, Delphine Baetz, Emmanuel Cabanes, Patrick Cozzone, Arnaud Lucien, and Danielle Feuvray. Changes in intracellular sodium and pH during ischaemia-reperfusion are attenuated by trimetazidine: Comparison between low- and zero-flow ischaemia. *Cardiovascular Research*, 47(4):688–696, 9 2000. ISSN 00086363. doi: 10.1016/S0008-6363(00)00136-X. URL [https://academic.oup.com/cardiovasres/article-lookup/doi/10.1016/S0008-6363\(00\)00136-X](https://academic.oup.com/cardiovasres/article-lookup/doi/10.1016/S0008-6363(00)00136-X).
- [43] G. E.C. Ellerby, C. P. Smith, F. Zou, P. Scott, and B. R. Soller. Validation of a spectroscopic sensor for the continuous, noninvasive measurement of muscle oxygen saturation and pH. *Physiological Measurement*, 34(8):859–871, 2013. ISSN 09673334. doi: 10.1088/0967-3334/34/8/859.
- [44] D. Ellis and R. C. Thomas. Microelectrode measurement of the intracellular pH of mammalian heart cells. *Nature*, 262(5565):224–225, 7 1976. ISSN 00280836. doi: 10.1038/262224a0. URL <https://www.nature.com/articles/262224a0>.
- [45] M. Elsherif, M.U. Hassan, A.K. Yetisen, and H. Butt. Hydrogel optical fibers for continuous glucose monitoring. *Biosensors and Bioelectronics*, 137:25–32, 2019. doi: 10.1016/j.bios.2019.05.002.
- [46] Mohamed Elsherif, Rosalia Moreddu, Muhammad Umair Hassan, Ali K. Yetisen, and Haider Butt. Real-time optical fiber sensors based on light diffusing microlens arrays. *Lab on a Chip*, 19(12):2060–2070, 2019. ISSN 14730189. doi: 10.1039/c9lc00242a. URL <http://xlink.rsc.org/?DOI=C9LC00242A>.
- [47] Larisa Florea, Cormac Fay, Emer Lahiff, Thomas Phelan, Noel E. O'Connor, Brian Corcoran, Dermot Diamond, and Fernando Benito-Lopez. Dynamic pH mapping in microfluidic devices by integrating adaptive coatings based on polyaniline with colorimetric imaging techniques. *Lab on a Chip*, 13(6):1079–1085, 3 2013. ISSN 14730189. doi: 10.1039/c2lc41065f. URL [www.rsc.org/loc](http://www.rsc.org/loc).
- [48] Paddy French. In-vivo microsystems: A review, 9 2020. ISSN 14248220. URL <https://www.mdpi.com/1424-8220/20/17/4953>.
- [49] M. T. Ghoneim, A. Nguyen, N. Dereje, J. Huang, G. C. Moore, P. J. Murzynowski, and C. Dagdeviren. Recent Progress in Electrochemical pH-Sensing Materials and Configurations for Biomedical Applications, 4 2019. ISSN 15206890. URL <https://pubs.acs.org/doi/abs/10.1021/acs.chemrev.8b00655>.
- [50] Glenn P. Gravlee. *Cardiopulmonary Bypass: Principles and Practice*. Wolters Kluwer Health/Lippincott Williams & Wilkins, 2008. ISBN 9780781768153. URL <https://books.google.fr/books?id=M5sbCxd5cioC>.
- [51] Jingjing Gong, Michael G. Tanner, Seshasailam Venkateswaran, James M. Stone, Yichuan Zhang, and Mark Bradley. A hydrogel-based optical fibre fluorescent pH sensor for observing lung tumor tissue acidity. *Analytica Chimica Acta*, 1134:136–143, 2020. ISSN 00032670. doi: 10.1016/j.aca.2020.07.063. URL <https://doi.org/10.1016/j.aca.2020.07.063>.
- [52] Sarah R Gutbrod, Matthew S Sulkin, John A Rogers, and Igor R Efimov. Patient-specific flexible and stretchable devices for cardiac diagnostics and therapy. *Progress in Biophysics and Molecular Biology*, 115:244–251, 2014. doi: 10.1016/j.pbiomolbio.2014.07.011. URL <http://dx.doi.org/10.1016/j.pbiomolbio.2014.07.011>.
- [53] R. Hajian, Z. Mehrayin, M. Mohagheghian, M. Zafari, P. Hosseini, and N. Shams. Fabrication of an electrochemical sensor based on carbon nanotubes modified with gold nanoparticles for determination of valrubicin as a chemotherapy drug: Valrubicin-DNA interaction. *Materials Science and Engineering C*, 49:769–775, 2015. doi: 10.1016/j.msec.2015.01.072.
- [54] Matthew R. Hartings, Nathan J. Castro, Kathryn Gill, and Zeeshan Ahmed. A photonic pH sensor based on photothermal spectroscopy. *Sensors and Actuators B: Chemical*, 301:127076, 12 2019. ISSN 09254005. doi: 10.1016/j.snb.2019.127076. URL <https://linkinghub.elsevier.com/retrieve/pii/S0925400519312754>.

- [55] Stuart J. Head, Milan Milojevic, David P. Taggart, and John D. Puskas. Current practice of state-of-the-art surgical coronary revascularization. *Circulation*, 136(14):1331–1345, 10 2017. ISSN 15244539. doi: 10.1161/CIRCULATIONAHA.116.022572. URL <https://pubmed.ncbi.nlm.nih.gov/28972063/>.
- [56] Yuki Hiruta, Naoto Yoshizawa, Daniel Citterio, and Koji Suzuki. Highly durable double sol-gel layer ratiometric fluorescent pH optode based on the combination of two types of quantum dots and absorbing pH indicators. *Analytical Chemistry*, 84(24):10650–10656, 12 2012. ISSN 00032700. doi: 10.1021/ac302178z. URL <https://pubs.acs.org/doi/10.1021/ac302178z>.
- [57] Carlos A. J. Gouveia, Jose M., and Pedro A.S. Refractometric Optical Fiber Platforms for Label Free Sensing. In *Current Developments in Optical Fiber Technology*. InTech, 6 2013. doi: 10.5772/55376. URL <http://dx.doi.org/10.5772/55376>.
- [58] Jiri Janata and Jiří Janata. Amperometric Sensors. In *Principles of Chemical Sensors*, pages 201–239. Springer US, 2009. doi: 10.1007/b136378{\\_}7. URL [https://link.springer.com/chapter/10.1007/b136378\\_7](https://link.springer.com/chapter/10.1007/b136378_7).
- [59] Dayeong Jeon, Wook Jae Yoo, Jeong Ki Seo, Sang Hun Shin, Ki Tek Han, Seon Geun Kim, Jang Yeon Park, and Bongsoo Lee. Fiber-optic pH sensor based on sol-gel film immobilized with neutral red. *Optical Review*, 20(2):209–213, 3 2013. ISSN 13406000. doi: 10.1007/s10043-013-0037-y. URL <https://link.springer.com/article/10.1007/s10043-013-0037-y>.
- [60] Ine L. Jernelv, Karina Strøm, Dag Roar Hjelme, and Astrid Aksnes. Infrared spectroscopy with a fiber-coupled quantum cascade laser for attenuated total reflection measurements towards biomedical applications. *Sensors (Switzerland)*, 19(23):5130, 11 2019. ISSN 14248220. doi: 10.3390/s19235130. URL <https://www.mdpi.com/1424-8220/19/23/5130>.
- [61] I. Kasik, J. Mrazek, T. Martan, M. Pospisilova, O. Podrazky, V. Matejec, K. Hoyerova, and M. Kaminek. Fiber-optic pH detection in small volumes of biosamples. *Analytical and Bioanalytical Chemistry*, 398(5):1883–1889, 11 2010. ISSN 16182642. doi: 10.1007/s00216-010-4130-9. URL <http://link.springer.com/10.1007/s00216-010-4130-9>.
- [62] D. Kattiparambil Rajan, M. Patrikoski, J. Verho, J. Sivula, H. Ihalainen, S. Miettinen, and J. Lekkala. Optical non-contact pH measurement in cell culture with sterilizable, modular parts. *Talanta*, 161:755–761, 2016. doi: 10.1016/j.talanta.2016.09.021.
- [63] Kamal R. Khabbaz, Fuad Zankoul, and Kenneth G. Warner. Intraoperative metabolic monitoring of the heart: II. Online measurement of myocardial tissue pH. *Annals of Thoracic Surgery*, 72(6):S2227–S2233, 12 2001. ISSN 00034975. doi: 10.1016/S0003-4975(01)03284-2. URL <https://linkinghub.elsevier.com/retrieve/pii/S0003497501032842>.
- [64] S. F. Khuri and W. A. Marston. On-line metabolic monitoring of the heart during cardiac surgery. *Surgical Clinics of North America*, 65(3):439–453, 1985. ISSN 00396109. doi: 10.1016/S0039-6109(16)43630-3. URL <https://pubmed.ncbi.nlm.nih.gov/3898425/>.
- [65] Soogeun Kim, Seung Ho Lee, Sun Young Min, Kyung Min Byun, and Soo Yeol Lee. Dual-modal cancer detection based on optical pH sensing and Raman spectroscopy. *Journal of Biomedical Optics*, 22(10):1, 2017. ISSN 1560-2281. doi: 10.1117/1.jbo.22.10.105002.
- [66] J R Knowles. Enzyme-catalyzed phosphoryl transfer reactions. *Annual review of biochemistry*, 49(1):877–919, 6 1980. ISSN 00664154. doi: 10.1146/annurev.bi.49.070180.004305. URL <http://www.annualreviews.org/doi/10.1146/annurev.bi.49.070180.004305>.
- [67] Jeffrey A. Kraut and Nicolaos E. Madias. Lactic Acidosis. *New England Journal of Medicine*, 371(24):2309–2319, 12 2014. ISSN 0028-4793. doi: 10.1056/NEJMra1309483. URL <http://www.nejm.org/doi/10.1056/NEJMra1309483>.

- [68] Mohamed Laimoud and Rehan Qureshi. Outcome of Postcardiac Surgery Acute Myocardial Infarction and Role of Emergency Percutaneous Coronary Interventions. *Cardiology Research and Practice*, 2020, 2020. ISSN 20900597. doi: 10.1155/2020/2014675.
- [69] Chee Hoon Lee, Min Ho Ju, Joon Bum Kim, Cheol Hyun Chung, Sung Ho Jung, Suk Jung Choo, and Jae Won Lee. Myocardial injury following aortic valve replacement for severe aortic stenosis: Risk factor of postoperative myocardial injury and its impact on long-term outcomes. *Korean Journal of Thoracic and Cardiovascular Surgery*, 47(3):233–239, 2014. ISSN 20936516. doi: 10.5090/kjtcs.2014.47.3.233. URL <https://pubmed.ncbi.nlm.nih.gov/pmc/articles/PMC4157473/>.  
?report=abstract<https://www.ncbi.nlm.nih.gov/pmc/articles/PMC4157473/>.
- [70] J. J. Lemasters, J. M. Bond, E. Chacon, I. S. Harper, S. H. Kaplan, H. Ohata, D. R. Trollinger, B. Herman, and W. E. Cascio. The pH paradox in ischemia-reperfusion injury to cardiac myocytes. *EXS*, 76:99–114, 1996. ISSN 1023294X. doi: 10.1007/978-3-0348-8988-9{\\_}7. URL [https://link.springer.com/chapter/10.1007/978-3-0348-8988-9\\_7](https://link.springer.com/chapter/10.1007/978-3-0348-8988-9_7)<https://pubmed.ncbi.nlm.nih.gov/8805791/>.
- [71] Wei Li, Hu Cheng, Min Xia, and Kecheng Yang. An experimental study of pH optical sensor using a section of no-core fiber. *Sensors and Actuators, A: Physical*, 199:260–264, 9 2013. ISSN 09244247. doi: 10.1016/j.sna.2013.06.004.
- [72] M. Liu, D. He, T. Yang, W. Liu, L. Mao, Y. Zhu, J. Wu, G. Luo, and J. Deng. An efficient antimicrobial depot for infectious site-targeted chemo-photothermal therapy. *Journal of Nanobiotechnology*, 16(1), 2018. doi: 10.1186/s12951-018-0348-z.
- [73] X. Liu, S.-Q. Zhang, X. Wei, T. Yang, M.-L. Chen, and J.-H. Wang. A novel “modularized” optical sensor for pH monitoring in biological matrixes. *Biosensors and Bioelectronics*, 109:150–155, 2018. doi: 10.1016/j.bios.2018.02.052.
- [74] Aleksandra Lobnik. ABSORPTION-BASED SENSORS. pages 77–98. Springer, Dordrecht, 2006. doi: 10.1007/1-4020-4611-1{\\_}5. URL [https://link.springer.com/chapter/10.1007/1-4020-4611-1\\_5](https://link.springer.com/chapter/10.1007/1-4020-4611-1_5).
- [75] Edward Lowenstein. Cardiac Surgery in the Adult. *Anesthesia & Analgesia*, 85(6):1418, 1997. ISSN 0003-2999. doi: 10.1213/00000539-199712000-00059.
- [76] Sayed A.M. Marzouk, Richard P. Buck, Larry A. Dunlap, Timothy A. Johnson, and Wayne E. Cascio. Measurement of extracellular pH, K<sup>+</sup>, and lactate in ischemic heart. *Analytical Biochemistry*, 308(1):52–60, 9 2002. ISSN 00032697. doi: 10.1016/S0003-2697(02)00220-8.
- [77] Erica A. Melkonian and Mark P. Schury. *Biochemistry, Anaerobic Glycolysis*. StatPearls Publishing, 10 2019. URL <http://www.ncbi.nlm.nih.gov/pubmed/31536301>.
- [78] Peyton Miesse. *Flexible Electrochemical Lactate Sensor*. PhD thesis, Old Dominion University, 2020. URL [https://digitalcommons.odu.edu/biomedengineering\\_etds/10](https://digitalcommons.odu.edu/biomedengineering_etds/10).
- [79] Satyendra Kumar Mishra, Bing Zou, and Kin Seng Chiang. Wide-Range pH Sensor Based on a Smart-Hydrogel-Coated Long-Period Fiber Grating. *IEEE Journal of Selected Topics in Quantum Electronics*, 23(2):284–288, 3 2017. ISSN 15584542. doi: 10.1109/JSTQE.2016.2629662.
- [80] D L Namay, K E Hammermeister, M S Zia, T A DeRouen, H T Dodge, and K Namay. Effect of perioperative myocardial infarction on late survival in patients undergoing coronary artery bypass surgery. *Circulation*, 65(6):1066–1071, 6 1982. ISSN 0009-7322. doi: 10.1161/01.CIR.65.6.1066. URL <https://www.ahajournals.org/doi/10.1161/01.CIR.65.6.1066>.
- [81] Scott P. Nichols, Mary K. Balaconis, Rebecca M. Gant, Kit Y. Au-Yeung, and Natalie A. Wisniewski. Long-term in vivo oxygen sensors for peripheral artery disease monitoring. In *Advances in Experimental Medicine and Biology*, volume 1072, pages 351–356. Springer New York LLC, 2018. doi: 10.1007/978-3-319-91287-5{\\_}56. URL <https://pubmed.ncbi.nlm.nih.gov/pmc/articles/PMC6367927/>.  
?report=abstract<https://www.ncbi.nlm.nih.gov/pmc/articles/PMC6367927/>.

- [82] Shuming Nie and Steven R. Emory. Probing single molecules and single nanoparticles by surface-enhanced Raman scattering. *Science*, 275(5303):1102–1106, 2 1997. ISSN 00368075. doi: 10.1126/science.275.5303.1102. URL <http://www.sciencemag.org><http://science.sciencemag.org/>.
- [83] Massimo Onor, Stefano Gufoni, Tommaso Lomonaco, Silvia Ghimenti, Pietro Salvo, Fiodor Sorrentino, and Emilia Bramanti. Potentiometric sensor for non invasive lactate determination in human sweat. *Analytica Chimica Acta*, 989:80–87, 10 2017. ISSN 18734324. doi: 10.1016/j.aca.2017.07.050.
- [84] Hong Jun Park, Jo Hee Yoon, Kyoung G. Lee, and Bong Gill Choi. Potentiometric performance of flexible pH sensor based on polyaniline nanofiber arrays. *Nano Convergence*, 6(1):9, 12 2019. ISSN 21965404. doi: 10.1186/s40580-019-0179-0. URL <https://nanoconvergencejournal.springeropen.com/articles/10.1186/s40580-019-0179-0>.
- [85] Margaret E. Payne, Alla Zamarayeva, Veronika I. Pister, Natasha A.D. Yamamoto, and Ana Claudia Arias. Printed, Flexible Lactate Sensors: Design Considerations Before Performing On-Body Measurements. *Scientific Reports*, 9(1):1–10, 12 2019. ISSN 20452322. doi: 10.1038/s41598-019-49689-7. URL <https://doi.org/10.1038/s41598-019-49689-7>.
- [86] Yolanda Picó. *Chemical Analysis of Food: Techniques and Applications*. Elsevier Inc., 2012. ISBN 9780123848628. doi: 10.1016/C2010-0-64808-5.
- [87] Muqsit Pirzada and Zeynep Altintas. micromachines Recent Progress in Optical Sensors for Biomedical Diagnostics. doi: 10.3390/mi11040356. URL [www.mdpi.com/journal/micromachines](http://www.mdpi.com/journal/micromachines).
- [88] S.E. Pischke, S Hyler, C Tronstad, J Bergsland, E Fosse, P.S. Halvorsen, H Skulstad, and T.I. Tønnessen. Myocardial tissue CO<sub>2</sub> tension detects coronary blood flow reduction after coronary artery bypass in real-time †. *British Journal of Anaesthesia*, 114(3):414–422, 3 2015. ISSN 00070912. doi: 10.1093/bja/aeu381. URL <https://linkinghub.elsevier.com/retrieve/pii/S000709121731807X>.
- [89] Søren Erik Pischke, Christian Tronstad, Lars Holhjem, Per Steinar Halvorsen, and Tor Inge Tønnessen. Perioperative detection of myocardial ischaemia/reperfusion with a novel tissue CO<sub>2</sub> monitoring technology. *European Journal of Cardio-thoracic Surgery*, 42(1):157–163, 2012. ISSN 10107940. doi: 10.1093/ejcts/ezr278.
- [90] Miroslav Pohanka. The Piezoelectric Biosensors: Principles and Applications, a Review. *Int. J. Electrochem. Sci*, 12:496–506, 2017. doi: 10.20964/2017.01.44. URL [www.electrochemsci.org](http://www.electrochemsci.org)<http://creativecommons.org/licenses/by/4.0/>.
- [91] C.S. Pundir, V. Narwal, and B. Batra. Determination of lactic acid with special emphasis on biosensing methods: A review. *Biosensors and Bioelectronics*, 86:777–790, 2016. ISSN 18734235. doi: 10.1016/j.bios.2016.07.076.
- [92] Brant Putnam, Scott Bricker, Peter Fedorka, Juliette Zelada, Saad Shebrain, Bassam Omari, and Frederic Bongard. The correlation of near-infrared spectroscopy with changes in oxygen delivery in a controlled model of altered perfusion. *American Surgeon*, 73(10):1017–1022, 2007. ISSN 00031348. doi: 10.1177/000313480707301021.
- [93] Jing Qi, Daying Liu, Xiaoyan Liu, Shiquan Guan, Fengli Shi, Hexi Chang, Huarui He, and Guangming Yang. Fluorescent pH Sensors for Broad-Range pH Measurement Based on a Single Fluorophore. *Analytical Chemistry*, 87(12):5897–5904, 6 2015. ISSN 15206882. doi: 10.1021/acs.analchem.5b00053. URL <https://pubs.acs.org/sharingguidelines>.
- [94] Yang Ran, Peng Xiao, Yongkang Zhang, Deming Hu, Zhiyuan Xu, Lili Liang, and Bai-Ou Guan. A Miniature pH Probe Using Functional Microfiber Bragg Grating. *Optics*, 1(2):202–212, 8 2020. ISSN 2673-3269. doi: 10.3390/opt1020016. URL <https://www.mdpi.com/2673-3269/1/2/16>.

- [95] Nahid Raoufi, Frederic Surre, Tong Sun, Muttukrishnan Rajarajan, and Kenneth T.V. Grattan. Wavelength dependent pH optical sensor using the layer-by-layer technique. *Sensors and Actuators, B: Chemical*, 169:374–381, 7 2012. ISSN 09254005. doi: 10.1016/j.snb.2012.05.024.
- [96] Liza Rassaei, Wouter Olthuis, Seiya Tsujimura, Ernst J. R. Sudhölter, and Albert van den Berg. Lactate biosensors: current status and outlook. *Analytical and Bioanalytical Chemistry*, 406(1):123–137, 1 2014. ISSN 1618-2642. doi: 10.1007/s00216-013-7307-1. URL <http://link.springer.com/10.1007/s00216-013-7307-1>.
- [97] Paul Regtien and Edwin Dertien. *Sensors for mechatronics*. Elsevier, 1 2018. ISBN 9780128138106. doi: 10.1016/C2016-0-05059-3.
- [98] Robert A. Robergs, Craig R. McNulty, Geoffrey M. Minett, Justin Holland, and Gabriel Trajano. Lactate, not lactic acid, is produced by cellular cytosolic energy catabolism, 1 2018. ISSN 15489221. URL [www.physiologyonline.org](http://www.physiologyonline.org).
- [99] Davorin Sef, Janko Szavits-Nossan, Mladen Predrijevac, Rajna Golubic, Tomislav Sipic, Kresimir Stambuk, Zvonimir Korda, Pascal Meier, and Marko Ivan Turina. Management of perioperative myocardial ischaemia after isolated coronary artery bypass graft surgery. *Open Heart*, 6(1):1027, 5 2019. ISSN 20533624. doi: 10.1136/openhrt-2019-001027. URL <http://openheart.bmj.com/>.
- [100] Benjamin Senst, Amandeep Goyal, and Rene R. Diaz. *Cardiac Surgery*. StatPearls Publishing, 6 2020. URL <http://www.ncbi.nlm.nih.gov/pubmed/30422530>.
- [101] Rinky Sha, Kikuo Komori, and Sushmee Badhulika. Amperometric pH Sensor Based on Graphene-Polyaniline Composite. *IEEE Sensors Journal*, 17(16):5038–5043, 8 2017. ISSN 1530437X. doi: 10.1109/JSEN.2017.2720634.
- [102] Manju Sharma and S. M.Paul Khurana. Biomedical engineering: The recent trends. In *Omics Technologies and Bio-engineering: Volume 2: Towards Improving Quality of Life*, pages 323–336. Elsevier, 1 2018. ISBN 9780128158708. doi: 10.1016/B978-0-12-815870-8.00017-6.
- [103] Priyanka Sharma, Vivek Semwal, and Banshi D. Gupta. Fiber optic surface plasmon resonance based lactate sensor using co-immobilization of lactate dehydrogenase and NAD<sup>+</sup>. *Optical Fiber Technology*, 49:22–27, 5 2019. ISSN 10685200. doi: 10.1016/j.yofte.2019.02.001. URL <https://doi.org/10.1016/j.yofte.2019.02.001>.
- [104] Kateryna Shavanova, Yulia Bakakina, Inna Burkova, Ivan Shteplyuk, Roman Viter, Arnolds Ubelis, Valerio Beni, Nickolaj Starodub, Rositsa Yakimova, and Volodymyr Khranovskyy. Application of 2D Non-Graphene Materials and 2D Oxide Nanostructures for Biosensing Technology. *Sensors*, 16(2):223, 2 2016. ISSN 1424-8220. doi: 10.3390/s16020223. URL <http://www.mdpi.com/1424-8220/16/2/223>.
- [105] Alina Sigaeva, Yori Ong, Viraj G. Damle, Aryan Morita, Kiran J. van der Laan, and Romana Schirhagl. Optical Detection of Intracellular Quantities Using Nanoscale Technologies. *Accounts of chemical research*, 52(7):1739–1749, 7 2019. ISSN 15204898. doi: 10.1021/acs.accounts.9b00102. URL <https://pubs.acs.org/sharingguidelines>.
- [106] Priti Singh, Shailendra Kumar Pandey, Jyoti Singh, Sameer Srivastava, Sadhana Sachan, and Sunil Kumar Singh. Biomedical Perspective of Electrochemical Nanobiosensor, 7 2016. ISSN 21505551. URL <https://link.springer.com/article/10.1007/s40820-015-0077-x>.
- [107] Stewart Smith. Special Lecture Series Biosensors and Instrumentation. Technical report.
- [108] William C. Stanley. Changes in cardiac metabolism: A critical step from stable angina to ischaemic cardiomyopathy. In *European Heart Journal, Supplement*, volume 3, pages 02–07. W.B. Saunders Ltd, 11 2001. doi: 10.1016/s1520-765x(01)90147-6. URL [https://academic.oup.com/eurheartjsupp/article-abstract/3/suppl\\_0/02/381043](https://academic.oup.com/eurheartjsupp/article-abstract/3/suppl_0/02/381043).

- [109] William C. Stanley, Fabio A. Recchia, and Gary D. Lopaschuk. Myocardial substrate metabolism in the normal and failing heart. *Physiological Reviews*, 85(3):1093–1129, 2005. ISSN 00319333. doi: 10.1152/physrev.00006.2004.
- [110] Charles Steenbergen and Nikolaos G. Frangogiannis. Ischemic heart disease. In *Muscle*, volume 1, pages 495–521. Elsevier Inc., first edit edition, 1 2012. ISBN 9780123815101. doi: 10.1016/B978-0-12-381510-1.00036-3. URL <http://dx.doi.org/10.1016/B978-0-12-381510-1.00036-3>.
- [111] S. Sun, Y. Wei, H. Wang, Y. Cao, and B. Deng. A novel electrochemiluminescence sensor coupled with capillary electrophoresis for simultaneous determination of quinapril hydrochloride and its metabolite quinaprilat hydrochloride in human plasma. *Talanta*, 179:213–220, 2018. doi: 10.1016/j.talanta.2017.10.050.
- [112] Jaison Chacha Sunny, Dinesh Kumar, Nalini Kotekar, and Nagaraj Desai. Incidence and predictors of perioperative myocardial infarction in patients undergoing non-cardiac surgery in a tertiary care hospital. *Indian Heart Journal*, 70(3):335–340, 5 2018. ISSN 00194832. doi: 10.1016/j.ihj.2017.08.010. URL [/pmc/articles/PMC6034009/?report=abstracthttps://www.ncbi.nlm.nih.gov/pmc/articles/PMC6034009/](https://pubmed.ncbi.nlm.nih.gov/pmc/articles/PMC6034009/).
- [113] E.W.Y. Tam, A. Feigenbaum, J.B.L. Addis, S. Blaser, N. MacKay, M. Al-Dosary, R.W. Taylor, C. Ackerley, J.M. Cameron, and B.H. Robinson. A novel mitochondrial DNA mutation in COX1 leads to strokes, seizures, and lactic acidosis. *Neuropediatrics*, 39(6):328–334, 2008. doi: 10.1055/s-0029-1202287.
- [114] Ali Tamayol, Mohsen Akbari, Yael Zilberman, Mattia Comotto, Emal Lesha, Ludovic Serex, Sara Bagherifard, Yu Chen, Guoqing Fu, Shideh Kabiri Ameri, Weitong Ruan, Eric L. Miller, Mehmet R. Dokmeci, Sameer Sonkusale, and Ali Khademhosseini. Flexible pH-Sensing Hydrogel Fibers for Epidermal Applications. *Advanced Healthcare Materials*, 5(6):711–719, 3 2016. ISSN 21922659. doi: 10.1002/adhm.201500553. URL <http://doi.wiley.com/10.1002/adhm.201500553>.
- [115] Ammar Ahmad Tarar, Umair Mohammad, and Soumya K. Srivastava. Wearable skin sensors and their challenges: A review of transdermal, optical, and mechanical sensors, 5 2020. ISSN 20796374. URL [/pmc/articles/PMC7345448/?report=abstracthttps://www.ncbi.nlm.nih.gov/pmc/articles/PMC7345448/](https://pubmed.ncbi.nlm.nih.gov/pmc/articles/PMC7345448/).
- [116] T. I. Tønnessen. Biological basis for PCO<sub>2</sub> as a detector of ischemia. *Acta Anaesthesiologica Scandinavica*, 41(6):659–669, 1997. ISSN 00015172. doi: 10.1111/j.1399-6576.1997.tb04764.x. URL [https://pubmed.ncbi.nlm.nih.gov/9241323/https://pubmed.ncbi.nlm.nih.gov/9241323/?dopt=Abstract](https://pubmed.ncbi.nlm.nih.gov/9241323/).
- [117] Z Q Tou, C C Chan, and Stephanie Leong. A fiber-optic pH sensor based on polyelectrolyte multilayers embedded with gold nanoparticles. *Measurement Science and Technology*, 25(7):075102, 7 2014. ISSN 13616501. doi: 10.1088/0957-0233/25/7/075102. URL <https://iopscience.iop.org/article/10.1088/0957-0233/25/7/075102>.
- [118] Christian Tronstad. *Developments in biomedical sensors based on electrical impedance*. PhD thesis, Oslo University Hospital, 2012. URL <http://hdl.handle.net/10852/34384>.
- [119] Aslan T. Turer and Joseph A. Hill. Pathogenesis of myocardial ischemia-reperfusion injury and rationale for therapy, 8 2010. ISSN 00029149. URL [/pmc/articles/PMC2957093/?report=abstracthttps://www.ncbi.nlm.nih.gov/pmc/articles/PMC2957093/](https://pubmed.ncbi.nlm.nih.gov/pmc/articles/PMC2957093/).
- [120] Sanne Vreugdenhil, Pedro J. Freire Jorge, Mels F. van Driel, and Maarten W. Nijsten. Ischemic priapism as a model of exhausted metabolism. *Physiological Reports*, 7(6):e13999, 3 2019. ISSN 2051-817X. doi: 10.14814/phy2.13999. URL <https://onlinelibrary.wiley.com/doi/abs/10.14814/phy2.13999>.

- [121] F. J.M. Walters, G. J. Wilson, D. J. Steward, R. J. Domenech, and D. C. MacGregor. Intramyocardial pH as an index of myocardial metabolism during cardiac surgery. *Journal of Thoracic and Cardiovascular Surgery*, 78(3):319–330, 9 1979. ISSN 00225223. doi: 10.1016/s0022-5223(19)38098-5.
- [122] Hong-Sheng Wang. Critical role of bicarbonate and bicarbonate transporters in cardiac function. *World Journal of Biological Chemistry*, 5(3):334, 2014. ISSN 1949-8454. doi: 10.4331/wjbc.v5.i3.334. URL /pmc/articles/PMC4160527/?report=abstracthttps://www.ncbi.nlm.nih.gov/pmc/articles/PMC4160527/.
- [123] Weizhong Jin, Lingxiang Wu, Yuanlin Song, Jinjun Jiang, Xiaodan Zhu, Dawei Yang, and Chunxue Bai. Continuous Intra-Arterial Blood pH Monitoring by a Fiber-Optic Fluorosensor. *IEEE Transactions on Biomedical Engineering*, 58(5):1232–1238, 5 2011. ISSN 0018-9294. doi: 10.1109/TBME.2011.2107514. URL http://ieeexplore.ieee.org/document/5696742/.
- [124] D. Wencel, A. Kaworek, T. Abel, V. Efremov, A. Bradford, D. Carthy, G. Coady, R.C.N. McMorro, and C. McDonagh. Optical Sensor for Real-Time pH Monitoring in Human Tissue. *Small*, 14(51), 2018. doi: 10.1002/sml.201803627.
- [125] Dorota Wencel, Tobias Abel, and Colette McDonagh. Optical Chemical pH Sensors. *Analytical Chemistry*, 86(1):15–29, 1 2014. ISSN 0003-2700. doi: 10.1021/ac4035168. URL https://pubs.acs.org/doi/10.1021/ac4035168.
- [126] Wikipedia. Bio-layer interferometry - Wikipedia, 2020. URL https://en.wikipedia.org/wiki/Bio-layer\_interferometry.
- [127] Z. Xia, H. Li, and M. G. Irwin. Myocardial ischaemia reperfusion injury: the challenge of translating ischaemic and anaesthetic protection from animal models to humans. *British Journal of Anaesthesia*, 117:ii44–ii62, 2016. ISSN 14716771. doi: 10.1093/bja/aew267.
- [128] Lizhi Xu, Sarah R. Gutbrod, Andrew P. Bonifas, Yewang Su, Matthew S. Sulkin, Nanshu Lu, Hyun Joong Chung, Kyung In Jang, Zhuangjian Liu, Ming Ying, Chi Lu, R. Chad Webb, Jong Seon Kim, Jacob I. Laughner, Huanyu Cheng, Yuhao Liu, Abid Ameen, Jae Woong Jeong, Gwang Tae Kim, Yonggang Huang, Igor R. Efimov, and John A. Rogers. 3D multifunctional integumentary membranes for spatiotemporal cardiac measurements and stimulation across the entire epicardium. *Nature Communications*, 5, 2014. ISSN 20411723. doi: 10.1038/ncomms4329.
- [129] Gan Xin Yan and André G. Kléber. Changes in extracellular and intracellular pH in ischemic rabbit papillary muscle. *Circulation Research*, 71(2):460–470, 1992. ISSN 00097330. doi: 10.1161/01.RES.71.2.460. URL http://ahajournals.org.
- [130] John T.W. Yeow. Biomedical Sensors. In *Wiley Encyclopedia of Biomedical Engineering*. John Wiley & Sons, Inc., Hoboken, NJ, USA, 4 2006. doi: 10.1002/9780471740360.ebs0155. URL http://doi.wiley.com/10.1002/9780471740360.ebs0155.
- [131] Yil Hwan You, Ashvin T. Nagaraja, Aniket Biswas, Jin Ha Hwang, Gerard L. Cote, and Michael J. McShane. SERS-Active Smart Hydrogels with Modular Microdomains: From pH to Glucose Sensing. In *IEEE Sensors Journal*, volume 17, pages 941–950. Institute of Electrical and Electronics Engineers Inc., 2 2017. doi: 10.1109/JSEN.2016.2636020.
- [132] Jakub Zajíc. Optical pH Detection with U-Shaped Fiber-Optic Probes and Absorption Transducers. *Conference Papers in Science*, 2015:1–8, 2015. ISSN 2356-6108. doi: 10.1155/2015/513621.
- [133] Nikolay V. Zaryanov, Vita N. Nikitina, Elena V. Karpova, Elena E. Karyakina, and Arkady A. Karyakin. Nonenzymatic sensor for lactate detection in human sweat. *Analytical Chemistry*, 89(21):11198–11202, 11 2017. ISSN 15206882. doi: 10.1021/acs.analchem.7b03662. URL https://pubmed.ncbi.nlm.nih.gov/29065687/.

- [134] Y. Zhao, Z. Zhang, Y. Zou, and Y. Yang. Visualization of Nicotine Adenine Dinucleotide Redox Homeostasis with Genetically Encoded Fluorescent Sensors. *Antioxidants and Redox Signaling*, 28(3):213–229, 2018. doi: 10.1089/ars.2017.7226.
- [135] Yong Zhao, Ming Lei, Shi Xuan Liu, and Qiang Zhao. Smart hydrogel-based optical fiber SPR sensor for pH measurements. *Sensors and Actuators, B: Chemical*, 261:226–232, 5 2018. ISSN 09254005. doi: 10.1016/j.snb.2018.01.120.
- [136] Xin Ting Zheng, Hong Bin Yang, and Chang Ming Li. Optical detection of single cell lactate release for cancer metabolic analysis. *Analytical Chemistry*, 82(12):5082–5087, 6 2010. ISSN 00032700. doi: 10.1021/ac100074n. URL <https://pubs.acs.org/sharingguidelines>.
- [137] Gaofeng Zhou, Yannian Wang, and Lujun Cui. Biomedical Sensor, Device and Measurement Systems. In *Advances in Bioengineering*. InTech, 7 2015. doi: 10.5772/59941. URL <http://dx.doi.org/10.5772/59941>.